Scuola Dottorale di Ingegneria Sezione di
Ingegneria dell'Elettronica Biomedica,
dell'Elettromagnetismo e delle Telecomunicazioni

XXVI Ciclo della formazione Dottorale

Signal processing techniques for cognitive radio networks

(Metodi di elaborazione numerica dei segnali per reti cognitive)

ING. ELENA GUZZON _____

Nome e Cognome del dottorando — Firma

PROF. GAETANO GIUNTA _____

Docente Guida/Tutor: Prof. — Firma

PROF. FRANCESCO BENEDETTO _____

Co-Tutor: Prof. — Firma

PROF. ALESSANDRO SALVINI _____

Coordinatore: Prof. — Firma

To my beloved brothers

Marco and Andrea

my partners in crime,

my harbor in time of storm

TABLE OF CONTENTS

LIST OF FIGURES

Chapter 1 INTRODUCTION

1.1 Research motivations

Telecommunication is one of the most noticeable technologic revolutions of the last century. It has changed forever the way we connected to each other, eliminating distance between continents, between countries, between persons. Its history begins in the far 1909, when Guglielmo Marconi and Carl Ferdinand Brown received the Nobel prize in "*recognition of their contributions to the development of wireless telegraphy*". The wireless communications have evolved since the 1909, starting from the telegraph, the telephone, to the mobile telecommunication, and lately to the diffusion of Internet, smartphones and tablets.

Figure.1-1 Guglielmo Marconi and its telegraph

In the last couple of decades, the telecommunications have experienced a drastic development. The proliferation of wireless services, and the diffusion of multifunctional

devices such as smartphones and tablets has opened the opportunity for the diffusion of new added values services. In addition, smartphones are becoming essential for most of us: 84% of people say they can't go a single day without a mobile phone [1]; the number of mobile devices sold every day worldwide is almost a million, twice the number of newborns [2]. Traditionally, the use of the radio spectrum has been regulated by governmental agencies that assign fixed frequency bands to licensed providers for exclusive access. The increasing demand of added value services, and the need of wide-band connections for supporting their diffusion, is rapidly saturating the frequencies available for communications. As a consequence, the spectrum scarcity problem has emerged: with all the spectrum bands already exclusively allocated, it is becoming extremely hard to find unused frequency bands to deploy new services, or enhance the existing ones. However, recent studies on the actual spectrum utilization have revealed that a large portion of the licensed spectrum is often under-utilized. Moreover, the spectrum usage is concentrated only in certain bands, while a significant amount of the radio spectrum is only sporadically used. To better understand the situation, international organizations such as the Federal Communication Commission (FCC), the Shared Spectrum Company (SSC), and the International Telecommunication Union (ITU), analysed which is the actual usage of the spectrum. The result is that in some cities like San Diego, New Orleans, and Atlanta up to 70% of the allocated spectrum is not continuously used [3]-[4]. In addition, the usage of GSM900/1800 in the city of Paris is less than 30%, while the UHF TV spectrum is used up to the 51% of its potential [5]. Moreover, not only some frequency bands are almost unused while other are oversaturated, but there are also problems related to traffic peaks in different moments of the day. The different requests of services drive to a spatial variation of the spectrum usage: in business areas there are principally data and voice communications, while in residential zones there are mostly television and entertainment communications. In practise, there are many frequency bands available for wireless communications, at different places and different times. It is evident that the spectrum scarcity problem is due to the spectrum fixed assignment policy, rather than to a physical shortage of usable frequencies. There are three major issues and inefficiencies in the current spectrum management policy:

(i) The majority of the spectrum is already allocated but the usage of the assigned bands is much lower than its potential.

(ii) The usage of the most requested bands varies in time and space.

(iii) Unassigned bandwidths with no specific policies, such as the Industrial Scientific and Medical (ISM) band, are growing in usage and number of accesses.

The underutilization of the radio spectrum and the inefficiency of the conventional assignment policy result in the need for a new communication paradigm to exploit the spectrum bands in a more efficient way.

The Cognitive Radio Networks (CRNs) that are the objects of this dissertations, have been proposed for solving these inefficiency issues [6]. In CRN the spectrum assignments is based on revolutionary policy, named Dynamic Spectrum Access (DSA) [7]-[8]. In particular, DSA allows breaking the spectrum barrier by enabling networks and their end-users to dynamically access the spectrum. The idea behind DSA is to authorize a finite number of devices, for a limited time, to share the same portion of the radio spectrum. The two key technologies of this revolution of the wireless communications are Software Defined Radio (SDR) and Cognitive Radio (CR). In particular, CR is the technology allowing a radio equipment to obtain knowledge of its radio environment and to dynamically adjust its operational parameters in order to improve its performance [9]. SDR technology is the natural platform on which to build in new cognitive features. In particular, SDR is a radio communication system where components that in the past have been typically implemented in hardware (e.g. mixers, filters, modulators/demodulators, detectors, etc.) are instead implemented by means of software. The list of SDR benefits is long, but some of the most important are interoperability with new and legacy radio systems; ability to squeeze a staggering amount of radio capability in a very small package; and the ability to implement networking tasks on each radio that run transparently to the user.

In a CRN there are two categories of users (and providers) usually referred to as the primary users (providers) and the secondary users (providers). The Primary User (PU) is the owner of the license for that frequency band and has always the right of using the radio resource. The Secondary User (SU) is an un-licensed user that can access the spectrum bands of a primary user guaranteeing that no interference is caused to the primary communications. A CRN consists of two "sub-networks": the primary network (PN), which is the network of primary transmitter and receivers, and the secondary network (SN), which conversely is the network of secondary receivers and transmitters. The PN has the license for accessing the spectrum bands, while the secondary networks does not. However, the SN can access the frequency bands left un-used by the PN. The un-used, or free, bands, suitable for a secondary communications, are named spectrum holes and their identification is one of the more critical implementation's issues of a cognitive system. The SN exploits its CR and SDR functionalities to sense the radio spectrum and identify spectrum opportunities. The CRNs, promise to bring along substantial benefits, such as:

- Reconfigurable and cost-effective architectures for wireless devices;
- Better utilization of the radio spectrum, which is expected to mitigate the ever increasing spectrum scarcity problem;
- Open the door for broadband usage in secure communications, which is currently restricted in available technologies;
- Enable open portability among different network technologies;
- Allow for economies of scale by their potential to harmonize the needs of commercial, public safety and military users.

Creating a set of standards acting as a common framework addressing the needs of all stakeholders would therefore allow for huge economies of scale for future SDR and CR products.

1.2 Research Objectives

In this dissertation, the spectrum scarcity problem is addressed in the scenarios of cognitive radio network, both at the primary and secondary network sides. The goal of the research activity has been proposing and implementing innovative methods for improving the spectrum utilization, mitigating the ever increasing spectrum scarcity problem, supporting the diffusion of CRNs and sustaining the coexistence of primary and secondary users.

More in details, the first part of the research activity has been focused on primary networks, studying the solutions for improving the spectrum utilization. The research has resulted in many scientific papers for scientific journals and international conferences [J3]-[J6]-[J7]-[J4]-[C3]-[C6]-[C9]-[C10]-[C11]-[C12] and in one patent [P1]. In particular we concentrated on fourth and five generation (4G and 5G) networks. In these systems, the Orthogonal Frequency Division Multiplexing (OFDM) is adopted to support high data rate multimedia transmission, while dynamically managing the spectrum resources. The main idea behind OFDM is to convert a frequency selective channel into a collection of frequency flat channels with partially overlapped spectra. The sub-carriers are orthogonal to each other, thus avoiding mutual interference. In addition, in 4G networks the orthogonal frequency division multiplexing access (OFDMA) is used for accessing the radio spectrum. OFDMA is a multi-user version of the OFDM, where different sub-channel's sets are assigned to different users. Although, OFDM and OFDMA allow using the available frequency bands in an agile, dynamic and efficient way, they heavily rely on the orthogonality of the uplink and downlink transmission and reception. Therefore, achieving and then maintaining timing and frequency synchronization are among the most critically procedures to be performed in OFDM system. In fact, even a small misalignment between the receiver and the transmitted signal can lead to dramatic degradation of the communication. For such reasons, the research activities in the field of primary networks have been mainly focused on the synchronization procedures in 4G and 5G networks. A detailed review of the state of art solutions is reported in [J6]-[J7].

The first part of the analysis has been focused on methods based on matched filter correlators. In these systems, the time uncertainty of the incoming signal is divided into a finite number of (timing) *cells*. Each cell corresponds to a sample of the time delay between the received signal and its local replica, generated at the receiver side. The cells are sequentially tested until a correct one is obtained. For each cell, a testing variable is compared with a pre-selected threshold: if the testing variable exceed the threshold true acquisition is achieved, otherwise the cell is discarded and the next one is tested. Taking the cell size as a fraction of the actual sample period could improve the acquisition performance, but unlike the case of one cell per sample, the detection variables between contiguous cells, are not independent and possibly strongly correlated. In such case it is extremely difficult to find a closed form expression for the systems error probabilities. The research activity in this context has resulted in the definition of a new class of functions, the extended-MGQ (EMGQ) functions that can express the false alarm and detection probabilities of the system in a closed form [J3]-[C4]. It has to be noted that the EMGQ are very generic functions and can be used for evaluating the performance of any testing procedure that uses two correlated testing variables. In addition, in order to consider the effects of cell correlation, a new test, namely the *twin test*, has been proposed. The main idea behind the twin test is to introduce an additional threshold to be jointly overcame by both the testing variable of two contiguous cells.

Another important research aspect has been improving the performance of initial synchronization in the 4G Long Term Evolution (LTE) systems [P1]-[J7]-[C9]-[C10]. LTE uses OFDM modulation and OFDMA technique for the downlink transmissions in order to provide high data rate and mobility. The initial synchronization process is especially important for LTE systems, which rely heavily on the orthogonality of the uplink and downlink transmission and reception to optimize the radio link performance. The design of the synchronization channel is being developed within the standardization activities of 3GPP Long Term Evolution and is it is one of the key issues in the design of the system. In this doctorate thesis an innovative signal processing method for the initial synchronization of LTE wireless networks is proposed. The method is based on a randomization operation performed over the samples of the received synchronization signal. The new method, can

be applied to every LTE transmission standard, since it requires modifications only at the receiver side.

The second part of the research activity has been dedicated to the secondary networks. One of the more important operation of a SN is identifying the under-utilized frequency bands that can used for secondary communications (i.e. the spectrum holes). The process of detecting PUs and identifying spectrum holes is the spectrum sensing [10]-[11]. Several strategies have been proposed in literature for spectrum sensing spanning from cumbersome techniques such as autocorrelation and auto-covariance-based methods to simpler algorithms (e.g. energy detectors), and a detailed review of the state-of-art solutions has been reported in [J5]-[J8]. Regardless the specific spectrum sensing strategy, the decision about the presence or absence the signal transmitted by the PU can be obtained by comparing a decision metric (e.g. the energy of the received signal in the energy detection approach) against a fixed threshold. Moreover, a CR should be able to operate in many different frequency bands, while detecting the presence of primary signals from various communications standards characterized by different parameters. Therefore, effective spectrum sensing strategies should be blind, i.e. they should need no a priori knowledge about the primary system. The research activity in this field has been manly focused on proposing effective, blind spectrum sensing methods. All the proposed algorithms have been applied for detecting primary communications in the 4G and 5G systems. The work in this field has resulted in many scientific papers for scientific journals and international conferences [J1]-[J2]-[J5]-[J8]-[C1]-[C2]-[C4]-[C5]-[C7]-[C8].

Spectrum sensing methods based on the autocorrelation of the received signal are very effective in detecting OFDM signals whose autocorrelation function exhibit strong periodicity features. A method for detection of OFDM signal based on the autocorrelation of the received signal has been proposed [C8]. Recently a “Rayleigh-ness test”, has been introduced for code acquisition purposes in Direct Sequence-Code Division Multiple Access (DS-CDMA) systems [12]. The test can be performed to decide on the presence of a statistically relevant mean value of a complex Gaussian model generating both Rayleigh

and Rice distributions. It has to be noted that code synchronization is a task that is conceptually similar to spectrum sensing: in both case the problem is modeled as a binary hypothesis testing, where a testing variable is compared to a proper pre-selected threshold. Then, the decision whether a primary user is active, or not, can be made on the presence of a non-zero mean value of a Gaussian distributed random variable. This is also equivalent to state whether the observed series is a portion of one realization of a Rayleigh (or Rice) distributed random process, and hence the Rayleigh-ness can be applied for spectrum sensing purposes. The Rayleigh-ness test in its original form makes use of matched filter correlation. Notwithstanding matched filter are the optimal detector, they require a priori knowledge about the signal of interest. Unfortunately in CR scenarios a priori knowledge about the signals of interest is typically very low. Therefore, the conventional Rayleigh-ness test has been accordingly modified, in order to provide a blind spectrum sensing method.

Another aspect that has been considered in this dissertaion is providing methods for the fast detection of primary users. In fact, secondary users are low priority users of the radio spectrum and they must yield to the primary user whenever he starts to access the band in operation. Then, the secondary communication should continue on another spectrum hole without interruptions. A cognitive radio device should be able to sense wide portion of the radio spectrum in order to identify multiple spectrum holes and select the more appropriate frequency band for communication. A possible solution for multiband sensing is using banks of band-pass filters. These methods are particularly suitable for OFDM systems, in which the signal consists of multiple orthogonal narrow band subcarriers. Conventional filter banks-based methods use analog hardware, because the imperfections of the devices' radio front end can be better handled in the analog domain. Also, digitizing a wideband signal with high dynamic range is a problem from the analog-to-digital conversion point of view. The research in this field results in an innovative SDR filter bank method that is based on the Fast Fourier Transform [C7]. Using SDR technology offers many benefits in terms of flexibility and re-configurability. More in details, the entire spectrum band is first scanned with the filter bank for selecting four adjacent sub-channel. Then, the energy of each band is measured and used as a testing variable for determine the presence of a primary user.

Recently, spectrum sensing methods based on high-order statistics of the received signal have been proposed in advance cognitive radio system. These methods allow overcoming the drawbacks of the conventional methods under noise uncertainty, without dramatically growing up the overall computational complexity. In fact one of the main drawbacks of many spectrum sensing strategies is that the noise variance has to be perfectly known in order to correctly set the threshold. Then, if this information is unavailable or not accurate, the system performance dramatically reduces. In order to overcame these limitations, in this dissertation an innovative spectrum sensing method, called the *normalized variance* (NV), is proposed [J1]. The basic rational behind the proposed method is as follows. First the second and fourth order moments of the received signal are evaluated. Then a new decision variable, namely the *normalized variance*, is derived as a function of these higher order moments.

Cooperative sensing has been recently proposed has a possible solution for the sensing problems arising in presence of noise uncertainty and fading. In cooperative spectrum sensing the final decision about the spectrum occupancy is obtained by combining the decision of each single SU. Conventional methods assume that the observations from the cooperative sensors are independent, in order to simplify the analysis. But, this assumption is not practical when the proximity of the sensors results in correlated observations. Then, in this dissertation a new test for the performance improvements of cooperative spectrum sensing in the presence of correlated users is proposed [C1]. In fact, in the presence of strong fading or shadowing effects, some correlated observations may be under the threshold of the conventional energy, even if the PU is effectively transmitting. This behavior results in a dramatic reduction of the detection probability of the system, thus increasing the interference with PUs. The proposed method which is based on a modified version of the twin test in [J2], allows to recovery these unlucky cases.

In addition, a new scenario and a security treat in CRN has been identified and a possible countermeasure proposed. In a CRN, the possibility of trading the radio spectrum offers new business opportunities for both PUs and SUs. In fact, a primary provider can rent its unused resources to secondary provider while maintaining the ownership of the spectrum. In this way, SUs can use the frequency bands which could not otherwise access. Unfortunately, in

this operating scenario there is also room for fraudulent users. In fact, a deceitful cognitive SU could use its technical advances for hiding himself under the noise floor, and not being charged for using the radio spectrum. The aim of such freeloader users (FLUs) is to use the spectrum secretly. Notwithstanding they do not directly damage the communications of active users (either PUs or SUs), they represent a relevant economic loss for CRN providers, and therefore must be promptly detected and blocked. This operating scenario, which to the best of our knowledge, is completely different from what has been studied in the literature about cognitive radio users, is fully addressed in this thesis and resulted in the paper [J2]. The main idea behind the proposed method is as follows. The second, fourth and sixth order moments of the received signal are evaluated. Then, an estimation of the fraudulent, active and noise signal power is derived from the above mention moments, and the fraudulent power used as a testing variable to determine the presence of such deceitful users.

Finally two applications of the FLUs detection procedure for conventional spectrum sensing have been proposed. More in details the second and fourth order moments of the received signal are derived and used for estimating the signal and noise power. The signal power can is used for determine the presence of a low power transmission in the frequency band of interest [C4]. On the other hand, the noise power can be exploited for determine if the SUs can safely accessing the band, without causing harmful interference to the primary users [C2].

1.3 Thesis organization

The remainder of this thesis is divided into three parts. Part 1 is an introduction to the cognitive radio network. Part 2 is dedicate to the primary networks while Part 3 is dedicated to the secondary network.

1.3.1 Part 1

Part 1 of the thesis is organized as follows:

Chapter 2 describes the cognitive radio networks, introduces the concepts of cognitive radio, software definer radio and dynamic spectrum access.

1.3.2 Part 2

Part 2 of the thesis is organized as follows:

Chapter 3 presents the synchronization processes in primary systems based on PN-OFDM, introducing the main concepts and state of art solutions. The basic framework of OFDM signals is also outlined.

Chapter 4 presents the twin test. The method is described in details, and the new EMGQ are fully derived. The performance of the method are evaluated both in analytic way (i.e. exploiting the EMGQ function) and by means of simulations.

Chapter 5 illustrates the innovative strategy for initial synchronization in LTE systems. The performances of the method have been analyzed in many practical operating scenarios, in order to assess its effectiveness.

1.3.3 Part 3

Part 3 of the thesis is organized as follows:

Chapter 6 introduces the concept of spectrum sensing and presents a review to the recent state of art solutions.

Chapter 7 presents the proposed spectrum sensing method based on a modified version of Rayleigh-ness test. First the original Rayleigh-ness is described, then the rational of the innovative method is outlined and its performance evaluated.

Chapter 8 describes the innovative software radio implementation of a bank of filter for spectrum sensing. The performances of the method are evaluated under different setting condition and compared with the state of art solution.

Chapter 9 is dedicated to the normalized variance method. The NV strategy is described in details and its performance theoretical evaluated. In addition, the results of several simulation trials are reported as proof of the validity of the theoretic analysis.

Chapter 10 introduces the innovative cooperative spectrum strategy based on a modified version of twin test. The performance of the method are numerically evaluated in many real case scenarios.

Chapter 11 presents the innovative scenario of the freeloader users that was not yet considered in the scientific literature. The freeloader detection method, based on the high order of the received signal is described in details, and its performance theoretical evaluated. Finally many simulations trial are conducted to validate effectiveness of the theoretical derivation.

Chapter 12 proposes two applications of the freeloader detection method, described in Chapter 11, for conventional spectrum sensing. The first part of the chapter focuses on low power users detection, while in the second part an estimation of the noise power is used for determine if the SUs can safely accessing the band, without causing harmful interference to the primary users.

Finally, the conclusion of this dissertation are reported in C*hapter 13*.

PERSONAL PUBBLICATIONS

JOURNALS

[J1]. F. Benedetto, G. Giunta, E. Guzzon, M. Renfors, "Normalized Variance-Based Spectrum Sensing Algorithm" in submitted to, *IEEE Trans. on Vehicular Technology*, 2014.

[J2]. F. Benedetto, G. Giunta, E. Guzzon, M. Renfors, "Effective Monitoring of Freeloading User in the Presence of Active User in Cognitive Radio Networks" in *Press, IEEE Trans. on Vehicular Technology*, 2013. DOI: 10.1109/TVT.2013.2290035. Impact Factor: 1.921.

[J3]. E. Guzzon, F. Benedetto, G. Giunta - "A New Test for Initial Code Acquisition of Correlated Cells", *IEEE Trans. on Vehicular Technology*, vol. 62. No. 5, pp. 2349-2358, 2013. 1. DOI: 10.1109/TVT.2013.2240325 . Impact Factor: 1.921

[J4]. F. Benedetto, G. Giunta, E. Guzzon "A novel "single-path" vs. "few-path" test based on higher order statistics to possibly start-up coherent combining", *invited paper to Special Issue on Telecommunications and Signal Processing of the Journal of Applied Research and Technology* (JART), 2013.

[J5]. E. Guzzon, F. Benedetto, G. Giunta "A Survey of Recent Patents on Spectrum Sensing for Cognitive Radios" *Recent Patents on Computer Science* , vol. 6, no. 2, pp. 137-144, 2013

[J6]. F. Benedetto, G. Giunta, E. Guzzon - "Recent Patents In Spread Spectrum Systems" in *Recent Patents on Electrical & Electronic Engineering*, vol. 6, no. 2, pp. 95-100, 2013

[J7]. F. Benedetto, G. Giunta, E. Guzzon - "Initial Code Acquisition in LTE Systems" - Recent Patents on Computer Science , vol. 6, no. 1,pp. 2-13, 2013.

[J8]. E. Guzzon, "Past, Present and Future of Spectrum Sensing in Cognitive Radio Networks" in *Recent Patents on Computer Science* vol. 5 n. 2 pp. 93-102, 2012

PATENTS

[P1]. F. Benedetto, G. Giunta, E. Guzzon " An Enhanced Receiver for 4G Mobile Cellular Networks (LTE), RM-2011-A-000253

INTERNATIONAL CONFERENCES

[C1]. F. Benedetto, G. Giunta, A.Tedeschi, E. Guzzon, "Performance Improvements of Cooperative Spectrum Sensing in Cognitive Radio Networks with Correlated Cognitive Users", *37th International Conference on Telecommunications and Signal Processing* (TSP), July 1-3, 2014, Berlin, Germany

[C2]. F. Benedetto, G. Giunta, E. Guzzon, M. Renfors, M. Arcangeli, - "Improving the Interference Temperature Estimation for Dynamic Spectrum Access in Cognitive Radios", *1st IEEE Global Conference on Signal and Information Processing* (GlobalSIP 2013), 3-5 Dec., Austin, Texas, USA

[C3]. F. Benedetto, G. Giunta, E. Guzzon, - "Reducing Mean Acquisition Time in Code Synchronization for Wireless Communications", *24th IEEE Int. Symp. on Personal, Indoor and Mobile Radio Communications* (PIMRC'13), 8-11 Sept. 2013, London, UK

[C4]. F. Benedetto, G. Giunta, E. Guzzon, M. Renfors - "Detection of Hidden Users in Cognitive Radio Networks", *24th IEEE Int. Symp. on Personal, Indoor and Mobile Radio Communications* (PIMRC'13), 8-11 Sept. 2013, London, UK

[C5]. S. Dikmese, J. L. Wong, A.Gokceoglu, E. Guzzon, M. Valkama, M. Renfors, "Reducing Computational Complexity of Eigenvalue Based Spectrum Sensing for Cognitive Radio", *IEEE 8th International Conference on Cognitive Radio Oriented Wireless Networks*, (CROWCOM2013), July 8–10 2013, Washington DC, USA.

[C6]. F.Benedetto, G.Giunta, E.Guzzon "A Rakeness Test for Coherent Signal Combining in Mobile Receivers", *36th International Conference on Telecommunications and Signal Processing* (TSP), July 2-4, 2013, Rome, (Italy).

[C7]. E. Guzzon, F. Benedetto, G. Giunta, M. Renfors, “A Software Radio Implementation for Spectrum Hole Sensing in Cognitive Mobile Networks” ICC'13 - IEEE ICC'13 - Workshop CoCoNet5, 6-13 June 2013, Budapest

[C8]. E. Guzzon, F. Benedetto, G. Giunta, “Performance Improvements of OFDM Signals Spectrum Sensing in Cognitive Radio” in *IEEE 76th Vehicular Technology Conference*, a Quebec City (Canada), 3-6 Sept. 2012.

[C9]. F. Benedetto, G. Giunta, E. Guzzon, “A Novel Procedure for Initial Cell Search in 3 GPP LTE Wireless Access Networks” in *IEEE Wireless Telecommunication Symposiums London* 17-24 April 2012

[C10]. F. Benedetto, G. Giunta, A. Vennarini, E. Guzzon “Improving the Code Acquisition of LTE Sysems”, *IEEE Wireless Telecommunication Symposiums* London 17-24 April 2012

[C11]. F. Benedetto, G.Giunta, E.Guzzon, "Enhanced TOA-Based Indoor-Positioning Algorithm for Mobile LTE Cellular System", *IEEE 8th Workshop on Positioning, Navigation and Communication* 2011 (WPNC'11), Dresden, Germany, 7-8 April 2011

[C12]. F. Benedetto, G. Giunta, E. Guzzon - "Effective Code Acquisition of Galileo BOC Signals " - *IEEE Int. Conf. on Localization and GNSS* (ICL-GNSS 2011), Tampere, Finland, June 29-30, 2011

Part 1

Introduction to Cognitive Radio Networks

Chapter 2 COGNITIVE RADIO NETWORKS

2.1 Introduction

Traditionally, the use of the radio spectrum has been regulated by governmental agencies that assign fixed frequency bands to licensed users for exclusive access. In the last couple of decades, the demand of radio spectrum has increased dramatically due to the proliferation of wireless services. As a consequence, the spectrum scarcity problem has emerged: with all the spectrum bands already exclusively allocated, it is becoming extremely hard to find unused frequency bands to deploy new services, or enhance the existing ones. Recent studies focusing on the actual spectrum utilization have revealed that a large portion of the licensed spectrum is often under-utilized and many frequency bands can be used for wireless communications, at different places and different times [3], [7]. These studies also indicate that the inefficient and inflexible spectrum allocation policy strongly contributes to the spectrum scarcity, perhaps even more than the physical shortage of radio spectrum. To support and maintain the development of the wireless industry, novel communications paradigms should be developed to exploit the spectrum bands more efficiently. The Dynamic Spectrum Access (DSA) has been recently proposed as a possible solution to these inefficiency problems [7]. In DSA there are two categories of user (and providers): the primary and the secondary users (providers). The Primary User (PU) is the owner of the license for that frequency band and has always the right of using the radio resource. The Secondary Users (SU) is an un-licensed user that can access the spectrum bands of a primary user assuring that no interference is caused to the licensed communications. With DSA, the radio spectrum can be reused in an opportunistic manner or shared over time, thus significantly improving the spectrum utilization. The technology enabling DSA is the Cognitive Radio (CR). A CR is defined as a context-aware intelligent radio device, potentially capable of autonomous reconfiguration, by learning from and adapting to the

communication environment [13]. The CR technology provides the SUs with the capability to use or share the spectrum in an opportunistic manner and to operate in the best available channel. More specifically, the CR technology enables SUs to: sense which portions of the spectrum are available (*spectrum sensing*), select the best available channel (*spectrum management*), coordinate spectrum access with other users (*spectrum sharing*), and vacate the channel when a primary user comes back (*spectrum mobility*).

Cognitive Radio enable the deployment of a new generation of networks, the Cognitive Radio Network, (CRN) that exploit CR technology for using the radio spectrum more efficiently [6]. A CRN consists of a primary network (PN), and a secondary network (SN). The primary network has the license for accessing spectrum bands, while the SN can access the frequency bands left un-used by the PN. The diffusion of CRN will change the business model of Telco, making unnecessary the need of licenses for spectrum bands since there will always be a free (unused or under-utilized) frequency that could be used for communicating. Moreover, CRNs offer new business opportunities for both PUs and SUs through the possibility of trading the radio spectrum [14]. PUs can rent unused resources to SUs while maintaining the ownership of the spectrum. On the other hand, SUs can use the frequency bands which could not otherwise access. In addition, in case of traffic peaks, it could be also possible to use the frequencies assigned to broadcasting, emergency services or army. The dynamic use of the spectrum causes adverse effects on the performance of conventional communication protocols, which were developed considering a fixed frequency band for communication. Therefore new adaptive network protocols should be developed. In Europe, projects like DRIVE and OVERDRIVE have been developed to explore DSA between mobile radio and Digital-TV (DVB-T and DVB-H) systems [15]. In particular, Dynamic Radio for IP Services in Vehicular Environments (DRiVE) project focuses on dynamic spectrum allocation in heterogeneous networks by assuming a common coordinated channel. The Uni- and Multicast Over Dynamic Radio Networks in Vehicular Environments (OverDRiVE) focuses on UMTS enhancements and coordination of existing radio networks into a hybrid network, to ensure spectrum efficient provision of mobile multimedia services. Then, the IEEE 802.22 standard has been developed to explore DSA

in the DVB-T band for bringing broadband internet connection to hard-to-reach rural environments [16].

CRNs can be used in many different situations, spanning form public safety and emergency, to military network or mesh networks [17]. For example, in the case of natural disasters, the existing communication infrastructure maybe temporarily disabled or destroyed. In such unfortunate cases CRNs can be used as an emergency networks (ENs). Since ENs deal with critical information, reliable communication should be guaranteed with minimum latency. In addition, ultra wide band are needed for handling huge volume of traffic including voice, video and data. CRNs can easily fulfill all these tasks, simply using the existing spectrum and without the need for a dedicated infrastructure. Another interesting potential applications of CRN is in the military radio environment. CRN can enable the military radios to arbitrary choose, carrier frequency, bandwidth, modulation schemes, and coding schemes, for adapting to the variable radio environment of a battlefield. Moreover, military networks have a strong need for security and protection of the communication. CRN allows military personnel to easily perform spectrum handoff to find secure spectrum band for themselves and their allies. Finally CR can be used for wireless mesh networks (WMNs). WMNs are emerging as a cost-effective technology for providing broadband connectivity. However, as the network density increases and the applications require higher throughput, mesh networks require higher capacity. Since the cognitive radio technology enables the access to larger amount of spectrum, they can be effectively used for deploying mesh networks [18].

The remainder of this chapter is organized as follows. Section 2 presents a brief description of the main DSA strategies, while section 3 describes the fundamental aspects of the CR technology. Finally, Section 4 introduces the architecture of the cognitive radio networks.

2.2 Dynamic Spectrum Access

2.2.1 Definition

DSA can be defined as:

> *"The real time adjustment of spectrum utilization in response to changing circumstances and objectives."*[19]

The term "changing circumstances" in the above definition includes (but it is not limited to) energy consumption, interference avoidance (either suffered or inflicted) spectrum usage efficiency targets, and changes in the radio state such as operational mode, battery life, location etc. Different strategies have been proposed in the scientific literature for DSA, which can be broadly organized in three general models: Dynamic Exclusive, Open Sharing and Hierarchical Access mode (See Fig 2-1).

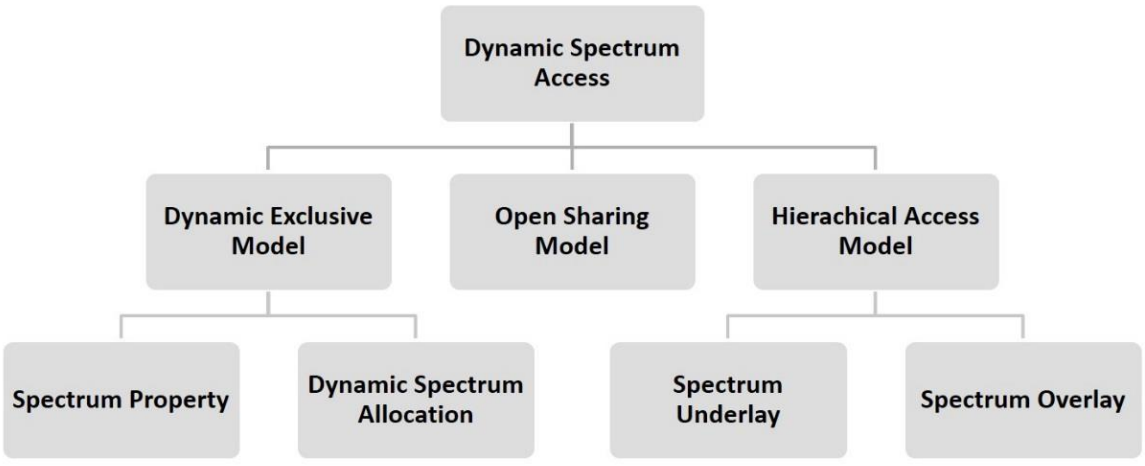

Figure 2-1 Dynamic Spectrum Access strategies categorization.

2.2.2 *Dynamic Exclusive Model*

In the Dynamic Exclusive Model (DEM) the spectrum bands are still allocated according to the current fixed spectrum regulation policy, but the assignment varies in a more dynamic and rapid way. The main idea behind DEM is to introduce flexibility to improve spectrum efficiency. Two approaches have been proposed under this model: spectrum property rights [20]-[21] and dynamic spectrum assignment [15]. The *spectrum property rights* allows licensees to sell or trade spectrum with unlicensed systems. Economy and market will thus play a fundamental role in driving toward the most profitable use of radio spectrum. The *dynamic spectrum assignment* approach aims at improving spectrum efficiency exploiting the spatial and temporal variations of traffic. In other words, in a given geographic region and at a given time instant, the spectrum is still allocated to services for exclusive use, but the allocation varies at a faster scale than the current policy. Notwithstanding DEM allows providers to use more efficiently the available spectrum, it is still based on the fixed assignment model, and hence, it cannot eliminate the spectrum holes that results from the bursting nature of wireless traffic.

2.2.3 *Open Sharing Model*

The Open Sharing Model, also referred to as Spectrum Commons, follows the same approach used in the ISM radio band (e.g., WiFi, Bluethooth). In this model "au pair" peer users can share the same frequency band at the same time and in the same geographic location without interfering with each other [22]. Then, sophisticated access protocols are needed for avoiding mutual interference.

2.2.4 Hierarchical access model

The hierarchical model adopts a "hierarchical" access structure with primary and secondary users. There are two main Hierarchical models: the Opportunistic Spectrum Access (OSA) Model [23], and the Concurrent Spectrum Access (CSA) Model [24].

2.2.4.1 The OSA model

The OSA model (Fig. 2-2) is the one predominantly studied in the scientific literature, and the de facto standard for DSA. According to this model SU can access a licensed spectrum band only if the PUs are not occupying it. Furthermore, the PU has the absolute priority on the spectrum band, and an SU that is occupying it must yield to the PU whenever the he starts to access the band.

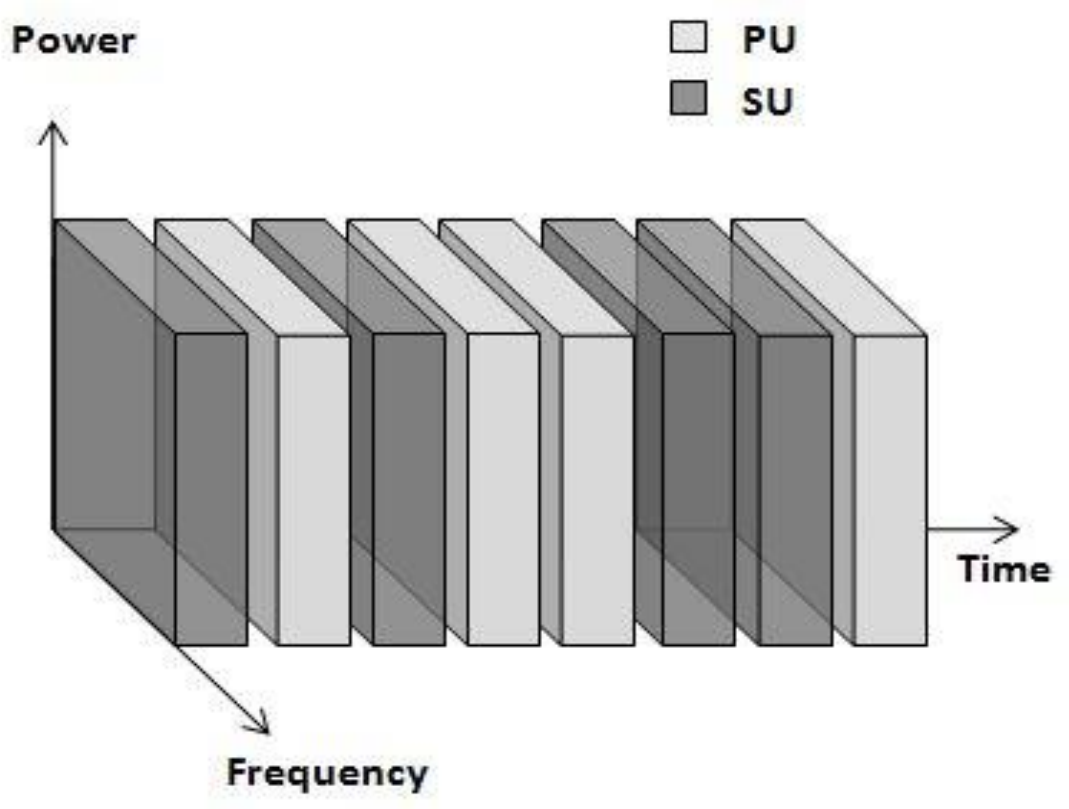

Figure 2-2 The Opportunistic Spectrum Access Model

The unused spectrum band, available for secondary communications, are referred to as spectrum holes (or white spaces). Spectrum holes are defined as multidimensional regions within frequency, time, and space [25]. A spectrum hole in space is the area around a primary Base Station (BS) that a SU can use to transmit at the same frequency. In fig. 2-3 (a) Tx_1 and Tx_2 are two primary stations transmitting in broadcast in the white area around them. The dark grey area is a guard area, in which the transmissions of a cognitive radio device could potentially interfere with the base station services while the light grey area is the spectrum hole. A spectrum hole in time (see again Fig. 2-3) is the time slot in which a spectrum band can be used by a secondary user. Finally a spectrum hole in frequency is defined as a frequency band in which a SU can transmit without interfering with any licensed user across different adjacent frequencies. In fact, due to the imperfections of filters and analog front-ends even if a SU finds an access opportunity in a certain frequency band, its transmission can still interfere with primary receivers operating in adjacent frequency bands.

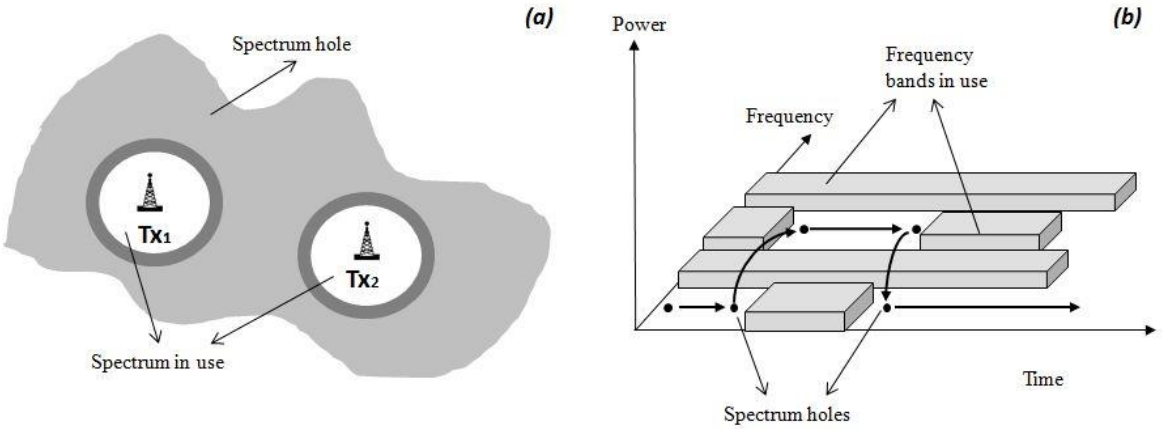

Figure 2-3 Spectrum holes: (a) Spectrum holes in the space domain, (b) spectrum holes in the time-frequency domain

2.2.4.2 The CSA model

In the CSA model (or underlay approach), both secondary and primary users can coexist together, at the same time and in the same geographic region, as long as the interference that SUs are causing to PUs is below a tolerable threshold (see Fig.2-4) [26]-[27]. There are two approaches to meet this constrain. A SU scan spread is transmit power over a wide range of frequency bands, so that the interference caused to the PU on each licensed band is below an interference threshold. This approach, which is taken by ultra-wide band (UWB) technology is typically used for short range communications. The second approach is called interference temperature. According to this approach, SUs can transmit with a higher power then in the previous approach, as long as the total interference that SUs are causing to PUs is below a tolerable threshold. (i.e. the interference temperature limit). The challenge here is how to measure the total interference and how to impose the interference temperature limit [28].

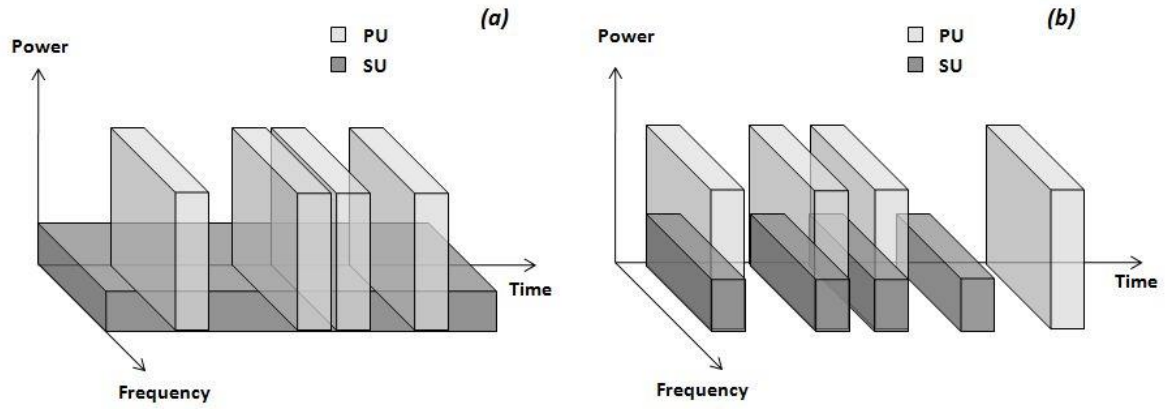

Figure 2-4 Concurrent Spectrum Access model. (a) Underlay model; (b) overlay model

Recently the overlay approach has been introduced under the concurrent spectrum access model. (Fig.2-4b). Similar to the underlay model, the overlay model allows SUs to transmit on a licensed spectrum band even when the PU is accessing it. However, rather than limiting the transmit power of SUs, the overlay model aims at maintaining the PU

performance. In other words, SUs are allowed to transmit simultaneously with PUs as long as the primary receiver experiences no performance deterioration. Specifically, when a PU is transmitting a packet that is known to an SU, the secondary transmitter splits is power into two parts, one to transmit its own packet, and the other to transmit the PU's packet, thus enhancing the power of the signal received at the primary receiver. Moreover, the SU could rely a PU's packet with a power high enough to not only maintaining the PU performance but actually improving it [29].

2.3 The Cognitive Radio Technology

2.3.1 Introduction and definitions

Cognitive radio technology refers to wireless architectures in which a communication system does not operate in a fixed assigned band, but continuously searches an appropriate band where to operate. The concept of CR was first introduced by Joseph Mitola III in a seminar at the Royal Institute of Technology in Stockholm in 1998 and, later, in an article, co-authored with Gerald Q. Maguire, Jr. in 1999 [9]. The Mitola's definition of CR was:

> "*The point in which wireless personal digital assistants (PDAs) and the related networks are sufficiently computationally intelligent about radio resources and related computer-to-computer communications to detect user communications needs as a function of use context, and to provide radio resources and wireless services most appropriate to those needs*." [9].

Following Mitola's definition, CR is a wireless technology that allows devices to understand the radio environment in which they operate and to react accordingly. The CR device scan the spectrum and select the best channel to tune in. However, Mitola's definition

is considered to be too broad. As a consequence, any device that responds to that standard is defined a "Full Cognitive Radio" device.

Then, the ICT definition of CR is:

> *"A radio that sense and is aware of its environment and can dynamically and autonomously adjust its radio operating parameters accordingly*" [30].

Finally, the IEEE 1900.1 standard defines a CR as follows:

> "*A type of radio in which communications systems are aware of their environment and internal state and can make decision about their radio operating behavior based on that information and predefined objectives*"[19]

From these definitions the two main characteristics of the cognitive radio can be defined as the cognitive capability and the re-configurability.

2.3.2 Cognitive capability

The cognitive capability refers to the ability of the radio technology to sense the radio environment, and then make decisions based on the acquired information. Through this capability, the portions of the spectrum that are unused at a specific time or location (i.e. spectrum holes) can be identified. Consequently, the best spectrum band and the relative operating parameters can be selected. In a CR device there is a "cognitive unit" which is the engine that uses cognitive capabilities to make decisions based on the received inputs [31]. The cognitive unit consists of a cognitive engine and a policy engine. The *cognitive engine* adapts the radio's parameters according to the received information and to the radio's current internal state. The *policy engine* ensures that the decisions of the cognitive engine

are in compliance with regulatory rules and policies external to the radio. The tasks that a CR needs to perform for adaptive operation are grouped in the cognitive cycle, which is shown in Fig. 2-5. The first task is the *spectrum sensing*. The CR senses the radio environment to determine which channels are available and which are not. In other words, the CR monitors the spectrum, captures information and then detects the spectrum holes. The second task is *Spectrum analysis*. The data collected during spectrum sensing are analyzed to determine the characteristics of the spectrum holes, detected during the previous stage. This identification process may also include communication with a subset of neighbor devices, in order to improve the decision process. Finally the last task is the *Spectrum decision*, in which a CR chooses the best channels to tune in and then adapts all its operating parameters for the transmission over the selected spectrum band.

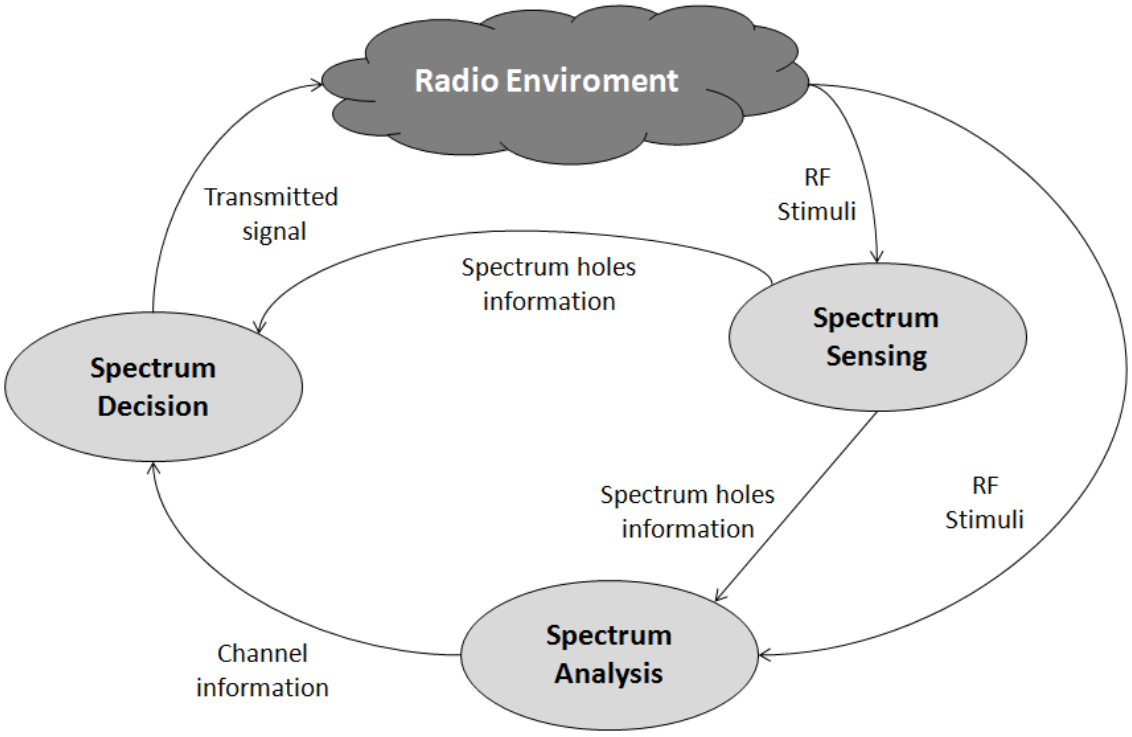

Figure 2-5 Cognitive cycle

Once a spectrum hole has been determined, the communication can be performed over the selected channel. However, since the radio environment changes over time and space, the cognitive radio should keep track of the changes of the radio environment. Moreover, if the spectrum band currently in use becomes unavailable, the "spectrum mobility" function is performed to provide a seamless transmission. In fact, CR users are low priority users of the spectrum, and they must release the licensed band as soon as a PU is detected. The secondary communication should continue in another spectrum hole, without interruptions.

2.3.3 Re-configurability

The re-configurability is the capability of adjusting the operating parameters without any modifications of the hardware components. This capability enables the CR to adapt to the dynamic environment. There are several re-configurable parameters that can be incorporated into a cognitive radio such as:

1. *Operating Frequency*: A cognitive radio should be capable of dynamically changing the operating frequency. In other words, based on the information about the radio environment, the most suitable operating frequency should be determined and used for communication.

2. *Modulation*: A cognitive radio should be able to adapt the modulation scheme to the user requirements and channel conditions. For example, in the case of delay sensitive applications, data rate is more important than the error rate, hence, modulation schemes with higher spectral efficiency should be selected. Conversely, in loss-sensitive applications the focus should be on the error rate, thus selecting modulation schemes with low bit error rate. The OFDM modulation thanks to its inherent flexibility in using the frequency bands, is one of the most promising candidate for CR communications [32].

3. *Transmission power:* the transmission power should be re-configured according to specific power constraints. In fact, if higher power operation is not necessary, the CR transmits with a lower power in order to decrease the interference and allow more users to share the spectrum hole.

4. *Communication technology*: A CR can also be used to provide interoperability among various communication systems. The transmission parameters of a CR can be re-configured not only at the beginning but also during the transmission. If the CR switches to a different spectrum band, the transmitting and receiving parameters should be changed according.

2.4 Physical architecture of the cognitive radio

A cognitive radio can receive and transmit on a variety of frequencies and to fully exploit this capability it needs a flexible hardware that can be dynamically and autonomously (re)-configured. Software Defined Radio (SDR) technologies are the natural platforms on which to build in this new cognitive features. In particular, SDR is a radio communication system where components that in the past have been typically implemented in hardware (e.g. mixers, filters, modulators/demodulators, detectors, etc.) are instead implemented by means of software. A SDR device typically consists of an analog RF front-end, and a digital processing engine, which may be a general-purpose processor (GP), a digital signal processor (DSP), or a customized field programmable gate array (FPGA) board. Most radio functions are implemented through software running on a digital processing engine [33]. A radio could be considered to be SDR if some or all the physical layer functions are accomplished through the use of DSP software, or FPGA firmware, or by a combination of software and FPGA firmware and both the software and firmware can be modified post deployment [19]. The list of SDR benefits is long, but some of the most important are: interoperability with new and legacy radio systems; the ability to squeeze a staggering

amount of radio capability in a very small package; and the ability to implement networking tasks on each radio that run transparently to the user.

A generic architecture of a cognitive radio transceiver, based on SDR platform, is shown in Fig. 2-6. The main components of a cognitive radio transceiver are the radio front-end and the baseband processing unit [34].

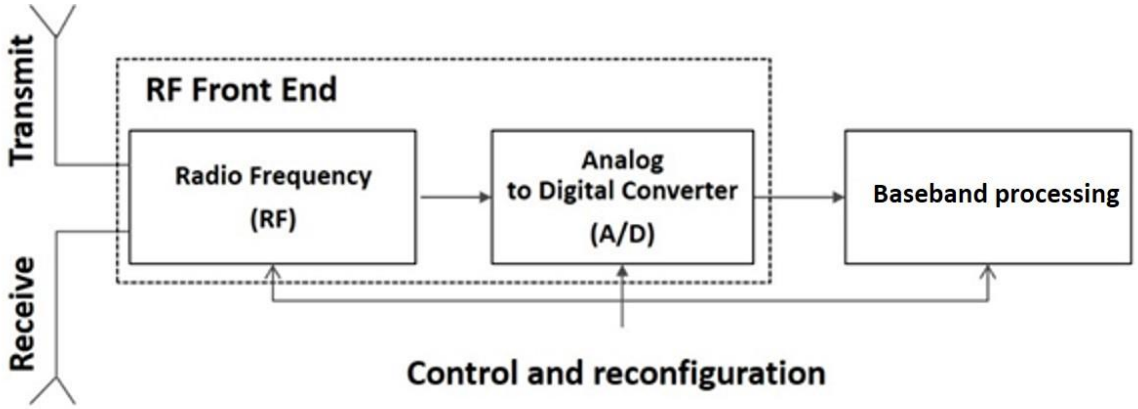

Figure 2-6 Physical architecture of the cognitive radio

Each component can be dynamically configured via a control bus to adapt to the time-varying RF environment. In the RF front-end, the received signal is amplified, mixed and A/D converted. In the baseband processing unit, the signal is modulated (demodulated) and encoded (decoded). The baseband processing unit of a CR is similar to existing transceivers, while the main novelties introduced by the CR technology are located at the RF front-end, which provides the cognitive device with wideband sensing capability. The front-end architecture for the CR has the structure is shown in Fig. 2-7.

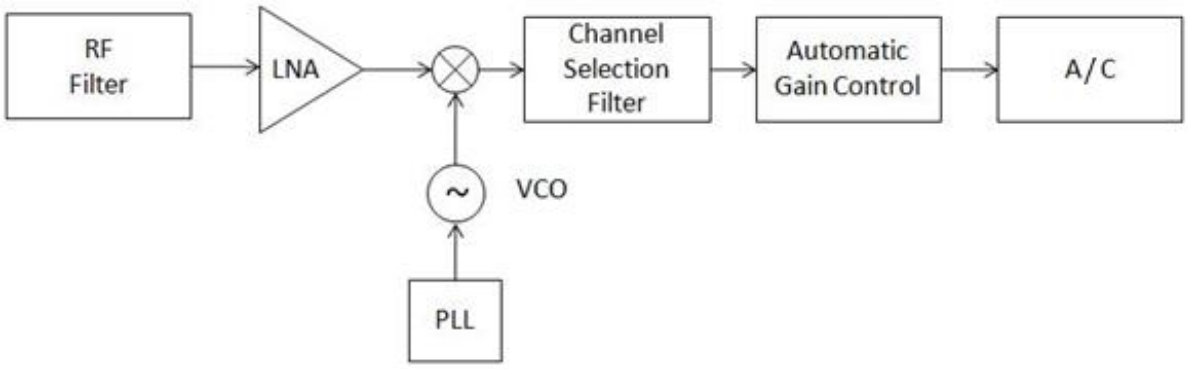

Figure 2-7 wideband RF/analog front-end architecture.

The components of a cognitive radio RF front-end are as follows:

- *RF filter*: The RF filter selects the desired band by filtering off noise and interference from the received RF signal.
- *Low noise amplifier (LNA)*: The LNA amplifies the desired signal and at the same time minimizes the noise component.
- *Mixer*: In the mixer, the received signal is mixed with locally generated RF frequency and converted to the baseband or the intermediate frequency (IF).
- *Voltage-controlled oscillator (VCO):* The VCO generates the signal at the desired frequency, for a given voltage, to mix with the incoming signal.
- *Phase locked loop (PLL)*: The PLL controls the VCO ensuring that the signal is locked on the desired frequency.
- *Channel selection filter*: The channel selection filter is used to select the desired channel while rejecting all the adjacent channels.
- *Automatic gain control (AGC):* The AGC maintains the gain level of the amplifier constant over a wide range of input signal levels.

In this architecture, a wideband signal is received through the RF front-end, sampled by the high speed analog-to-digital (A/D) converter, and processed by the baseband front-end. However, there exist some limitations on developing the cognitive radio front-end. The wideband RF antenna receives signals from many transmitters operating at various frequencies, power levels, bandwidths, and locations. As a consequence it should be able to detect very weak signals in a large dynamic range. This capability requires a multi-GHz speed A/D converter with high resolution, which might be still infeasible with the available technologies. The dynamic range of the signal can be reduced before the A/D conversion by filtering strong signals with tunable notch filters. Another approach is to use multiple antennas so that signal filtering is performed in the spatial domain rather than in the frequency domain. Notwithstanding the implementation of RF wideband front-end and A/D converter are still critical issues in the development of CR device, the current trend of technology evolution is going to time compensate for such limitations, allowing the implementation of full SDR cognitive devices.

2.5 Cognitive Radio Network Architecture

2.5.1 Definition

A CRN is a new generation network in which transmission happens using the spectrum holes. A possible definition of a CRN is the following:

> "*A type of network in which the behavior of each radio is controlled by a cognitive control mechanisms to adapt to changes in topology, operating conditions or user's needs*" [19]

It has to be noted that, according to this definition, nodes in CRN do not have to be cognitive radios. Rather, a CRN is a network of radio in which the nodes are subject to cognitive

control mechanisms. The architecture CRN, is shown in Fig. 2-8. A CRN consists of two networks: the primary network and the secondary network.

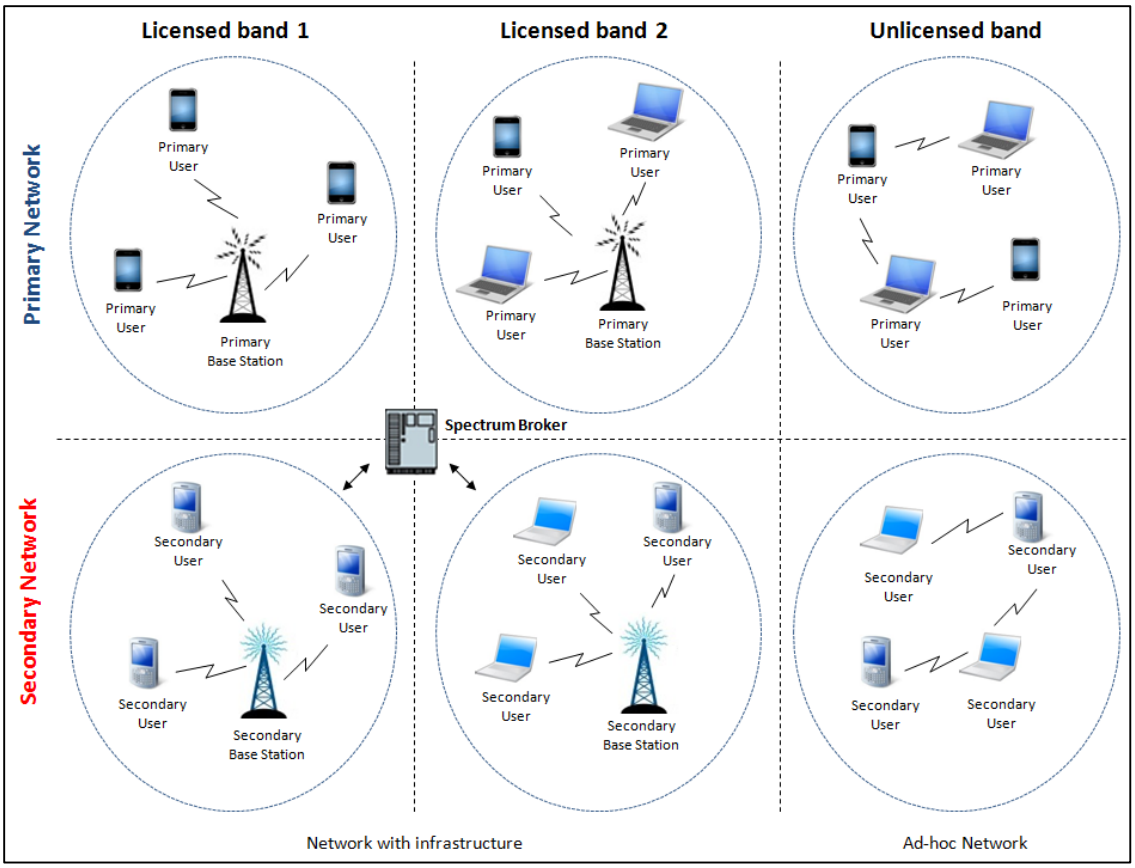

Figure 2-8 Cognitive Radio network architecture

2.5.2 Primary network

An existing network infrastructure which has an exclusive right to a certain spectrum band is generally referred to as the primary network. Common examples include the cellular and TV broadcast networks. The components of the primary network are as follows:

– *Primary base-station*: Primary base-station (or licensed base-station) is a fixed infrastructure network component which has a spectrum license, e.g. the base-station transceiver system (BTS) in a cellular system. In principle, the primary base-station does not have any CR capability for sharing spectrum with the secondary users. However, it may have both legacy and CR/DSA protocols for managing the access of both primary a secondary users.

– *Primary user*: The primary user (or licensed user) has a license to operate in a certain spectrum band. This access can only be controlled by the primary base-station and should not be affected by the operations of any other unlicensed users. Primary users do not need any modification or additional functions for coexistence with secondary base-stations and users.

2.5.3 Secondary network:

The secondary network (or cognitive radio network, Dynamic Spectrum Access network, unlicensed network) does not have the license to operate in a frequency band, but can opportunistically access the spectrum bands of a primary network. The components of an SN are as follows:

– *Secondary user*: the secondary user (or unlicensed user, cognitive radio user) has no spectrum license hence, it should be equipped with additional cognitive functionalities for sharing the licensed band with primary users.

– *Secondary base-station*: the secondary base-station (or unlicensed base-station, secondary base-station) is a fixed infrastructure component with CR capabilities. The secondary base-station provides single hop connection to SUs allowing them to access other networks, without the need of any spectrum access license.

– *Spectrum broker*: Spectrum broker (or scheduling server) is the central network entity responsible for dynamic assignment of spectrum access rights. The spectrum broker can be connected to primary and secondary network and can serve as a spectrum information manager to enable coexistence of multiple CRNs.

Secondary networks could operate under different spectrum environment consisting of both licensed and unlicensed band. The functionalities required for accessing and communicated in each band vary according to whether the spectrum is licensed or unlicensed. In a CRN operating licensed bands, a SU can access the radio spectrum only when the PUs are not occupying it. Therefore, spectrum sensing functionalities are needed to detect the presence of primary users and select the best available channel. In fact, the channel capacity depends on the interference caused at the nearby primary users. Thus, interference avoidance is of the most important issue in the deployment of SNs. Furthermore, if a PU appears in the spectrum band in operation, the SN should immediately vacate it and switch to the new available channel. In unlicensed bands, such as in the ISM band, there are no license holders, and all network entities have the same right to access the spectrum bands. Then, sophisticated spectrum sharing methods are required for managing the interference among users.

Part 2

Code acquisition in primary networks

Chapter 3 SYNCHRONIZATION IN 4G PRIMARY NETWORKS

3.1 Introduction

In order to mitigate the spectrum inefficiency problem in fourth and five generation (4G and 5G) systems the Orthogonal Frequency Division Multiplexing (OFDM) modulation has be introduced for dynamic frequency assignment. The idea behind OFDM is to convert a frequency selective channel into a collection of frequency-flat sub-channels with partially overlapping spectra. This can be achieved by splitting the input data stream into a number of sub-streams that are transmitted in parallel over orthogonal subcarriers [33],[34]. Fast Fourier Transform (FFT) operations are used for mapping the data stream on the orthogonal subcarriers. Compared to conventional single-carrier systems, OFDM offers several advantages, such as high spectral efficiency, robustness to fading channel, and immunity to impulse interference. Moreover, it provides good performance-complexity tradeoff for high data rate transmission, over frequency selective channels. Due to its favorable features OFDM technique has developed into a very popular scheme for wide-band digital wireless communication: for example, it is used in the wireless local area networks standards (i.e. IEEE 802.11x family protocols), in the Long Term Evolution (LTE) as well as in the DVB-T systems. Moreover, it is going to be a key technology for the future of broadband wireless telecommunications [35].

OFMD's underlying sensing and spectrum shaping capabilities together with its flexibility and adaptability makes it the best transmission technology for CR systems. By employing OFMD transmission in CR communications adaptive aware and flexible systems can be realized that can operate in many scenarios, while interoperate with the current technology. One of the most important elements of CR systems is the ability to identify and then exploit the unused frequency bands in a fast and efficient way. The use of FFT

operation in OFDM systems eases spectrum sensing in the frequency domain. In OFDM systems, conversion from time to frequency domain is achieved by using FFT. This means that all the points in a time-frequency grid of an OFDM systems can be scanned without any extra hardware technology or computation. In other words, the same hardware configuration used for signal transmission can be re-used for spectrum sensing purposes. Another very important aspect of CR systems is to control all the waveform parameters such as signal bandwidth, power level and center frequency: OFDM can provide such flexibility. In fact, by disabling a set of subcarriers, the spectrum of OFDM signal can be adaptively shaped to fit into the required spectrum assignment needs [32].

In addition, there is currently a strong interest in extending the OFDM concept to multiuser communications. A prominent example of this trend is represented by the Orthogonal Frequency Division Multiple Access (OFDMA) technology, which results from a combination of OFDM with a frequency division multiple access (FDMA) protocol. In OFDMA systems, the spectrum is still dived into orthogonal sub-carries, but now the available subcarriers are assigned to distinct users for simultaneous transmission. The assignment is not fixed, but on the contrary it varies according to channel conditions and user's needs [36]. The orthogonality among subcarriers guarantees intrinsic protection against multiple access interference (MAI) while the adoption of a dynamic subcarrier assignment strategy provides the system with high flexibility in resource management. Furthermore, OFDMA inherits from OFDM the ability to compensate channel distortions without the need of computationally demanding equalizers.

Despite its appealing features, the design of an OFDM/OFMDA system poses several technical challenges. One of the main issue is related to the stringent requirement on frequency and timing synchronization. In fact, both OFDM, and OFDMA are extremely sensitive to timing errors and carrier frequency offsets between the incoming waveform and the local references signal at the receiver side. Inaccurate compensation of the frequency offset destroys orthogonality among subcarriers and produces inter-channel interference (ICI) as well as MAI. On the other hand, timing errors result in inter-block interference (IBI) and must be promptly correct to avoid severe error rate degradations. Therefore achieving

at then maintaining time and frequency synchronization is one of the most imports tasks to be performed in an OFDM system. Addressing some of these issues, this chapter focuses of initial synchronization in OFMD systems.

The remainder of this chapter is organized as follows. Section 2 presents the basic framework of OFDM systems, while Section 3 illustrated the conventional method for code acquisition.

3.2 The OFMD system model

The OFDM is a multi-carrier transmission technique, which employs Frequency Division-carries Multiplexing (FDM) of orthogonal sub-carriers, each modulating a different low bit-rate digital stream. In conventional FDM systems, the total bandwidth is divided into *N* non overlapping frequency sub-channels (see Fig. 3-1a). Each channel is modulated with a different stream and the *N* channels are frequency multiplexed. In addition, guarding bands are added to eliminate ICI. Notwithstanding, the use of non-overlapping bands prevents ICI, the need for guards bands leads to a non-efficient use of the radio spectrum. OFDM allows overcoming these inefficiency issues, eliminating the need for guard bands. In OFDM the total bandwidth is still divided into *N* sub-channels, but now the sub-carries are mathematical orthogonal to each other. Hence, even if the bands are partially overlapped orthogonality prevents ICI (see Fig. 3-1b).

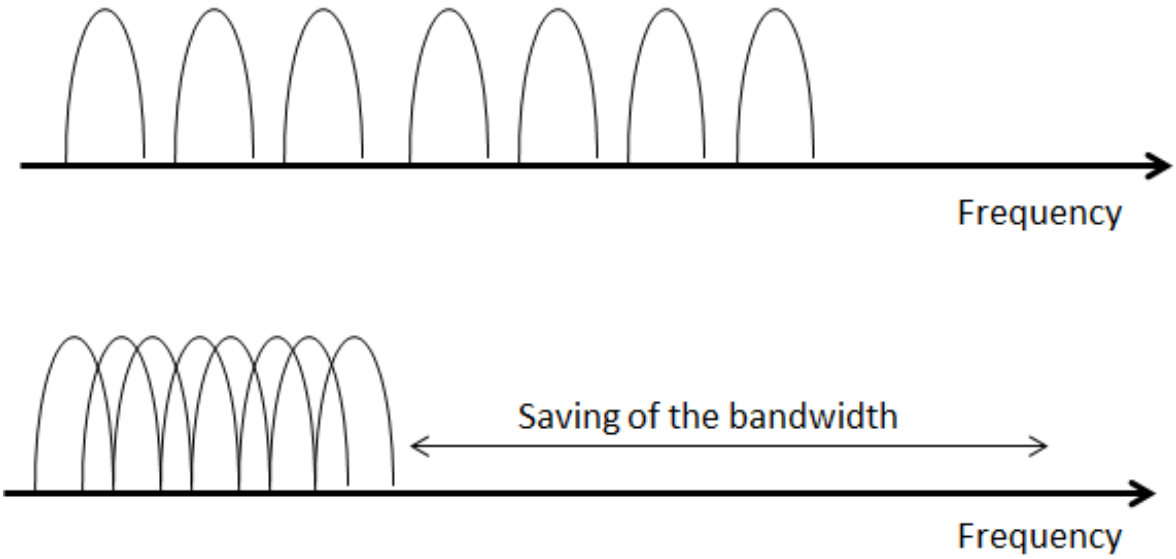

Figure 3-1 FDM Vs OFDM modulation. (a) The FDM modulation technique. (b) The OFDM modulation technique.

In addition, the process of modulating many sub-carriers simultaneously is equivalent to a Discrete Fourier Transform operation, for which efficient Fast Fourier Transform (FFT) algorithms exist. Thus integrated circuit implementations of OFDM modulators and demodulators are feasible for affordable mass-produced transmitters and receivers. In fact, the orthogonal carriers required for the OFDM signal can be easily generated performing the Inverse Fast Fourier Transform (IFFT). Since each bin (sample) of an IFFT corresponds to the amplitude and phase of a set of orthogonal sinusoids, the process guarantees that the carriers generated are orthogonal. The block diagram of a typical OFDM system is shown in Fig. 3-2.

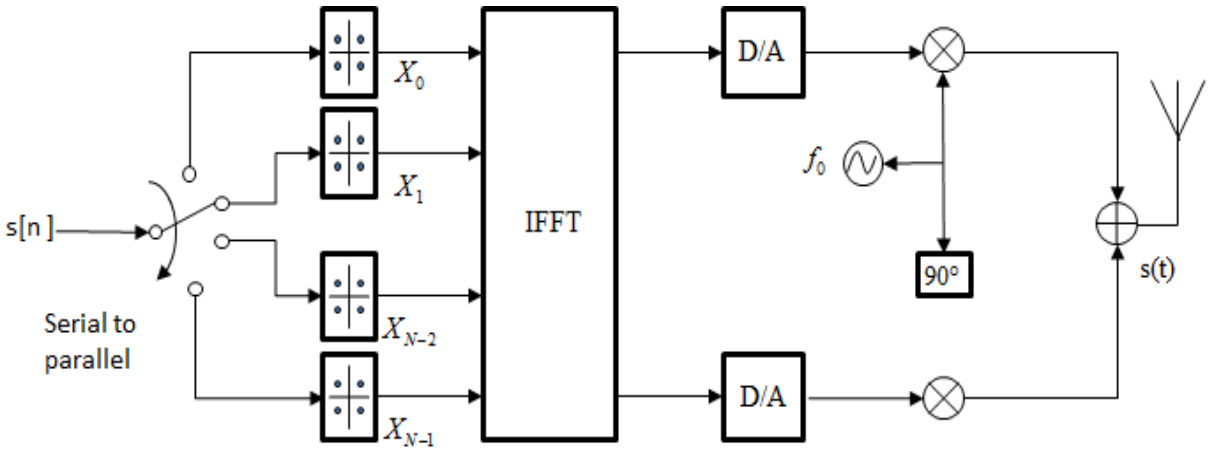

Figure 3-2 basic scheme of an OFMD modulator

The input digital stream is first covert to parallel stream and encoded with a digital modulator (i.e. PSK, QAM, 64-QAM). The result stream of *M* symbols is then zero padded to get *N* symbols that are fed to a *N*-points IFFT module. The output of the IFFT is the basic OFDM symbol, which is expressed as follows:

$$c(n) = \frac{1}{\sqrt{N_c}} \sum_{k=0}^{N_c-1} X_k \, \mathrm{e}^{\,j\frac{2\pi kn}{N_c}} \tag{3.1}$$

Where X_k is the modulated symbol to be transmitted over the *k*th sub-carrier, N_c is the number of subcarriers, *n* is a discrete time index and *k* is a discrete frequency index. The symbol are then converted to a serial stream by parallel-to-serial conversion, and the last N_{CP} symbols are added in front of the block, thus forming a cyclic prefix (CP). The baseband signal is digital-to-analog transformed and up-converted to the RF and finally transmitted through the channel. The CP is used as guard interval in between successive OFDM data blocks to alleviate inter-block interference and Inter-Symbol Interference. The length of CP is one of the more critical tradeoffs in the design of an OFDM system. In fact, since the CP carries no information, it should be as short as possible; but at the same time, it must be chosen longer the channel impulse response, in order to avoid ICI. In addition, the symbol

duration should be much larger than the CP. However an increase in the symbol length implies a corresponding increase in the number of sub-carries and thus an increase in the system complexity. The spectrum the OFDM symbol, generated according to:

$$S(f) = \frac{1}{\sqrt{N_c}} \sum_{k=0}^{N_c-1} X_k \delta(\mathrm{f} - \mathrm{f}_k) \mathrm{sinc}\left(nN_c\right) \tag{3.2}$$

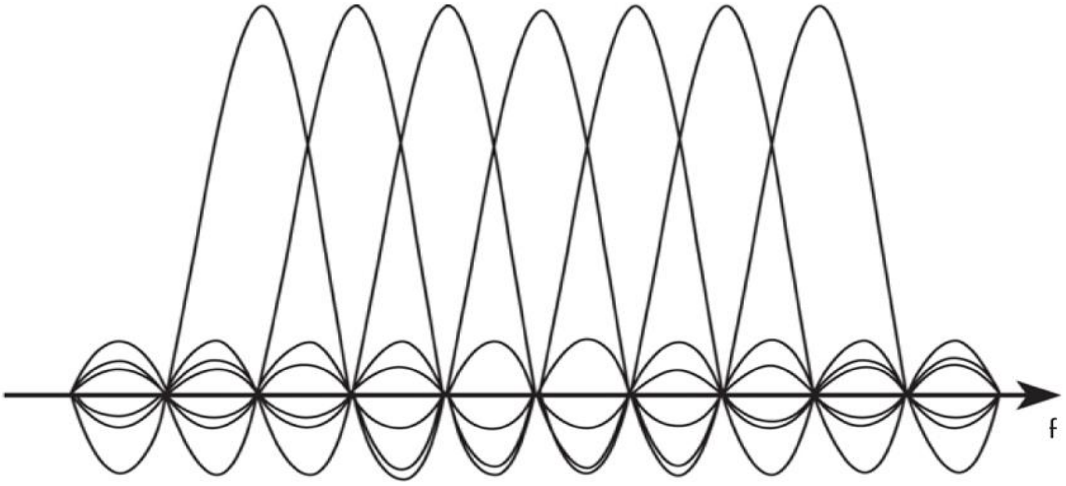

Figure 3-3 The OFDM spectrum

3.2.1 Orthogonality of Carriers

The orthogonality of carriers is the necessary condition for the proper functioning of an OFDM system. It is well kwon functions f(x) and g(x) are said to be orthogonal in the period [0 T] if

$$\frac{1}{T}\int_0^T x(\mathrm{n}) y^*(\mathrm{n}) dn = 0 \tag{3.3}$$

In the case of OFDM, carriers are sinusoidal. Consider two sinusoidal functions $e^{j\frac{2\pi k_1 n}{N_c}}$ and $e^{j\frac{2\pi k_2 n}{N_c}}$. Then, the integral in (3.3) becomes:

$$\frac{1}{N_c}\int_0^{N_c} e^{j\frac{2\pi k_1 n}{N_c}} e^{-j\frac{2\pi k_2 n}{N_c}} dn = \begin{cases} 0, & k_1 \neq k_2 \\ 1, & k_1 = k_2 \end{cases} \tag{3.4}$$

Equation (3.4) shows that all harmonics of a sinusoid of frequency *k* are orthogonal to each other. This property is used in the generation of orthogonal carriers for OFDM signals.

3.3 Code acquisition in OFDMA based primary networks

In OFDM/OFDMA systems achieving and maintaining time and frequency synchronization are two of the most critical procedure to be performed, since, if these tasks are not performed with sufficient accuracy, the orthogonality among the sub-carries is lost, and the communication system suffers from inter symbol and inter carrier interference. If the receiver is frequency synchronized with the transmitter, all the contributions from the other sub-carriers sum to zero, as shown Fig.3-4(a). On the other hand, if there is no synchronization the receiver may sample the received signal away from the peak, at a point where the contributions from the other signals do not cancel each other, see Fig.3-4(b). This will lead to a degradation of the signal which could in turn lead to an increase of the error rate.

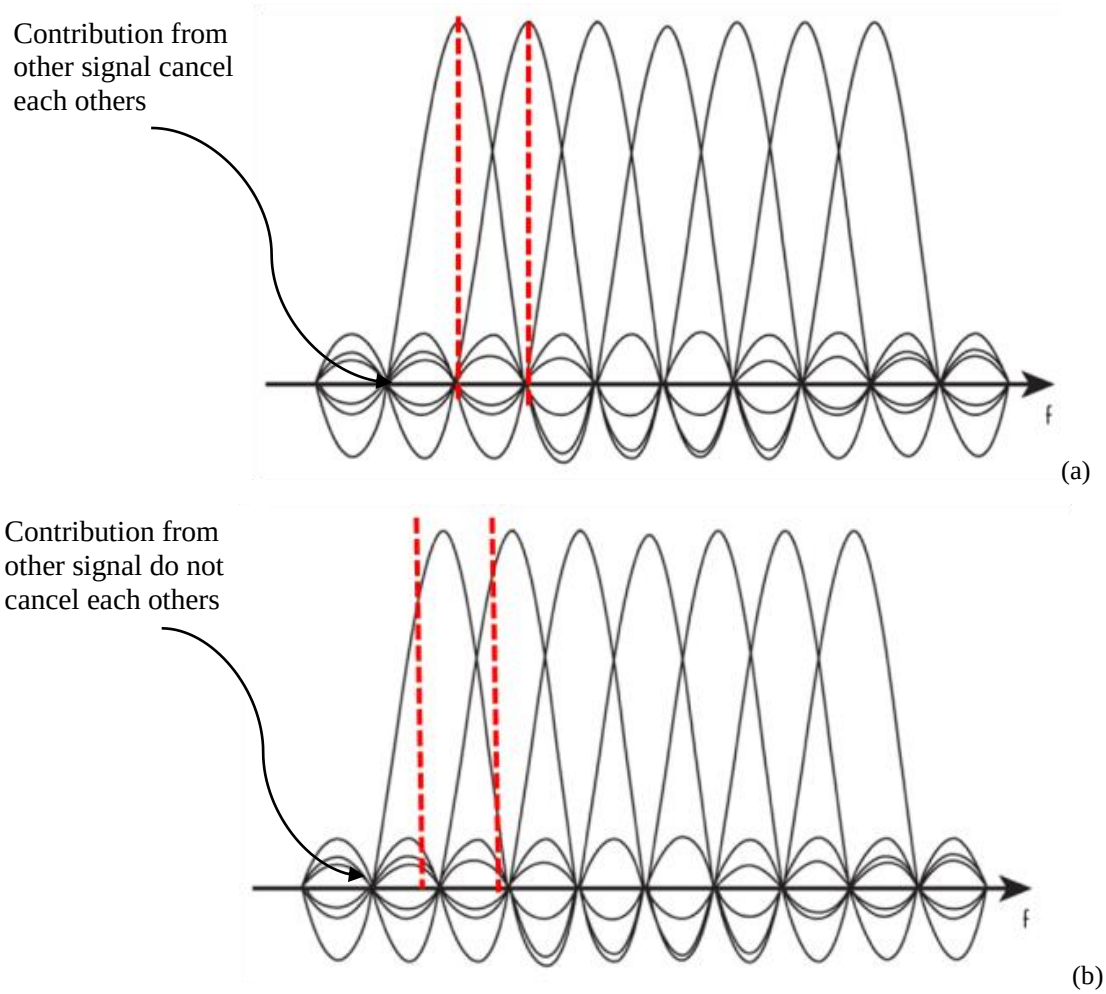

Figure 3-4 demodulation of a received OFDM symbol. (a) synchronization between the receiver and the transmitter. (b) no synchronization between the receiver and the transmitter.

Moreover, the carrier spacing used at the receiver side is based on its internal clock rate. If the receiver clock rate differs from that used within the transmitter, even if the first carrier is correctly sampled, there will be a growing discrepancy with each carrier away from the first one (Fig. 3-6). In other words, if the timing synchronization is not accurate the sampling interval will not be correct and orthogonality will be reduced

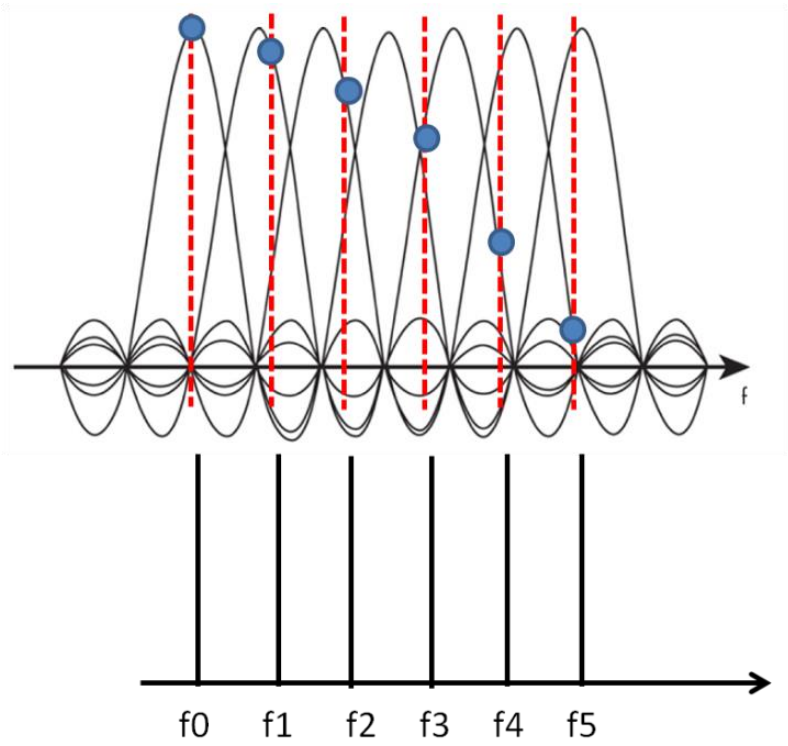

Figure 3-5 OFDM synchronization problem with clock offset problem

In OFMDA systems, synchronization is usually accomplished in three-steps. Firstly, the MS performs frequency and timing estimation by exploiting a synchronization signal transmitted by the BS on dedicated channels. The estimated parameters are exploited by each user not only to detect the downlink data stream, but also as synchronization references for the uplink transmission. However, due to Doppler shifts and propagation delays, the uplink signals arriving at the BS may still be affected by residual synchronization errors. As a consequence, the second step of the synchronization process is frequency and timing estimation in the uplink. This is a challenging task since, contrarily to the downlink, the uplink received waveform is a mixture of signals transmitted by different users, each affected by exclusive synchronization errors. Once the uplink timing and frequency offsets have been estimated, the BS has to restore orthogonality among subcarriers. This operation is commonly referred to as timing and frequency correction, and represents the final step of

the synchronization process. Several strategies have been proposed for timing and frequency synchronization in OFMD based systems [37]-[46].

One possible solution is using the correlation that exists between the CP and the corresponding portion of the OFDM symbol. However since the CP is usually affected by ISI, the performance of the estimator heavily depends on the channel quality. Alternatively pilot symbol based on a repeated maximum length could be used. The algorithm proposed by Schmidl [39] is the most popular one. It uses a training symbol containing two same halves to estimate the symbol timing and, then, computes the phase difference between the two halves to estimate the fractional frequency offset. However this method suffers from broad autocorrelation function (ACF) which may result in large timing estimation errors

It is well known that pseudo-noise (PN) sequences have very good auto-correlation proprieties. Therefore, using PN codes as preamble in OFDM systems can improve the performance of the synchronization process [41]-[42]. Moreover, with PN preamble is possible to use matched filter correlator at the receiver side [39],[46]. An improved version of the Schmidl and Cox algorithm, based on PN sequences has been recently proposed in [46]. The two identical halves are generated by transmitting a PN code on the even frequencies and zeros on the odd ones. Moreover, PN sequence and training sequence (TS) are used in TDS-OFDM, employed in the television/terrestrial multimedia broadcasting (DTMB) standard.

3.4 Code acquisition based on PN sequences

3.4.1 System model

In OFDM systems based on PN sequences, the receivers must synchronize the locally generated PN code with the received PN code. The conventional method is based on matched filter correlation. According to this method, the time uncertainty of the incoming signal is divided into a finite number of (timing) *cells*. Each cell corresponds to a sample of the time delay between the received and the locally generated PN codes (i.e., each cell is a different timing alignment). The cells are tested on a cell-by-cell-based procedure until a

correct cell is obtained. For each cell, a testing variable is compared with a pre-selected threshold: if the testing variable exceed the threshold true acquisition is achieved, otherwise the cell is discarded and the next one is tested. Conventional code acquisition method rely on the power detector, in which the testing variable is the squared modulus of the cross-correlation function. The power test distinguishes between two different hypotheses: the *in-sync* condition (hypothesis H_1), which corresponds to the case of presence of the tested code with the correct time offset; and the *out-of-sync* case (hypothesis H_0) which conversely states the absence of that code with the considered offset [47]. The typical structure of a matched filter (MF) receiver is shown in Fig. 3-7.

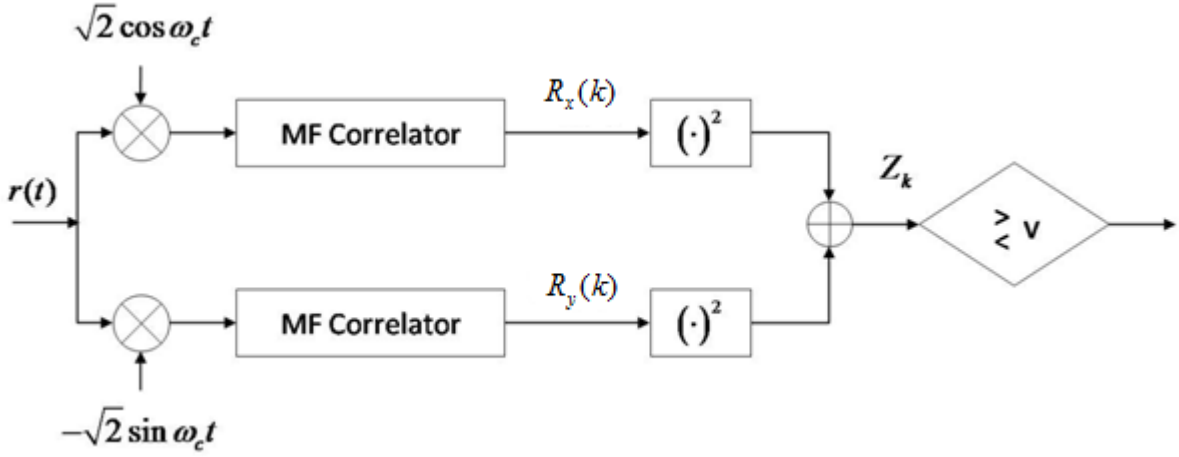

Figure 3-6 The typical of a matched filter detector

The received signal is

$$r(t) = \sqrt{2S}c(t-\tau)\cos\left(\omega_c t + \theta\right) + n(t) \tag{3.5}$$

Where S, ω_c, θ are the carrier power, frequency and phase, respectively and $c(t)$ is the PN sequence; τ is the timing offset to be acquired ad $n(t)$ is the AWGN noise with one-side power spectral density of N_0 [Watts/Hertz]. In the rest of this chapter, for the sake of compactness and without loss of generality, the effects of modulation and frequency offset

on the synchronization process will not be considered. The received signal is first down-converted to the in-phase and quadrature components. Then each component is processed by a MF correlator whose structure is depicted in Figure 3-7. Finally, the outputs of the MF correlators are squared the sum is the decision variable used for threshold comparison.

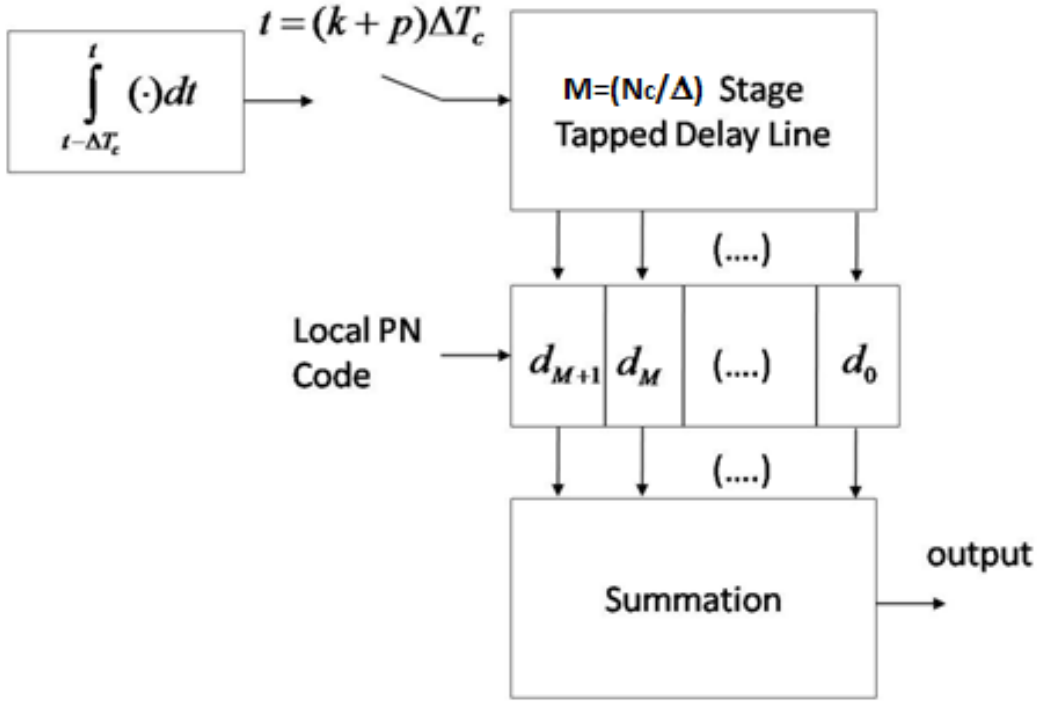

Figure 3-7 The matched filter correlator

At the MF, the received signal is sampled with a sampling period $t = (k + p)\Delta T_c$, where $k = 0,1,..$ and $0 \leq p \leq 1$ takes into account the effects of sample-offset (i.e. $p = 0$ for synchronous communications). The time uncertainty of the incoming signal is quantized into a finite number of (timing) cells so that each MF correlator performs correlation between the received and the locally generated waveform $\{d_0,\ldots,d_{M-1}\}$, using a $M = N_c/\Delta$-stage tapped delay line, with a tap spacing of ΔT_c, where N_c is the number of samples of the received signal over which the correlation is computed; T_c is the sample period; and $\Delta = 1, 1/2, 1/3,...$ is the fractional cell size.

Assuming, for the sake of compactness and without loss of generality, the sample synchronous model, i.e. $p = 0$ and $\tau = 0$, the in-phase and quadrature outputs of the MF correlators are defined as, respectively:

$$R_x(k) = \sqrt{S}\cos(\theta)\Delta T_c \sum_{j=0}^{M-1} d_{k+j} d_j + \sum_{j=0}^{M-1} n_x(k+j) d_j \tag{3.6}$$

$$R_y(k) = \sqrt{S}\sin(\theta)\Delta T_c \sum_{j=0}^{M-1} d_{k+j} d_j + \sum_{j=0}^{M-1} n_y(k+j) d_j \tag{3.7}$$

where $n_x(k)$ and $n_y(k)$ are the band-base mutually independent Gaussian noise components with zero-mean values and marginal variance $\sigma_n^2 = N_0/2$. Now, let has define the mean value of the correlator outputs in (3.6) and (3.7) are as follows:

$$E\left[R_x(k)\right] = W\cos(\theta)\sum_{j=0}^{M-1} d_{k+j} d_j = m_\Delta L \tag{3.8}$$

$$E\left[R_y(k)\right] = W\sin(\theta)\sum_{j=0}^{M-1} d_{k+j} d_j = m_s L \tag{3.9}$$

Where $W = \sqrt{S}\Delta T_c$, and $E[\cdot]$ is the expectation operator, and

$$m_\Delta = \begin{cases} m/\Delta, & \mathrm{k} = 0 \\ m, & |\mathrm{k}| = 1 \\ 0, & otherwise \end{cases} \tag{3.10}$$

Now using (3.8) and (3.9), the expression (3.6) and (3.7), can be re-written as:

$$R_x(k) = m_\Delta L + \sum_{j=0}^{L-1} n_c(k+j) d_j \tag{3.11}$$

$$R_y(k) = m_y L + \sum_{j=0}^{L-1} n_y(k+j) d_j \tag{3.12}$$

Finally, the decision variable at each lag *k* is defined as follows:

$$Z_k = R_x^2(k) + R_y^2(k) \tag{3.13}$$

This is the testing variable to be compared with a pre-selected threshold, to state whether true acquisition has been achieved or not.

Usually the testing variables between two contiguous cells (i.e. z_i and z_{i+1}) are independent. However, is some cases, such as when the cell size is a fraction of the sampling time (i.e. more than one cell per sample), the testing variable are no longer independent and possible strongly correlated [48]-[49]. Notwithstanding choosing the cell size as a fraction of the sample time (e.g Δ=1/2) could improve the system performance, the resulting correlation between testing variables has some effects on the acquisition process that should be taken into proper account. These effects are described in the next section.

3.4.2 Effects of cell correlation on the code acquisition process

In this section we describe the meaning of cell correlation and its effects on the acquisition process. Let us define the correlation coefficient between two consecutive MF outputs, i.e *R*(*k*-*i*) and *R*(*k*), as follows:

$$\rho_{|k-j|} = \frac{E\left[\left(R_\alpha(k) - E\left[R_\alpha(k)\right]\right)\left(R_\alpha(k-i) - E\left[R_\alpha(k-i)\right]\right)\right]}{E\left[R_\alpha(k) - E\left[R_\alpha(k)\right]^2\right]} \tag{3.14}$$

where $\alpha = c$ or $\alpha = s$ for the in-phase and quadrature components, respectively. In the following analysis, we assume that the PN sequence have ideal autocorrelation proprieties: i.e. we assume that different PN sequences are orthogonal and that the correlation between a PN code and a translated version of itself is zero. It has to be noted that in real cases the

cross-correlation between two non-synchronized PN sequences is not exactly zero. However, for very long sequences, such as those used for code synchronization in 3G and 4G systems, the output of the MF correlator for an incorrect time offset is very small and the ideal model can be effectively used. Then, under the ideal model, correlation sequences at the output of MF correlator have zero mean (i.e. $m = 0$) in the out-of-sync hypothesis (i.e. H_0 hypothesis) and non-zero mean (i.e. $m = W$) in the alternate one. Under such assumptions we have:

$$E\left[R_\alpha(k) - E\left[R_\alpha(k)\right]^2\right] = N_c \cdot \sigma_n^2$$

$$E\left[\left(R_\alpha(k) - E\left[R_\alpha(k)\right]\right)\left(R_\alpha(k-i) - E\left[R_\alpha(k-i)\right]\right)\right] = \begin{cases} \sigma_n^2 - \sum_{j=0}^{N_c-|i|-1} d_j d_{j+i}, & 0 \le |i| \le N_c - 1 \\ 0, & otherwise \end{cases} \tag{3.15}$$

And the correlation coefficient can be evaluated as follows:

$$\rho_{|k-j|} = \begin{cases} \dfrac{\sigma_n^2 - \sum_{j=0}^{N_c-|i|-1} d_j d_{j+i}}{\sigma_n^2}, 0 \le |i| \le N_c - 1 \\ 0, \quad otherwise \end{cases} \tag{3.16}$$

For very large M, ρ can be approximated by

$$\rho_{|k-j|} = \begin{cases} 1 - \Delta|k-j|, & 0 \le |k-j| \le 1/\Delta - 1 \\ 0, & |k-j| \ge 1/\Delta \end{cases} \tag{3.17}$$

When the cell size is equal to the sample period, $\Delta = 1$, there is no correlation between two contiguous cells and the correlations coefficient simplifies as:

$$\rho_{|k-j|} \approx \begin{cases} 1, & k = j \\ 0, & k \ne j \end{cases} \tag{3.18}$$

However, when the cell size is a fraction of the sample duration (e.g., $\Delta \neq 1$), contiguous cells are not independent and possibly strongly correlated. In order to explain how the correlation impacts on the synchronizing procedure, in the following analysis we refer to the simple case of $\Delta = ½$ (i.e. shift delay of $T_c/2$), but the same derivation can be easily extended for every Δ.

Let d_k with $\{k=0,1,..M-1\}$ be the local generated replica of the synchronization signal, and $r_{i,z,\alpha}$ with $\{i=0,1,..L-1\}$ the series of samples of the received signal, where $\alpha = x,y$ for the in-phase and quadrature component, respectively. z =..-1,0,1,… denotes the periods of the series, and b =1,2 denotes the even and odd samples , respectively.

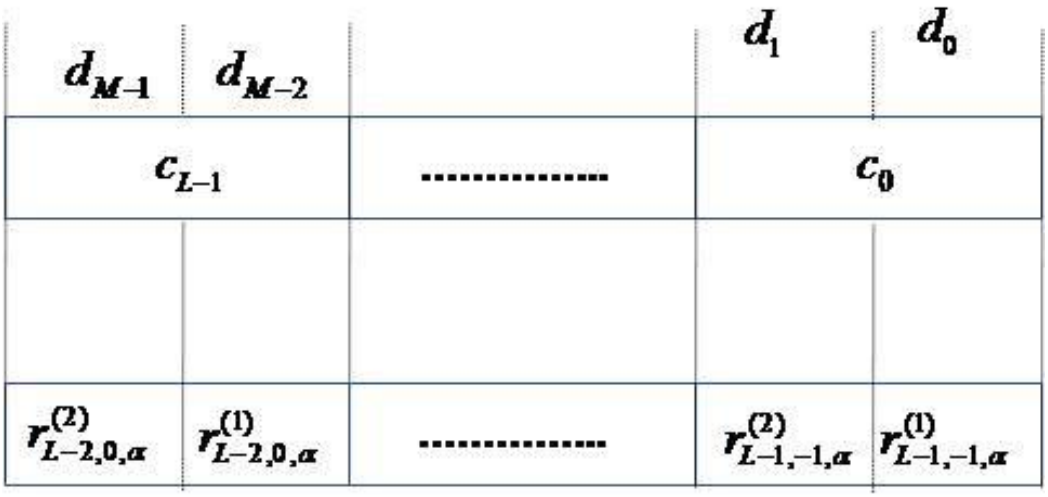

Figure 3-8 A possible alignment between the received and the local generated code.

At every correlation step the received sequence is first shifted of ΔT_c s and then, correlated with its local replica. Fig.3-8 shows a possible alignment between the received and the local generated code. Then, considering a shift delay of $T_c/2$, and two cells per sample, we can define two "sub-sequences" as follows:

$$S_0 = d_0, d_2, d_{4,\ldots\ldots,} d_{M-2}$$
$$S_1 = d_1, d_3, d_{5,\ldots\ldots,} d_{M-1} \qquad (3.19)$$

Now, the sub-correlations between the received samples and the two sub-sequences S_0, S_1 , for the in-phase and quadrature components can be expressed as, respectively:

$$\begin{aligned}
&\vdots \\
&x_{-1} = r^{(1)}_{0,0,x}C_0 + r^{(1)}_{1,0,x}C_1 + r^{(1)}_{2,0,x}C_2 + \ldots + r^{(1)}_{L-1,0,x}C_{L-1} \\
&x_0 = r^{(2)}_{0,0,x}C_0 + r^{(2)}_{1,0,x}C_1 + r^{(2)}_{2,0,x}C_2 + \ldots + r^{(1)}_{L-1,0,x}C_{L-1} \\
&x_1 = r^{(1)}_{1,0,x}C_0 + r^{(1)}_{2,0,x}C_1 + r^{(1)}_{3,0,x}C_2 + \ldots + r^{(1)}_{0,1,x}C_{L-1} \\
&\vdots
\end{aligned} \tag{3.20}$$

$$\begin{aligned}
&\vdots \\
&y_{-1} = r^{(1)}_{0,0,y}C_0 + r^{(1)}_{1,0,y}C_1 + r^{(1)}_{2,0,y}C_2 + \ldots + r^{(1)}_{L-1,0,y}C_{L-1} \\
&y_0 = r^{(2)}_{0,0,y}C_0 + r^{(2)}_{1,0,y}C_1 + r^{(2)}_{2,0,y}C_2 + \ldots + r^{(2)}_{L-1,0,y}C_{L-1} \\
&y_1 = r^{(1)}_{1,0,y}C_0 + r^{(1)}_{2,0,y}C_1 + r^{(1)}_{3,0,y}C_2 + \ldots + r^{(1)}_{0,1,y}C_{L-1} \\
&\vdots
\end{aligned} \tag{3.21}$$

The cross-correlation at every lag is obtained as the sum of the two contiguous sub-correlations. In other words, the series of at the output of the MF correlator for the in-phase and quadratrure components are defined as:

$$\begin{aligned}
&\vdots && \vdots \\
&R_x(0) = x_0 + x_{-1} && R_y(0) = y_0 + y_{-1} \\
&R_x(1) = x_1 + x_0 && R_y(1) = y_1 + y_0 \\
&\vdots && \vdots
\end{aligned} \tag{3.22}$$

The correlation $R_\alpha(k) = \alpha_k + \alpha_{k-1}$ in each lag k consists of two terms: one from the current lag (i.e. α_k) and one from the previous one (i.e. α_{k-1}). The testing variable, $R_x(k)^2 + R_y(k)^2 = \left(x_k + x_{k-1}\right)^2 + \left(y_k + y_{k-1}\right)^2$, of the cell($k$) and the testing variable of the cell(k-1), $R_x(k-1)^2 + R_y(k-1)^2 = \left(x_{k-1} + x_{k-2}\right)^2 + \left(y_{k-1} + y_{k-2}\right)^2$, are *correlated* with each other since they both share the terms x_{k-1} and y_{k-1}. As a consequence, the final result of the decision process in cell(k) depends also on the result of the test in the cell(k-1). In other words, the probability of declaring true acquisition in the current cell depends on the "*state*" of the system. The state-transition diagram of the system is depicted in Fig.3-9.

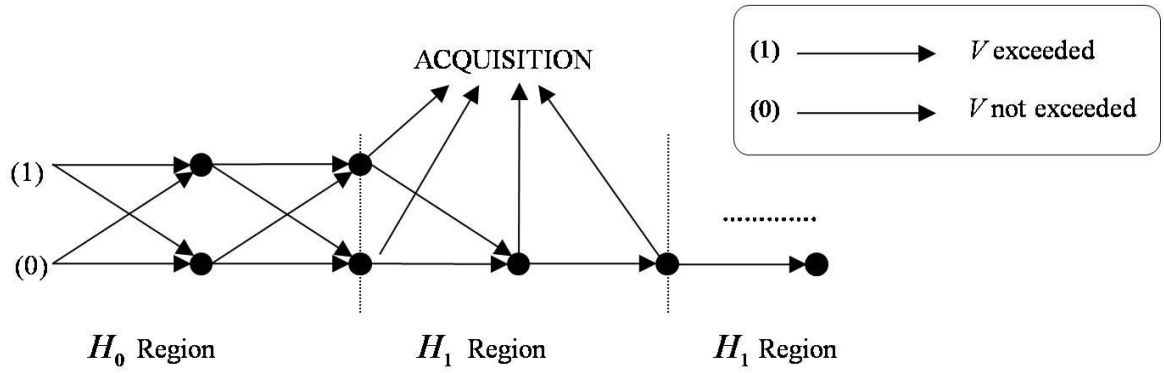

Figure 3-9 Transition Diagram for a single dwell system

where (0) , (1) are the two possible states of threshold exceeded or not exceeded. Now, the probability of going form (0) to (1) is expressed is $\Pr_{(0)-(1)} = \Pr\{z_k > V_{t1} \mid z_{k-1} > V_{t1}\}$, while the probability of going form (1) to (1) is $\Pr_{(1)-(1)} = \Pr\{z_k > V_{t1t1}\}$. The probability of going form (1) to (0) and from (0) to (0) can be obtained as the complement of $\Pr_{(0)-(1)}$ and $\Pr_{(1)-(1)}$, respectively. As it can be seen from the graph, in the case of perfect alignment between the transmitter and the receiver there exists three cells in the H_1 region. However, in most practical cases perfect compensation of the timing-synchronization error, is not possible and there exists only two possible H_1 cells. Finding a close form expression for the above mentioned probabilities is a trivial task. A first solution to such problem was proposed in [48] for the case of two cell per sample with a correlation coefficient of 1/2. The authors define a special class of function, the MGQ function expressing the system probabilities in a closed form. In this doctorate thesis we move further defining a new class of function, the Enhanced-MGQ functions, that can be used for describing the false alarm and detection probabilities of the system without making any a priori assumption on the correlation coefficient. The new functions, along with an innovative method for code acquisition with correlated cells are described in the next chapter of this thesis.

Chapter 4

A New Test for Initial Code Acquisition of Correlated Cells

4.1 Introduction

In serial-search code acquisition, the time uncertainty of the incoming signal is divided into a finite number of (timing) cells. The cells are tested on a cell-by-cell-based procedure until a correct cell is obtained. Taking the cell size as a fraction of the actual chip period could improve the acquisition performance, but unlike the case of one cell per chip, the detection variables between contiguous cells, for sizes less than one chip period, are not independent and possibly strongly correlated [48], [49]. As we showed in the previous chapter, cells' correlation has some effects on the acquisition process that must be taken into proper account. In addition it is extremely difficult to find a closed form expression for the systems error probabilities. In [48], a solution of such a problem is provided only in the simple case of two testing variables and a correlation coefficient $\rho = 1/2$, exploiting a new family of functions, namely, the modified generalized-Q (MGQ) functions. Then novelty introduced in this chapter is twofold. First, a new testing procedure is proposed for the performance improvements of initial code acquisition, taking into account correlated cells. Then, a closed-form expression for the system error probabilities is derived, without making any a priori assumptions. We modify the conventional power approach, to consider the effects of cell correlation, defining a new test, namely the *twin test*. Moreover, we define a new class of function, the extended MGQ (EMGQ) function, to express the false alarm and detection probabilities of the system in a closed form. The remainder of this chapter is organized as follows. Section 2 introduces the system model with correlated cells along with the new

twin test for initial code acquisition with correlated cells, whereas the new EMGQ functions are derived in Section 3, along with an efficient computational method. Closed-form expressions for the system error probabilities are shown in Section 4. Theoretical and simulation results in presence of cell correlation are shown in Section 5 and finally, our conclusions are given in Section 6.

4.1 Introducing the New Twin Test

In asynchronous communications, and due to the timing uncertainty of the incoming code, the maximum of the cross-correlation function may not be equal to the cross-correlation peak that is essential in the indication of the code synchronization. The receiver may sample the received signal with a timing offset uniformly distributed in a chip period [50]. Hence, the cross-correlation maximum may incur in a significant reduction since the receiver is now sampling the cross correlation in the neighborhood of the peak. However, while the maximum of the cross correlation reduces, the adjacent cross-correlation sample assumes a value greater than before. In the presence of timing offsets [see Fig. 4-1(a)], the maximum (sample) of the cross-correlation function (i.e., cell i) decreases, whereas the adjacent cross-correlation sample (i.e., cell $i + 1$) assumes a greater value. The problem is that, in many cases, these two correlated correlation's values (i.e., cell i and cell $i + 1$) are under the conventional threshold. As a consequence, searching for the correct timing offset with the conventional power test could result in a dramatic reduction of the detection probability.

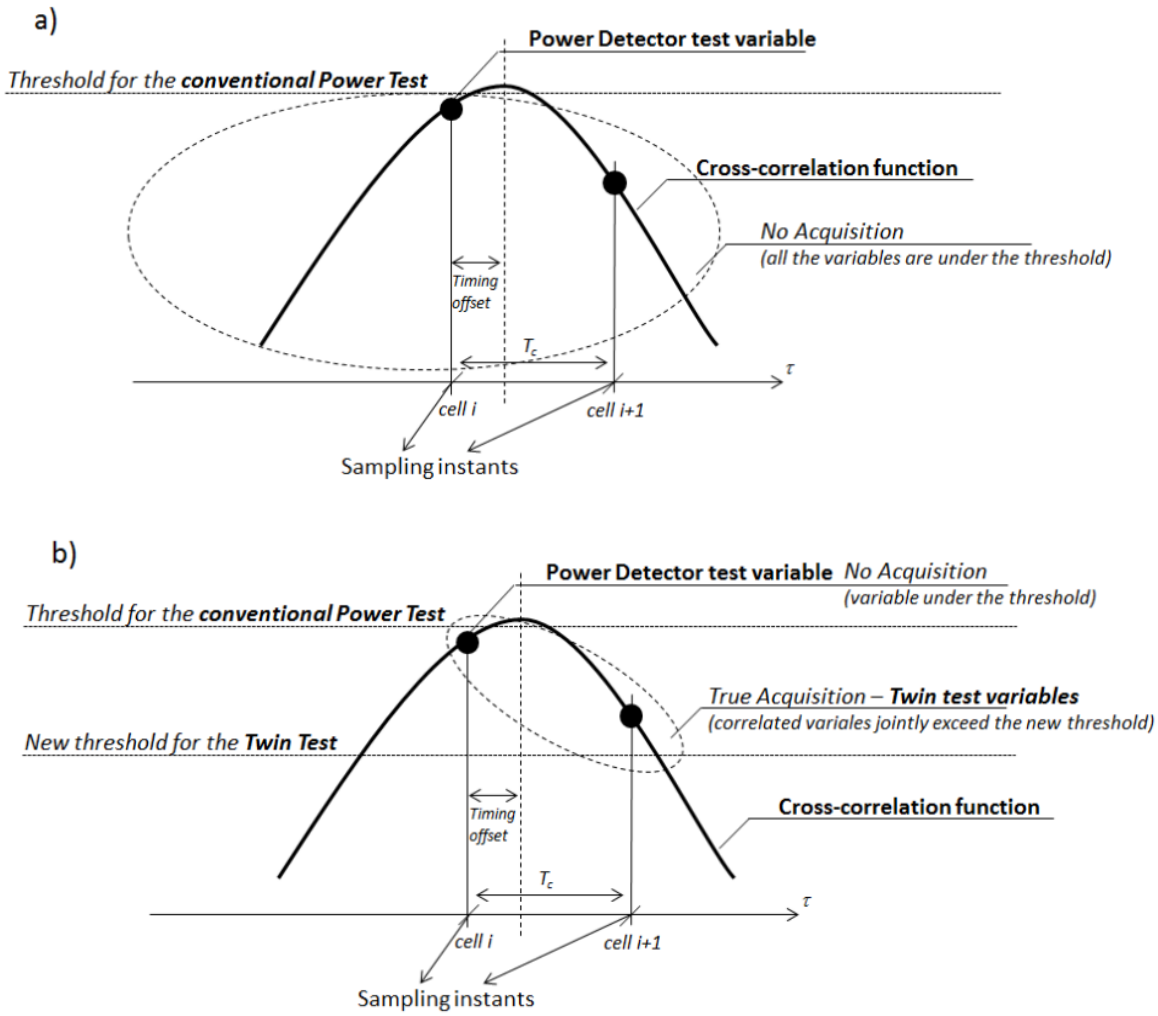

Figure 4-1 Decision variables of the: a) Conventional Power test (in presence of a timing offset); b) Conventional and Twin tests in presence of cell correlation and timing offset

The new method proposed in this doctorate thesis, aims at recovering these unlucky cases, and allows to compensate for the reduction of the cross-correlation maximum, meanwhile ensuring a faster rejection of H_0 cells. The rationale behind the proposed approach is as follows. In addition to the conventional threshold, we introduce another threshold v (lower than the conventional one). This threshold must be jointly exceeded by both the testing variables of the two correlated cells in order to declare acquisition . More in details, if the testing variables are under the upper threshold V' (different from the

conventional threshold *V*) but at the same they jointly exceed the lower threshold *v*, it is still possible to declare true acquisition. In the power test, the cells are tested on a cell-by-cell basis and true acquisition is achieved only if the testing variable z_i of the i-*th* cell exceeds the threshold *V* (i.e. $|z_i|>V'$). The twin test uses two correlated cells (e.g. cells *i* and *i+1*) and declares true acquisition if one of the corresponding testing variable exceeds the upper threshold *V'* (i.e $|z_i|>V'$ or $|z_{i+1}|>V'$) or if they both exceed the lower one (i.e. $v<|z_i|<V'$ and $v<|z_{i+1}|<V'$), see Fig.4-2. Moreover, since the testing variables are strictly correlated, if they are jointly below the lower threshold it is unlikely to have true acquisition in one of them. In this case, the cells are both discarded and the next pair is tested.

The pair of threshold (*v*, *V'*) is chosen according to the Constant False Alarm Rate (CFAR) criterion. In particular, the CFAR test is usually accomplished in two successive parts: first, a threshold *V* is determined to limit the false-alarm probability (P_{FA}), at a given chosen value under the H_0 hypothesis; second, the probability of detection (P_D) is evaluated under the hypothesis H_1 for the previously determined threshold. The probability of false alarm must be tuned to guarantee a very low number of possible false alarms (typical values are $P_{FA}=10^{-3}$, $P_{FA}=10^{-4}$), eventually implying a relevant penalty time. Large probabilities of detection (up to 100%) are typical of well-performing tests. In our case, there is more than one possible pair (*v*, *V'*) that meet the CFAR criterion, and the best one is chosen as the pair maximizing the P_D. More in details, fixing the P_{FA} to a desired target value, P_{FA}^{target}, the threshold evaluation step can described as the following constrained-optimization problem: find the unique pair (*v*, *V'*) that maximize P_D, with the constraint $P_{FA}=P_{FA}^{target}$.

4.2 Derivation of the EMGQ Function

In this section the new function E-MGQ function are derived in details. Following the

same notations of the previous chapter[1], let now $\{z_i = r_i e^{\theta i}\}$ with $i=1....\ N_c/\Delta$ be the correlator outputs taken at different cells. In particular, we are assuming that these random variables are Gaussian distributed and correlated with a correlation coefficient ρ. Since the test is a non-coherent one, the testing variables consist of the magnitude of correlator outputs, taken at different times $r_i = |z_i|$. Since our derivation is spherical invariant, as in all non-coherent tests working on signal magnitude, we have assumed a in-phase/quadrature notation for the complex variables $z_i = \{x_i + jy_i\}$. For each cell we define two Gaussian random variables $\{x_i, y_i\}$ randomly distributed with variances $\left\{\sigma_i^2\right\}$ and mean values $\{m_i, 0\}$, where $\{m_i = 0\}$ in the H_0 hypothesis, and $\{m_i \neq 0\}$ in the H_1 hypothesis. Since the variance is related to the channel noise, we are assuming without loss of generality the same variance for the two testing variables. However, all the analysis can be extended for variables with different variances.

First we evaluate the joint probability $Pr\{(r_i < V_i, r_{i+1} > V_{i+1})\}$ under both the two hypotheses, thus defining the new EMGQ function. Then, we express detection and false alarm probabilities will be in terms of the EMGQ functions. It has to be noted that in order to be as generic as possible, in the following analysis we are assuming different thresholds for each cell.

[1] Actually, we are using here $V = \sqrt{V_t}$ and $z_i = \sqrt{Z_k}$ with respect to the definitions of V_t and Z_k given in the previsours chapters

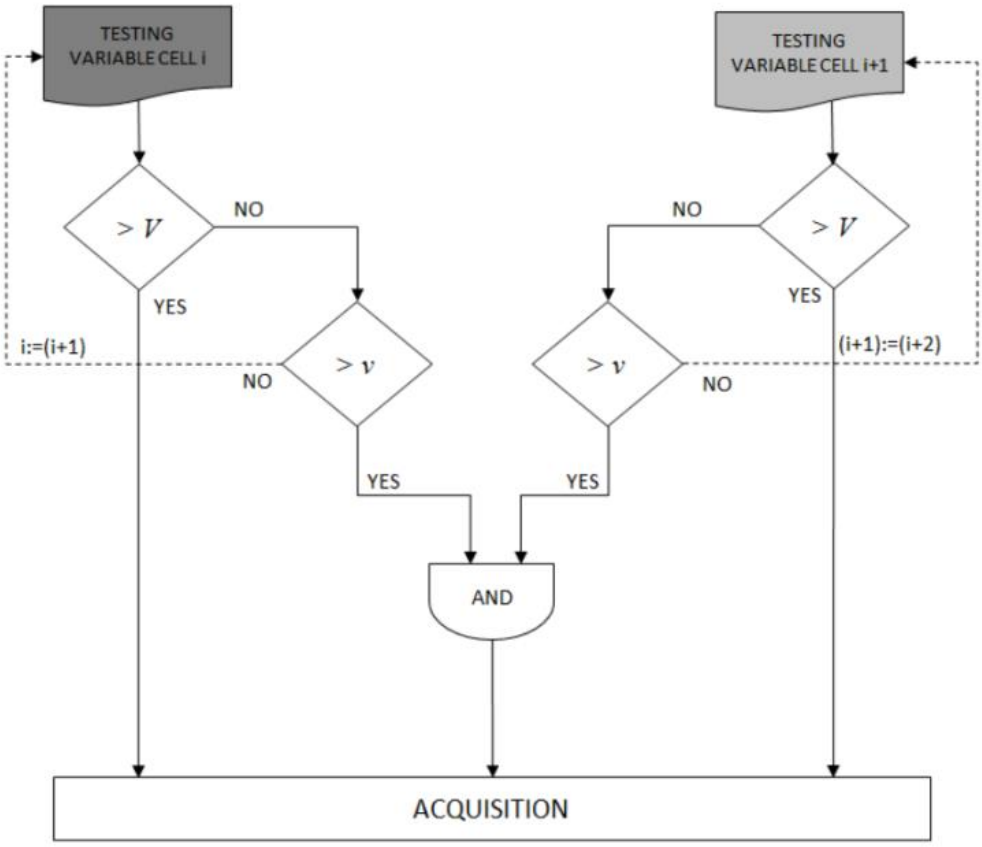

Figure 4-2 Equivalent scheme for the detection procedure of the twin-test

4.2.1 Hypothesis H_1

In order to evaluate the joint probability $Pr\{(r_i < V_i, r_{i+1} > V_{i+1})\}$, we first evaluate the joint probability density function (PDF) $p(x_i, x_{i+1}, y_i, y_{i+1}, m_i, m_{i+1}, \sigma)$ of the variables $[x_i, x_{i+1}, y_i, y_{i+1}]$ with mean values $[m_i, m_{i+1}, 0, 0]$ and the same variance σ^2. The covariance matrix of the above mentioned variables and the expression of the PDF are given by:

$$K = \begin{pmatrix} \sigma^2 & \rho\sigma^2 & 0 & 0 \\ \rho\sigma^2 & \sigma^2 & 0 & 0 \\ 0 & 0 & \sigma^2 & \rho\sigma^2 \\ 0 & 0 & \rho\sigma^2 & \sigma^2 \end{pmatrix} \tag{4.1}$$

$$p(x_i, x_{i+1}, y_i, y_{i+1}, m_i, m_{i+1}, \sigma) = \frac{1}{(2\pi)^2 \sigma^4 (1-\rho^2)} e^{\left\{ -\frac{(x_i - m_i)^2 + y_i^2 + y_{i+1}^2 + (x_{i+1} - m_{i+1})^2 - 2\rho\left[y_i y_{i+1} + (x_i - m_i)(x_{i+1} - m_{i+1}) \right]}{2\sigma^2 (1-\rho^2)} \right\}} \cdot \tag{4.2}$$

Now, let us made the following useful substitutions:

$$x_i = r_i \cos\theta_i; \quad y_i = r_i \sin\theta_i; \quad x_{i+1} = r_{i+1} \cos\theta_{i+1}; \quad y_{i+1} = r_{i+1} \sin\theta_{i+1}. \tag{4.3}$$

Substituting the previous expression for x_i, x_{i+1}, y_i and y_{i+1} into (4.2) the PDF becomes:

$$\begin{aligned} p(x_i, x_{i+1}, y_i, y_{i+1}, m_i, m_{i+1}, \sigma) &= \frac{1}{(2\pi)^2 \sigma^4 (1-\rho^2)} \\ \cdot \exp\Bigg\{ & \frac{-1}{2\sigma^2 (1-\rho^2)} \Big[m_{i+1}^2 + m_i^2 - 2 m_i m_{i+1} \rho + r_i^2 + r_{i+1}^2 \\ & + r_{i+1} (2 m_i \rho - 2 m_{i+1}) \cos\theta_{i+1} - 2 r_i (m_i - m_{i+1} \rho) \cos\theta_i - 2 r_i r_{i+1} \rho \cos(\theta_i - \theta_{i+1}) \Big] \Bigg\}. \end{aligned} \tag{4.4}$$

Then, the expression of the joint probability $Pr\{r_i < V_i, r_{i+1} > V_{i+1}\}$ can be obtained exploiting a new special function, the EMGQ function, defined as follows:

$$\begin{aligned} & Pr\{r_i < V_i, r_{i+1} > V_{i+1} \mid H_1\} = EMGQ(V_i, V_{i+1}, m_i, m_{i+1}, \sigma, \rho) \\ & = \frac{1}{(2\pi)^2 \sigma^4 (1-\rho^2)} \int_0^{V_i} \int_{V_{i+1}}^{\infty} e^{-\frac{m_{i+1}^2 + m_i^2 - 2 m_i m_{i+1} \rho + r_i^2 + r_{i+1}^2}{2\sigma^2 (1-\rho^2)}} r_i r_{i+1} dr_i dr_{i+1} \\ & \cdot \left(\int_0^{2\pi} \int_0^{2\pi} e^{-\frac{r_{i+1}(2 m_i \rho - 2 m_{i+1}) \cos\theta_{i+1} - 2 r_i (m_i - m_{i+1} \rho) \cos\theta_i - 2 r_i r_{i+1} \rho \cos(\theta_i - \theta_{i+1})}{2\sigma^2 (1-\rho^2)}} d\theta_i d\theta_{i+1} \right). \end{aligned} \tag{4.5}$$

The angular integral in the joint probability (4.5) can be computed in terms of the regulaized Hypergeometric function ${}_2\bar{F}_1(\cdot)$ [16], by the series derived in the following (see Appendix I at the end of this chapter for details):

$$\begin{aligned}&\int_0^{2\pi}\int_0^{2\pi} e^{-\frac{r_{i+1}\left(2m_i\rho-2m_{i+1}\right)\cos\theta_{i+1}-2r_i\left(m_i-m_{i+1}\rho\right)\cos\theta_i-2r_ir_{i+1}\rho\cos\left(\theta_i-\theta_{i+1}\right)}{2\sigma^2\left(1-\rho^2\right)}} d\theta_i d\theta_{i+1}\\&=\sum_{n=0}^{\infty}\sum_{p=0}^{\infty}\sum_{k=0}^{\infty}\sum_{s=0}^{\infty}\left(\frac{1}{n!\,p!k!s!}2^{2(1+s)}\Gamma\left[\frac{1+s}{2}\right]^4\cdot\left[\frac{r_i\left(m_i-m_{i+1}\rho\right)}{\sigma^2\left(1-\rho^2\right)}\right]^n\left[\frac{r_{i+1}\left(m_{i+1}-m_i\rho\right)}{\sigma^2\left(1-\rho^2\right)}\right]^p\left[\frac{r_ir_{i+1}\rho}{\sigma^2\left(1-\rho^2\right)}\right]^{s+k}\right.\\&\left.\cdot\,{}_2\bar{F}_1\left(\frac{1+s}{2},-n-k,1+s,2\right){}_2\bar{F}_1\left(\frac{1+s}{2},-p-k,1+s,2\right)\right).\end{aligned}\tag{4.6}$$

Now, using (4.6) in (4.5) we can obtain the following expression:

$$\begin{aligned}&EMGQ\left(V_i,V_{i+1},m_i,m_{i+1},\sigma,\rho\right)=\frac{e^{-\frac{m_{i+1}^2+m_i^2-2\rho m_im_{i+1}}{2\sigma^2\left(1-\rho^2\right)}}}{\left(2\pi\right)^2\sigma^4\left(1-\rho^2\right)}\\&\cdot\sum_{n=0}^{\infty}\sum_{p=0}^{\infty}\sum_{k=0}^{\infty}\sum_{s=0}^{\infty}\left(\frac{2^{2(1+s)}}{n!\,p!k!s!}\Gamma\left[\frac{1+s}{2}\right]^4\cdot\left[\frac{m_i-m_{i+1}\rho}{\sigma^2\left(1-\rho^2\right)}\right]^n\left[\frac{m_{i+1}-m_i\rho}{\sigma^2\left(1-\rho^2\right)}\right]^p\right.\\&\left.\cdot\left[\frac{\rho}{\sigma^2\left(1-\rho^2\right)}\right]^{s+k}\cdot{}_2\bar{F}_1\left(\frac{1+s}{2},-n-k,1+s,2\right){}_2\bar{F}_1\left(\frac{1+s}{2},-p-k,1+s,2\right)\cdot\int_0^{V_i}e^{-\frac{r_i^2}{2\sigma^2\left(1-\rho^2\right)}}r_i^{n+s+k+1}dr_i\int_{V_{i+1}}^{\infty}e^{-\frac{r_{i+1}^2}{2\sigma^2\left(1-\rho^2\right)}}r_{i+1}^{p+s+k+1}dr_{i+1}\right).\end{aligned}\tag{4.7}$$

All the power terms of (4.7), multiplied by exponential factors, can be evaluated as follows:

$$\int_0^V x^k e^{-Ax^2} dx = \frac{\Gamma\left(\frac{k+1}{2}\right)}{2\,A^{\frac{2+1}{2}}}\Gamma_1\left(AV_2^2;\frac{k+1}{2}\right),$$
$$\int_V^\infty x^k e^{-Ax^2} dx = \frac{\Gamma\left(\frac{k+1}{2}\right)}{2A^{\frac{2+1}{2}}}\overline{\Gamma}_1\left(AV_2^2;\frac{k+1}{2}\right), \tag{4.8}$$

where $\Gamma_1(\cdot,\cdot)$ and $\overline{\Gamma}_1(\cdot,\cdot) = 1-\Gamma_1(\cdot,\cdot)$ are the well-known incomplete Gamma function and its complement [17], respectively. Now, the EMGQ function re-writes as:

$$EMGQ(V_i,V_{i+1},m_i,m_{i+1},\sigma,\rho) = \frac{e^{-\frac{m_{i+1}^2+m_i^2-2\cdot\rho\cdot m_i m_{i+1}}{2\sigma^2\left(1-\rho^2\right)}}}{(2\pi)^2\,\sigma^4\left(1-\rho^2\right)}$$
$$\cdot\sum_{n=0}^{\infty}\sum_{p=0}^{\infty}\sum_{k=0}^{\infty}\sum_{s=0}^{\infty}\frac{2^{2(1+s)}}{n!\,p!\,k!\,s!}\Gamma\left(1+\frac{s}{2}\right)^4\cdot\frac{\Gamma\left(\frac{n+s+k+2}{2}\right)}{2\left[\frac{1}{2\sigma^2\left(1-\rho^2\right)}\right]^{\frac{n+s+k+2}{2}}}\cdot\frac{\Gamma\left(\frac{p+s+k+2}{2}\right)}{2\left[\frac{1}{2\sigma^2\left(1-\rho^2\right)}\right]^{\frac{p+s+k+2}{2}}} \tag{4.9}$$
$$\cdot\Gamma_1\left[\frac{V_i^2}{2\sigma^2\left(1-\rho^2\right)};\frac{n+s+k+2}{2}\right]\cdot\overline{\Gamma}_1\left[\frac{V_{i+1}^2}{2\sigma^2\left(1-\rho^2\right)};\frac{p+s+k+2}{2}\right]\cdot\left[\frac{m_i-m_{i+1}\rho}{\sigma^2\left(1-\rho^2\right)}\right]^n$$
$$\left[\frac{m_{i+1}-m_i\rho}{\sigma^2\left(1-\rho^2\right)}\right]^p\left[\frac{\rho}{\sigma^2\left(1-\rho^2\right)}\right]^{s+k}\cdot{}_2\overline{F}_1\left(\frac{1+s}{2},-n-k,1+s,2\right){}_2\overline{F}_1\left(\frac{1+s}{2},-p-k,1+s,2\right).$$

After some simplifications, the final expression is given by:

$$EMGQ(V_i,V_{i+1},m_i,m_{i+1},\sigma,\rho) = \frac{e^{-\frac{m_{i+1}^2+m_i^2-2\cdot\rho\cdot m_i m_{i+1}}{2\sigma^2\left(1-\rho^2\right)}}}{\pi^2}$$
$$\cdot\sum_{n=0}^{\infty}\sum_{p=0}^{\infty}\sum_{k=0}^{\infty}\sum_{s=0}^{\infty}\frac{2^{\frac{(2k+p+n+6s)}{2}}}{n!\,p!\,k!\,s!}\left(\frac{1}{\sigma}\right)^{n+p}\rho^{k+s}\cdot\left(\frac{1}{1-\rho^2}\right)^{\frac{n+p-2}{2}}$$
$$\cdot\Gamma\left(\frac{1+s}{2}\right)^4(m_i-m_{i+1}\rho)^n(m_{i+1}-m_i\rho)^p\cdot\Gamma\left(\frac{n+s+k+2}{2}\right)\cdot\Gamma\left(\frac{p+s+k+2}{2}\right)$$
$$\cdot\Gamma_1\left[\frac{V_i^2}{2\sigma^2\left(1-\rho^2\right)};\frac{n+s+k+2}{2}\right]\cdot\overline{\Gamma}_1\left[\frac{V_{i+1}^2}{2\sigma^2\left(1-\rho^2\right)};\frac{p+s+k+2}{2}\right] \tag{4.10}$$
$$\cdot{}_2\overline{F}_1\left(\frac{1+s}{2},-n-k,1+s,2\right)\cdot{}_2\overline{F}_1\left(\frac{1+s}{2},-p-k,1+s,2\right).$$

4.2.2 Hypothesis H_0

In the H_0 hypothesis the two testing variables are zero-mean Gaussian variables and the PDF in $x_i = r_i\cos\theta_i;\quad y_i = r_i\sin\theta_i;\quad x_{i+1} = r_{i+1}\cos\theta_{i+1};\quad y_{i+1} = r_{i+1}\sin\theta_{i+1}$.

(4.2) can be simplified as:

$$p(x_i, x_{i+1}, y_i, y_{i+1}, 0, 0, \sigma) = \frac{e^{-\frac{x_i^2 + y_i^2 + x_{i+1}^2 + y_{i+1}^2 - 2\rho(y_i y_{i+1} + x_i x_{i+1})}{2\sigma^2(1-\rho^2)}}}{(2\pi)^2 \sigma^4 (1-\rho^2)}. \tag{4.11}$$

Performing the same change of variables as in (4.3), we obtain:

$$p(r_i, r_{i+1}, \theta_i, \theta_{i+1}, 0, 0, \sigma) = \frac{e^{-\frac{r_i^2 + r_{i+1}^2 - 2r_{i+1}r_{i+1}\rho\cos(\theta_i - \theta_{i+1})}{2\sigma^2(1-\rho^2)}}}{(2\pi)^2 \sigma^4 (1-\rho^2)}. \tag{4.12}$$

Finally, the joint probability $\Pr\{r_i < V_i, r_{i+1} > V_{i+1}\}$ is expressed as:

$$Pr\{r_i < V_i, r_{i+1} > V_{i+1} \mid H_0\} = \frac{1}{(2\pi)^2 \sigma^4 (1-\rho^2)} \cdot \int_0^{V_i} \int_{V_{i+1}}^{\infty} e^{-\frac{r_i^2 + r_{i+1}^2}{2\sigma^2(1-\rho^2)}} r_i r_{i+1} \cdot \left(\int_0^{2\pi} \int_0^{2\pi} e^{\frac{2r_i r_{i+1}\rho\cos(\theta_i - \theta_{i+1})}{2\sigma^2(1-\rho^2)}} d\theta_i d\theta_{i+1} \right) dr_i dr_{i+1}. \tag{4.13}$$

The angular integral can be expressed in terms of the zero-order Bessel function of the first kind, which is defined as:

$$I_0(z) = \frac{1}{2\pi} \int_0^{2\pi} e^{z\cos(\theta_1 - \theta_2)} d\theta_1 \text{ , for any } \theta_2 . \tag{4.14}$$

Since the result is independent from the value of the parameter θ_2, the integration can be separately accomplished if we begin with the first variable $\{\theta_i\}$ and proceed with the second one $\{\theta_{i+1}\}$. The joint probability in (4.13) can be now expressed as:

$$EMGQ(V_i,V_{i+1},0,0,\sigma,\rho)=\frac{1}{\sigma^4\left(1-\rho^2\right)}\int_0^{V_i}\int_{V_{i+1}}^{\infty} e^{-\frac{r_i^2+r_{i+1}^2}{2\sigma^2\left(1-\rho^2\right)}} I_0\left(\frac{r_i r_{i+1}}{\sigma^2\left(1-\rho^2\right)}\right) r_i r_{i+1} dr_i dr_{i+1} \tag{4.15}$$

which can be computed in terms of the power expansion of the Bessel function of the first kind:

$$I_0(z)=\sum_{n=0}^{\infty}\left(\frac{1}{2}\right)^{2n} z^{2n}\frac{1}{(n!)^2}, \tag{4.16}$$

and finally allows to compute (4.13) as follows:

$$EMGQ(V_i,V_{i+1}0,0,\sigma,\rho)=\frac{1}{\sigma^4\left(1-\rho^2\right)}\cdot\sum_{n=0}^{\infty}\left(\frac{1}{2}\right)^{2n}\cdot\left[\frac{\rho}{\sigma^2\left(1-\rho^2\right)}\right]^{2n}\cdot\frac{1}{(n!)^2}\cdot\int_0^{V_i} e^{-\frac{r_i^2}{2\sigma^2\left(1-\rho^2\right)}} r_i^{2n+1} dr_i \int_{V_{i+1}}^{\infty} e^{-\frac{r_{i+1}^2}{2\sigma^2\left(1-\rho^2\right)}} r_{i+1}^{2n+1} dr_{i+1} \tag{4.17}$$

Following the same approach as in (4.8), equation (4.17) can be re-written as follows:

$$\begin{aligned} EMGQ(V_i,V_{i+1},0,0,\sigma,\rho)&=\frac{1}{\sigma^4\left(1-\rho^2\right)}\sum_{n=0}^{\infty}\left(\frac{1}{2}\right)^{2n}\left(\frac{1}{n!}\right)^2 \\ &\cdot\frac{\Gamma(n+1)}{2\left(\frac{1}{2\sigma^2\left(1-\rho^2\right)}\right)^{n+1}}\frac{\Gamma(n+1)}{2\left(\frac{1}{2\sigma^2\left(1-\rho^2\right)}\right)^{n+1}}\left(\frac{\rho}{\sigma^2\left(1-\rho^2\right)}\right)^{2n}\Gamma_1\left(\frac{V_i^2}{2\sigma^2\left(1-\rho^2\right)};n+1\right)\overline{\Gamma_1}\left(\frac{V_{i+1}^2}{2\sigma^2\left(1-\rho^2\right)};n+1\right) \end{aligned} \tag{4.18}$$

And after some simplifications the final expression is given by:

$$\begin{aligned} &EMGQ(V_i,V_{i+1},0,0,\sigma,\rho)= \\ &\left(1-\rho^2\right)\cdot\sum_{n=0}^{\infty}\rho^{2n}\cdot\Gamma_1\left(\frac{V_i^2}{2\sigma^2\left(1-\rho^2\right)};n+1\right)\cdot\overline{\Gamma}_1\left(\frac{V_{i+1}^2}{2\sigma^2\left(1-\rho^2\right)};n+1\right). \end{aligned} \tag{4.19}$$

4.2.3 Evaluation of the joint probability

In this section, the joint probability $Pr\{v < r_i < V, v < r_{i+1} < V\}$ is evaluated. In the following analysis, for the sake of simplicity and without loss of generality, the attention will be focused only on the H_0 hypothesis. However, the same procedure can be easily extended to the H_1 hypothesis. In addition, for the sake of compactness and without loss of generality, we consider $V_i=V_{i+1}=V$ and $v_i=v_{i+1}=v$, as happens in the conventional operating cases. The joint probability under investigation can be expressed as in (4.13) but with a different integration domain (i.e. $[v,V,0,2\pi]$), as follows:

$$\Pr\{v < r_i < V, v < r_{i+1} < V \mid H_0\} = \frac{1}{(2\pi)^2 \sigma^4 (1-\rho^2)} \cdot \int_v^V \int_v^V e^{-\frac{r_i^2 + r_{i+1}^2}{2\sigma^2(1-\rho^2)}} r_i r_{i+1} \cdot \left(\int_0^{2\pi} \int_0^{2\pi} e^{\frac{2r_i r_{i+1}\rho\cos(\theta_i - \theta_{i+1})}{2\sigma^2(1-\rho^2)}} d\theta_i d\theta_{i+1} \right) dr_i dr_{i+1}. \tag{4.20}$$

We can now express the angular integral in (4.20) in terms of the Bessel function of the first kind:

$$\Pr\{v < r_i < V, v < r_{i+1} < V \mid H_0\} = \frac{1}{\sigma^4(1-\rho^2)} \cdot \int_v^V \int_v^V e^{-\frac{r_i^2 + r_{i+1}^2}{2\sigma^2(1-\rho^2)}} \cdot I_0\left(\frac{2r_i r_{i+1}\rho}{2\sigma^2(1-\rho^2)}\right) dr_i dr_{i+1} \tag{4.21}$$

which can again be computed in the terms of the power expansion of the Bessel function:

$$\Pr\{v < r_i < V, v < r_{i+1} < V \mid H_0\} = \frac{1}{\sigma^4(1-\rho^2)} \cdot \sum_{n=0}^{\infty} \left(\frac{1}{2}\right)^{2n} \left[\frac{\rho}{\sigma^2(1-\rho^2)}\right]^{2n} \cdot \frac{1}{(n!)^2} \cdot \left(\int_0^V e^{-\frac{r_i^2}{2\sigma^2(1-\rho^2)}} r_i^{2n+1} dr_i - \int_0^v e^{-\frac{r_i^2}{2\sigma^2(1-\rho^2)}} r_i^{2n+1} dr_i \right) \cdot \left(\int_0^V e^{-\frac{r_{i+1}^2}{2\sigma^2(1-\rho^2)}} r_{i+1}^{2n+1} dr_{i+1} - \int_0^v e^{-\frac{r_{i+1}^2}{2\sigma^2(1-\rho^2)}} r_{i+1}^{2n+1} dr_{i+1} \right). \tag{4.22}$$

All the power terms of the above series multiplied by exponential factors can still be formally integrated in terms of the well know incomplete Gamma function, with the following useful relation:

$$\begin{aligned}&\int_{v}^{V} x^k e^{-Ax^2}\,dx = \int_{0}^{V} x^k e^{-Ax^2}\,dx - \int_{0}^{v} x^k e^{-Ax^2}\,dx \\ &= \frac{\Gamma\left(\frac{k+1}{2}\right)}{2A^{\frac{k+1}{2}}}\left[\Gamma_1\left(AV^2;\frac{k+1}{2}\right)-\Gamma_1\left(Av^2;\frac{k+1}{2}\right)\right].\end{aligned} \tag{4.23}$$

Substituting (4.23) in (4.22) and after some simplifications, the final expression is given by:

$$\begin{aligned}&\Pr\{v<r_i<V, v<r_{i+1}<V \mid H_0\} = \left(1-\rho^2\right) \\ &\cdot\sum_{i=0}^{\infty}\rho^{2i}\left[\Gamma_1\left(\frac{V^2}{2\sigma^2\left(1-\rho^2\right)};i+1\right)-\Gamma_1\left(\frac{v^2}{2\sigma^2\left(1-\rho^2\right)};i+1\right)\right] \\ &\cdot\left[\Gamma_1\left(\frac{V^2}{2\sigma^2\left(1-\rho^2\right)};i+1\right)-\Gamma_1\left(\frac{v^2}{2\sigma^2\left(1-\rho^2\right)};i+1\right)\right].\end{aligned} \tag{4.24}$$

Exploiting the Gamma function and its complement, (4.24) can be written as:

$$\begin{aligned}&\Pr\{v<r_i<V, v<r_{i+1}<V \mid H_0\} = \left(1-\rho^2\right)\sum_{n=0}^{\infty}\rho^{2n} \\ &\cdot\left[-\Gamma_1\left(\frac{V^2}{2\sigma^2\left(1-\rho^2\right)};n+1\right)\bar{\Gamma}_1\left(\frac{V^2}{2\sigma^2\left(1-\rho^2\right)};n+1\right)\right. \\ &+\Gamma_1\left(\frac{V^2}{2\sigma^2\left(1-\rho^2\right)};n+1\right)\bar{\Gamma}_1\left(\frac{v^2}{2\sigma^2\left(1-\rho^2\right)};n+1\right) \\ &+\Gamma_1\left(\frac{v^2}{2\sigma^2\left(1-\rho^2\right)};n+1\right)\bar{\Gamma}_1\left(\frac{V^2}{2\sigma^2\left(1-\rho^2\right)};n+1\right) \\ &\left.-\Gamma_1\left(\frac{v^2}{2\sigma^2\left(1-\rho^2\right)};n+1\right)\bar{\Gamma}_1\left(\frac{v^2}{2\sigma^2\left(1-\rho^2\right)};n+1\right)\right],\end{aligned} \tag{4.25}$$

which can be effectively expressed as the sum of four EMGQ functions:

$$\begin{aligned}&\Pr\{v < r_i < V, v < r_{i+1} < V \mid H_0\}\\&= -EMGQ(V,V,\sigma,0,0,\rho) + EMGQ(V,v,\sigma,0,0,\rho) + EMGQ(v,V,\sigma,0,0,\rho) - EMGQ(v,v,\sigma,0,0,\rho).\end{aligned} \quad (4.26)$$

Following the same procedure, in the H_1 hypothesis we obtain the following expression:

$$\begin{aligned}&\Pr\{v < r_i < V, v < r_{i+1} < V \mid H_1\}\\&= -EMGQ(V,V,\sigma,m_i,m_{i+1},\rho) + EMGQ(V,v,\sigma,m_i,m_{i+1},\rho)\\&\quad + EMGQ(v,V,\sigma,m_i,m_{i+1},\rho) - EMGQ(v,v,\sigma,m_i,m_{i+1},\rho).\end{aligned} \quad (4.27)$$

4.3 Performance Analysis

In this Section, we express the performance of both the conventional and the twin test in terms of in terms of false alarm (i.e P_{FA}) and detection probability (i.e P_D) Moreover, we express P_{FA} and P_D of both methods are expressed in terms of the EMG-Q function.

4.3.1 Conventional Test

4.3.2 False alarm probability

The false-alarm probability (P_{FA}) is the probability of declaring acquisition in a wrong cell. In other words, is the probability of exceeding the threshold V in the H_0 hypothesis. The P_{FA} of the *ith*-cell can be computed as follows:

$$\Pr\{r_i > V\} = \frac{1}{2\pi\sigma^2} \cdot \int_{V_i}^{\infty} \int_{0}^{2\pi} e^{-\frac{r_i^2}{2\sigma^2}} r_i \cdot d\theta_i dr_i = \int_{V}^{\infty} e^{-\frac{r_i^2}{2\sigma^2}} r_i dr_i = e^{-\frac{V^2}{2\sigma^2}} \quad (4.28)$$

The false alarm probability of the *(i+1)th*-cell, conditioned to a non-false-alarm situation in the *ith*-cell is given by $\Pr\{r_{i+1} > V \mid r_i < V\} = \Pr\{r_{i+1} > V, r_i < V\} / \Pr\{r_i < V\}$. The probability

$\Pr\{r_i < V\}$ can be easily obtained from the complement of (4.28), while the joint probability $\Pr\{r_{i+1} > V, r_i < V\}$ is expressed by the EGM-Q in (4.19). Hence, the false alarm probability of the *(i+1)th*-cell can be derived as:

$$\Pr\{r_{i+1} > V \mid r_i < V\} = \frac{\Pr\{r_{i+1} > V, r_i < V\}}{1 - \Pr\{r_i < V\}} = \frac{EMGQ(V, V, 0, 0, \sigma, \rho)}{1 - e^{-\frac{V^2}{2\sigma^2}}} \tag{4.29}$$

Finally, the false alarm probability of the conventional test can be written as the sum of (4.29) and (4.28) as follows:

$$P_{FA}^{(conv)} = \Pr\{r_i > V\} + \Pr\{r_{i+1} > V \mid r_i > V\} = e^{-\frac{V^2}{2\sigma^2}} + \left(1-\rho^2\right)\sum_{n=0}^{\infty}\rho^{2n}\Gamma_1\left(\frac{V^2}{2\sigma^2\left(1-\rho^2\right)}; n+1\right)\cdot\bar{\Gamma}_1\left(\frac{V^2}{2\sigma^2\left(1-\rho^2\right)}; n+1\right)\Bigg/\left(1-e^{-\frac{V^2}{2\sigma^2}}\right) \tag{4.30}$$

4.3.3 Probability of Detection

The probability of detection (i.e. P_D) is the probability of declaring acquisition in a correct cell. In other words, is the probability of exceeding the threshold V in the H_1 hypothesis. Following the same methodology as before, the P_D of the conventional test can be evaluated as follows. The P_D of the ith-cell can be computed by means of the GQ_1 function of the first order [51]:

$$\Pr\{r_i > V\} = GQ_1(\mathrm{V}, \mathrm{m}_i, \sigma) = \mathrm{e}^{-\frac{m_i^2}{2\sigma^2}}\sum_{t=0}^{\infty}\frac{m_i^{2t}}{t!2^t\sigma^{2t}}\bar{\Gamma}_1\left(\frac{V^2}{2\sigma^2}; t+1\right) \tag{4.31}$$

The P_D of the (i+1)th-cell conditioned to a non-detection in the ith-cell is given by: $\Pr\{r_{i+1} > V \mid r_i < V\} = \Pr\{r_{i+1} > V, r_i < V\} / \Pr\{r_i < V\}$. The probability $\Pr\{r_i < V\}$ can be easily obtained from the complement of (4.31), while the joint probability $\Pr\{r_{i+1} > V, r_i < V\}$ is expressed by the EGM-Q in (4.10). In the case under consideration the detection probability can be written as:

$$\Pr\{r_{i+1} > V \mid r_i < V\} = \frac{\Pr\{r_{i+1} > V, r_i < V\}}{1 - \Pr\{r_i < V\}} = \frac{EMGQ(V, V, m_i, m_{i+1}\sigma, \rho)}{1 - GQ_1(V, m_i, \sigma, \rho)} \tag{4.32}$$

Hence, the P_D of the conventional single-threshold test, can be written as the sum of the two probabilities in (4.31) and (4.32):

$$\begin{aligned} P_D^{(conv)} = & \\ & \frac{\mathrm{e}^{-\frac{m_{i+1}^2 + m_i^2 - 2\cdot\rho\cdot m_i m_{i+1}}{2\sigma^2(1-\rho^2)}}}{\pi^2} \left[\sum_{n=0}^{\infty}\sum_{p=0}^{\infty}\sum_{k=0}^{\infty}\sum_{s=0}^{\infty} \frac{2^{\frac{2k+p+n+6s}{2}}}{n!\,p!\,k!\,s!} \left(\frac{1}{\sigma}\right)^{n+p} \right. \\ & \cdot \rho^{k+s} \left(\frac{1}{1-\rho^2}\right)^{\frac{1}{2}(n+p-2)} \Gamma\left[\frac{1+s}{2}\right]^4 (m_i - m_{i+1}\rho)^n (m_{i+1} - m_i\rho)^p \\ & \cdot \Gamma\left(\frac{n+s+k+2}{2}\right) \Gamma\left(\frac{p+s+k+2}{2}\right) \cdot \Gamma_1\left(\frac{V^2}{2\sigma^2(1-\rho^2)}; \frac{n+s+k+2}{2}\right) \\ & \cdot \overline{\Gamma}_1\left(\frac{V^2}{2\sigma^2(1-\rho^2)}; \frac{p+s+k+2}{2}\right) {}_2\overline{F}_1\left(\frac{1+s}{2}, -n-k, 1+s, 2\right) \\ & \left. \cdot {}_2\overline{F}_1\left(\frac{1+s}{2}, -p-k, 1+s, 2\right) \right] \Bigg/ \left(1 - \mathrm{e}^{-\frac{m_i^2}{2\sigma^2}} \sum_{t=0}^{\infty} \frac{m_i^{2t}}{t!\,2^t\,\sigma^{2t}} \overline{\Gamma}_1\left(\frac{V^2}{2\sigma^2}; t+1\right) \right) \\ & + \mathrm{e}^{-\frac{m_i^2}{2\sigma^2}} \sum_{t=0}^{\infty} \frac{m_i^{2t}}{t!\,2^t\,\sigma^{2t}} \overline{\Gamma}_1\left(\frac{V^2}{2\sigma^2}; t+1\right) \end{aligned} \tag{4.33}$$

4.3.4 Twin test

4.3.5 False alarm probability

Then, let us focus on the probability of false alarm of the Twin Test. To evaluate the P_{FA} of the new test, we need to take also into account the P_{FA} of the lower threshold v, i.e. $\Pr\{v < r_i < V, v < r_{i+1} < V\}$ that can be effectively computed as the combination of four EMGQ functions, as shown in (4.26). Then, the P_{FA} for the twin-test, can be evaluated as the sum of (4.30) and the four EMGQ in (4.26), and it is expressed as follows:

$$P_{FA}^{(twin)} = e^{\frac{-V^2}{2\sigma}} + \left(1-\rho^2\right)\left[\sum_{n=0}^{\infty}\rho^{2n}\bar{\Gamma}_1\left(\frac{V^2}{2\sigma^2\left(1-\rho^2\right)};n+1\right)\cdot\Gamma_1\left(\frac{V^2}{2\sigma^2\left(1-\rho^2\right)};n+1\right)\right]\Bigg/\left(1-e^{\frac{-V^2}{2\sigma}}\right)+\left(1-\rho^2\right)\sum_{n=0}^{\infty}\rho^{2n}\cdot\left[\Gamma_1\left(\frac{V^2}{2\sigma^2\left(1-\rho^2\right)};n+1\right)-\Gamma_1\left(\frac{v^2}{2\sigma^2\left(1-\rho^2\right)};n+1\right)\right]\cdot\left[\Gamma_1\left(\frac{V^2}{2\sigma^2\left(1-\rho^2\right)};n+1\right)-\Gamma_1\left(\frac{v^2}{2\sigma^2\left(1-\rho^2\right)};n+1\right)\right] \quad (4.34)$$

4.3.6 Probability of Detection

Finally, to evaluate the probability of detection of the Twin Test, we now need to compute also the P_D relative to the lower threshold $\Pr\{v < r_i < V, v < r_{i+1} < V\}$, expressed in (4.27)

$$P_D^{(lower)} = \frac{e^{-\frac{\left(m_{i+1}^2+m_i^2-2\cdot\rho\cdot m_i m_{i+1}\right)}{2\sigma^2(1-\rho^2)}}}{\pi^2}\sum_{n=0}^{\infty}\sum_{p=0}^{\infty}\sum_{k=0}^{\infty}\sum_{s=0}^{\infty}\frac{2^{\frac{1}{2}(2k+p+n+6s)}}{n!\,p!\,k!\,s!}\left(\frac{1}{\sigma}\right)^{n+p}\cdot\rho^{k+s}\left(\frac{1}{1-\rho^2}\right)^{\frac{1}{2}(n+p-2)}$$
$$\cdot\Gamma\left[\frac{1+s}{2}\right]^4(m_i-m_{i+1}\rho)^n(m_{i+1}-m_i\rho)^p\cdot\Gamma\left(\frac{n+s+k+2}{2}\right)\Gamma\left(\frac{p+s+k+2}{2}\right)$$
$${}_2\overline{F}_1\left(\frac{1+s}{2},-n-k,1+s,2\right){}_2\overline{F}_1\left(\frac{1+s}{2},-p-k,1+s,2\right) \qquad (4.35)$$
$$\left[\Gamma_1\left(\frac{V^2}{2\sigma^2(1-\rho^2)};\frac{n+s+k+2}{2}\right)-\Gamma_1\left(\frac{v^2}{2\sigma^2(1-\rho^2)};\frac{n+s+k+2}{2}\right)\right]$$
$$\left[\Gamma_1\left(\frac{V^2}{2\sigma^2(1-\rho^2)};\frac{n+s+k+2}{2}\right)-\Gamma_1\left(\frac{v^2}{2\sigma^2(1-\rho^2)};\frac{n+s+k+2}{2}\right)\right].$$

Hence, the P_D of the innovative test can be derived as the sum of (4.31), (4.32) and the additional term expressed by (4.35).

$$P_D^{(Twin)}=\mathrm{e}^{-\frac{m_i^2}{2\sigma^2}}\sum_{t=0}^{\infty}\frac{m_i^{2t}}{t!2^t\sigma^{2t}}\bar{\Gamma}_1\left(\frac{V^2}{2\sigma^2};t+1\right)+\frac{1}{\pi^2}\mathrm{e}^{-\frac{\left(m_{i+1}^2+m_i^2-2\cdot\rho\cdot m_i m_{i+1}\right)}{2\sigma^2(1-\rho^2)}}$$
$$\cdot\sum_{n=0}^{\infty}\sum_{p=0}^{\infty}\sum_{k=0}^{\infty}\sum_{s=0}^{\infty}\frac{2^{\frac{2k+p+n+6s}{2}}}{n!\,p!k!s!}\left(\frac{1}{\sigma}\right)^{n+m}\rho^{k+s}\cdot\left(\frac{1}{1-\rho^2}\right)^{\frac{(n+p-2)}{2}}\Gamma\left[\frac{1+s}{2}\right]^4(m_i-m_{i+1}\rho)^n$$
$$\cdot(m_{i+1}-m_i\rho)^p\cdot\Gamma\left(\frac{n+s+k+2}{2}\right)\Gamma\left(\frac{m+s+k+2}{2}\right)\Gamma_1\left(\frac{V^2}{2\sigma^2(1-\rho^2)};\frac{n+s+k+2}{2}\right)$$
$$\cdot\bar{\Gamma}_1\left(\frac{V^2}{2\sigma^2(1-\rho^2)};\frac{p+s+k+2}{2}\right){}_2\bar{F}_1\left(\frac{1+s}{2},-n-k,1+s,2\right)$$
$$\cdot{}_2\bar{F}_1\left(\frac{1+s}{2},-p-k,1+s,2\right)\Bigg/\left[1-\mathrm{e}^{-\frac{m_i^2}{2\sigma^2}}\sum_{t=0}^{\infty}\frac{m_i^{2t}}{t!2^t\sigma^{2t}}\bar{\Gamma}_1\left(\frac{V_i^2}{2\sigma^2};t+1\right)\right]$$
$$+\frac{\mathrm{e}^{-\frac{\left(m_{i+1}^2+m_i^2-2\cdot\rho\cdot m_i m_{i+1}\right)}{2\sigma^2(1-\rho^2)}}}{\pi^2}\sum_{n=0}^{\infty}\sum_{p=0}^{\infty}\sum_{k=0}^{\infty}\sum_{s=0}^{\infty}\frac{2^{\frac{1}{2}(2k+p+n+6s)}}{n!\,p!k!s!}\left(\frac{1}{\sigma}\right)^{n+p}\cdot\rho^{k+s}\left(\frac{1}{1-\rho^2}\right)^{\frac{1}{2}(n+p-2)}$$
$$\cdot\Gamma\left[\frac{1+s}{2}\right]^4(m_i-m_{i+1}\rho)^n(m_{i+1}-m_i\rho)^p\cdot\Gamma\left(\frac{n+s+k+2}{2}\right)\Gamma\left(\frac{p+s+k+2}{2}\right)$$
$${}_2\bar{F}_1\left(\frac{1+s}{2},-n-k,1+s,2\right){}_2\bar{F}_1\left(\frac{1+s}{2},-p-k,1+s,2\right)$$
$$\left[\Gamma_1\left(\frac{V^2}{2\sigma^2(1-\rho^2)};\frac{n+s+k+2}{2}\right)-\Gamma_1\left(\frac{v^2}{2\sigma^2(1-\rho^2)};\frac{n+s+k+2}{2}\right)\right]$$
$$\left[\Gamma_1\left(\frac{V^2}{2\sigma^2(1-\rho^2)};\frac{n+s+k+2}{2}\right)-\Gamma_1\left(\frac{v^2}{2\sigma^2(1-\rho^2)};\frac{n+s+k+2}{2}\right)\right].$$

(4.36)

4.4 Truncation Error

The series expansion in (4.28)-(4.36) are defined over an infinite number of terms. However, this is an ideal definition and in practical cases the sums can be computed only over a limited number of terms. In this section, in order to assess the effectiveness of those series expansion we evaluated the error due to the approximation of these expressions by a relatively small number of terms.

4.4.1 Probability of false alarm: Conventional Test

Let us consider the expression of the false alarm probability of the conventional test, see eq. (4.30) and assume that we can compute this expression (and the EMGQ function involved) only while the indices of the sums are limited to a known value M. The truncation error $\varepsilon^{(conv)}$ (i.e. the remainder of the infinite sum) due to such approximation is defined as:

$$\begin{aligned}\varepsilon^{(conv)} &= \frac{EMGQ(V,V,0,0,\sigma,\rho)}{1-e^{-\frac{V^2}{2\sigma^2}}} - \frac{EMGQ_{TRUNC}(V,V,0,0,\sigma,\rho)}{1-e^{-\frac{V^2}{2\sigma^2}}} \\ &= \frac{\left(1-\rho^2\right)\sum_{n=0}^{\infty}\rho^{2n}\Gamma_1\left(\frac{V^2}{2\sigma^2\left(1-\rho^2\right)};n+1\right)\overline{\Gamma}_1\left(\frac{V^2}{2\sigma^2\left(1-\rho^2\right)};n+1\right)}{\left(1-e^{-\frac{V^2}{2\sigma^2}}\right)}\end{aligned} \tag{4.37}$$

The two Gamma functions in (4.37) are expressed in terms of the ratio $V^2/2\sigma^2\left(1-\rho^2\right)$ and of the current index *n*. The gamma function is limited in the following interval $0 \le \Gamma_1(x,a) \le 1$ by definition, hence, the maximum value of the product of the two Gamma functions is equal to 1/4. In fact, we must evaluate the maximum of $x(1-x)$ which is, effectively, 1/4. Thus, the truncation error in (4.37) is bounded by the following

$$\varepsilon_{\max}^{(conv)} = \frac{\left(1-\rho^2\right)\frac{1}{4}\sum_{n=M+}^{\infty}\rho^{2n}}{1-e^{-\frac{V^2}{2\sigma^2}}} = \frac{\frac{1}{4}\left(\rho^2\right)^{M+1}}{1-e^{-\frac{V^2}{2\sigma^2}}} \tag{4.38}$$

4.4.2 Probability of false alarm: Twin Test

To evaluate the truncation error of the false alarm probability of the twin test, see eq. (4.34), we need to consider the P_{FA} relative to the lower threshold, shown in (4.34). The maximum value of the difference between the two Gamma functions in (4.34), with the constrain $v < V$, is equal to 1. Therefore, we obtain the following expression for the upper bound of the truncation error of the twin test:

$$\varepsilon_{\max}^{(conv)} = \frac{1}{4}\left(1-\rho^2\right)\frac{\sum_{n=M+1}^{\infty}\rho^{2n}}{1-e^{-\frac{V^2}{2\sigma^2}}} + \left(1-\rho^2\right)\sum_{n=M+}^{\infty}\rho^{2n} = \frac{1}{4}\frac{\left(\rho^2\right)^{M+1}}{1-e^{-\frac{V^2}{2\sigma^2}}} + \left(\rho^2\right)^{M+1} \tag{4.39}$$

4.4.3 Probability of detection: Conventional Test

Let us now evaluate the truncation error for the expression of the detection probability in (4.33), that involves the computation of the EMGQ expressed in (4.10) and of the GQ_1 in [51]. This computation involves also the Hypergeometric function, but a detailed analysis of the truncation error for such a function is out of the focus of this dissertation and can be found in [52] and references therein. From the definition of the Hypergeometric function [52], the maximum value of the product of the two Hypergeometric functions in (4.33) is 1, and since the maximum value of the product of the two Gamma functions is ¼, we obtain the following expression for the upper bound of the truncation error of the EMGQ function:

$$\varepsilon_{EMGQ\max} = \frac{e^{-\frac{m_{i+1}^2+m_i^2-2\cdot\rho\cdot m_i m_{i+1}}{2\sigma^2\left(1-\rho^2\right)}}}{\pi^2}\cdot\sum_{n=0}^{\infty}\sum_{p=0}^{\infty}\sum_{k=0}^{\infty}\sum_{s=0}^{\infty}\frac{2^{\frac{(2k+p+n+6s)}{2}}}{n!\,p!\,k!\,s!}\left(\frac{1}{\sigma}\right)^{n+p}\rho^{k+s}\cdot\left(\frac{1}{1-\rho^2}\right)^{\frac{n+p-2}{2}} \tag{4.40}$$
$$\cdot\Gamma\left(\frac{1+s}{2}\right)^4\left(m_i-m_{i+1}\rho\right)^n\left(m_{i+1}-m_i\rho\right)^p\cdot\Gamma\left(\frac{n+s+k+2}{2}\right)\cdot\Gamma\left(\frac{p+s+k+2}{2}\right)$$

The truncation error of the GQ_1 function is expressed as follows [51]:

$$\varepsilon_{GQ}=\mathrm{e}^{-\frac{m_i^2}{2\sigma^2}}\sum_{t=T+1}^{\infty}\frac{m_i^{2t}}{t!2^t\sigma^{2t}} \tag{4.41}$$

Finally, the truncation error of the detection probability for the conventional test can be derived as:

$$\varepsilon_{\max}^{(conv)}=\frac{e^{-\frac{m_{i+1}^2+m_i^2-2\cdot\rho\cdot m_i m_{i+1}}{2\sigma^2\left(1-\rho^2\right)}}}{\pi^2}\cdot\sum_{n=0}^{\infty}\sum_{p=0}^{\infty}\sum_{k=0}^{\infty}\sum_{s=0}^{\infty}\frac{2^{\frac{(2k+p+n+6s)}{2}}}{n!p!k!s!}\left(\frac{1}{\sigma}\right)^{n+p}\rho^{k+s}\cdot\left(\frac{1}{1-\rho^2}\right)^{\frac{n+p-2}{2}} \tag{4.42}$$
$$\cdot\Gamma\left(\frac{1+s}{2}\right)^4\left(m_i-m_{i+1}\rho\right)^n\left(m_{i+1}-m_i\rho\right)^p\cdot\Gamma\left(\frac{n+s+k+2}{2}\right)\cdot\Gamma\left(\frac{p+s+k+2}{2}\right)\frac{1}{4}\frac{1}{\mathrm{e}^{-\frac{m_i^2}{2\sigma^2}}\sum_{t=T+1}^{\infty}\frac{m_i^{2t}}{t!2^t\sigma^{2t}}}+\mathrm{e}^{-\frac{m_i^2}{2\sigma^2}}\sum_{t=T+1}^{\infty}\frac{m_i^{2t}}{t!2^t\sigma^{2t}}$$

4.4.4 Probability of detection: Twin Test

To evaluate the truncation error of the detection probability of the twin test in (4.36), we need to consider the P_D relative to the lower threshold, (4.35). Following the same approach as before, and after some algebra, we can finally write the expression of the truncation error for the twin test as follows:

$$\varepsilon_{EMGQ\max}=\frac{e^{-\frac{m_{i+1}^2+m_i^2-2\cdot\rho\cdot m_i m_{i+1}}{2\sigma^2\left(1-\rho^2\right)}}}{\pi^2}\cdot\sum_{n=0}^{\infty}\sum_{p=0}^{\infty}\sum_{k=0}^{\infty}\sum_{s=0}^{\infty}\frac{2^{\frac{(2k+p+n+6s)}{2}}}{n!p!k!s!}\left(\frac{1}{\sigma}\right)^{n+p}\rho^{k+s}\cdot\left(\frac{1}{1-\rho^2}\right)^{\frac{n+p-2}{2}} \tag{4.43}$$
$$\cdot\Gamma\left(\frac{1+s}{2}\right)^4\left(m_i-m_{i+1}\rho\right)^n\left(m_{i+1}-m_i\rho\right)^p\cdot\Gamma\left(\frac{n+s+k+2}{2}\right)\cdot\Gamma\left(\frac{p+s+k+2}{2}\right)\frac{1}{4}\frac{1}{\mathrm{e}^{-\frac{m_i^2}{2\sigma^2}}\sum_{t=T+1}^{\infty}\frac{m_i^{2t}}{t!2^t\sigma^{2t}}}+\mathrm{e}^{-\frac{m_i^2}{2\sigma^2}}\sum_{t=T+1}^{\infty}\frac{m_i^{2t}}{t!2^t\sigma^{2t}}$$

Finally, it has to be noted that (4.38)-(4.43) become zero for sufficiently high M, confirming the validity of the approximation of the series to a finite number of terms.

4.5 Numerical results

Several simulation trials have been performed to validate the twin-test acquisition procedure, versus the conventional power detector approach, in the case of correlated cells. The P_D of the new detector is evaluated under the CFAR procedure versus Signal-to-Noise-Ratios (SNR) of practical interest, and for different values of the synchronization delay between the transmitter and receiver. The P_D has been evaluated both in analytic way, i.e. using eq. (4.34) and (4.36) and by means of simulation.

In the reported analysis, a $P_{FA}=10^{-4}$ and additive white Gaussian noise (AWGN) have been used. We consider a correlation coefficient between contiguous cells of 1/2 and 2/3 that corresponds, respectively, to consider 2 cells per sample and three cells per sample. Three cases of interest are investigated, namely *best*, *middle* and *worst* operating case. The best case represent an ideal case of perfect synchronization between transmitter and receiver, while the worst case of erroneous synchronization will happen if the cross-correlation computed for an offset, which is just in the middle between two cells. The middle case is an intermediate case of timing offset is randomly located between the best and worst cases. The P_D of both the conventional and new test is shown in Fig. 4-3 versus different values of the SNR for the best operating case, i.e. perfect synchronization between transmitter and receiver. The simulation results (markers) well match the theoretical ones (solid lines), thus validating the correctness of the mathematical analysis and assumptions of the previous Sections. The performance of the two detection strategies almost perfectly overlaps, for all the considered correlation coefficient values. This is not surprising, in fact, when there is no timing offset, the maximum of the cross-correlation function is equal to the cross-correlation peak and true acquisition is achieved in correspondence of the upper threshold. However, the best case is not the typical operating case in asynchronous communization. Then, in order to stress the different behavior of the new twin test the worst and middle operating cases have been considered. The resulting P_D for the worst operating case is depicted in Fig. 4-4. In this case, the twin test outperforms the conventional method for each correlation coefficient value. In fact, when there is a non-zero timing offset between

the incoming and locally generated code, the maximum of the cross-correlation function is not equal to the cross-correlation peak and the conventional testing variable may be under the conventional threshold (see Fig 4-1a and Fig. 4-1b). The best and worst cases represent the upper and lower bounds of the system's performance, respectively. Then, in order to assess the performance also in intermediate cases, typical of asynchronous acquisition systems, we consider also a middle timing offset. Fig. 4-5 reports the P_D for the middle case versus different SNR values. The new acquisition method outperforms the conventional approach also in this case.

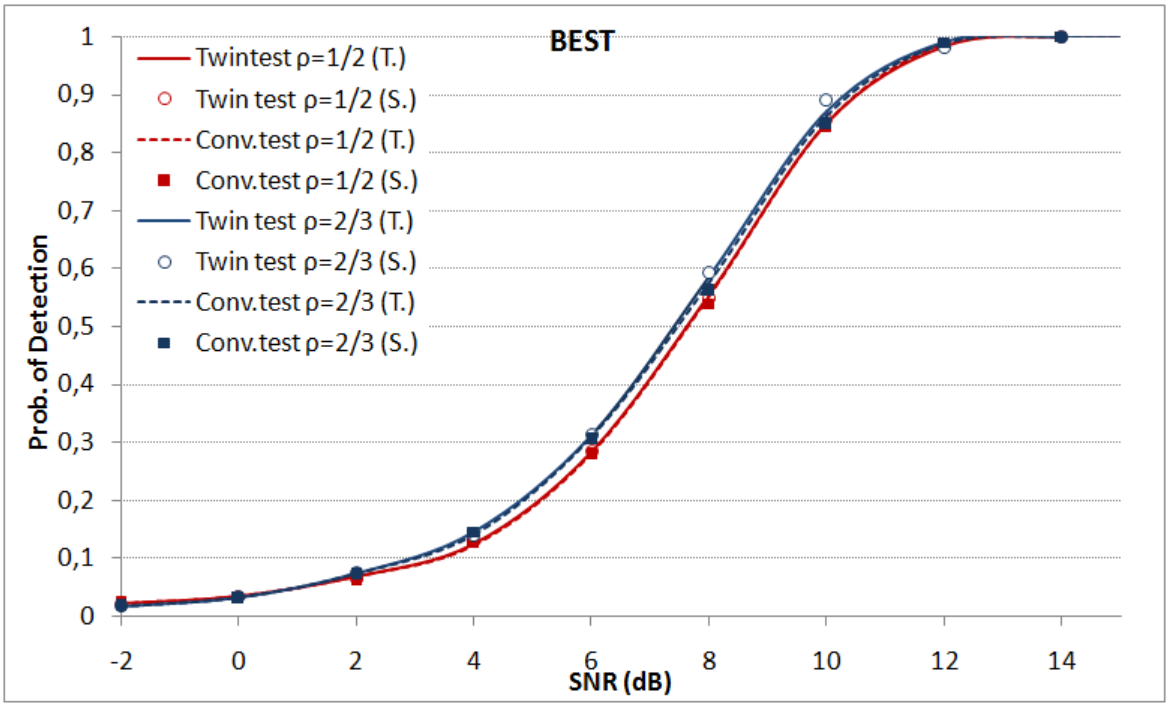

Figure 4-3 Simulated (S.) and theoretical (T.) results for the P_D versus SNR (with a $P_{FA} = 10^{-3}$) of both the conventional and twin test methods in the best case.

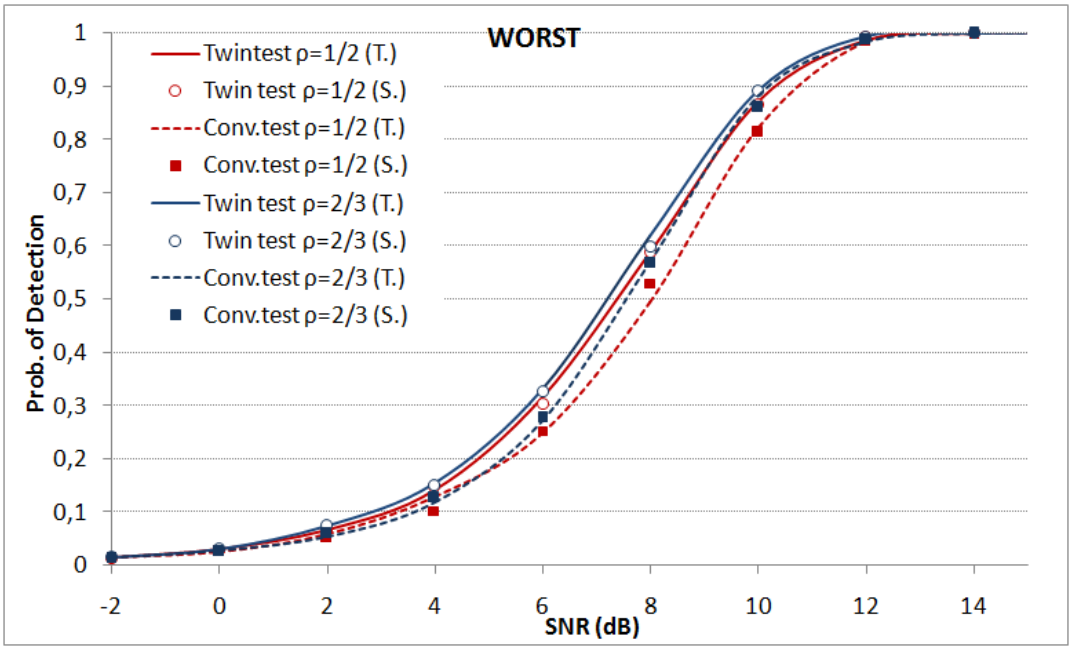

Figure 4-4 Simulated (S.) and theoretical (T.) results for the P_D versus SNR (with a P_{FA} =10^{-3}) of both the conventional and twin test methods in the worst case.

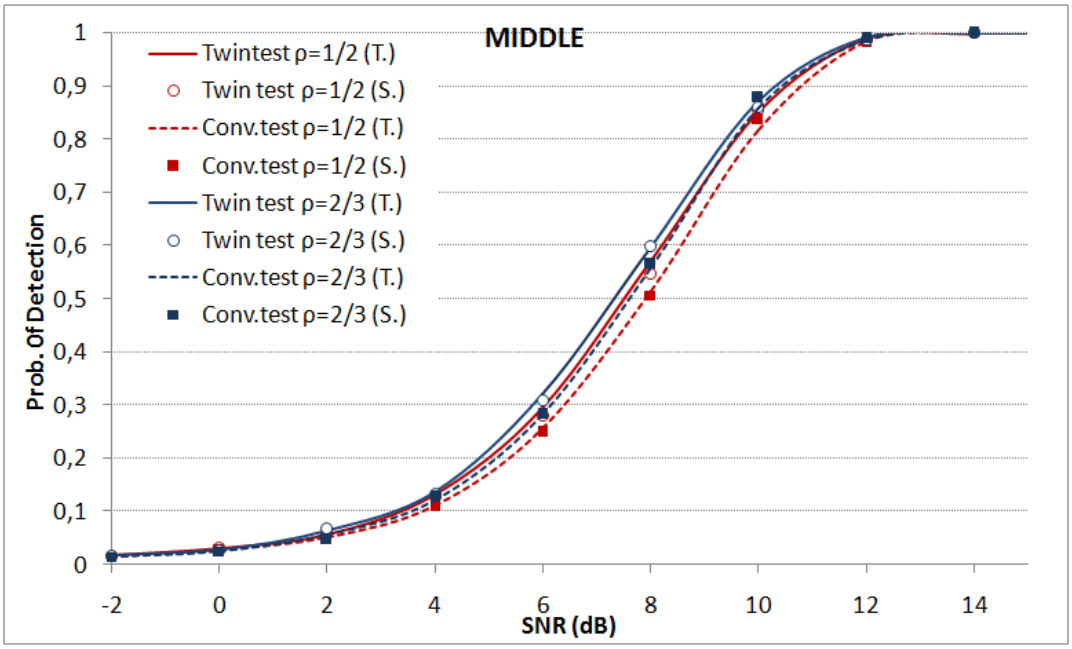

Figure 4-5 Simulated (S.) and theoretical (T.) results for the P_D versus SNR (with a P_{FA} =10^{-3}) of both the conventional and twin test methods in the middle case

As it can be seen from the graph, the two detection approaches have the same behaviour in the best case, but the performance of the novel test strongly increases when the timing offset starts worsening for a wide range of typical operating cases. In particular, the proposed method increases the detection probability up to 10% and 5% in the worst and middle case, respectively. Such a performance increasing results in a relative detection gain of 30% (in the worst case) and 10% (in the middle case) versus the conventional approach, considering a $P_D = 0.5$.

This performance gain is extremely relevant in typical code acquisition scenarios. In fact, it has a great impact on the minimization of the mean acquisition time (MAT) that is a relevant parameter for evaluating the performance of code acquisition strategies [47],[48],[51],[53]. In fact, in high-mobility communications scenarios, where initial cell search procedures are very frequent, code acquisition should be as fast as possible. Hence, effective methods are needed for ensuring fast and reliable code acquisition, such as the one introduced in this thesis. The MAT is defined as the time needed, on average, for acquiring a correct cell, and it can be expressed as follows:

$$T_{ACQ} = q \cdot [N_c + T_p P_{FA}] \cdot \frac{2 - P_D}{2 \cdot P_D}, \tag{4.44}$$

where $q = 1/\Delta$ is the number of cells per sample, N_c is the test's duration for each code offset candidate, T_p is the penalty time for an erroneous (i.e. false) acquisition. The MAT is directly related to the probability of detection, and a higher P_D results in a lower MAT. Fig. 4-6 shows the MAT of the two methods for the best operating case, while the worst and middle cases are reported in Fig. 4-7 and Fig. 4-8, respectively.

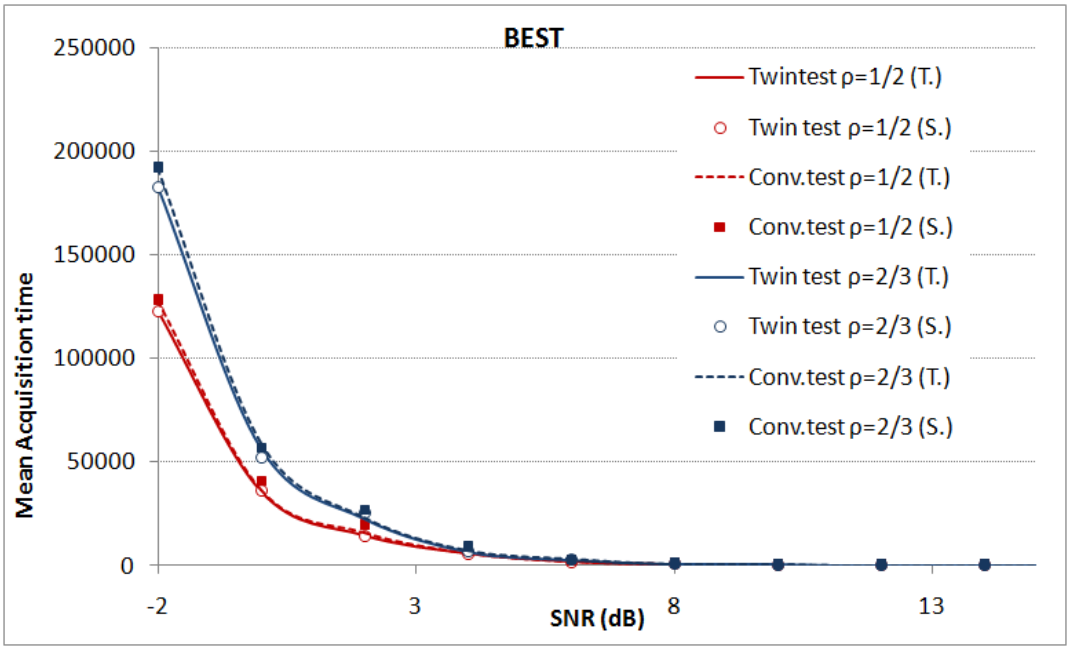

Figure 4-6 Simulated and theoretical results for the *MAT* of the conventional and twin test methods in the best case

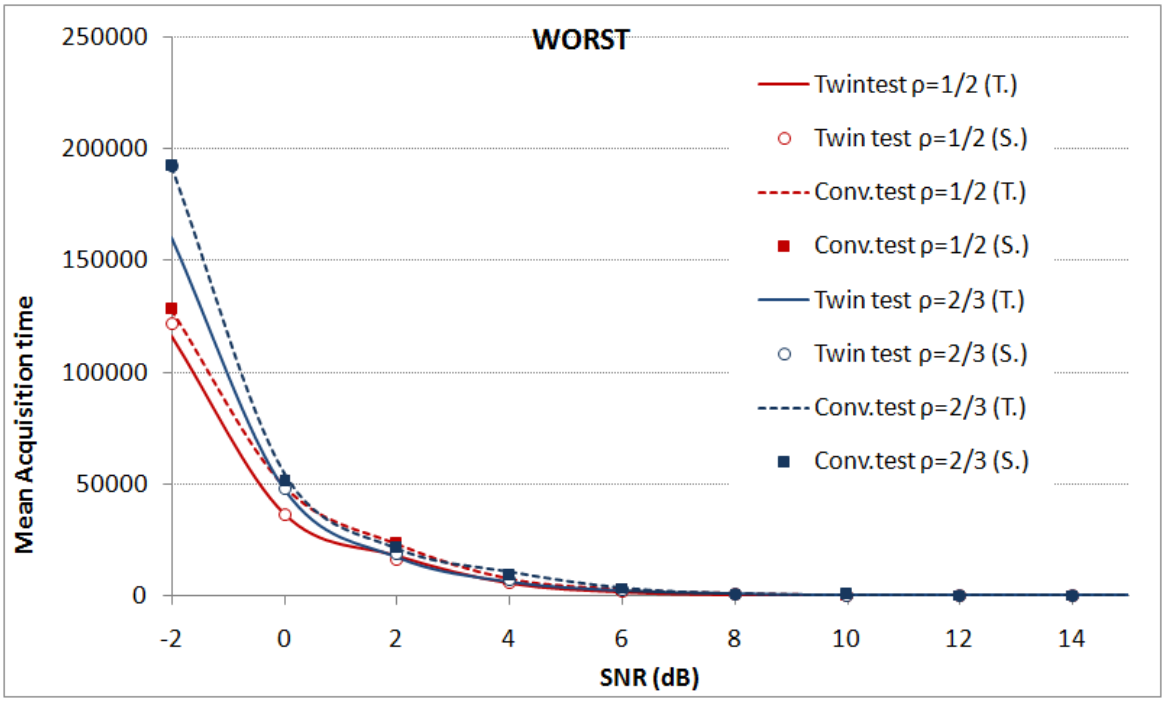

Figure 4-7 Simulated and theoretical results for the *MAT* of the conventional and twin test methods in the worst case.

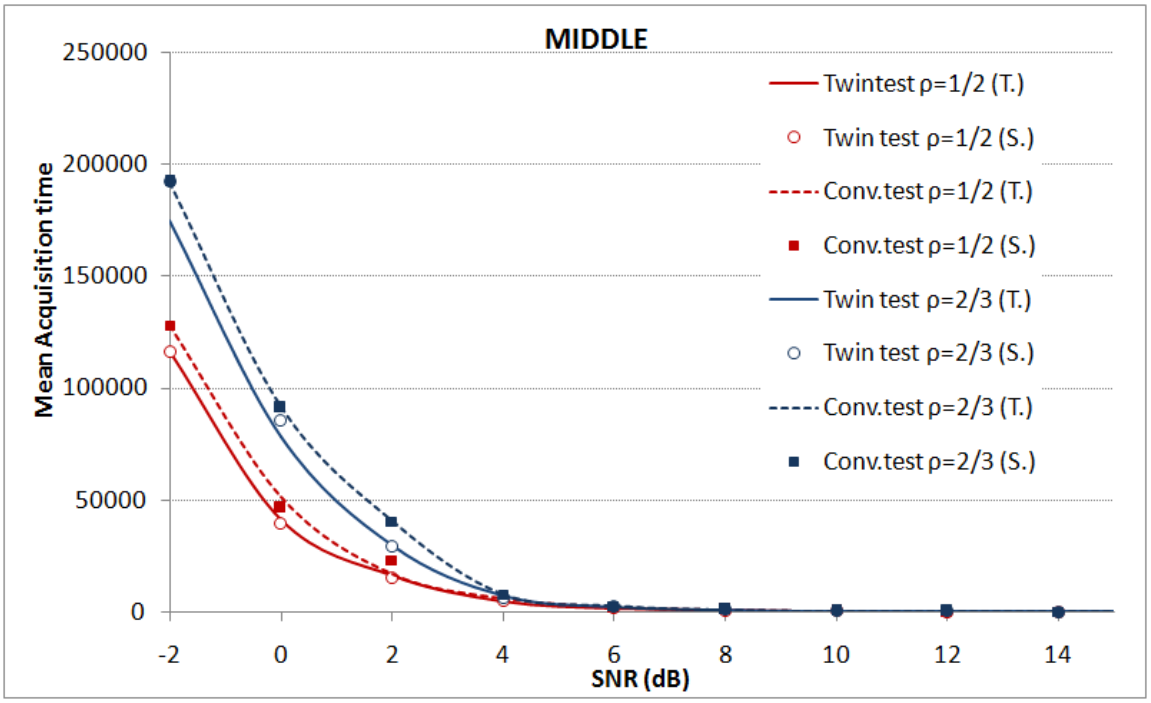

Figure 4-8 Simulated and theoretical results for the *MAT* of the conventional and twin test methods in the middle case

Again, the performance of the two methods are almost the same in the best case, but the performance of the twin test strongly increases when the timing offset starts worsening for a wide range of typical operating cases.

It has to be noted that the term $q \cdot [N_c + T_p \cdot P_{FA}]$ is the same for both the two methods. It depends on the number of cells q, on the number of samples over which the correlation is computed N_c, on the penalty time T_p, and probability of false alarm P_{FA}. All these parameters are related only to the correlation step, which is the same for both the procedures. Then, to better assess how much the increasing in the P_D reflects in a MAT gain, we define the MAT ratio, R_T, as the ratio between the MAT of the conventional and twin test, respectively. The MAT ratio for the best case is depicted in Fig. 4-9 while Fig. 4-10 shows the worst case, for different P_{FA}. Finally, Fig. 4-11 depicts the MAT ratio in the middle case. Again, the twin-test outperforms the conventional approach (maximum gain is about 20%).

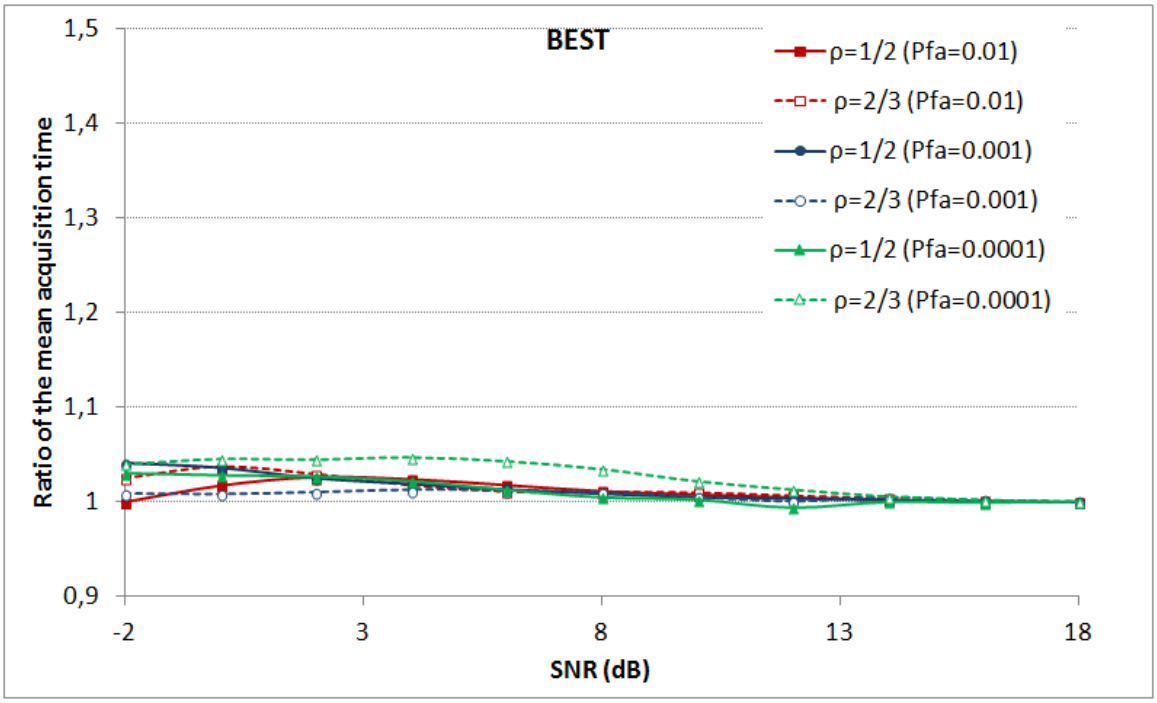

Figure 4-9 Results of the MAT ratio for different P_{FA} in the best case

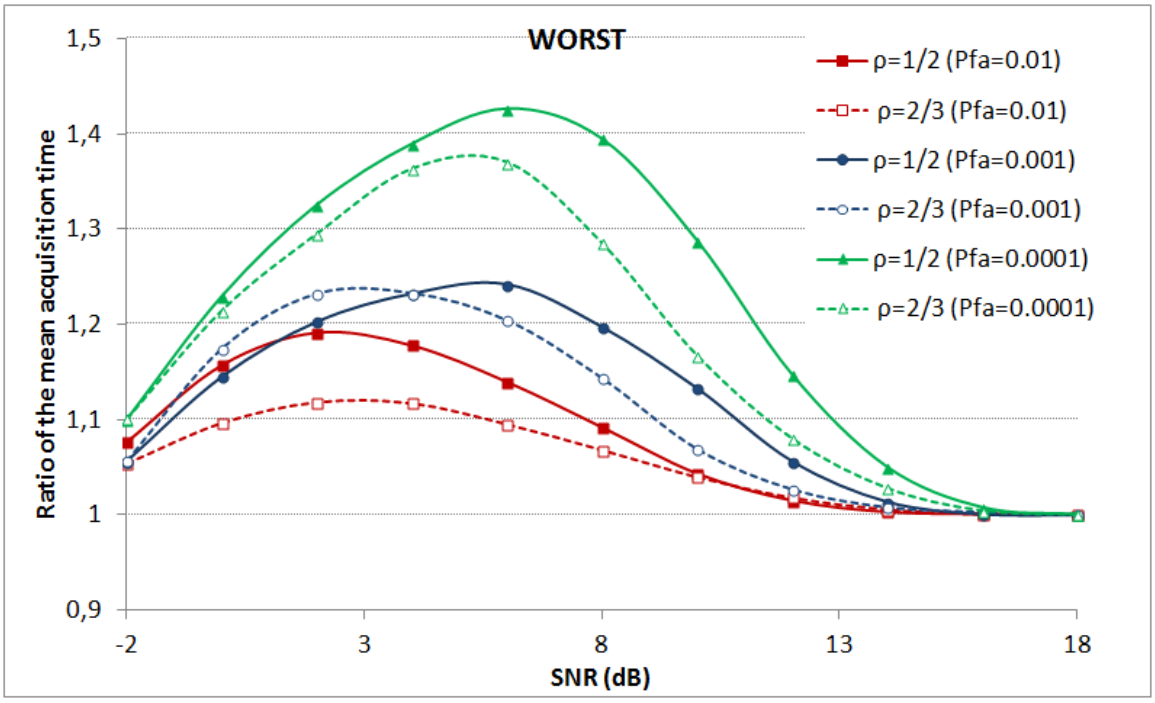

Figure 4-10 Results of the MAT ratio for different P_{FA} in the worst case.

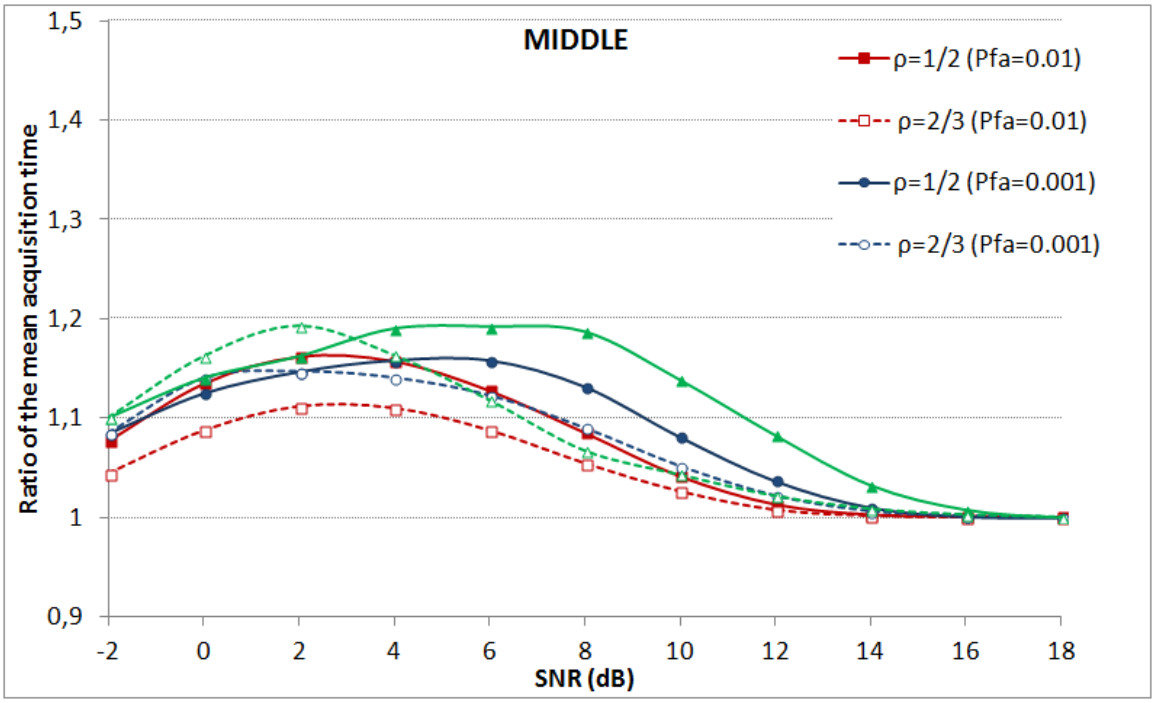

Figure 4-11 Results of the MAT ratio for different P_{FA} in the middle case

It can be easily seen from Figs. 3-5 that the new method with $\rho = 2/3$ is only marginally better than the case $\rho = 1/2$. In fact, as the cell size decreases (i.e. as the number of cells per sample increases), the correlation between two contiguous cells becomes higher and the detection performance improves. But, this results in an increasing of the MAT, that is proportional to the number of cells per sample, according to (4.44).

In fact, the more performing method in terms of P_D ($\rho = 2/3$) becomes poorer in terms of MAT, which increases of 50% and 35% in the best and worst case, respectively.

Hence, we can consider the scenario of $\rho = 1/2$ as the common operating scenario and evaluate the P_D of both the conventional and twin test for different timing offset. The P_D versus different code offsets (i.e. from the best to the worst operating case) is depicted in Fig. 4-12. The two detection approaches have the same behaviour in the best case, but the performance of the novel test strongly increases when the timing offset starts worsening for a wide range of typical operating cases.

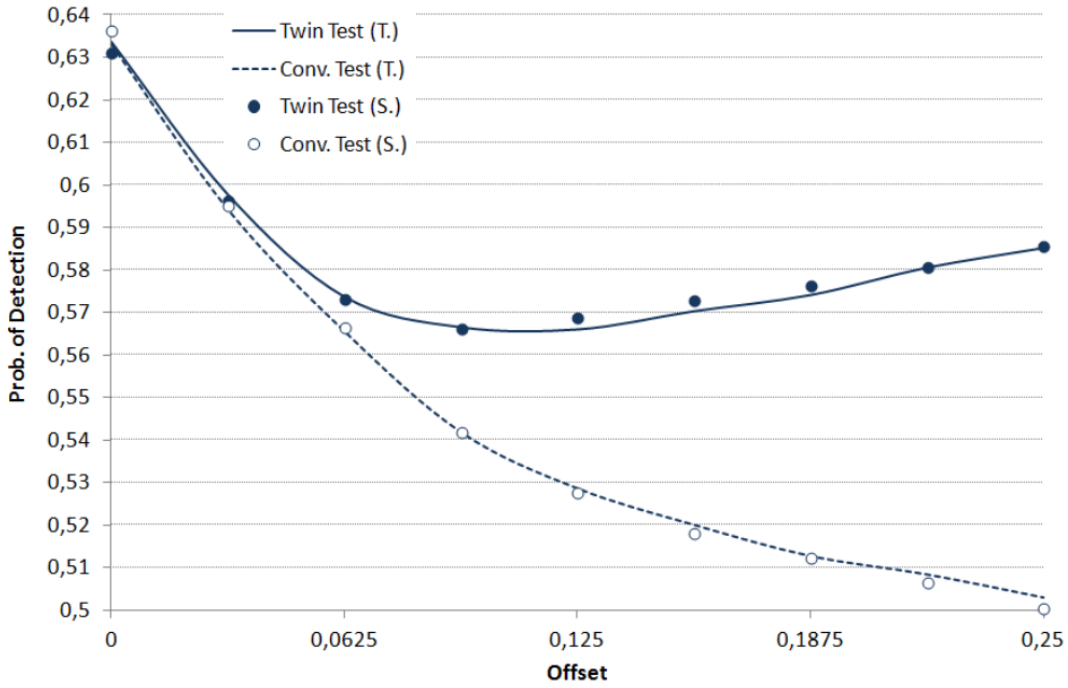

Figure 4-12 Simulated (S.) and theoretical (T.) results for the P_D of both the conventional and twin test methods versus the actual time offset, SNR=8 dB, $P_{FA}=10^{-3}$ and $\rho = ½$.

Moreover, it has to be noted that only negligible increasing of the system computational complexity is introduced by the twin test. In fact, code acquisition consists of a serial search over the correlator's output, over-sampled at more than one cell per sample. Then, the conventional procedure compares each variable to one threshold, while the new method tests each pair of variables with two thresholds. Therefore, the computational cost is mainly due to the former correlation stage that is identical for both the methods, while the new approach requires just one more comparison per cell operated on the same testing variables followed by a Boolean operation. In addition, it has to be noted that the threshold setting stage is usually performed off-line because is time-consuming. In practice, the thresholds are usually pre-computed and stored on look-up tables for several SNR values. Therefore, the computational required for solving the constrained optimization problems and setting the pair of threshold by is neglible for the implementation point of view.

4.6 Conclusions

In this chapter, the design and analysis of serial search code acquisition systems with correlated (timing) cells has been discussed. The novelty introduced in this thesis is twofold. First a new method, the twin test, has been introduced for the performance improvement of initial code acquisition, taking into account correlated cells. Then, a new special function is here derived to express the system error probabilities in a closed form. The analytical results show that the new procedure can offer better performance than the conventional scheme based on the cell-by-cell detection, with a negligible increasing of the system computational complexity. Moreover, the twin test can be effectively used for reducing the mean acquisition time in code synchronization wireless communications.

4.7 Appendix

We now give a proof of the series expansion in equation (4.6). The angular integral in (4.5) is in the form:

$$\int_0^{2\pi}\int_0^{2\pi} e^{x\cos\theta_1 + y\cos\theta_2 + z\cos(\theta_1-\theta_2)}d\theta_1 d\theta_2 \tag{A1}$$

The exponential function in the above expression can be written as the product of four exponential functions as follows

$$\int_0^{2\pi}\int_0^{2\pi} e^{x\cos\theta_1 + y\cos\theta_2 + z\cos(\theta_1-\theta_2)}d\theta_1 d\theta_2 = \int_0^{2\pi}\int_0^{2\pi} e^{x\cos\theta_1} e^{y\cos\theta_2} e^{z\cos\theta_1\cos(\theta_2)} e^{z\sin\theta_1\sin(\theta_2)}d\theta_1 d\theta_2 \tag{A2}$$

We can expand each of the four exponential functions in term of the Taylor's series $e^x = \sum_{n=0}^{\infty}\frac{x^n}{n!}$ as follows:

$$\int_0^{2\pi}\int_0^{2\pi} e^{x\cos\theta_1} e^{y\cos\theta_2} e^{z\cos\theta_1\cos\theta_2} e^{z\sin\theta_1\sin\theta_2}d\theta_1 d\theta_2 =$$
$$\int_0^{2\pi}\int_0^{2\pi}\sum_{n=0}^{\infty}\frac{(x\cos\theta_1)^n}{n!}\sum_{p=0}^{\infty}\frac{(y\cos\theta_2)^p}{p!}\sum_{k=0}^{\infty}\frac{(z\cos\theta_1\cos\theta_2)^k}{k!}\sum_{s=0}^{\infty}\frac{(z\sin\theta_1\sin\theta_2)^s}{s!} \tag{A3}$$

Now, interchanging the operations of summation and integration, it is possible to split the double integral in (A3) in two single integrals

$$\sum_{n=0}^{\infty}\sum_{p=0}^{\infty}\sum_{k=0}^{\infty}\sum_{s=0}^{\infty}\frac{x^n y^p z^{s+k}}{n!}\int_0^{2\pi}(\cos\theta_1)^{n+k}(\sin\theta_1)^s d\theta_1\int_0^{2\pi}(\cos\theta_2)^{p+k}(\sin\theta_2)^s d\theta_2 \tag{A4}$$

Hence, considering $q=n+k$ for the first integral and $q=p+k$ for the second one, all the computation can be reduced to the problem of solving the following basic integral:

$$\int_0^{2\pi}(\cos\theta)^p(\sin\theta)^s d\theta \tag{A5}$$

which has non-zero values only when q and p are even, and can be computed in term of the hypergeometric regularized function (see ref [10]):

$$\int_0^{2\pi}(\cos\theta)^p(\sin\theta)^s d\theta = 2^{2(1+s)}\Gamma\left[\frac{1+s}{2}\right]^2 {}_2\bar{F}_1\left(\frac{1+s}{2},-q,1+s,2\right) \tag{A7}$$

Finally, with the above expression, the integral in (A1) can be computed as follows:

$$\int_0^{2\pi}\int_0^{2\pi} e^{x\cos\theta_1}e^{y\cos\theta_2}e^{z\cos\theta_1\cos\theta_2}e^{z\sin\theta_1\sin\theta_2}d\theta_1 d\theta_2 =$$
$$\sum_{n=0}^{\infty}\sum_{p=0}^{\infty}\sum_{k=0}^{\infty}\sum_{s=0}^{\infty}\frac{x^n y^p z^{s+k}}{n!}2^{2(1+s)}\Gamma\left[\frac{1+s}{2}\right]^4 {}_2\bar{F}_1\left(\frac{1+s}{2},-n-k,1+s,2\right){}_2\bar{F}_1\left(\frac{1+s}{2},-p-k,1+s,2\right) \tag{A8}$$

Where:

$${}_2\bar{F}_1(a,b,c,z) = \begin{cases} \sum_{k=0}^{\infty}\frac{(a)_k(b)_k z^k}{\Gamma(c+k)k!}, & |z|<1 \\ \frac{\pi}{\sin[\pi(b-a)]}\left(\frac{(-z)^{-a}}{\Gamma(b)\Gamma(c-a)}\sum_{k=0}^{\infty}\frac{(a)_k(a-c+1)_k z^{-k}}{\Gamma(a-b+k+1)} - \frac{(-z)^{-b}}{\Gamma(a)\Gamma(c-b)}\sum_{k=0}^{\infty}\frac{(b)_k(b-c+1)_k z^{-k}}{\Gamma(-a+b+k+1)}\right), & |z|>1\wedge(a-b)\notin Z \end{cases} \tag{A9}$$

And

$(a)_k = \frac{\Gamma(a+k)}{\Gamma(a)}$ is the Pochhammer symbol

Chapter 5 THE RAND METHOD FOR CODE ACQUISTION IN LONG TERM EVOLUTION

5.1 Introduction

In the last years, there has been an explosive growth in wireless/mobile networks and obviously an ever-growing demand for platforms with mobile multimedia application support. Users are requesting more and more high rate data transmissions, and to answer their needs the Long Term Evolution (LTE) standards have been developed in the 3rd Generation Partnership Project (3GPP) as the future wireless communication system [60]. LTE is intended to enhance third Generation (3G) systems in order to guarantee higher peak data rate and extreme high mobility support [61]. It aims at supporting a wide range of cellular deployment scenarios, including indoor, urban, sub-urban and rural environments, covering both low and high User Equipment (UE) mobility conditions (up to 350 or even 500 km/h). Deployed carrier frequencies are likely to range from 400 MHz to 4 GHz, with bandwidths ranging from 1.4 to 20 MHz. LTE uses OFDM modulation and OFDMA technique for the downlink transmissions in order to provide high data rate and mobility [62]. In these modulations at each user is assigned one of the sets of orthogonal sub-carries in which the total bandwidth is divided. The sub-carrier assignment is not fixed, but on the contrary it can change according to the specific service requirements, traffic congestion or channel conditions.

The initial cell search process is especially important for LTE systems, which rely heavily on the orthogonality of the uplink and downlink transmission and reception to optimize the radio link performance. As in conventional cellular systems, the mobile terminal in an LTE system acquires time and frequency synchronization by processing the synchronization channel. A mobile device wishing to access a LTE system must undertake an initial cell search procedure, which enables the UE to achieve both time and frequency

synchronization with the serving base station (eNodeB). LTE aims at providing very high mobility support and high data rate. Hence, a key requirement for the LTE cell search procedure is that the delay for the UE to detect a newly appearing cell and report it to the eNodeB should be less than a prescribed acceptable threshold [63]. The design of the synchronization channel is being developed within the standardization activities of 3GPP Long Term Evolution and is it one of the key issues in the design of the system. The contribution of this chapter is to resolve some of the issues in the deployment of the design of an efficient synchronization process, focusing the attention on the initial cell search procedure. In particular, an innovative signal processing method for the initial cell search of 3GPP LTE wireless networks is proposed. The new method, can be applied to every LTE transmission standard, since it requires modifications only at the receiver side.

The reminder of this chapter is organized as follows. Section 2 illustrates the basic framework about the initial cell search in LTE systems, along with the conventional methods. In Section 3 the new acquisition method is illustrated. Finally, simulation results and comparisons are outlined in Section 4.

5.1 System model

A LTE downlink radio frame (10 ms) consists of 10 sub-frames, each split into two time slots of 0.5 ms. Each slot comprises 7 OFDM symbols in the case of the normal CP length or 6 if the extended CP is configured in the cell. In the frequency domain, resources are grouped in units of 12 sub-carriers that occupies a total of 180 kHz. One unit of 12 sub-carriers for a duration of one slot is termed a Resource Block (RB). The smallest unit of resource is the Resource Element (RE), which consists of one sub-carrier for the duration of one OFDM symbol. A resource block consists in 84 resource elements in the case of the normal cyclic prefix length, and in 72 resource elements if the extended cyclic prefix is configured in the cell [63]. The time and frequency structure of a LTE for the normal prefix case is depicted in Fig. 5-1.

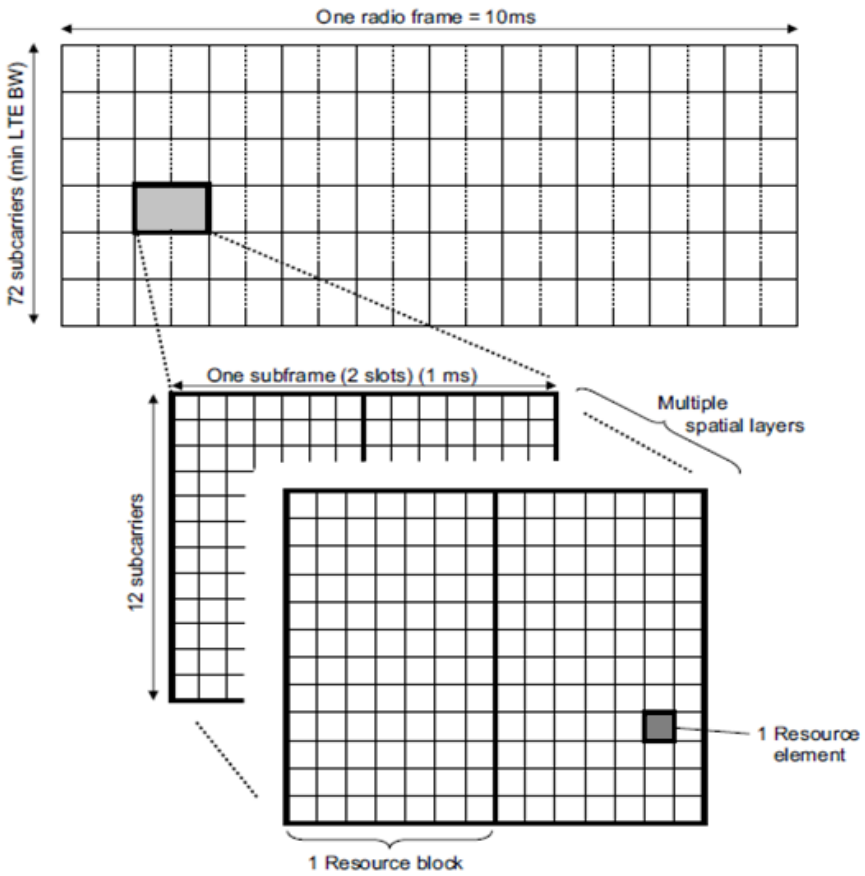

Figure 5-1 Basic time-frequency resource structure of LTE (normal cyclic prefix case).

In LTE systems, the initial cell search procedure is based on the detection of two signals transmitted in the downlink, the Primary Synchronization Signal (PSS) and the Secondary Synchronization Signal (SSS). The cell search is a two stage procedure, firstly the UE detects the PSS, and secondly detects the SSS. The PSS and SSS are transmitted in the central six RBs, and they both occupy the central frequency: 1.08MHz of 72 subcarriers 62 of which for the signal itself and 2 sets of 5 guard-bands' sub-carriers. The allocations is the same regardless of the transmission bandwidth, (e.g. 5MHz, 10MHz and 20MHz) [64]-[65]. This choice enables the UE to synchronize with the network without any a priori knowledge about the systems bandwidth. The primary purposes of these two signals are to enable time and frequency synchronization, to provide the UE with the physical layer cell identity, and to inform the UE whether the cell uses Frequency Division Duplex (FDD) or Time Division Duplex (TDD).

The synchronization signals are transmitted periodically, twice per radio frame (10 ms). The PSS and SSS structure in time for the FDD case is shown in Figure 5-2 whereas Fig. 5-3 shows the TDD case. In an *FDD* cell, the PSS is always located in the last OFDM symbol of the first and 11th slots of each radio frame, thus enabling the UE to acquire the slot boundary timing independently of the Cyclic Prefix length. The SSS is located in the symbol immediately preceding the PSS. This design choice enables coherent detection of the SSS, under the assumption that the channel coherence duration is significantly longer than one OFDM symbol. In a *TDD* cell, the PSS is located in the third symbol of the 3rd and 13th slots, while the SSS is located three symbols earlier. Coherent detection can be used, under the assumption that the channel coherence time is significantly longer than four OFDM symbols.

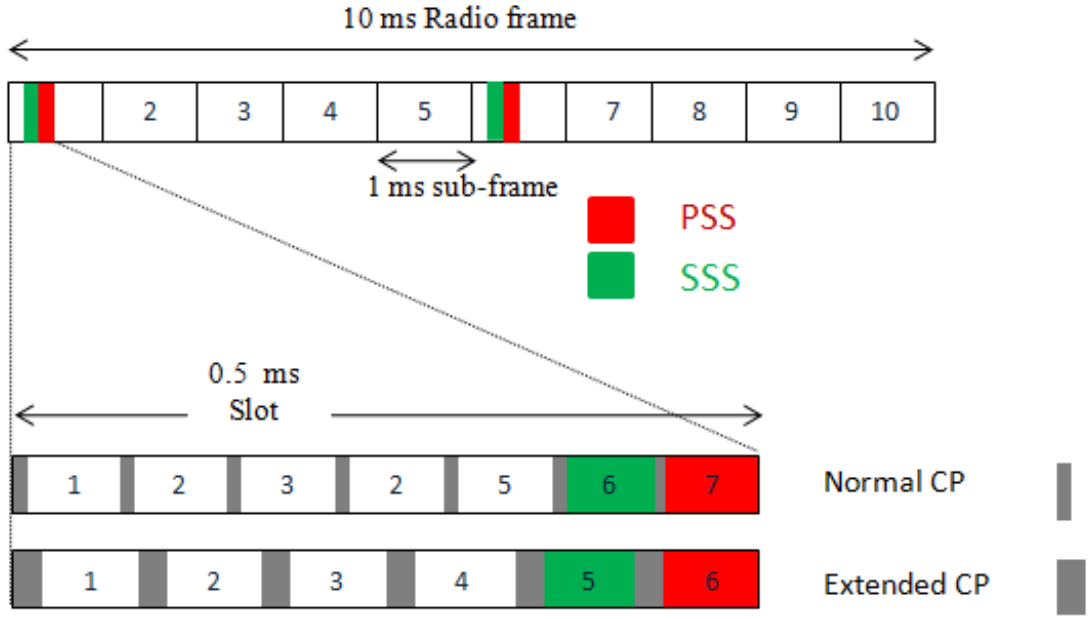

Figure 5-2 PSS and SSS frame and slot structure in time domain in the FDD case

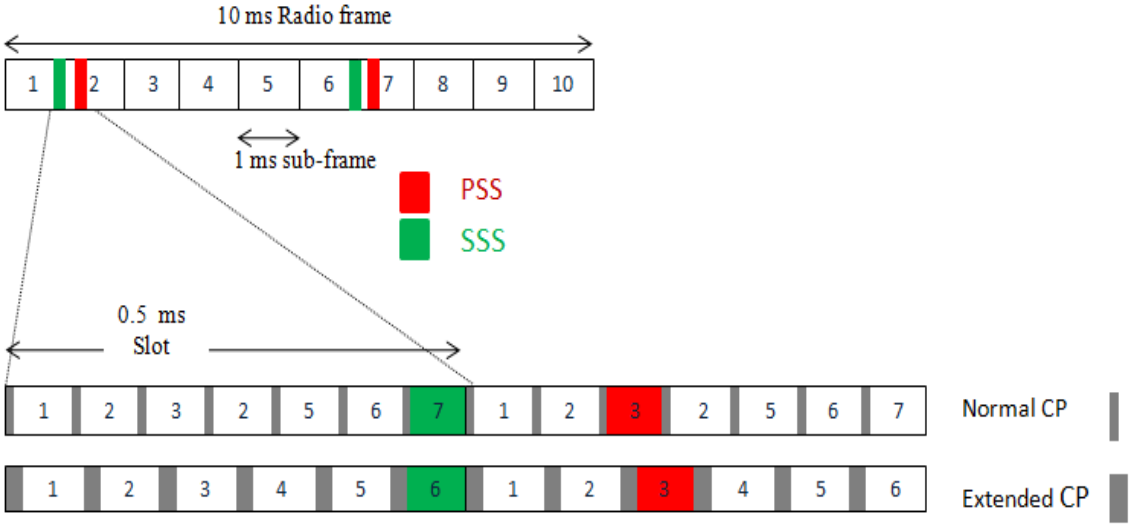

Figure 5-3 PSS and SSS frame and slot structure in time domain in the TDD case

A large number of physical layer cell identities simplify the task of network planning. The *Physical layer cell identities* assignment of LTE are reported in Fig. 5-4. There are 504 unique physical layer cell identities, $N_{ID}^{(2)}$, grouped into 168 *physical layer cell identity*

groups, $N_{ID}^{(1)}$, of three identities [66]. The grouping is such that each physical layer cell identity is part of one and only one physical layer cell identity group [67]. A physical layer cell identity $N_{ID}^{cell} = 3N_{ID}^{(1)} + N_{ID}^{(2)}$ is uniquely defined by a number in the range of 0 to 167, representing the physical layer cell identity group, and a number in the range of 0 to 2, representing the physical-layer identity within the physical layer cell identity group [68]. The Physical layer cell identity and the Physical layer identity can be recognized using the PSS and the SSS, respectively as shown in Fig.5-4.

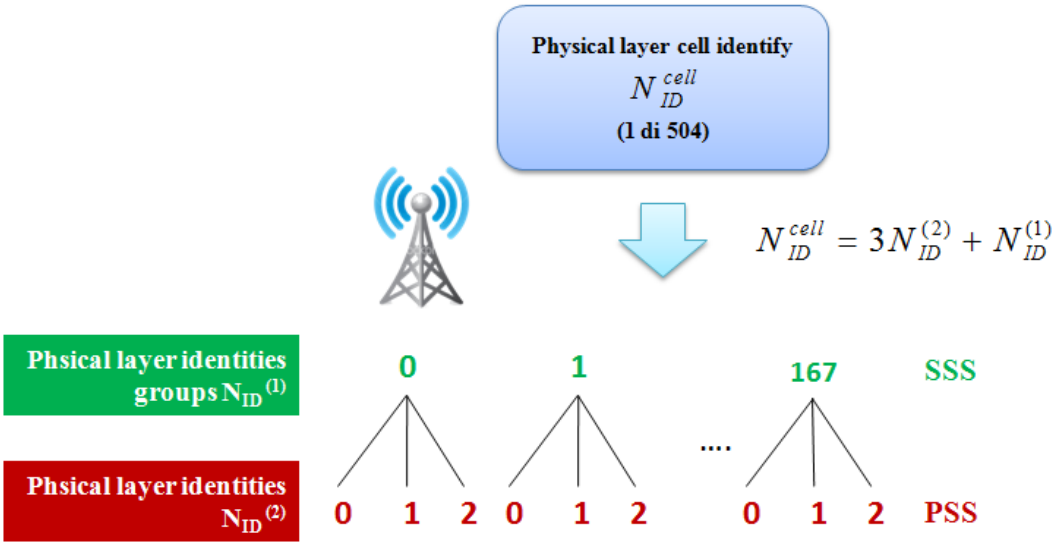

Figure 5-4 Physical layer cell identities in LTE

5.2 Conventional LTE initial cell search algorithms

5.2.1 Conventional method

The detection of the PSS is of the most critical issues of the synchronization process in LTE systems. In fact, since this is the first step to be achieved, its performance directly impacts all the synchronization process. The cell search procedure directly impacts on the performance improvements of the system, and hence synchronization with the eNodeB must be quickly accomplished and then easily maintained. The conventional method to detect the presence of the PSS is represented by the power detection approach [69]. Power detector is chosen to limit the computational costs of the decision device. In fact, as shown in the previous chapter, the power test first estimates the cross-correlation between the received signal and its locally generated replica. Then, it accumulates *W* blocks of the square magnitude of the estimated cross-correlation $R_w(\tau)$, in order to avoid the effect of the frequency and phase uncertainty:

$$Z_k(\tau) = \frac{1}{W}\sum_{w=1}^{W}\left|R_w(\tau)\right|^2 \qquad (5.1)$$

Finally, it compares the (*k*-th) currently examined decision variable $Z_k(\tau)$ to a pre-selected threshold *v* [17c]. Fig. 5 reports here the scheme conventional power detector method for LTE systems. The testing variable is represented by the (ordinate of the) maximum of the cross-correlation function between the received signal and its locally generated replica.

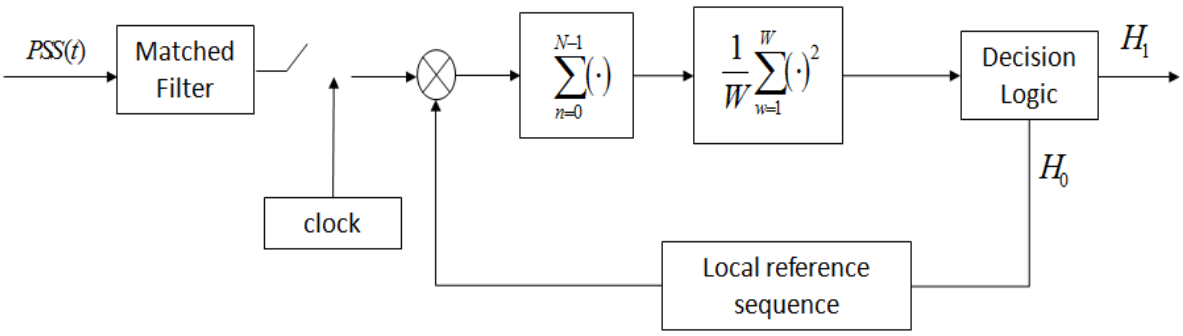

Figure 5-5 Block scheme of the conventional LTE power detector method, based on matched filter.

5.2.1 The PSS structure

To facilitate the timing and frequency offset detection within the eNodeB, three PSS symbol structures have been proposed in the scientific literature: repetitive pattern, symmetrical-and-periodic pattern, and non-repetitive pattern. In particular, a PSS symbol structure with time domain repetitive block is proposed in [70] and [71]. Specifically, Fig. 5-6a shows here the PSS symbol in the time domain with L (= 4 in this example) blocks of equal length (namely PSCH) and with the CP attached at the beginning of the structure. In [72], a symmetrical-and-periodic pattern is proposed for the PSS symbol structure. This solution is depicted in Fig. 5-6b where the block PSCHR is symmetrical reverse to the block PSCH. Finally, [73] proposes a PSS symbol structure with a non-repetitive pattern, as shown in Fig. 5-6c.

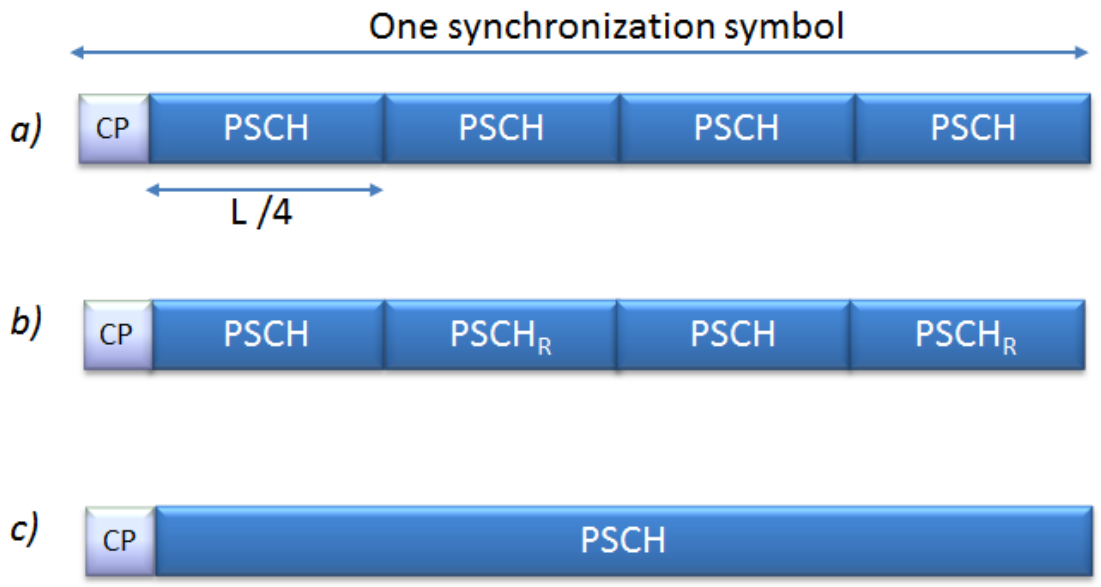

Figure 5-6 Symbol structure for synchronization with: a) repetitive pattern; b)symmetrical-and-periodic pattern; c) non-repetitive pattern

Regardless the specific structure, the PSS is generated from a frequency-domain Zadoff-Chu (ZC) sequence of length n = 63, with the DC element punctured, as expressed in the following:

$$d_u(n) = \begin{cases} e^{-j\frac{\pi un(n+1)}{63}} & n = 0,1,.....30 \\ e^{-j\frac{\pi un(n+1)(n+2)}{63}} & n = 31,.....61 \end{cases} \qquad u = 25, 29, 34 \tag{5.2}$$

The PSS expressed by (5.2) is then translated in the time domain through a Discrete Time Fourier Transform (DFT), whose length is usually equal to 128 or 256 bins [63]. The ZC sequences (also known as Generalized Chirp-Like sequences) are non-binary unit-amplitude sequences, which satisfy a Constant Amplitude Zero Autocorrelation (CAZAC) property [74]. The Zadoff-Chu are specially generated pseudorandom polyphase sequences

with perfect correlation properties. In particular, the most relevant ZC sequences' properties are as follows:

- The ZC sequence is periodic with period N_{ZC};
- The Discrete Fourier Transform (DFT) of a ZC sequence is another ZC sequence conjugated, scaled and time scaled; This means that a ZC sequence can be generated directly in frequency domain without the need for a DFT operation. For this reason, correct acquisition can be performed either in frequency or in time domain.
- The ZC sequence has ideal cyclic autocorrelation;
- The cross correlation between two prime length ZC sequences, i.e. With different *u*, is constant and equal $1/\sqrt{N_{ZC}}$

All these properties make PSS particularly interesting to obtain accurate time and frequency synchronization metrics. Nonetheless the ZC sequences have ideal cyclic autocorrelation properties, it has to be noted that LTE receivers perform *linear* cross-correlation between the incoming (noisy) ZC sequence and its locally generated replica. Unfortunately, the linear autocorrelation of a ZC sequence is not ideal and presents side-lobs that may originate errors and consequently false acquisitions. In particular, Fig. 5-7 reports the ideal (i.e. without noise) autocorrelation of a ZC sequence and two more autocorrelations in presence of a contribution of noise equal to -10dB and -15dB, respectively. As it can be easily seen from the graphs, the side lobs of the autocorrelation in absence of noise are not very distant from the main peak, and this difference reduces as the noise on the channel increases. At SNR = -15dB the side lobes sometimes can be even greater than the main peak, causing errors and consequently false alarms. Moreover, the PSS sequence transmitted in the LTE cell is always the same for each synchronization block (and for each of the three PSS structures). This means that the averaging operation expressed by (5.2) is necessary to mitigate the noise effects introduced by the channel but is not sufficient to avoid or eliminate the side-lobs of the cross-correlation.

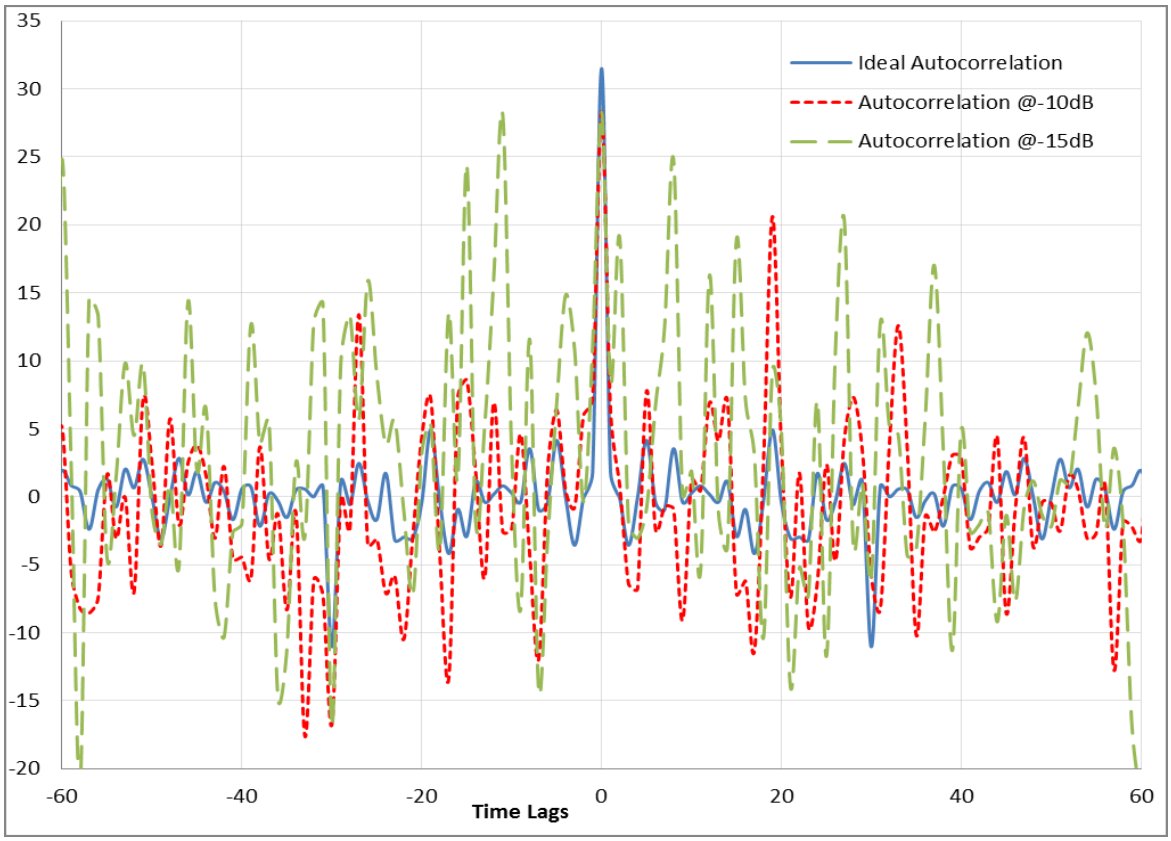

Figure 5-7 Ideal (i.e. in absence of noise) autocorrelation of a ZC sequence and two autocorrelations presence of noise at SNR = -10dB and -15 dB, respectively

5.3 Innovative LTE initial cell search algorithm

In this doctorate dissertation a novel cell search procedure, named the Rand method, for LTE system is proposed. The method can be applied to any PSS symbol structure and to any LTE transmission standard, since all the required modification is localized only at the receiver side. In particular, the proposed procedure maximizes the main peak of the cross-correlation and, at the same time, minimizes the side-lobes. This goal can be achieved with the following operations.

1. The samples of the received PSS sequence are first scrambled with a randomized rule that change from one synchronization block to another.
2. The samples are grouped into L (≥ 2) blocks of equal length, (in Fig. 5-8 $L = 2$). It is important to underline that the PSS samples are randomly chosen from the

received PSS signal and the randomization rule is different for each synchronization block.

3. The same operations are performed also on the locally generated replica of the synchronization signal.
4. The cross-correlation function between the locally generated and the received PSS is evaluated (one for each block).
5. A decision variable is obtained, as expressed by (5.2).

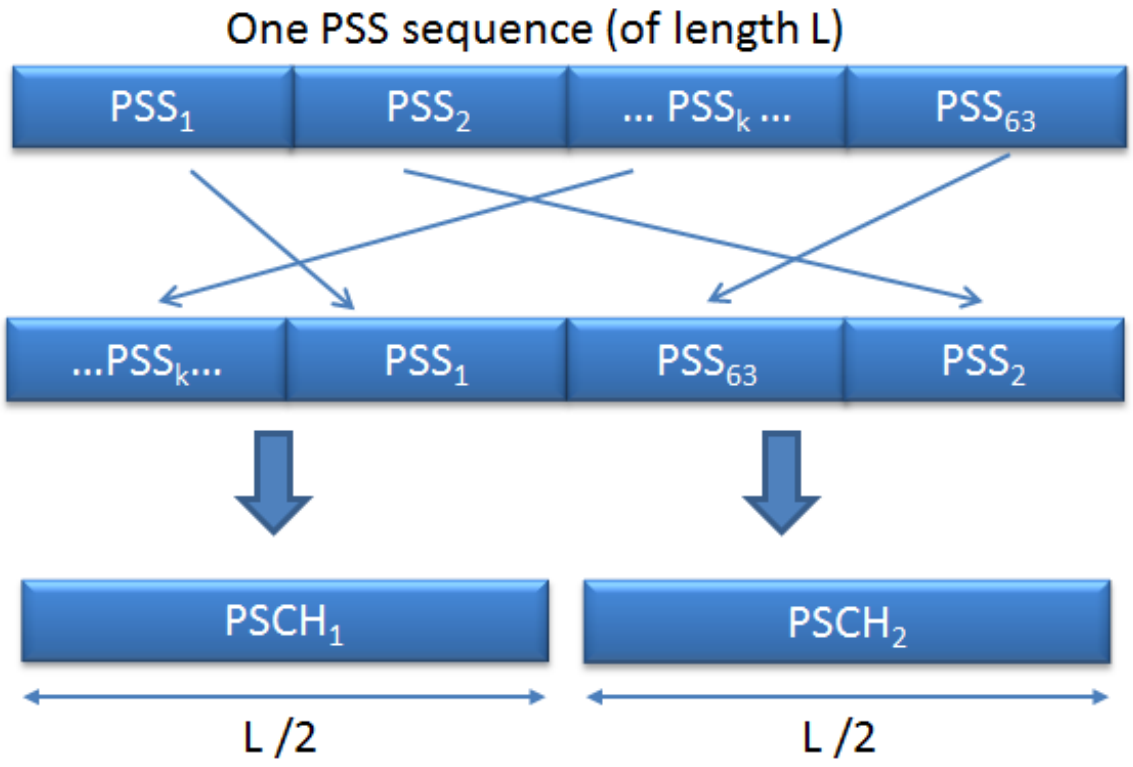

Figure 5-8 Example of randomization and division in 2 blocks

The rationale behind the proposed method is as follows. The employed randomization rule is different from one block to the following one, hence, the cross-correlation between the received and the local PSS averaged over a number *W* of synchronization symbols, presents always the same main peak, but different values of the side-lobs. In other words, the cross-

correlation value at lag 0 is the same as in the conventional procedure, whereas the cross-correlations for all the other lags are always different from one symbol to the following one. Conversely, in the conventional approach the cross-correlation is always the same (in absence of noise) for each lag and for each synchronization block [74]. As a consequence, averaging the decision variable over a number *W* of synchronization symbols reduce the noise contribution but allows no mitigation of the side-lobs that can hence originate false locks [75]. In the new method, this is avoided because of the randomization rule that has been applied: averaging over *W* synchronization symbols allows maximizing the ratio between the main peak and the values of the side-lobs. In addition, averaging over a number of blocks allows us to consider the decision variable expressed by (5.2) as an asymptotically Gaussian variable according to the central limit theorem. The testing variable is then compared with a threshold value, according to the desired false alarm probability, and the test threshold evaluated from a straightforward evaluation of the Gaussian integral as follows:

$$v = E\left[Z_k(\tau)\right] H_0 + \frac{1}{\sqrt{2\,\mathrm{var}\left[Z_k(\tau)\right] H_0}} erfc^{-1}\left(2P_{FA}\right) \tag{5.3}$$

5.4 SIMULATION RESULTS

Several simulation trials were performed to validate the innovative cell search procedure, versus the conventional power detector approach. The probability of detection P_D of the new detector is evaluated under the CFAR procedure versus Signal-to-Noise ratio (SNR) of practical interest and for different lengths of the DFT (128 and 256 bins). In the reported results, a constant P_{FA} (= 10^{-3}) and both additive white Gaussian noise (AWGN) and multipath channels have been used. Moreover, several Monte–Carlo simulation trials (10^6 independent runs) have been implemented to numerically evaluate the detection probabilities of the two methods. The P_D of both methods versus different values of the SNR for the best case, i.e. perfect synchronization between transmitter and receiver is shown in Fig. 5-9.

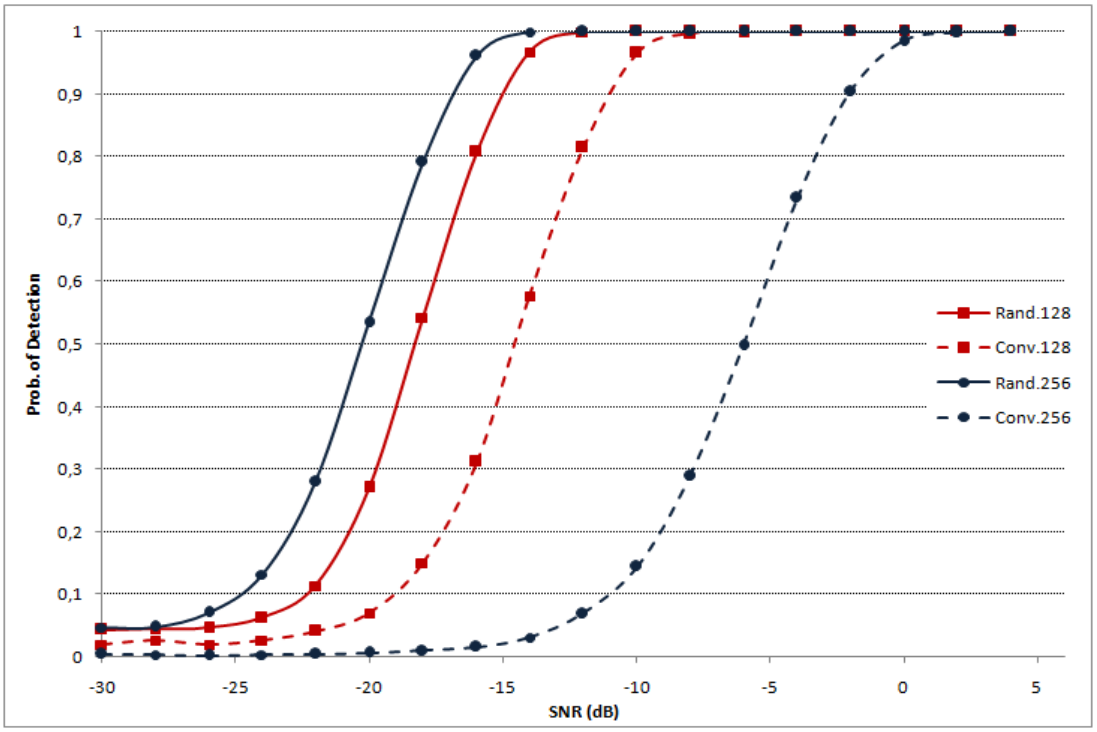

Figure 5-9 Best Case: P_D (10^6 Monte-Carlo runs) of the conventional power test and new method versus SNR for different DFT lengths

It can be easily seen from the graph that the curves referring to the new method are always higher than the ones referring to the conventional method. This situation corresponds to higher detection probabilities of the proposed strategy versus the conventional one. The best case is not a typical operating case of chip asynchronous system. Hence, in to order better assess the behavior of both methods other two scenarios have been considered: the worst operating scenario and the middle operating scenario. Fig. 5-10 shows here the resulting P_D for the worst case, i.e. timing offset just in the middle between two sampling periods. It can be easily seen from the graph, that worst case has a non-negligible impact on the performance of both methods. However, the proposed solution greatly outperforms the conventional one, thus proving its effectives for code acquisition in asynchronous communications. Finally, in order to evaluate the performance also in intermediate cases, typical of asynchronous systems, the middle case, i.e. timing offset randomly located between the best and worst cases, has been considered (see Fig. 5-11). According to the obtained results, the new acquisition method outperforms the conventional approach also in this case.

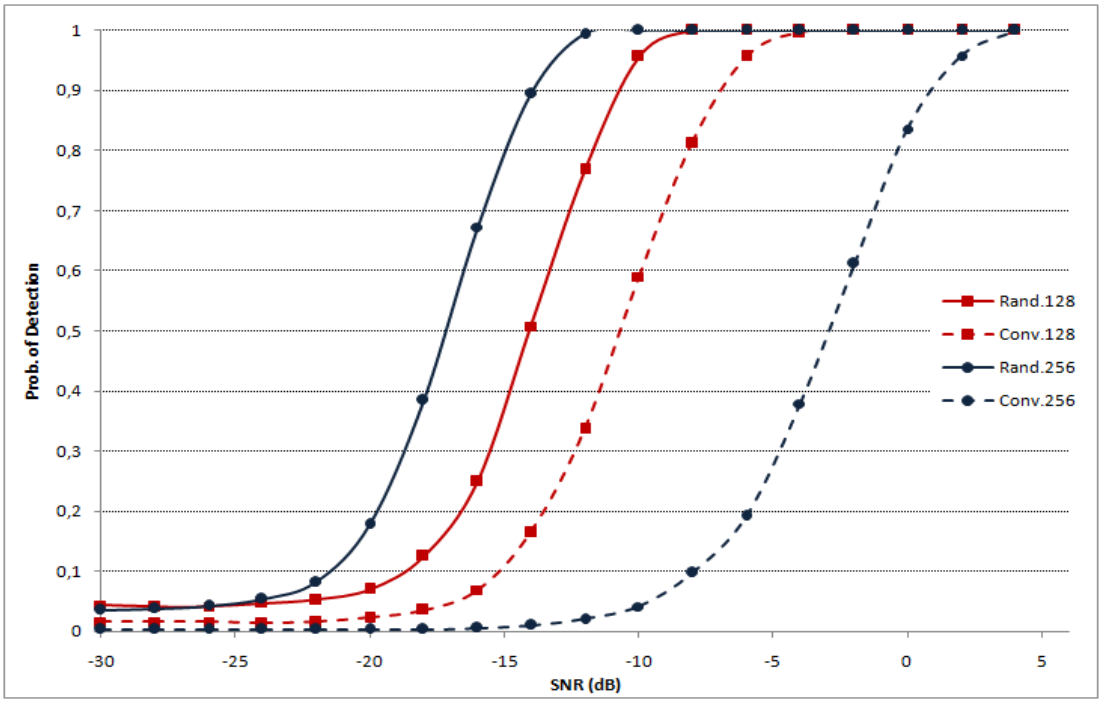

Figure 5-10 Worst Case: P_D (10^6 Monte-Carlo runs) of the conventional power test and new method versus SNR for different DFT lengths

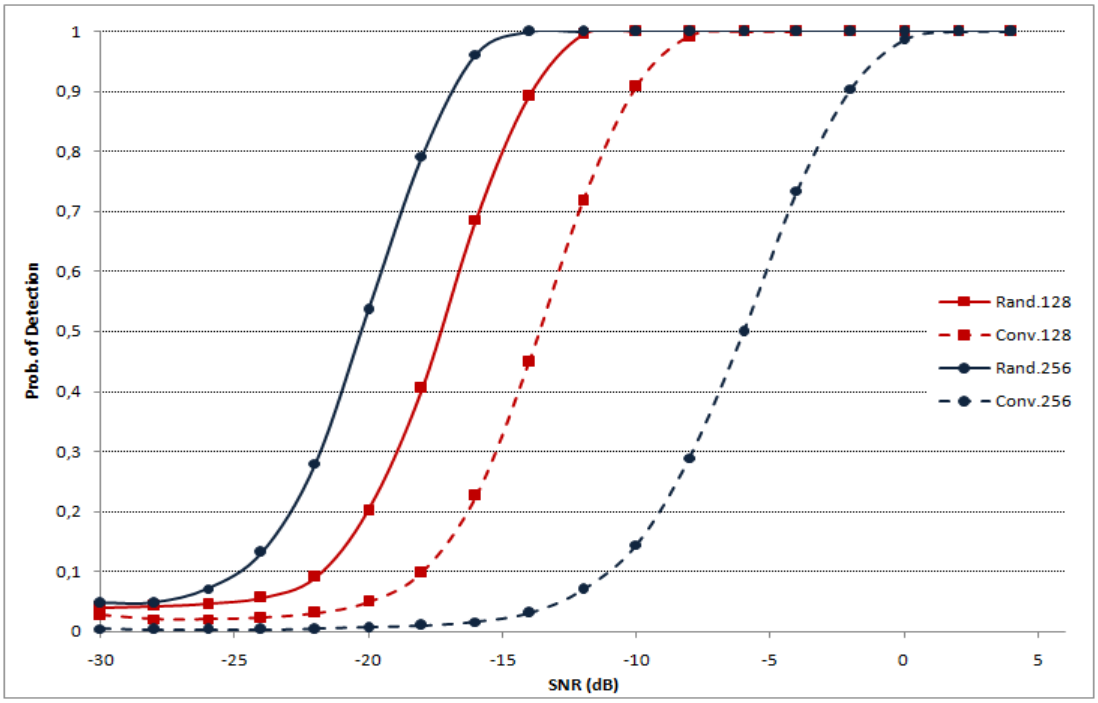

Figure 5-11 Middle Case: P_D (10^6 Monte-Carlo runs) of the conventional power test and new method versus SNR for different DFT lengths

The graphs shows that as the number of DFT bins becomes higher, the performances of the proposed method increase. This due to the fact that as the number of DFT bins increases, the correlation between the PSS samples in the time domain decreases. As a consequence, the scrambling process, acting over uncorrelated samples is more effective in making the cross-correlation samples of two consecutive PSS repetitions independent. In other words, averaging over W synchronization symbols strongly reduces the cross-correlation side-lobs, since the original PSS samples are now less correlated.

Then, in order to assess the performance of the proposed method in channel conditions typical of operating cases, we evaluated the P_D of the new detector under different multi-path conditions. We consider a uniformly distributed random timing jitter and assume that the channel is affected by flat fading. For the sake of comparison, three channel models have been used: the 6-path Rayleigh-faded channel model with exponential path decay [76], namely Case I, and the two IEEE standard channels of [77], namely Case II (pedestrian channel model) and Case III (vehicular channel model). In particular, the pedestrian (speed: 3 Km/h) and vehicular (speed: 120 km/h) scenarios are characterized by three paths with the following properties.

Pedestrian model:

- First path: amplitude 0 dB, delay = 0 ns.
- Second path: amplitude 0 dB and delay = 976 ns,
- Third path: amplitude 0 dB and delay = 20000 ns.

Vehicular model:

- First path: amplitude 0 dB, delay 0 ns.
- Second path: amplitude -3 dB, delay = 260 ns
- Third path: amplitude -6 dB, delay = 521 ns.

Fig.5-12 reports the detection probabilities of the both methods for the best case versus the SNR, while the worst and middle case are reported in Fig.5-13 and Fig.5-14 respectively. It can be easily seen from the graphs that the curves referring to the new method are always higher than the ones referring to the conventional method, in each multi-path scenario.

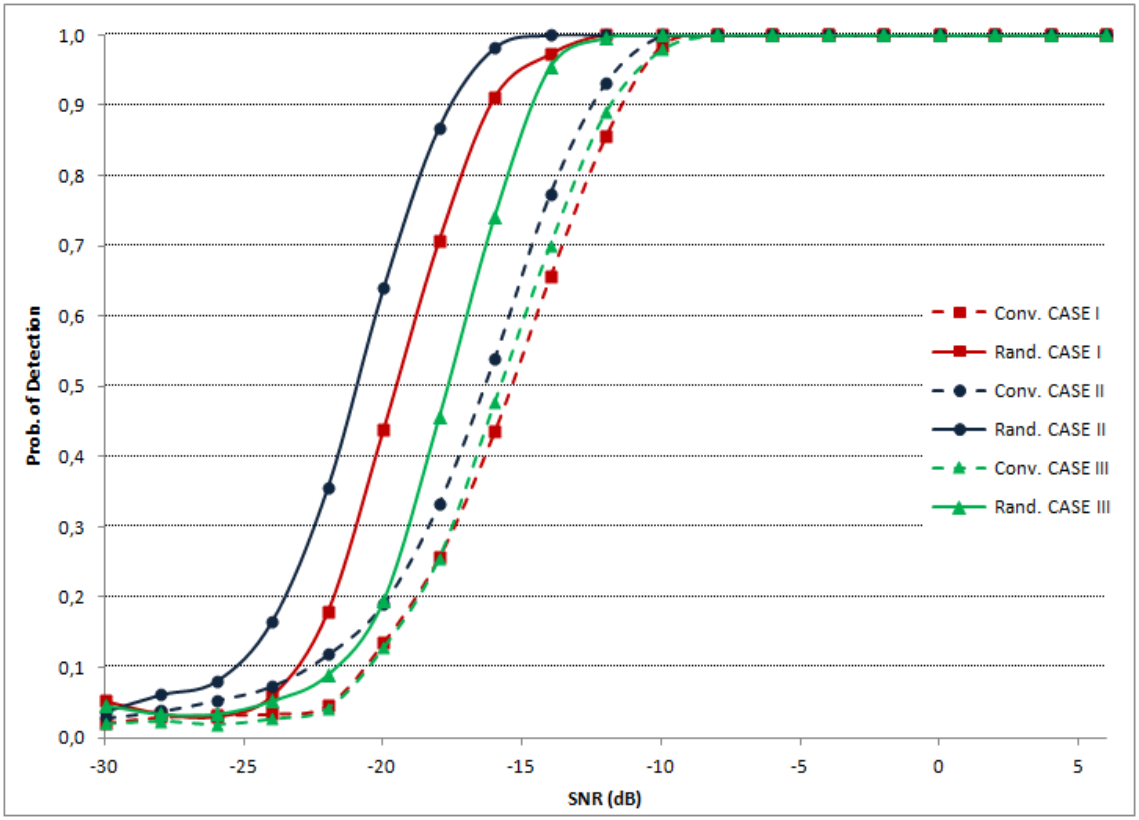

Figure 5-12 Detection probability of the power test (Conv.) and new method (Rand.) versus SNR for different multi-path channels in the Best Case.

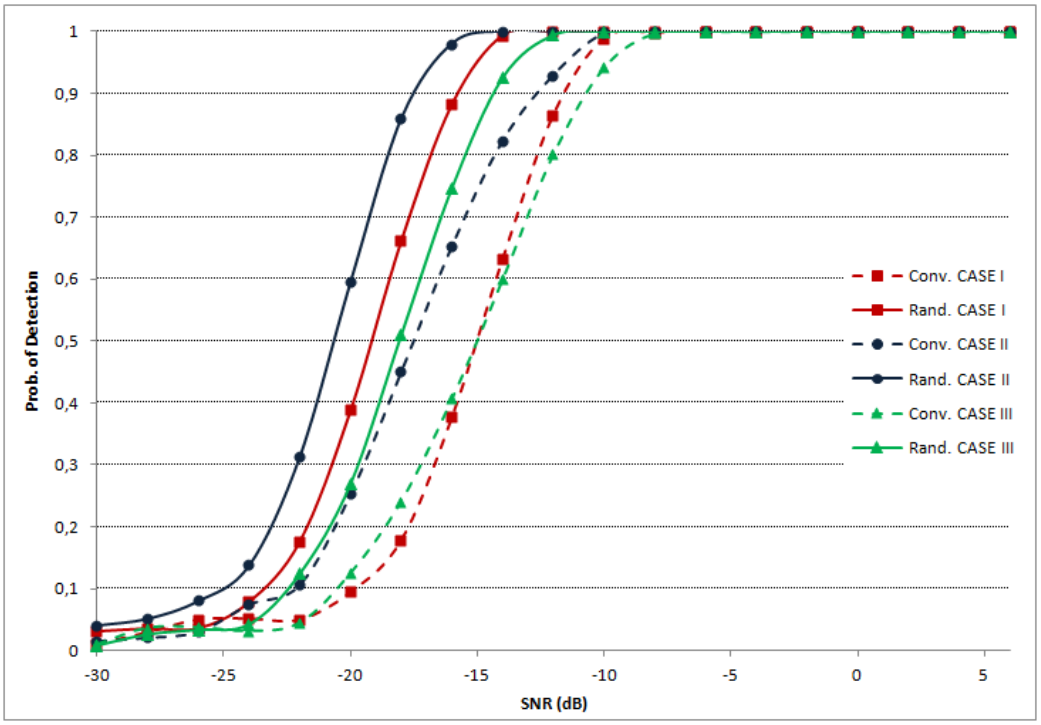

Figure 5-13 Detection probability of the power test (Conv.) and new method (Rand.) versus SNR for different multi-path channels in the Worst Case

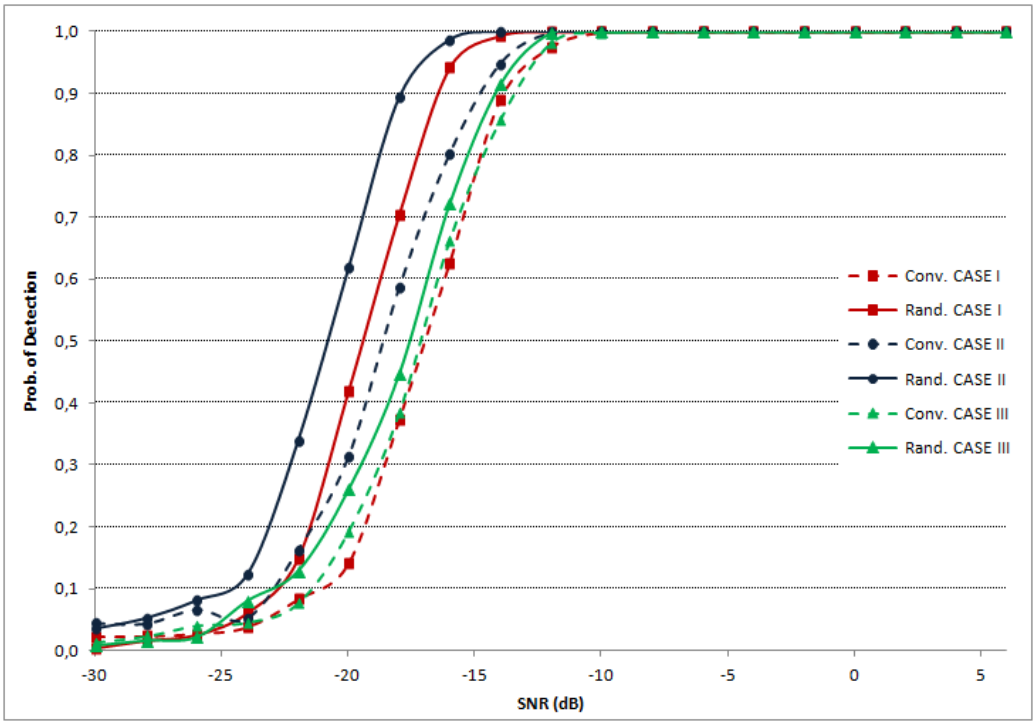

Figure 5-14 Detection probability of the power test (Conv.) and new method (Rand.) versus SNR for different multi-path channels in the Middle Case

Another relevant parameter for evaluating the performance of the code acquisition procedure is the MAT, which is defined as the time needed, on average, for performing a true acquisition. Figure 5-15 reports the MAT of the conventional and Rand method for all the considered multi-path scenarios, in the best operating case, while Fig. 5-16 and Fig. 5-17 illustrates the MAT of the two methods for the worst and middle operating cases, respectively. It is clearly visible that the innovative acquisition technique is superior to the conventional method, also in terms of MAT.

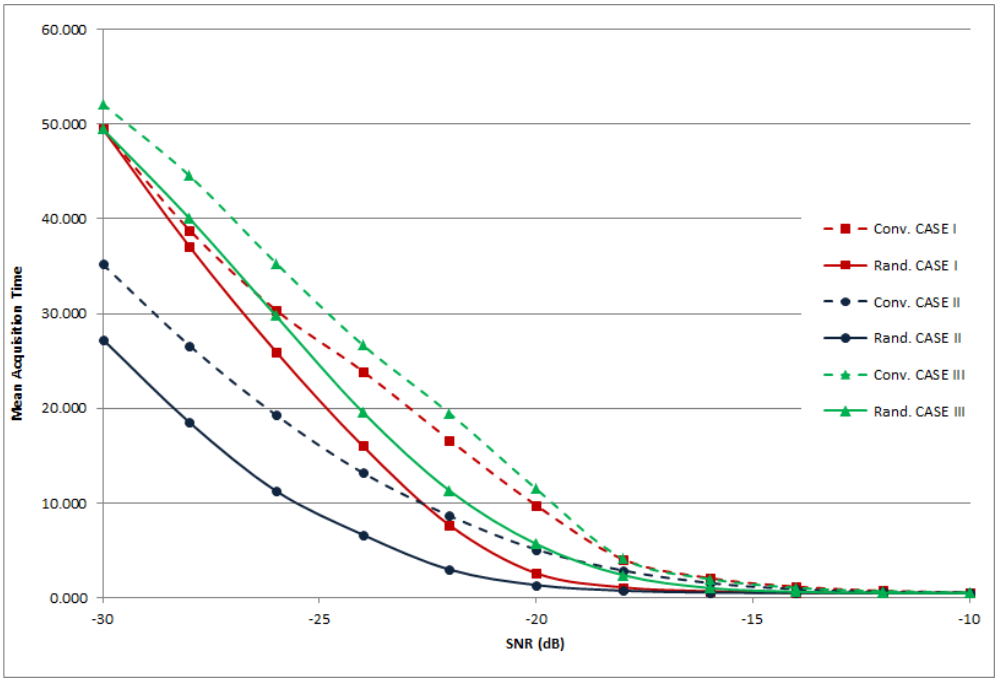

Figure 5-15 Mean Acquisition Time of the power test (Conv.) and new method (Rand.) versus SNR for different multi-path channels in the Best case.

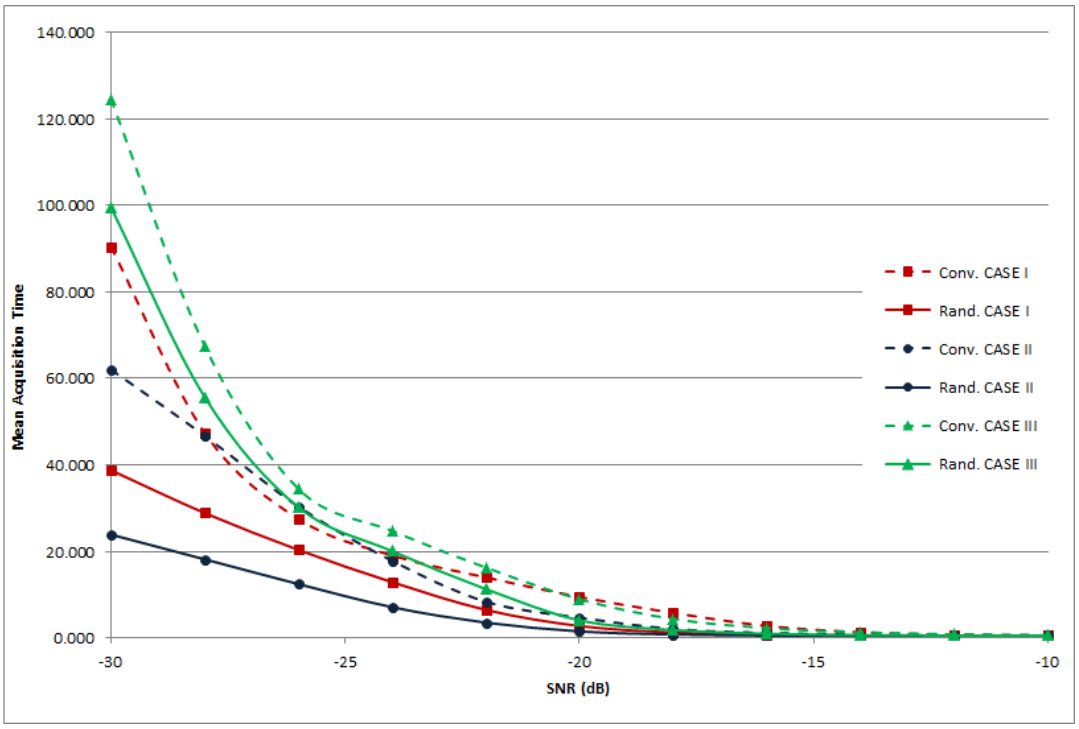

Figure 5-16 Mean Acquisition Time of the power test (Conv.) and new method (Rand.) versus SNR for different multi-path channels in the Worst case.

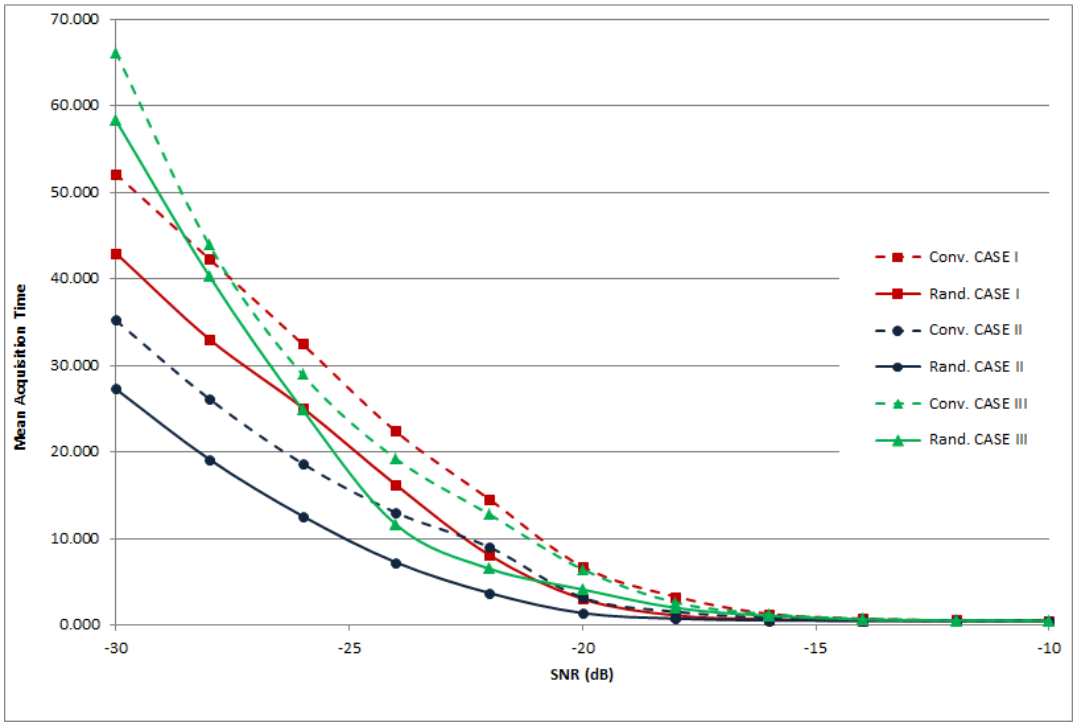

Figure 5-17 Mean Acquisition Time of the power test (Conv.) and new method (Rand.) versus SNR for different multi-path channels in the Middle case.

Moreover, it has to be noted that the rand method requires modification only at the receiver side; therefore it needs no alteration of the LTE standards. This reflects in a minor increasing of the computational complexity and processing throughput required to implement the new acquisition system, since our method can be performed either via hardware or via software implementation. In addition, near the total amount of the required computation is due to the cross-correlation process, while the additional operations introduced by our method are negligible from the implementation and computational point of view. Moreover, the current trend, providing higher and higher-speed microprocessors, is going to timely compensate for the request computational cost, allowing the development of LTE handsets in which all the additional operations can be performed via software implementation.

5.5 Conclusions

This chapter has presented an effective cell search algorithm for 3GPP LTE systems. By means of the proposed method, we have obtained a performance improvement in the initial code acquisition stage versus the conventional approach (i.e. power detector). The proposed procedure exploits the primary synchronization signal, and can be applied to any LTE transmission standard. The rationale behind the new approach is to maximize the main peak of the cross-correlation between the received signal and its locally generated replica, at the same time minimizing the side-lobes. Performance analysis is carried out in comparison with the conventional approach, based on the power detector test. The numerical results, obtained from wide simulation trials under operating settings, have evidenced that the devised method outperforms the conventional approach for all the timing offsets.

Part 3

Spectrum Sensing In Cognitive Radio Networks

Chapter 6 STATE OF ART SPECTRUM SENSING IN COGNITIVE RADIO NETWORKS

6.1 Introduction

The fundamental task of each CR device in CRN is to detect the licensed users and identify the available spectrum holes. This process, which is achieved by sensing the RF environment, is called spectrum sensing. The design of a spectrum sensing strategy is one of the most critical task of CRN since the performance of spectrum sensing has a great impact on the performances of both the primary and the secondary network. In fact, CRs must not cause harmful interference to PUs by either switching to an available band or limiting interference with PUs at an acceptable level. As a consequence, they should guarantee both fast and reliable detection of spectrum holes. On the other hand, the secondary network should efficiently identify and exploit the spectrum holes for satisfying its throughput and quality-of service (QoS) requirements. Spectrum sensing's performance can be primarily determined on the basis of two metrics: probability of false alarm, which denotes the probability declaring that a PU is present when the spectrum is actually free, and probability of detection, which conversely denotes the probability of declaring that a PU is present when the spectrum is indeed occupied by the PU. A miss detection (i.e. declaring empty an occupied band) will cause interference with the PUs, on the other hand a false alarm will reduce the spectral efficiency at the SN. Therefore optimal spectrum sensing performance is a trade-off between high detection probability and low false alarm. Several strategies have been proposed in literature for spectrum sensing [10, 11] spanning from cumbersome techniques (e.g. autocorrelation and auto-covariance-based methods [77], and cyclostationary feature detection [78, 79]), to simpler algorithms (e.g. energy detectors [80]-[82]). The conventional approach which is taken from code acquisition, is based on the energy (or power) detector [81]. In this method the energy (or power) of the received signal in a certain band is first measured, and then compared with a pre-selected threshold to state whether a PU is present or not. However, in realistic environments, the

CR receiver might operate at low Signal-to-Noise Ratio (SNR) regimes, due to the channel fading, and under noise uncertainty [82]. Unfortunately, at low SNR values, the performance of the Energy Detector (ED) dramatically reduces and reliable spectrum sensing is very difficult to achieve [83]. Therefore, alternative spectrum sensing methods have been investigated to answer these issues. The eigenvalue-based detection technique is one of the most attractive solutions, since this method is quite robust against the noise uncertainty problem [84]. Unfortunately, eigenvalue-based methods are computationally prohibitive because of the need to perform eigenvalue decomposition. Alternative solutions are represented by the autocorrelation-based and cyclostationary feature detectors. The periodicity of the autocorrelation function and the inherent cyclostationarity properties of digital modulated signals are exploited in order to distinguish them from the channel noise. Although these detectors can operate much better than the energy-based ones, they are generally too complex [79]. Recently, spectrum sensing methods based on high-order statistics of the received signal have been proposed for PU detection in cognitive radio networks. These methods allow overcoming the drawbacks of energy detection, without dramatically growing up the overall computational complexity of the system. An alternative solution to the spectrum sensing is represented by the use of spectrum databases. A CR, wishing to access the spectrum, can select one of the available frequency bands in the database, without performing spectrum sensing. This solution is very attractive especially in wireless systems characterized by fixed spectrum band time-occupation, such as the Digital Video Broadcasting (DVB) System [85].

The remainder of this chapter is organized as follows. The basic framework about spectrum sensing is presented is section 2. Section 3 introduces filter based method, while Energy detection is presented in section 4. Section 5 described features detection method. Receiver detection methods are described in Section 6, while interference temperature is presented in section 7. Section 8 focuses on cooperative spectrum sensing, and section 9 on spectrum databases.

6.2 Basic Framework on spectrum sensing

The spectrum sensing is the key functionality enabling SUs to detect and then to opportunistically access the unused frequency bands. Regardless the specific spectrum sensing strategy, the decision about the presence or absence of a signal of interest (i.e., the signal transmitted by the PU) can be obtained by comparing a decision metric (e.g. the energy of the received signal in the ED approach) against a fixed threshold. This is equivalent to discriminate between two alternate hypotheses, as usually happens in the case of code acquisition [86]: the H_1 hypothesis which states the presence of the signal of interest, and the H_0 hypothesis, which states the absence of this signal (i.e. a spectrum hole is detected). Let $s(t)$ be the signal transmitted by the PU, which is assumed to be affected by complex additive white Gaussian noise (AWGN) $n(t)$, with zero-mean and variance $2\sigma_n^2$. Then, the received signal $r(t)$ is $r(t) = s(t) + n(t)$ in the H_1 hypothesis and $r(t) = n(t)$ in the H_0 hypothesis. For the sake of the compactness in the remainder of this dissertation, all the signals are expressed in terms of their representative vectors. The signal $r(t)$ represented by the vector $\mathbf{r} = \mathbf{s} + \mathbf{n}$ is sampled at the receiver side with a sampling period T_s. The sequences (of N samples) of the received signal, of the primary signal, and of the noise are defined as, respectively:

$$\begin{aligned} \mathbf{r} &= [r_1, r_2, r_3 \ldots r_N]^T \\ \mathbf{s} &= [s_1, s_2, s_3 \ldots s_N]^T \\ \mathbf{n} &= [n_1, n_2, n_3 \ldots n_N]^T \end{aligned} \tag{6.1}$$

Then, a decision metric is extracted from N samples of the received signal and the metric is compared with a fixed threshold to discriminate between the two hypotheses. The hypothesis testing problem is expressed as:

$$\begin{aligned} H_0 &: \mathbf{r} = \mathbf{n} \\ H_1 &: \mathbf{r} = \mathbf{n} + \mathbf{s} \end{aligned} \tag{6.2}$$

Many spectrum sensing strategies have been proposed in the scientific literature. They can be broadly divided into two main categories: receiver detection and transmitter detection. Receiver detection-based strategies rely on the detection of PUs [87], while transmitter detection strategies are based on detecting the primary transmissions [10], and the great majority of spectrum sensing methods falls in this category.

6.3 Matched filter

In CRN, matched filter-based spectrum sensing is the optimal solution when the primary signal is known to the CR device. As happens in conventional synchronization and code acquisition methods, in MF-based spectrum sensing, the received noisy signal is correlated with a locally generated replica of the signal of interest in order to distinguish it from the channel noise [88]. In wireless communication systems, synchronization usually takes place by means of synchronization signals broadcasted by the base station on dedicated channels. Then, in order to perform correlation between the local replica and the received (primary) signal, time synchronization between primary and secondary users is needed. However, it is extremely difficult, if not impossible, for a CR to detect the synchronization signal, and then perform synchronization without having any a priori knowledge about the synchronization protocol. However, matched filter based detection has the great advantage of requiring a very short time to achieve the final decision, in comparison to other detection strategies. Unfortunately, some a priori knowledge about the primary signal (i.e. modulation type, coding, packet format, etc.) is needed and if this information is unavailable, or not accurate, matched filter strategies are useless. Notwithstanding most of the wireless networks and systems have pilots, preambles, or synchronization signals that are known to the receiver, in CRN the a priori knowledge about the signals of interests is typically very low, and hence, matched filter detectors are rarely used in practices. However, in specific scenarios, such as in the digital television systems, the primary signal is known to the CR receivers, and matched filter can be effectively used.

6.4 Energy Detection

The Energy detection (ED) is the simplest and most well know spectrum sensing strategy. In this approach the energy (or power) of *N* samples of the received signal is first evaluated, and then compared with a pre-determined threshold to state if a PU is present or not [89]. Following the mathematical notations used before, the decision variable is expressed as follows:

$$P_R = \frac{1}{N}\sum_{i=1}^{N}|r_i|^2 \tag{6.3}$$

Where $\{r_i\}$ with i=1,2..N is the sequence of the received samples. The operations in (6.3) require no information about the signal of interest, and the energy detector has a very simple and economic structure. As usually happens in the case of code acquisition, the CFAR procedure is adopted to determine the threshold value:

$$\gamma = Q^{-1}\left(P_{FA}\right)\sqrt{4\sigma_n^4/N} + 2\sigma_n^2 \tag{6.4}$$

Where P_{FA} is the false alarm probability (i.e., the probability of declaring empty an occupied band). Q^{-1} is the inverse of the Marcum Q-Function and σ_n^2 is the marginal noise variance (i.e. the variance of the real or imaginary component only). One of the main drawbacks of ED is that the noise variance has to be perfectly known in order to correctly set the threshold. When there is no uncertainty and the noise variance is completely known, we can use the central limit theorem to approximate the test statistic (under the H_0 hypothesis) as Gaussian with mean $2\sigma_n^2$ and variance $4\sigma_n^4$. Unfortunately, in most practical cases exact knowledge of the noise variance is not possible; hence the assumption is that the noise variance is expected to be in the range $[1/\rho\sigma_n^2 ; \rho\sigma_n^2]$ where ρ (with ρ >1) is a parameter related to the size of the uncertainty [82]. With a given noise uncertainty ρ, there is a minimum SNR value under which a primary signal cannot be reliably detected, not even increasing the number of the received samples. This nominal SNR threshold is called the SNR *wall* for the detector.

A possible solution to mitigate the SNR wall problem is proposed in [81], where a novel cognitive device is proposed. The device consists of two independent receiving chains each comprising: low-noise amplifiers, mixer amplifiers, pre-filters and ADC. The received signal is first processed by each of the two chains, independently. Then, the signals at the output of each chain are cross-correlated together and the energy of the resulting signal is evaluated. The authors also show that the SNR wall is directly proportional to the correlation coefficient between the noises added by the receiving chains, and in particular it is zero if the noises are totally uncorrelated. This is an ideal case and in practices there is always a certain degree of correlation between the two chains. However, since the noises are strongly uncorrelated the SNR wall can be effectively reduced.

Notwithstanding the energy detector can be used to determine whether a spectrum band is occupied or not, it cannot be used to decide if the detected transmission belongs to a primary or a secondary user. In [90], a spectrum sensing approach able to distinguish between primary and secondary users is proposed, which combines simple ED with optimum matched filter. The method consists of two consecutive stages: a fast coarse sensing stage, followed by a finer sensing stage. More in details, in the first stage ED is exploited to decide on the presence of a received signal. Then, during the second (or finer) stage a matched filter is used to determine whether the received signal is transmitted from a primary or a secondary system. Moreover, the threshold for the energy detector can be dynamically controlled to avoid performing the finer stage when there are no active primary users

6.5 Feature detection methods

Features detection-based spectrum sensing methods have been investigated to answer the challenges behind the ED approach. Eigenvalue-based detection technique is one of the most attractive solutions, since this method is quite robust against the noise uncertainty problem [84]. Unfortunately, eigenvalue-based methods are computationally prohibitive because they need to perform eigenvalue decomposition. In [C5], we have proposed some methods for reducing the computational complexity of eigenvalue decomposition. In

particular, the power method and the inverse-power method are used to decrease the number of computations needed for the inversion of the covariance matrix. The periodicity of the autocorrelation function and the inherent cyclostationarity properties of digital modulated signals can be exploited to distinguish them from the channel noise.

In [78] the authors propose an effective method for the detection of an OFDM signal. In particular, they exploit the periodicity of the correlation coefficient at delays equal to the symbol length of an OFDM block. In fact, the presence of the CP gives OFDM signals the following well-known propriety: the autocorrelation coefficients $\rho = E\left[x(t)x^*(t+\tau)\right] / E\left[x(t)x^*(t)\right]$ are non-zero only at delays equal to $\tau = \pm T_d$, where T_d is the symbol length and T_c is the CP length. The main rational behind the method in [78] is that the auto-correlation coefficients at $\tau = \pm T_d$, assume a zero value in the H_0 hypothesis (i.e. absence of the PU) and a non-zero value otherwise. Then, the hypothesis testing problem becomes:

$$\begin{aligned} H_0 &: \rho(\pm T_d) = 0 \\ H_1 &: \rho(\pm T_d) = \rho_1 \end{aligned} \tag{6.5}$$

where:

$$\rho_1 = \frac{T_c}{T_c + T_d} \frac{\sigma_s^2}{\sigma_s^2 + \sigma_w^2} \tag{6.6}$$

σ_s^2, σ_w^2 are the signal and noise marginal variance, respectively. The decision is based on an estimation of the correlation coefficient from a set of M observations (with $M >> T_d$) of the received signal [$x(0)$, $x(1)$....$x(T_d+M-1)$]. In other terms, the testing variable is expressed as the maximum likelihood estimate of the correlation coefficient [19]:

$$\hat{\rho}_{ML} = \frac{\frac{1}{M}\sum_{t=0}^{M-1} x(t)x(t+T_d)}{\frac{1}{2(M+T_d)}\sum_{t=0}^{M+T_d-1} |x(t)|^2} \tag{6.7}$$

For large values of M, the testing variable in (6.7) is asymptotically Gaussian, because of the central limit theorem. The hypothesis testing can be written as follows:

$$\begin{aligned} H_0 &: \hat{\rho}_{ML} \sim N\left(0, \frac{1}{2M}\right) \\ H_1 &: \hat{\rho}_{ML} \sim N\left(\rho_1, \frac{\left(1-\rho_1^2\right)^2}{2M}\right) \end{aligned} \tag{6.8}$$

The test threshold can be now tuned from a straightforward evaluation of the Gaussian integral for a fixed probability of false alarm:

$$v = \frac{1}{\sqrt{M}} erfc^{-1}\left(2\, P_{FA}\right) \tag{6.9}$$

Moreover, the detection probability (P_D) can be determined by means of the error function under the H_1 hypothesis:

$$P_D = \frac{1}{2} erfc\left(\sqrt{M}\,\frac{v-\rho_1}{1-\rho_1}\right) \tag{6.10}$$

In the case that the CP is known to the receiver, the performances of the overall system can be strongly improved. In fact, in this case, and assuming perfect synchronization between the receiver and the transmitter, the test statistics in (6.7) can be expressed as:

$$\begin{aligned} H_0 &: \rho_{cML} \sim N\left(0, \frac{1}{2M_c}\right) \\ H_1 &: \rho_{cML} \sim N\left(\rho_{c1}, \frac{\left(1-\rho_{c1}^2\right)^2}{2M_c}\right) \end{aligned} \tag{6.11}$$

with:

$$\rho_{c1} = \frac{\sigma_s^2}{\sigma_s^2 + \sigma_w^2} \tag{6.12}$$

and $M_c = T_c \cdot N_s$, where N_s is the number of OFDM blocks over which the autocorrelation coefficient is estimated. As a consequence, the mean of the estimate has increased by a factor T_s/T_c under the hypothesis H_1, effectively increasing the detection probability. It has to be noted that, even if the CP length may be known to the receiver, since it is related to the communications standard, perfect synchronization between the transmitter and the receiver is not a typical operating case. The method is quite simple and extremely efficient in terms of computational complexity. Unfortunately, it requires some knowledge about the transmitted signal (e.g. the length of the cyclix prefix). On the other hand, a cognitive radio should be able to operate in many different frequency bands, while detecting the presence of primary signals from various communications standards characterized by different parameters. For example, in the Digital Video Broadcasting-Terrestrial system, different lengths of the cyclic prefix are used. Therefore, effective spectrum sensing strategies should be blind, i.e. they should need no a priori knowledge of the communication scenario. Autocorrelation and cyclostationarity features detection can perform much better than the energy detector and they can distinguish not only the interference from the target signal, but also different types of transmitted signals. However, they are generally computationally expensive and time consuming. Moreover, it has to be underlined that features detection based spectrum sensing methods are not always better than plain ED, since they usually incur an initial SNR-loss, because the feature contains only a fraction of the transmission power.

Recently, spectrum sensing methods based on high-order statistics of the received signal have been proposed for primary user detection in cognitive radio networks. These methods allow overcoming the drawbacks of energy detection, under noise uncertainty, without dramatically growing up the overall computational complexity of the system. The authors in [91] propose a spectrum sensing method, in which the third-order cumulant is first estimated, and then applied for binary hypothesis testing. In fact, the third-order cumulant,

which accounts for the asymmetry of the probability distribution, is zero for Gaussian processes and can be used for separating the signal from the noise. However, this approach cannot be used for signals characterized by symmetric probability distributions (e.g., such as constant modules signals).

6.6 Receiver detection methods

Receiver detection methods are based on the detection of the leakage power emitted by the RF front end of the primary receivers. In fact, due to the imperfections of the receiver's front end, a portion of the power (i.e. the leakage power) emitted by the Local Oscillator (LO) might couple back with the antenna and be radiated out.

A spectrum sensing approach based on the detection of the LO leakage power is proposed in [92]. The CR system consists of several low cost sensor-nodes mounted close to the primary receivers. Each node first detects the LO leakage power emitted by the PU to determine on which channel the receiver is tuned, and then relays this information to the CRN. The front-end of the sensor node consists of a radio frequency amplifier, a filter and a bank of local oscillators, each tuned such that the received LO leakage power falls into a fixed IF band. However, in order to determine the RF band on which the LO is tuned, its IF should be known in advance. As a consequence, if this information is unavailable or inaccurate, receiver detection cannot be used. In addition, the LO leakage power is typically very low, and varies depending on the specific hardware technology. Hence, sophisticated strategies are needed for leakage power detection [93]. Moreover, the sensor nodes need to be mounted closed to the PU receivers, which is not very practical. Finally, the sensor network increases the system's deployment and maintenance costs. As a consequence, receiver detection-based spectrum sensing is rarely used in practice.

6.7 Interference Temperature Limit

The Interference Temperature (IT) has been proposed by the FCC as a metric for measuring the interference perceived by licensed users [27, 56]. The Interference Temperature is the decision metric used in CRNs based on the concurrent spectrum access model, to state whether SUs can access the spectrum without interfering with the PUs. The concept of IT is very similar to that of noise temperature: it is a measure of the power and bandwidth occupied by the interference. The basic idea behind interference temperature approaches is that by taking a single measurement, a SU can completely characterize both the interference and the noise. The conventional method for estimating the IT is based on the ED technique. According to this method, the energy (or power) of the received signal is first evaluated and then used for estimating the interference experienced by the PU in a certain frequency band and at a specific time instant. There are two IT models: *the ideal model* and the *generalized model*. The ideal model assumes that the power of the signal transmitted by the PU is known to the CR device. Then, the noise (or interference) power can be derived, and exploited for IT evaluation. Conversely, in the generalized model, the SU has no information about the licensed signal and hence the power of the received signal is used for the interference estimation. More in details, the IT is evaluated as follows:

$$T_I = \frac{P_R}{K \cdot B} \tag{6.13}$$

Where P_R is the received power defined in (6.3), B [Hertz] is the signal bandwidth, and $K = 1.38 \cdot 10^{-23}$ [Joules per Kelvin degree] is the well-known Boltzmann's constant. The non-interference condition is expressed by:

$$T_I + \frac{P_{SU}}{K \cdot B} < T_L^G \tag{6.14}$$

Where P_{SU} is the SU power and T_L^G is the IT limit. For a given geographic area, the FCC would establish an interference temperature limit. This value is the maximum amount of tolerable interference for a given frequency band in a particular location. Any unlicensed transmitter utilizing this band must guarantee that their transmissions added to the existing

interference do not exceed the interference temperature limit at a licensed receiver. There are two main challenges in the evaluation of the IT. In the ideal model the CR should be able to identify the licensed signals. However, energy detection cannot be used for distinguishing the noise from the transmitted signal, and some a priori knowledge about the primary signal is needed. One common approach is assuming that the locations of the PUs are known to the CR and exploiting this information for identifying the licensed users. Notwithstanding this assumption is not always true (especially for mobile users), in some specific scenarios, such as in the DVB system, the primary transmitters are located in fixed, well-known positions and the ideal IT model can be effectively used. However, in CR networks the a priori information about the signal of interest is typically very low, and hence, the ideal model is rarely used in practice. In the generalized model the received power P_R is used for the interference's estimation, but P_R includes both noise and useful signal powers. The noise increases the IT value but the licensed signal does not. Hence, with the generalized model, the IT may be incorrectly estimated, thus providing bad working conditions for the SU.

6.8 Cooperative detection methods

Conventional spectrum sensing methods decide on the presence of a primary user from the local observations of a single CR device. However, sensing the spectrum using only one CR has a number of drawbacks and limitations. For example, a CR may not be able to detect a primary transmitter located behind a high building (see Fig. 6-1a). Furthermore, a CR might miss the detection of a primary transmitter, blocked by a primary user (see Fig. 6-2b). These effects are known as the 'hidden terminal problem': in both cases (i.e. shadowing from a high obstacle or shadowing from primary receiver) a CR fails to detect the PU and may access the radio spectrum, thus interfering with the licensed users. Another relevant limitation of the single node sensing is that the sensitivity of a single device is often limited because of energy constraints (e.g. limited battery power).

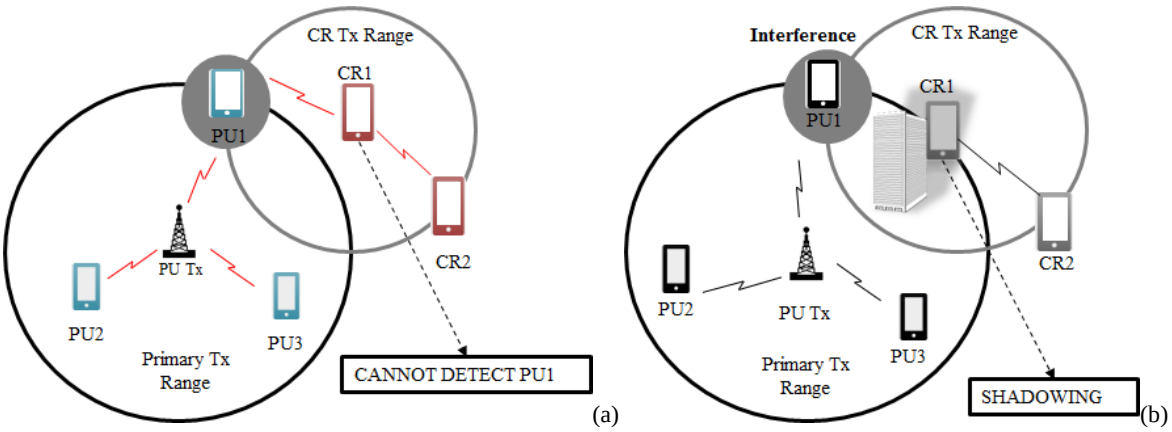

Figure 6-1 The hidden node problem: a) shadowing from an high building, b) shadowing from a primary user.

Cooperative sensing has been proposed as a possible solution to these limitations [94], [98]. The main idea behind this strategy is to sense the radio spectrum with multiple sensors and combine their measurements into one common decision. The collaboration of multiple CR users can be used for: (*i*) improving the detection performance, (*ii*) increasing the sensitivity of the CR devices, (*iii*) mitigating the hidden terminal problem, and (*iv*) reducing the detection time. Cooperative detection strategies can be divided into two main categories: centralized and distributed [98]. In the first case, there is a central node (i.e. the Fusion Centre, FC) that collects and combines the sensing data of each CRs. On the other hand, in distributed detection there is no central node and the sensing information is shared among all the CR devices.

In [99], a centralized cooperative detection strategy is proposed. The devised method exploits spatial, time and frequency diversity for improving the detection performance. The main advantage of this procedure is that when some nodes cannot directly report to the central node, due to the shadowing phenomena, relay diversity can be used for compensating the reduced sensing diversity. This scenario is depicted in Fig. 6-2. Let us assume that CR_1 cannot directly report to the FC because it is blocked by a high building. In this case, CR_1 can share the results of its spectrum measurements with CR_2 which, then, relays this information to the FC.

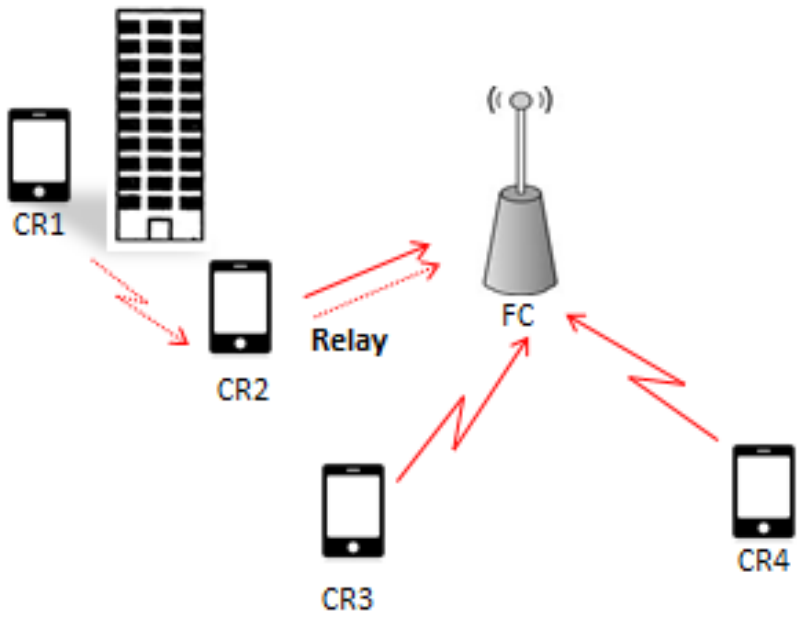

Figure 6-2 A cooperative detection's scenario with relay diversity

Conventionally, the participation to the cooperative sensing is mandatory: the FC selects which sensor nodes will take part in the detection and broadcasts a message to join the cooperative sensing to all the selected nodes. In [100], an alternative selection method is proposed.

Each CR receives an invitation to join the cooperative sensing, and can autonomously decide whether to participate or not, based on its internal state (e.g. battery level, channel quality information, etc.). This approach allows a more efficient management of the system resources since CR devices with critical conditions (e.g. low battery level) will not take part in the spectrum sensing.

Finally, in [101], a weighted combing procedure is described. In more details, a weighting factor is assigned to each CR node: nodes that are further away from the FC are associated with lower weights, while higher weights are assigned to the closer nodes. The main idea behind this approach is to reduce the influence of the furthest nodes in the final decision, since the sensing information of these nodes may be incorrect, due to propagation loss.

6.9 Spectrum Databases

Usually, spectrum sensing procedures suffer from some fundamental drawbacks, regardless the specific implemented strategy. The sensitivity levels imposed by the governing authorities to protect the licensed system are often difficult to achieve, especially in the presence of high power adjacent channel signals. Moreover, the spectrum sensing does not provide a mechanism to allow governing authorities to exclude some CR devices from any particular channel, if required. Finally, there are many types of primary signals and the CR may be capable of detecting only certain types, which leaves those undetectable primary users unprotected. The use of spectrum databases has been proposed as a possible solution to the limitations of conventional spectrum sensing procedures [102]. The main idea behind this approach is to provide CRs with large and adaptive databases than can be inquired for an available frequency band, without performing spectrum sensing. In [103], an effective spectrum database approach is proposed. The cognitive device provides the database with its current location, and the database responds with a list of available channels that the CR may use. This list includes: (*i*) the number of vacant channels, (*ii*) the maximum allowed transmitting power on each channel, and (*iii*) the time interval in which each channel can be used by secondary users.

A method that combines database inquiries with conventional spectrum sensing is proposed in [104]. A CR registers with a spectrum database, using variable resolution geo-location information. Upon receiving a spectrum access request with the current CR's location, the database responds with a map of available spectrum bands. The CR analyzes the spectrum map and conducts spectrum sensing on the available frequency bands. Finally, it combines the sensing results with the spectrum map to select the best radio channel. Variable geo-location resolution resolves the problem of determining the location of a CR in indoor environments. Spectrum databases can be also used to determine the most suitable sensing time duration for each frequency band. In [105], a method for deciding the time duration of the sensing interval is proposed. The database locally stores an association of channels and categories. There are three possible categories: *inuse*, *backup* and *other* and

each channel has an association with at least two categories. The sensing time for the in use category is the shortest one, the sensing time for the other category is the longest one, while the sensing time for the backup category is just in the middle between them. First, the cognitive device selects the in use and backup channels, and then performs spectrum sensing in each of the selected channels, with the respective time interval duration.

Although spectrum database approaches are quite simple and efficient, they suffer from some fundamental drawbacks and limitations. The CR need to be equipped with location-aware devices which increase the overall cost of the system. The geo-location information must be very precise, in order to correctly determine the available channels. However, it is impossible to have perfect location information, and hence, the database generally assume that the CR may be anywhere within an area indicated by the lowest level of geo-location accuracy. As a consequence, the database should be programmed to protect the primary users by returning conservative inquiry results, which compromises the efficiency of the spectrum utilization. Finally, with spectrum databases is not possible to detect an incoming PU in the frequency band in operation. Nevertheless, spectrum holes' databases are very powerful instrument, especially if used together with the spectrum sensing.

Chapter 7 Performance Improvements of OFDM-Signals Spectrum Sensing

7.1 Introduction

The OFMD is becoming very popular modulation scheme in wireless communication: for example, it is used in the wireless local area networks standards (i.e. IEEE 802.11x family protocols), in the Long Term Evolution, as well as in the DVB-T systems. Moreover, it is going to be a key technology for the future of broadband wireless telecommunications. Therefore, it is fair to assume that many primary users will operate in an OFDM – based system. Autocorrelation-based spectrum sensing methods are very effective in detecting OFDM signals whose autocorrelation presents strongly periodicity proprieties. Recently, the authors in [78] have proposed an efficient method for the detection of OFDM based primary users. The method (see Chapter 6 for details) exploits the periodicity of the correlation coefficient at delays equal to the symbol length of an OFDM block. Detection is based on an estimation of the autocorrelation coefficient which should provide a zero-mean value in the H_0 hypothesis (absence of primary user) and non-zero value otherwise. The method is quite simple and extremely efficient in terms of computational complexity. Unfortunately, it requires some knowledge about the transmitted signal (e.g. the length of the CP), and if this information is unviable or not accurate, the method performs poorly. In addition, effective spectrum sensing strategies should be as blind as possible in order to detect the presence of primary signals belonging to various communications standards and characterized by different parameters.

Addressing some of these issues, this chapter presents an innovative blind spectrum sensing strategy that can be effectively applied for the detection of OFDM-based primary users. The proposed method is based on a modified version the “Rayleigh-ness test”, which was recently introduced for code acquisition purposes in Direct Sequence-Code Division Multiple Access (DS-CDMA) systems [12]. The Rayleigh-ness aims to state whether a real

positive series is a portion of one realization a Rice or Rayleigh distributed random process. The test can be also performed to decide on the presence of a statistically relevant mean value of a complex Gaussian model generating both Rayleigh and Rice distributions. In this dissertation, we move further proposing a modified version of the Rayleigh-ness test for advanced spectrum sensing in cognitive radio networks.

The rationale behind the proposed method is as follows. The decision whether a primary user is active, or not, can be made on the presence of a non-zero mean value of a Gaussian distributed random variable; but this is also equivalent to state whether the observed series is a portion of one realization of a Rayleigh (or Rice) distributed random process. The Rayleigh-ness test in its original form makes use of matched filter correlation. Notwithstanding matched filter are the optimal detector, they require a priori knowledge about the signal of interest. Therefore, we have accordingly modified the conventional Rayleigh-ness test, in order to provide a blind spectrum sensing method, i.e. no assumptions on the system parameters in are needed in the propose strategy. The new method is applied for the detection of an OFMD primary signal and its performance matched to the conventional method [78] under the same settings and channel conditions.

The reminder of this chapter is organized as follows. In section 2 the original Rayleigh-ness is introduced. Section 3 outlines the rationale of our new spectrum sensing strategy, while simulation results and comparisons are showed in section 4. Finally the chapter's conclusions are briefly depicted in Section 5.

7.2 The Rayleigh-ness test

In this section the original Rayleigh-ness test for code acquisition is introduced. In code acquisition systems, the receiver must be able to synchronize the locally generated PN code with the incoming PN code. The conventional acquisition method is based on MF correlation (see chapter 3 and 4). This test distinguishes between two different hypotheses: the in-sync condition (hypothesis H_1), which corresponds to the case of presence of the

tested code with the correct timing offset; and the out-of-sync case (hypothesis H_0) which conversely states the absence of that code with the considered offset. These cases differ because the output of a matched filter is ideally constant in the former condition, while it randomly varies in the latter one. In fact, it is well known that the user codes employed in DS-CDMA are orthogonal only if the users are chip-synchronized with each other.

Let us assume that the observed signal after the matched filter is periodically corrupted by unknown phase factors. In addition, let us consider an additive independent and identically distributed (i.i.d.) complex random series $H=[\eta_1, \ldots, \eta_k]^T$ that affects the estimated cross-correlation sample. This series accounts for both the background noise and the interference due to the other co-users in the same cell or to the same code with erroneous shift. If the number of interferers is large, the series H can be assumed as asymptotically Gaussian with zero-mean and variance $2\sigma^2$, as a direct consequence of the central limit theorem. Then, the series at the output of the non-coherent MF correlator is express as follows:

$$\Gamma = \left[|R_1|, ... |R_N| \right]^T = \left[|\mu + \varepsilon_1| ..... |\mu + \varepsilon_N| \right]^T \tag{7.1}$$

Where $\{\varepsilon_k\} = \{\eta_k e^{-j\phi_K}\}$ is a zero-mean complex i.i.d. Gaussian random series accounting for phase uncertainty and channel noise effects. In H_1 hypothesis, we have $\mu \neq 0$ and series at the output of the MF correlator is $\Gamma = \left[|\mu + \varepsilon_1| ..... |\mu + \varepsilon_K| \right]^T$. On the other hand, in the H_0 hypothesis, $\mu = 0$ and the series at the output of the MF correlator consists only on the noise samples, i.e. $\Gamma = \left[\left|\varepsilon'_1\right| ..... \left|\varepsilon'_K\right| \right]^T$.

The statistical distribution of the observed series is the Rice probability density function (PDF) in the former hypothesis, while it reduces to the Rayleigh PDF in the latter case. As a consequence, the hypothesis testing is equivalent to decide for the "best fitting" statistical model of the real and positive-valued observed series **Γ** between the Rayleigh and the Rice cases. Such decision can be made on the presence of a statistically relevant mean of the complex Gaussian model $R_k = \mu + \varepsilon_k$ generating both Rayleigh ($\mu = 0$) and Rice ($\mu \neq 0$)

distributions by the magnitude of the complex Gaussian variable $|R_k|$. In fact, it is well kwon, that a random variable $Z=\sqrt{(X^2+Y^2)}$ is Rice distributed if the two marginal variables (i.e. *X*, *Y*) are statistically independent Gaussian variables with same variance and mean values μ_x, μ_y, respectively. Moreover, if the marginal variable have zero mean value (i.e. $\mu_x=\mu_y=0$) *Z* follows a Rayleigh distribution. In our case, when $\mu = 0$, the observed series $|R_k|$ consists only on the noise samples: since the noise is assumed to be a Gaussian zero mean process, $|R_k|$ is Rayleigh distributed.

The Rayleigh–ness test is based on the following useful propriety. Let $\xi=|\zeta|$ be a Rice disturbed variable generated as the magnitude of a complex variable ζ with mean λ. Then:

$$\begin{aligned}|\lambda|^4 &= 2E\left(\xi^2\right)^4 - E\left(\xi^4\right) \\ &= 2E\left(|\zeta|^2\right)^4 - E\left(|\zeta|^4\right)\end{aligned} \tag{7.2}$$

Now, if $\lambda \neq 0$, $|\zeta|$ is a Rice distributed random variable, otherwise if $\lambda = 0$, $|\zeta|$ reduces to a Rayleigh variable. Then, the testing variable is evaluated as:

$$x = 2\hat{M}_2^2 - \hat{M}_4 \tag{7.3}$$

Where $\hat{M}_2$ and $\hat{M}_4$ are the estimation of the second and fourth order moment of the of the magnitude of observed series, that are obtained as, respectively:

$$\begin{aligned}\hat{M}_2 &= \frac{1}{N}\sum_{k=1}^{N}|R_k|^2 \\ \hat{M}_4 &= \frac{1}{N}\sum_{k=1}^{N}|R_k|^4\end{aligned} \tag{7.4}$$

Then the test is finally express as follows:

$$x \underset{H_0}{\overset{H_1}{\gtrless}} \upsilon_x \tag{7.5}$$

It means that if the testing variable is greater than the threshold value $|R_k|$ follows a Rice distribution and true acquisition is achieved, otherwise $|R_k|$ is Rayleigh distributed. The threshold υ_x can be tuned form a straight evaluation of the Gaussian integral under the CFAR procedure.

7.3 The proposed method

In this section, the innovative spectrum sensing strategy is discussed. The basic rational behind the proposed method is as follows. The original Rayleigh-ness test [12] exploits the mean vale μ of a complex Gaussian model for deciding whether the observed series is Rayleigh (or Rice) distributed. The spectrum sensing method proposed in [78], follows a similar approach. In fact, the testing variable in (6.7) has zero mean (i.e. $E\left[\hat{\rho}_{ML}\right]=0$) in the H_0 hypothesis (i.e. absence of a primary user) and non-zero mean (i.e. $E\left[\hat{\rho}_{ML}\right]=\rho_1$) in the in the H_1 hypothesis (i.e. presence of a primary user). Therefore, the decision whether a primary user is active, or not, can be made on the presence of a non-zero mean value of a Gaussian distributed random variable. But this is also equivalent to state whether the observed series is a portion of one realization of a Rayleigh (or Rice) distributed random process, and hence, the Rayleigh-ness test can be effectively applied for spectrum sensing in CRN.

The main drawback of this procedure is that the Rayleigh-ness test is based on a matched filter correlation. Notwithstanding matched filter is known as the optimal detector in stationary Gaussian noise, it requires some a priori knowledge about the signal of interest. However, in cognitive radio scenarios, a priori knowledge about signals under investigation is generally very low, and so matched filter detectors are rarely used in practices. In addition, a CR should be able to operate in many different frequency bands, detecting the presence of primary signals belonging to various communications standards. Therefore, effective spectrum sensing strategies should be as blind as possible. Then, in order to effectively apply the Rayleigh-ness test for the detection of a primary signal, we replaced the cross-correlation samples of the received signal with the *auto-correlation* samples.

Let $s(t)$, be the transmitted complex OFDM signal with symbol length T_d and CP length T_c, which is assumed to be affected by additive complex circular Gaussian white noise $n(t)$. The received signal is $x(t) = s(t)+n(t)$ under the H_1 hypothesis and $x(t)=n(t)$ otherwise. In addition, let $\Lambda = \left[|C_1|,....|C_N|\right]^T$ be the series of the auto-correlation. Then, following the same approach as in the previous section, the testing variable of the new method is expressed as:

$$X_c = 2\left[\frac{1}{M}\sum_{k=0}^{M-1}|C_k|^2\right]^2 - \frac{1}{M}\sum_{k=0}^{M-1}|C_k|^4 \tag{7.6}$$

The testing variable is the compared to a preselected threshold in order to discriminate between the two hypotheses. The test threshold can be tuned from a straightforward evaluation of the Gaussian integral for a fixed probability of false alarm:

$$v = E\left[X_c\right]|H_0 + \frac{1}{\sqrt{2var\left[X_c\right]|H_0}} erfc^{-1}\left(2\,P_{FA}\right) \tag{7.7}$$

and the probability of detection is determined by means of the error function in the H_1 hypothesis:

$$P_D = \frac{1}{2} erfc\left(\frac{v - E\left[X_c\right]|H_1}{\sqrt{2var\left[X_c\right]|H_1}}\right) \tag{7.8}$$

7.4 Numerical results

Several simulations trials have been performed to validate the proposed method, versus the conventional approach [78], under the same settings and channel. The probability of detection of the new detector is evaluated under the CFAR procedure versus SNR of practical interest conditions. The reported analysis, a $P_{FA}=10^{-3}$ and white Gaussian noise have been used. Moreover, several Monte-Carlo simulation trials (10^6 independent runs)

have been implemented to numerically evaluate the detection probabilities of the two methods.

Following the same approach of [78], we have considered an OFDM signal with a 16-QAM modulation and a symbol length of T_d=256. The P_D of both the conventional and new procedure are shown in Fig. 7-1 for a CP length of $T_c=T_d/4$ (i.e. the length of the CP for the WLAN system). The simulated (dotted) lines well matched the theoretical ones, thus validating the correctness of the mathematical analysis of the previous sections. Notwithstanding the curves referring to new procedure are very close to the one referring to the conventional procedure, the conventional test slightly outperforms the new method. However, the reduced performance is greatly compensated by the "blindness" of our method that requires no additional information on the parameters of the signal of interest. Moreover, if the CP duration is known to the receiver the performance of the conventional test can be obviously even higher (see again Fig. 7-1). It has to be underlined that this is the best case, where all the signal's parameters are known to the detector. However, this is not a typically operating case; hence we refer to this situation as the upper limit of the system performance.

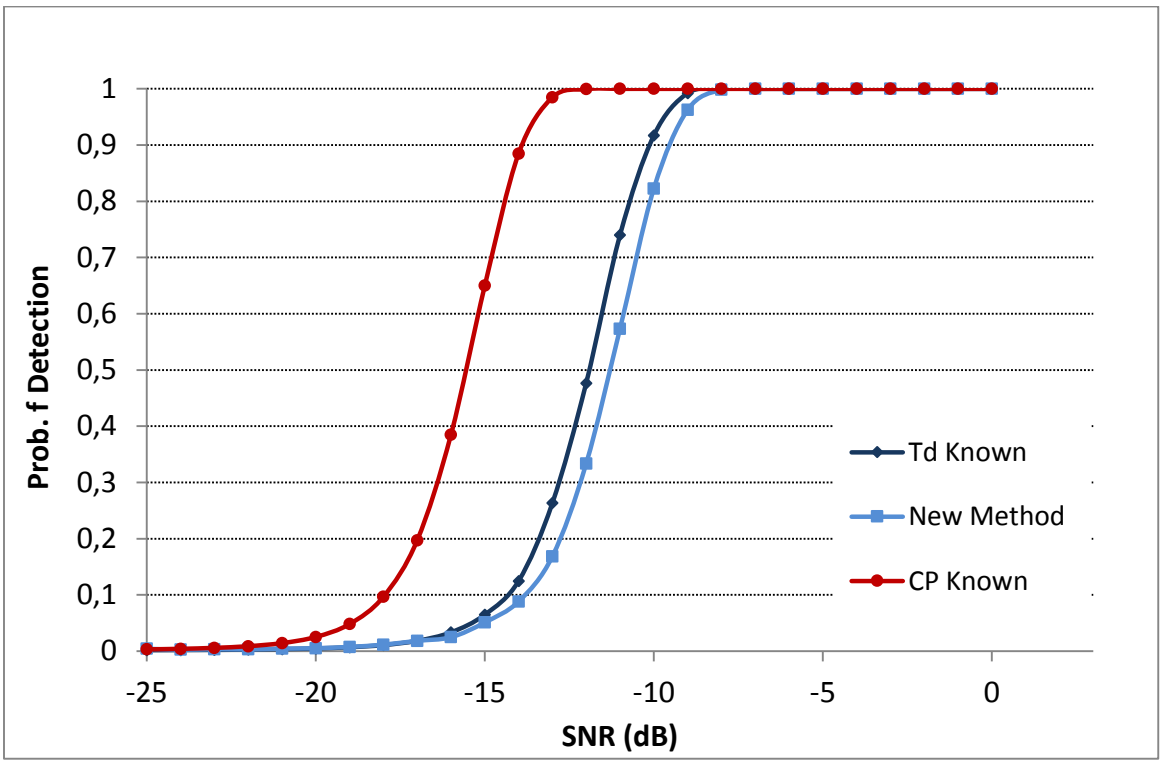

Figure 7-1 P_D versus SNR ($P_{FA}=10^{-3}$), of both the new (blind) and conventional method for a CP length of $T_c=T_d/4$

Many communication systems support multiple choices for the CP length (i.e. in the case of DVB-T, T_c varies from $T_d/4$, to $T_d/16$). Then, in order to assess the performance of the proposed method in real case scenarios, we evaluated the P_D with values of the CP length spanning from $T_d/8$, to $T_d/16$. Results are shown in Fig.7-2, where it can be easily seen that the new method drastically outperforms the conventional one, in all the addressed cases. Moreover the performance of the conventional strategy strongly depends on the length of the CP and lower P_D are obtained with lower T_c. On the other hand, the performance of the proposed methods are almost the same, for every CP length. This is due to the blindness of our procedure that is not affected by variations in the CP length.

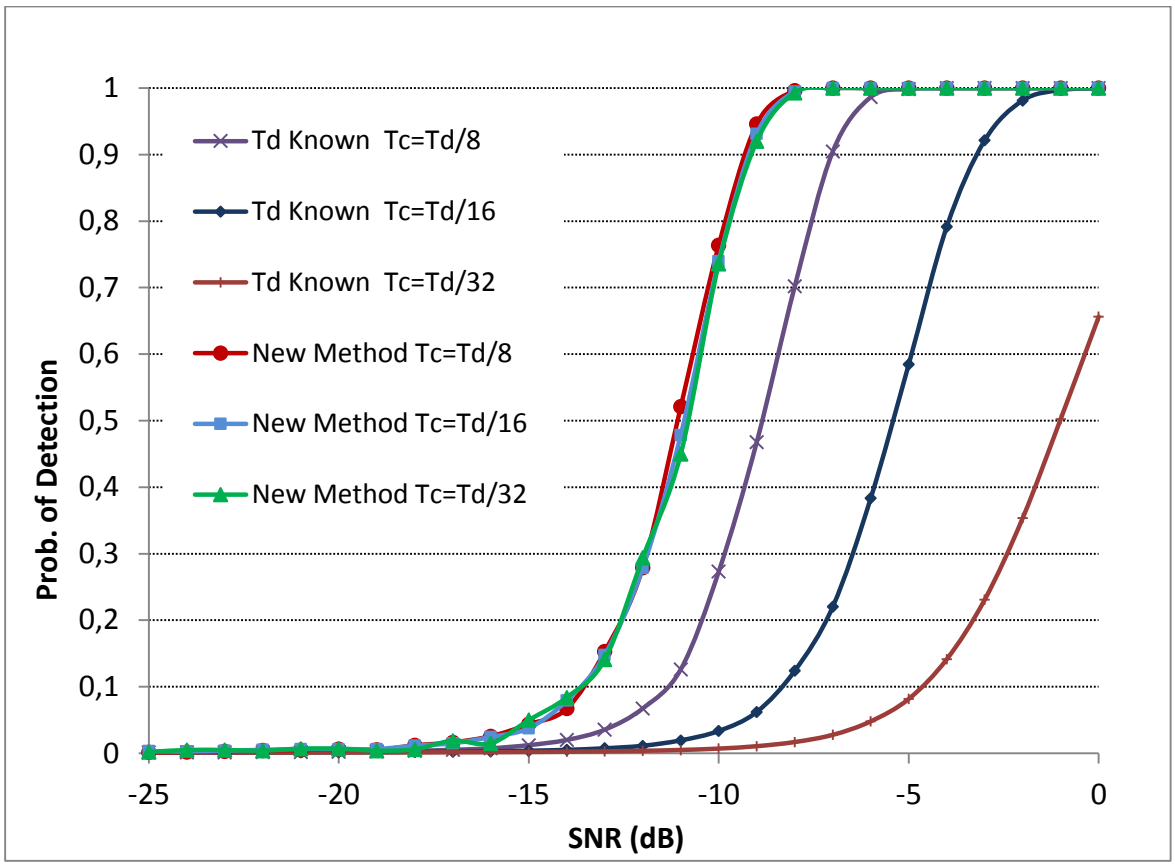

Figure 7-2 P_D versus SNR ($P_{FA}=10^{-3}$), of both the new and conventional method for a CP length of $T_c=T_d/8$

7.5 Conclusions

This Chapter has presented an effective detection strategy for an OFDM-based primary signal. The proposed method requires no a priori knowledge of the signal interest, since it exploits the autocorrelation of the received signal. The performance of the new method has been analyzed in comparison a spectrum sensing approach [78], based on the autocorrelation coefficient. The numerical results, obtained from wide simulation trials have evidenced the effectiveness of the devised method in different operating scenarios. We have applied our method using typical operating parameters for OFDM signal of wireless local area networks (i.e. IEEE 802.11x protocols) and multimedia communications (i.e. Digital

video Broadcasting-Terrestrial systems, DVB-T), thus proving the applicability of the new method for spectrum sensing in CRNs.

Chapter 8 A Software Radio Implementation for Spectrum Hole Sensing in Cognitive Radio Networks

8.1 Introduction

One of the main requirements of the spectrum sensing is the fast and reliable detection of primary users. In fact, SUs are low priority users of the radio spectrum and they must release the frequency bands in use as soon as a PU is detected. Cognitive radios should be able to sense wide portions of spectrum and identify more than one spectrum hole suitable for communications. In this way, if a PU appears in the band currently in use, the SU can easily switch to one of the other spectrum holes. The simplest and most natural way of dealing with a wideband frequency band is to divide it into multiple sub-channels. Then, the problem is to determine which sub-channels are occupied and which are available. Generally all the sub-channels are assumed to be independent so that, the multiband sensing problem reduces to the conventional hypothesis testing of type (6.2) for each sub-channel. In practice, there many cases in which the sub-channels are not independent, due to the correlation among adjacent frequencies. In these cases, the detection problem, becomes a composite hypothesis testing that grows exponentially with the number of sub-channels. However, in many cases, such as in the DVB-T system there is not noteworthy correlation between adjacent channels and the independent channel model can be effectively used. In such case digital filter banks based on the FFT transform can be used for sensing multiple sub-bands in parallel [106]-[107]. These methods are particularly suitable for OFDM systems, in which the signal consist of multiple orthogonal narrow band subcarriers. Applications of FFT filter bank to the WLAN standards can be found in [108]-[109], while Bluetooth signals detection is investigated in [110]. However, conventional filter banks methods makes use of analog hardware, because the RF imperfections (i.e. the leakage effects of filters, nonlinearity of the amplifier stages, …) can be better handled in the analog domain. Also, digitizing a wideband signal with high dynamic range is a problem from the

ADC conversion point of view. In fact, the system bandwidth is often large enough so that it cannot be digitalized and processed all at once. Hence, SDR concepts cannot be always fully exploited.

Recently, the authors in [111] have proposed a fast two-stage sensing strategy for spectrum holes detection in the DVB-T frequency bands. The method consists in two consecutive stages: a preliminary coarse resolution sensing (CRS) followed by a fine resolution sensing (FRS). The overall system band is first scanned with a coarse resolution bandwidth to identify a set of potentially vacant bands. Then, the selected frequency bands are scanned with a finer resolution bandwidth for detecting a spectrum hole. In the two-stages sensing approach, both analog phase locked loops (PLL) and filters are used to generate the carrier frequency and, then, to select the band of interest. This solution strongly reduces the system flexibility, and restricts the range of frequency bands over which the CR device can operate. Moreover, in such approach ADC limitations are significant in the first (CRS) stage, due to the CSB large bandwidth. Conversely, digital filters can be effectively exploited in the FRS stage, in which the band of each channel is narrow enough to be processed by digital filter banks without any ADC conversion issues.

In this dissertation SDR concepts and FFT filter bank are exploited for spectrum holes detection in DVB-T systems. A new method is proposed that uses short FFT and detects more than one spectrum hole at the same time, without increasing the system complexity. The performance of the proposed method are matched to the one in [111] under the same signal and channel conditions. The obtained results evidence that the innovative strategy allows both higher detection probabilities and lower mean detection time with respect to the conventional method.

The remainder of this chapter is organized as follows. Section 2 depicts the system model, while the proposed method is detailed in section 3. Section 4 the performance of both method are evaluated in terms of the mean number of operations required for achieving a decision over the channel occupancy. Results are shown in Section 5, before the conclusion briefly depicted in Section 6.

8.2 System model

Let us assume that the entire spectral band comprises N contiguous discrete frequency channels of band B_c, which also represents the band of a the signal of interset. There are L, with $L << N$, spectrum holes, randomly scattered over the N channels. The total spectrum is divided into β contiguous coarse sensing block (CSBs) of bandwidth B_{csb}, each one consisting of $\alpha = N/\beta$ channels of equal bandwidth B_c (see Fig.8-1). First, the overall system band is scanned with the coarse resolution bandwidth (i.e. $B_{sense} = B_{csb}$) and a candidate CSB is identified. Then, the selected CSB is scanned with the finer resolution bandwidth (i.e. $B_{sense} = B_c$) and a spectrum hole is detected.

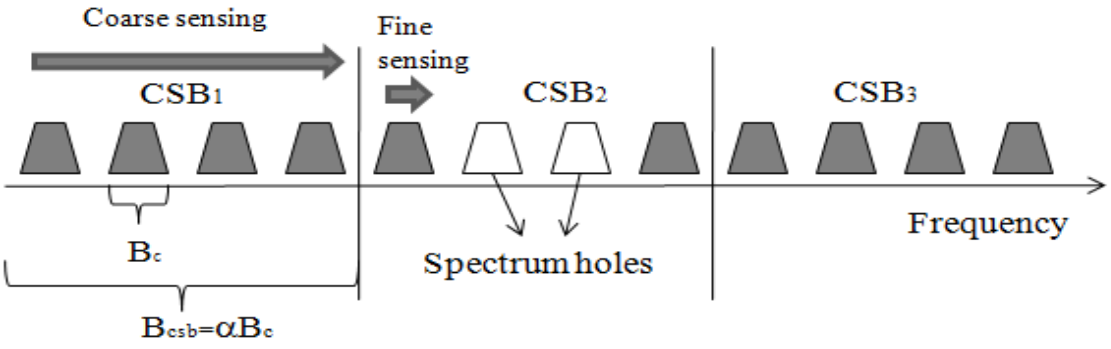

Figure 8-1 Two-stage spectrum sensing for DVB- T.

In both stages, energy detection is used to keep the computational complexity as low as possible. Following the same notation of the previous chapters, let assume that $\mathbf{r} = [r_1, r_2, r_3 ... r_N]^T, \mathbf{s} = [s_1, s_2, s_3 ... s_N]^T, \mathbf{n} = [n_1, n_2, n_3 ... n_N]^T$ are the sequence (of N samples) of the received signal, of the primary signal, and of the noise, respectively. Then the decision variable of the ED is evaluate as in shown in eq. (6.3) and here reported for the sake of readability:

$$X = \frac{1}{N}\sum_{i=1}^{N} |r_i|^2 \qquad (8.1)$$

8.3 Proposed method

One motivation for the analog two-stage approach, or at least for doing the first step on the analog side, is that the RF imperfections can be better handled in the analog domain. However, while these limitations are significant in the CRS stage, due to the CSB bandwidth, digital filters can be effectively exploited in the FRS stage. Therefore, in the following, we assume that a CSB has already been selected and we focus our attention on the FRS stage only.

The FFT filter bank (FFTFB) is a computationally efficient technique for implementing the equivalent of a bank of band-pass filters. FFTFBs can be effectively used for sensing more than one frequency band at the same time, effectively reducing the time required for identify spectrum access opportunities. In the basic FFTFB implementation, the received wideband signal is processed by an FFT modulus and the Power Spectrum Density (PSD) of each frequency band is evaluated. The sensing bandwidth of the filters is inversely proportional to the number of samples (N_{FFT}) over which the FFT is computed. However, FFTs with a high number of bins are computational expensive and time consuming. Therefore, the optimum value of N_{FFT} is a trade-off between performance and computational efforts.

The method proposed in this chapter allows implementing FFTFBs with small N_{FFT}, and without decreasing the system performances. The rationale behind the new procedure is as follows. The received signal is dived into W blocks of data, and the FFT is performed on each block. Then, in every block, a group of contiguous bins is used to evaluate the power estimate in each channel. Finally, the PSD of the channel is obtained by averaging the power estimates of each the block. The key of the innovative method is the averaging operation, which allows to effectively exploit FFTFBs with a small number of bins (i.e. $N_{FFT} = 4, 8, 16$) and without decreasing the system performances.

More in details and following the same system model of the previous the entire system bandwidth is divided into α channels of equal bandwidth B_c, while the signal is divided into

$W=N_s/N_{FFT}$ groups of data. The W consecutive groups of data can be defined by the following vectors:

$$\mathbf{B}_j = \left[r_{j\cdot N_{FFT}}, r_{j\cdot N_{FFT}+1} \ldots . r_{j\cdot N_{FFT}+N_{FFT}-1} \right], \qquad 0 \le j \le W-1 \tag{8.2}$$

The vectors $\mathbf{B}_j$ are then transformed by a FFT of length N_{FFT} as follows:

$$\mathbf{Y}_j = FFT(\mathbf{B}_j) = \left[y_{j,0}, y_{j,1} \ldots y_{j,N_{FFT}-1} \right], \quad 0 \le j \le W-1 \tag{8.3}$$

Now, in each FFT-vector, $K=N_{FFT}/\alpha$ bins are assigned to each channel to compute the PSD. In particular, for each vector $\mathbf{Y}_j$, a vector $\boldsymbol{Z_j} = \left[z_{j,0}, z_{j,1} \ldots . z_{j,\alpha-1} \right]$ of length α is formed by summing the power over K contiguous bins. The elements of $\mathbf{Z}$ are given by:

$$z_{j,i} = \sum_{k=0}^{K-1} \left| y_{j,i\cdot K+k} \right|^2, \quad 0 \le i \le \alpha-1;\ 0 \le j \le W-1 \tag{8.4}$$

Finally, the decision statistic for the i-th channel is obtained by averaging the power estimates in (8.4) over the W blocks:

$$Z_i = \frac{1}{W} \sum_{j=1}^{W} z_{j,i}, \qquad 0 \le i \le \alpha-1 \tag{8.5}$$

The testing variable in (8.5) is then compared with a threshold value, calculated according to the desired false alarm probability. Since the testing variable is Gaussian from direct application of the central limit theorem, the test threshold can be evaluated from a straightforward evaluation of the Gaussian integral as follows:

$$v_i = E\left[Z_i \right] | H_0 + \frac{1}{\sqrt{2var\left[Z_i \right] | H_0}} erfc^{-1}\left(2\, P_{FA} \right) \tag{8.6}$$

A different threshold for each channel could be used. However, assuming statistical independence between channels, the same threshold for all the channels can be used (i.e. $v_I = v$).

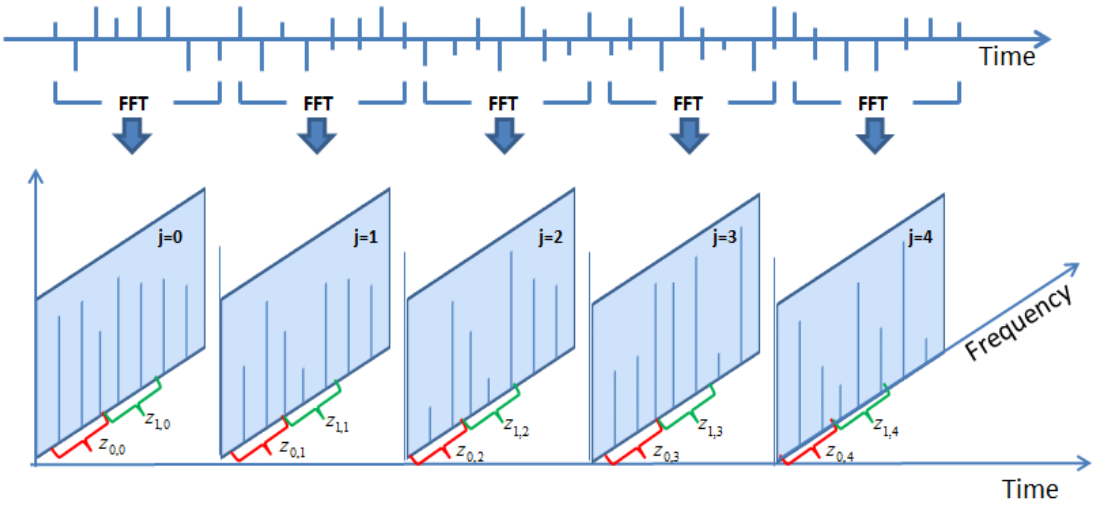

Figure 8-2 Basic scheme of the proposed procedure

8.4 Mean number of required operation

A relevant parameter for evaluating the performance of a spectrum sensing algorithm is the mean detection time required for identifying a spectrum hole. The mean detection time depends on the average number of steps required for detecting a spectrum hole (S_{det}), and the time needed for reaching a decision (T_D) about the occupancy of the channel. However, while S_{det} depends only on the performance of the sensing algorithm (i.e. on both P_D, and P_{FA},), T_D is strongly related to the specific hardware architecture. Therefore, in the rest of this chapter, we refer to the *mean number of operations* (MNO) as the number of (real) sums and multiplications, on average, requested to perform the selected operation [76].

8.4.1 MNO of the Conventional method

In the two-stage sensing approach, a single channel is first selected and the energy of the received signal is computed. The number of arithmetic operations needed for computing the energy of the received signal can be derived from (8.1): 1 complex sum and 2 complex multiplications are needed for computing each of the N_s square modulus. It is well known

that one complex sum is implemented with two real sums, while one complex multiplication requests 4 real multiplications and two real sums.Then:

- 1 real sum and 2 real multiplications are needed for computing each of the N_s square modulus.
- N_s-1 real sums are required for accumulating all the (square) modulus.

Finally, the total number of required real arithmetic operations (i.e. sums and multiplications) is given by:

$$N_{\text{op}} = 3N_s + N_s - 1 = 4N_s - 1 \tag{8.7}$$

In [111], random search is used in the CRS stage, while serial search is performed in the FRS stage. The mean number of steps required for successfully detecting a candidate CSB in the first stage is defined as follows:

$$S_{CRS} = \frac{1/[1-\left(\frac{N-L}{N}\right)^{\alpha} P_D^c]}{1-\sum_{k=1}^{\alpha}\binom{\alpha}{k}\frac{L^k(N-L)^{\alpha-k}}{(N^\alpha-(N-L)^\alpha)}(1-P_D^f)^k} \tag{8.8}$$

where $P_D{}^c$ is the probability of successfully identifying a spectrum hole and $P_{FA}{}^c$ is the probability of declaring empty a busy channel. In the FRS stage, two opposite cases should be considered: the FRS is performed after a correct detection ($S^{cor}{}_{FRS}$), or after a false alarm ($S^{fal}{}_{FRS}$) in the previous stage. The average number of steps is under these tow case is expressed as, respectively:

$$S_{frs}^{cor} = \sum_{i=1}^{\alpha}\binom{\alpha}{i}\frac{L^i(N-L)^{\alpha-i}}{(N^\alpha-(N-L)^\alpha)}\frac{P_{FA}^f(\alpha-i)J+\alpha}{P_D^f i} \tag{8.9}$$

$$S_{frs}^{fal} = \frac{P_{FA}^c(N-L)^\alpha(\alpha+J\alpha P_{FA}^f)}{P_D^c(N^\alpha-(N-L)^\alpha)} \tag{8.10}$$

where *J* is a penalty factor that takes into account the consequences of a false alarm in the FRS stage, and P_D^f and P_{FA}^f are the detection and false alarm probabilities of the FRS stage, respectively. Finally, the mean number of operations required for detecting a spectrum hole is given by:

$$MNO = N_{op}(S_{CRS} + S_{FRS}) = (4N_s - 1)\cdot \left(\frac{1/[1-\left(\frac{N-L}{N}\right)^{\alpha} P_D^c]}{1-\sum_{k=1}^{\alpha}\binom{\alpha}{k}\frac{L^k(N-L)^{\alpha-k}}{(N^{\alpha}-(N-L)^{\alpha})}(1-P_D^f)^k} + \sum_{i=1}^{\alpha}\binom{\alpha}{i}\frac{L^i(N-L)^{\alpha-i}}{(N^{\alpha}-(N-L)^{\alpha})}\frac{P_{FA}^f(\alpha-i)J+\alpha}{P_D^f i} + \frac{P_{FA}^c(N-L)^{\alpha}(\alpha+J\alpha P_{FA}^f)}{P_D^c(N^{\alpha}-(N-L)^{\alpha})} \right) \quad (8.11)$$

8.4.2 MNO of the proposed method

The *MNO* required by the proposed method for determining the testing variable in (8.5) can be evaluated as follows:

- The number of multiplications and sums needed to perform a power-of-two N_{FFT}-point FFT is given in [20] and equal to:

$$N_{op}^{FFT} = [4N_{FFT}\log_2(N_{FFT})\text{-}6\,N_{FFT}+8] \quad (8.12)$$

- $W \cdot (4\,N_{FFT}\text{-}1)$ complex sums and multiplications are needed for computing the square modulus in eq. (8.4)
- $W\cdot(K\text{-}1)$ sums are required for accumulating all the (square) modulus in eq. (8.4).
- $(W\text{-}1)$ sums are needed to accumulate all the power estimates in eq. (8.5).

In conclusion, after some algebra, the total number of required operation is expressed as:

$$\bar{N}_{op} = W[4N_{FFT}\log(N_{FFT})\text{-}2\,N_{FFT}+7+K]\text{-}1 \quad (8.13)$$

It has to be noted that most of the required arithmetic operations is due to the FFT stage, while the latter stages have a minor impact on the overall computation complexity. High FFT lengths are needed to process very wideband signals. On the other hand, as the FFT length becomes higher, the computational complexity increases and the benefits of using FFTFBs become less significant. Due to such bandwidth constrains, in the subsequent analysis, it assumed that a candidate CSB has already been selected and we focus on the FRS stage only. Assuming that no false alarm has occurred in the CRS stage, all the α channels in a CSB can be simultaneously tested. Under such assumption equations (8.9) and (8.10) rewrite as, respectively:

$$S_{frs}^{cor} = 1 \tag{8.14}$$

$$S_{frs}^{fal} = \frac{P_{FA}^{c}(N-L)^{\alpha}(\alpha + J\alpha P_{FA}^{f})}{P_{D}^{c}(N^{\alpha} - (N-L)^{\alpha})} \tag{8.15}$$

The mean number of steps in the FRS stage, can be now expressed as:

$$S_{frs} = 1 + \frac{P_{FA}^{c}(N-L)^{\alpha}(\alpha + J\alpha P_{FA}^{f})}{P_{D}^{c}(N^{\alpha} - (N-L)^{\alpha})} \tag{8.16}$$

Finally, the mean number of operations required for spectrum holes detection in the FRS stage is given by:

$$MNO_{frs} = S_{frs}\bar{N}_{op}$$
$$\frac{N_s}{N_{FFT}}\left([4N_{FFT}\log(N_{FFT}) - 2N_{FFT} + 8 + \frac{N_s}{N_{FFT}}]\right)\cdot\left(1 + \frac{P_{FA}^{c}(N-L)^{\alpha}(\alpha + J\alpha P_{FA}^{f})}{P_{D}^{c}(N^{\alpha} - (N-L)^{\alpha})}\right) \tag{8.17}$$

The formulas show that the number of operation required for each step is higher than in the conventional method. However, such increasing is fully compensated by the reduced number of steps needed for spectrum holes detection. In addition, if short FFTs are used (i.e. N_{FFT} = 4, or N_{FFT} = 8) the FFT can be computed with fast and multiplication free implementations, the effectively reducing the MNO.

8.5 Numerical Results

Several simulations have been performed to validate the proposed spectrum sensing procedure versus the two-stage sensing approach. The performances of the two methods are evaluated in terms of detection and false alarm probability. Furthermore, we have evaluated the mean number of arithmetic operations required by the two methods to detect a spectrum hole in the band of interest. Several Monte-Carlo simulation trials (10^5 independent runs) have been implemented to numerically evaluate the performance of the two methods. We assume that each CSB consists of $\alpha = 4$ channels of bandwidth B_c (= 6 MHz). In all the addressed cases DVB-T signals and white Gaussian noise have been used. In order to assess the performance of the new method in many different operating cases, various FFT lengths have been used (i.e. N_{FFT} = 4, 8, 16, 64, 128). The receiver operating characteristic (ROC) curves, i.e. P_D vs. P_{FA}, varying the length of the FFT, are shown in Fig. 8.3, in correspondences of SNR= -10dB. As it can be seen, for small N_{FFT}, the conventional method outperforms the proposed one. However, as the value of N_{FFT} increases, the curves referring to the two methods become closer, and they perfectly overlap for sufficiently high N_{FFT} (i.e. N_{FFT} = 256). The reason for such behavior can be explained as follows. The conventional energy detector assumes using ideal sensing filter, with rectangular frequency response. In the proposed method, if short FFTs are used (i.e. N_{FFT} =4), the filter frequency response is actually a *sinc*(·) function (where *sinc(x)=sin(x)/x*). The signals' bandwidth is narrow compared to the *sinc*-filter bandwidth, and hence, the captured energy is reduced. As a consequence, the mean of the test statistic under the hypothesis H_1 reduces and the performance of the proposed method decreases. However, with longer FFTs, this effect appears significantly only in the edge sub-bands, and the performance of the proposed method starts increasing. Moreover, the same number of samples has been used for both the considered methods. In particular, N_s =1024 time-samples are used in the conventional method for achieving the final decision over the occupancy of one single channel. On the other hand, only $N_s/4$ are used by the new method. In fact, the total number of samples used by the proposed method is still N_s but now the final decision is done over $\alpha = 4$ channels. This means that, for each channel, $N_s/4$ different samples are actually used. Thus, with the

same number of samples (i.e. N_s = 1024), we can now test four channels all together, effectively reducing the mean number of arithmetic operations. The MNO required by the two methods is shown in Fig. 8-4 versus the ratio between the number of spectrum holes and the total number of channels (i.e. *L/N*).

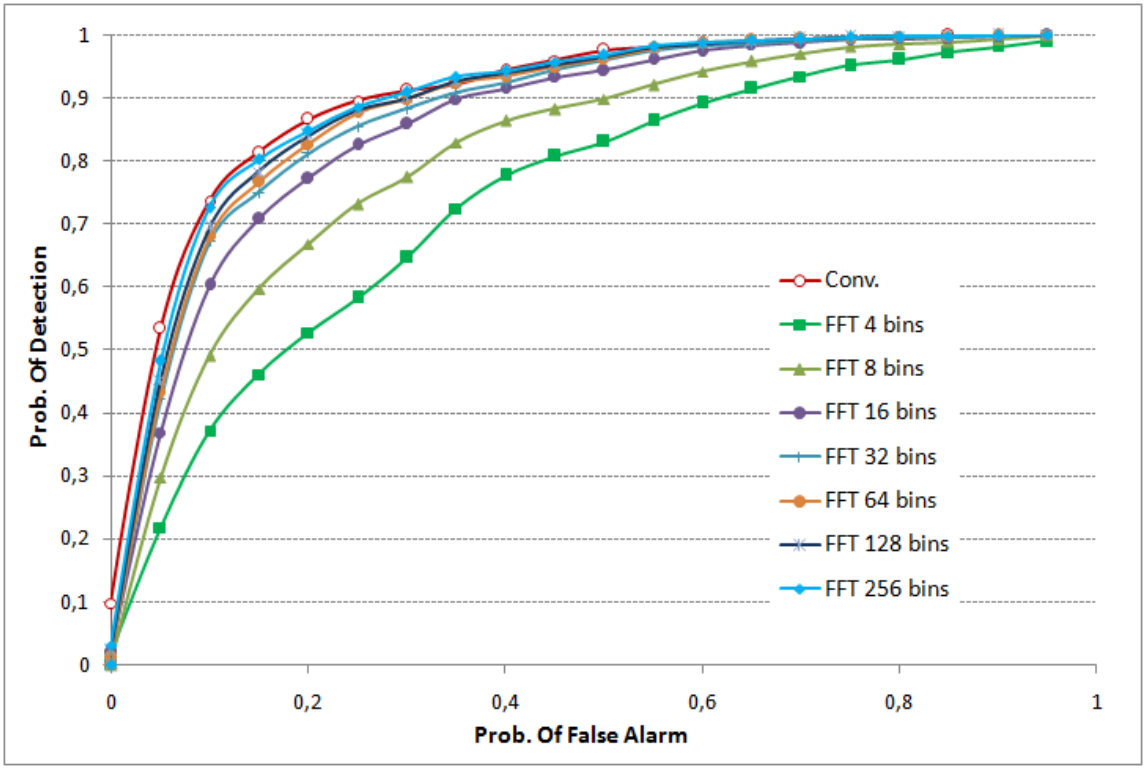

Figure 8-3. ROC curves of both the new and the conventional approach, for N_s=1024 and for signal-to- noise ratio SNR=-10dB

As the number of spectrum holes increases (i.e. L/N → 1) the MNO of the two methods becomes closer. That is because the probability of identify a spectrum holes in the first scanned channels becomes higher and fast detection in possible even with the conventional method. However, in most practical cases, spectrum holes are very rare. When L/N<<1 the proposed method drastically outperforms the conventional one. The detection performances of the innovative approach can be improved by increasing the number of sensing samples of each channel. Then, for a sufficiently high number of samples, i.e. N_s=4096, even with short FFTs, the proposed method outperforms the conventional one.

A performance comparison between the two strategies is depicted in Fig. 8-5, where 1024 and 4096 samples are used by the two-stage and the proposed scheme, respectively. In particular, the conventional method exploits 1024 samples for achieving the final decision over one single channel.

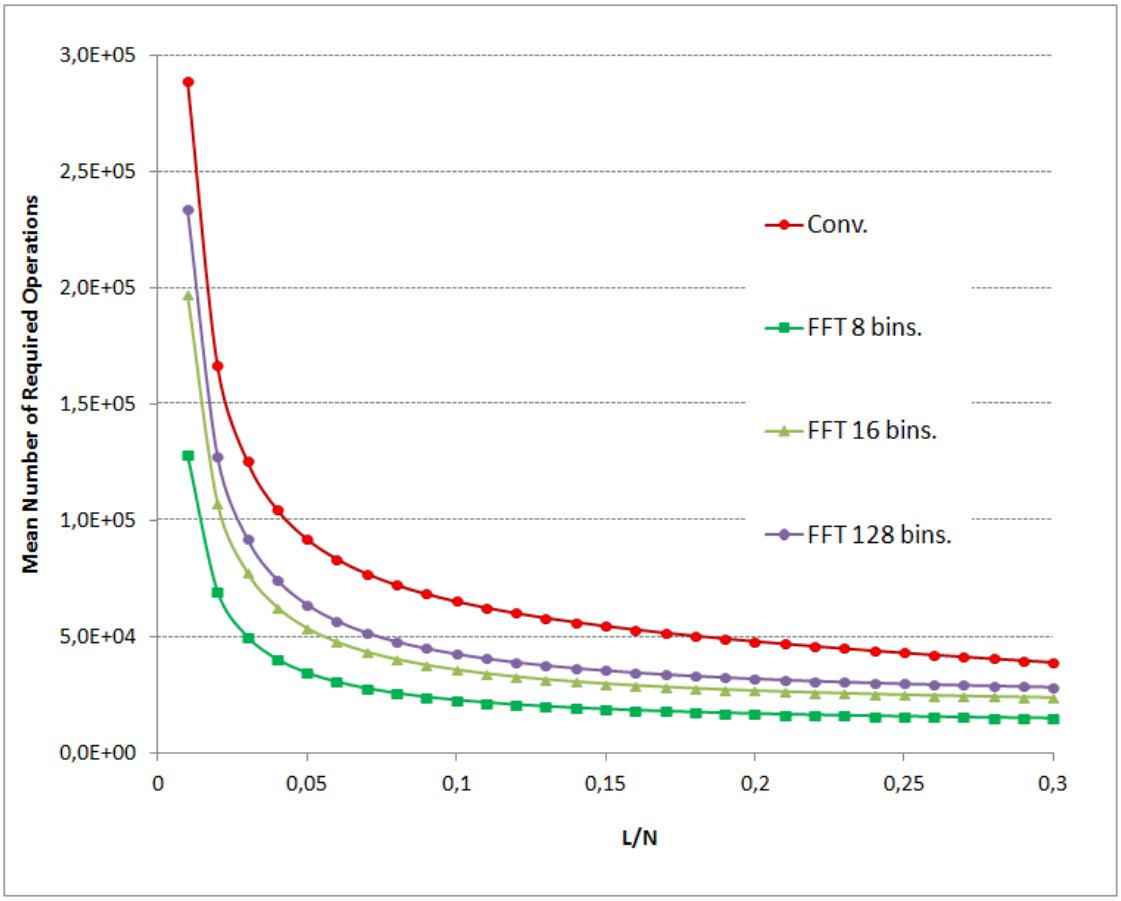

Figure 8-4 Mean number of required operations of both the conventional approach and the FFT method versus the ratio between the number of spectrum holes and the total number of channels (L/N), for N_s=1024

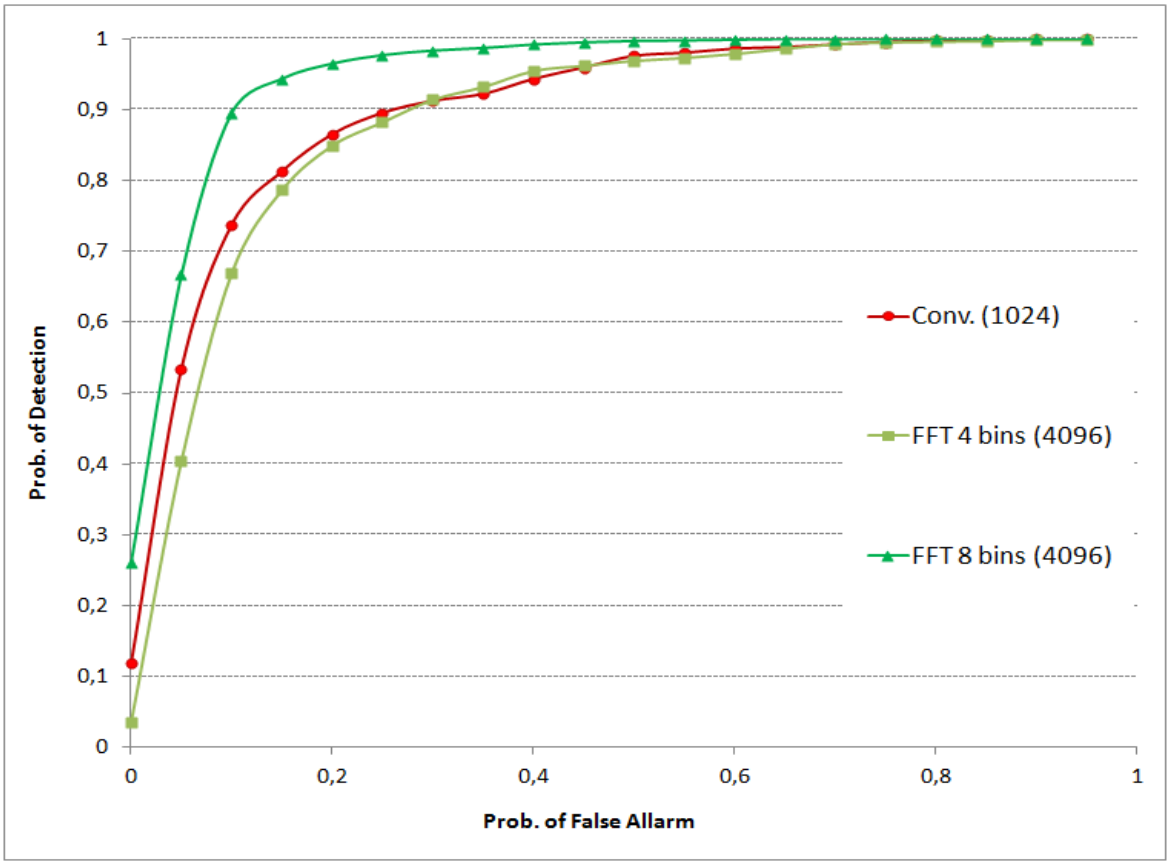

Figure 8-5 ROC of the conventional and proposed FFT methods for different numbers of received samples (1024 and 4096) and for SNR=-10dB.

Then, $N_s/4=1024$ samples, for each channel, are used by the proposed method. It is evident from the graph that, with a FFT of only 8 bins, our method drastically outperforms the conventional one. It has to be noted that the increase of the number of samples has only a neglible impact on the MNO. Fig. 8-6 shows the MNO in this news scenario. It can be seen that the FFT-based method with $N_s=4096$ is still faster than the two-stage approach with $N_s=1024$

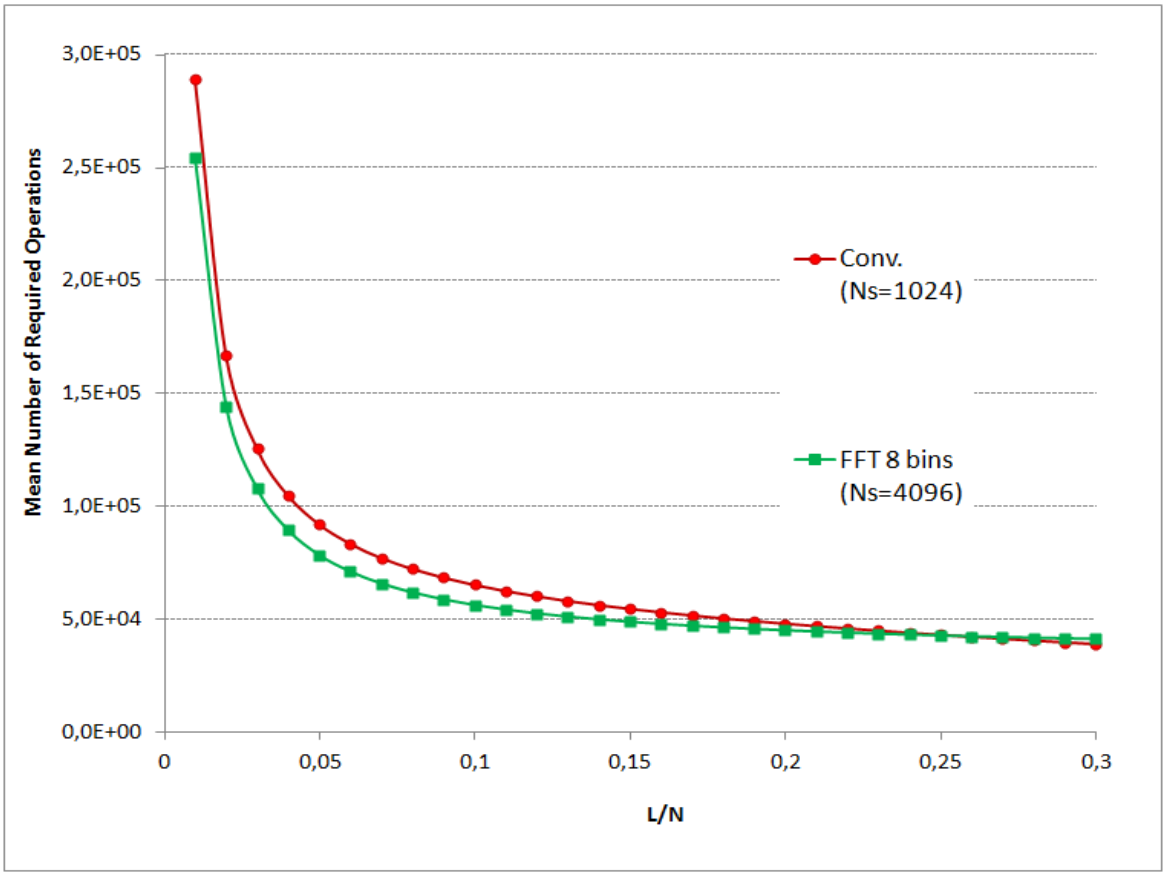

Figure 8-6. Mean number of required operations of both the conventional approach (N_s = 1024) and the FFT method (N_s = 4096) vs. the ratio between the number of spectrum holes and the total number of channels (L/N).

8.6 Conclusions

This chapter has presented a software radio implementation for multi-channel spectrum sensing method in CRN that exploits FFT filter banks. A performance analysis of the proposed method has been carried out in comparison with a two stage sensing approach that exploits analog band-pass filters. Numerical results show that the FFT filter banks allows achieving both higher detection probabilities and lower mean detection time. Different FFT lengths have been used, and the obtained results have evidenced that good performances can be achieved even with small FFT lengths, with the advantages of free multiplication implementations.

Chapter 9 NORMALIZED VARIANCE-BASED SPECTRUM SENSING

9.1 Introduction

Recently, spectrum sensing methods based on high-order statistics (HOS) of the received signal have been proposed in advance cognitive radio system. These methods allow overcoming the drawbacks of energy detection under noise uncertainty, without dramatically growing up the overall computational complexity. In fact the main drawbacks of ED is that the noise variance has to be perfectly known in order to correctly set the threshold, however in most practical cases exact knowledge of the noise variance is not possible. Hence, the assumption is that the noise variance is expected to be in the range $[(1/\rho)\cdot \sigma^2, \rho\cdot\sigma^2]$ where ρ is the parameter related to the size of the uncertainty. Hence, accurate estimates of the noise variance are needed to overcome the drawbacks of weak signal detection and noise uncertainty, without dramatically growing up the overall computational complexity of the system. Many HOS have been proposed in the scientific literature. In [91], the authors first estimate the third-order cumulant (accounting for the asymmetry of the probability distribution) and then use this value as the testing variable to decide about the presence of the primary user in a certain band. Unfortunately, this method cannot be used for signals characterized by symmetric distribution, such as constant modulus (CM) signals. However, this assumption is usually verified in CR communications, since primary transmissions often take place by means of CM waveforms that are also highly desirable for portable digital radios [112]. Important examples are represented by the cases of: the wireless microphones [113], the phase shift keying (PSK) modulation used in the Direct Sequence-Code Division Multiple Access (DS-CDMA) technique [114], and the Gaussian Minimum Shift Keying (GMSK) modulation employed by both the GSM cellular network and the Bluetooth system [51]. Therefore, it is fair to assume that many PUs will be CM based.

In this dissertation, a novel HOS-based spectrum sensing technique, called the *normalized variance* (NV) method is proposed. The method allows fast and reliable detection of primary users. The rationale behind the new strategy is as follows. First the second and fourth order moments of the received signal are evaluate. Then a new decision variable, namely the *normalized variance* (Ω), is derived as a function of these higher order moments and compared to a preselected threshold for determine the presence of PUs. It has to be noted that no a priori knowledge about the signal of interest is needed by the innovative method, and the sole assumption made is to work with constant-modulus (CM) signals.

The remainder of this chapter is organized as follows. The new method is described in Section 2. Performance analysis is carried out in Section 3, while results are reported in Section 4. Finally, chapter conclusion are depicted in section 5.

9.2 The NV method

The main idea behind the new procedure is that the normalized variance of the received signal is lower when the primary user is present (H_1 hypothesis), while it is higher in the alternate H_0 (i.e. when we have only noise, H_0 hypothesis). In fact, the signal of the primary user is a realization of a CM process with power P_s. Conversely, the same consideration is not more valid for the channel noise which is a realization of a Gaussian process. Hence, the normalized variance of the received signal can be effectively used for discriminating between the presence and absence of the signal of interest. In same case and applications, the primary signal level may be very week at signal samples; hence, we introduce an integration operation that is realized as follows. The received signal is first dived into L blocks of K samples. Then, the second and fourth order moments of each block are estimated, and the normalized variance of each j-th block evaluated. Finally, the normalized variance over L blocks is derived as the sum of each j-th normalized variance, and then used as the testing variable to state whether a primary user is present or not.

More in details, let the vectors of the received signal, of the primary user's signal, and of the noise, in the *j*-th data block, be defined as follows:

$$\begin{aligned}\mathbf{R}_j &= \left[r_{j\cdot K}, r_{j\cdot K+1}....r_{j\cdot K+K-1} \right] \\ \mathbf{S}_j &= \left[s_{j\cdot K}, s_{j\cdot K+1}....s_{j\cdot K+K-1} \right] \\ \mathbf{N}_j &= \left[n_{j\cdot K}, n_{j\cdot K+1}....n_{j\cdot K+K-1} \right]\end{aligned} \tag{9.1}$$

with $0 \le j \le L-1$. Now, let $M_{2,j}$ be the second-order moment of the received signal in the *j*-th block and expressed as follows:

$$M_{2,j} = E\left[\left| \mathbf{S}_j + \mathbf{N}_j \right|^2 \right] = E\left[\mathbf{S}_j \cdot \mathbf{S}_j^* \right] + E\left[\mathbf{N}_j \cdot \mathbf{N}_j^* \right] + E\left[\mathbf{S}_j \cdot \mathbf{N}_j^* \right] + E\left[\mathbf{N}_j \cdot \mathbf{S}_j^* \right] \tag{9.2}$$

where $E[\cdot]$ denotes the expectation operator, $|\cdot|$ stands for the absolute value, and $(\cdot)^*$ denotes the complex conjugate operator. Assuming that the signal and the noise are zero-mean, mutually independent random processes, we have:

$$\begin{aligned}E\left[\mathbf{S}_j \cdot \mathbf{N}_j^* \right] &= 0 \\ E\left[\mathbf{S}_j^* \cdot \mathbf{N}_j \right] &= 0.\end{aligned} \tag{9.3}$$

Eq. (4) can now be re-written as follows:

$$M_{2,j} = E\left[\mathbf{S}_j \cdot \mathbf{S}_j^* \right] + E\left[\mathbf{N}_j \cdot \mathbf{N}_j^* \right] = P_{S,j} + P_{N,j} \tag{9.4}$$

where $P_{S,j}$ and $P_{N,j}$ are the signal and noise powers in the *j*-th block, respectively. Now, let $M_{4,j}$ denote the fourth order moment of the *j*-th block and expressed by:

$$\begin{aligned}M_{4,j} &= E\left[\left| \mathbf{S}_j + \mathbf{N}_j \right|^4 \right] \\ &= E[(\mathbf{S}_j \cdot \mathbf{S}_j^*)^2 + (\mathbf{N}_j \cdot \mathbf{N}_j^*)^2 + (\mathbf{S}_j \cdot \mathbf{N}_j^*)^2 + (\mathbf{S}_j^* \cdot \mathbf{N}_j)^2 + 4(\mathbf{S}_j \cdot \mathbf{S}_j^* \cdot \mathbf{N}_j \cdot \mathbf{N}_j^*) \\ &+ 2(\mathbf{S}_j \cdot \mathbf{S}_j^* \cdot \mathbf{S}_j \cdot \mathbf{N}_j^*) + 2(\mathbf{S}_j \cdot \mathbf{S}_j^* \cdot \mathbf{S}_j^* \cdot \mathbf{N}_j) + 2(\mathbf{N}_j \cdot \mathbf{N}_j^* \cdot \mathbf{S}_j \cdot \mathbf{N}_j^*) + 2(\mathbf{N}_j \cdot \mathbf{N}_j^* \cdot \mathbf{S}_j^* \cdot \mathbf{N}_j)]\end{aligned} \tag{9.5}$$

Assuming that the real and imaginary components of the noise and signal processes are orthogonal, we have:

$$\begin{aligned} &E[\mathbf{S}_j \cdot \mathbf{S}_j^* \cdot \mathbf{N}_j \cdot \mathbf{N}_j^*] = 0 \\ &E[\mathbf{S}_j \cdot \mathbf{S}_j^* \cdot \mathbf{S}_j \cdot \mathbf{N}_j^*] = 0 \\ &E[\mathbf{S}_j \cdot \mathbf{S}_j^* \cdot \mathbf{S}_j^* \cdot \mathbf{N}_j] = 0 \\ &E[\mathbf{N}_j \cdot \mathbf{N}_j^* \cdot \mathbf{S}_j \cdot \mathbf{N}_j^*] = 0 \\ &E[\mathbf{N}_j \cdot \mathbf{N}_j^* \cdot \mathbf{S}_j^* \cdot \mathbf{N}_j] = 0 \end{aligned} \quad , \tag{9.6}$$

Then, the fourth order moment re-writes as follows:

$$\begin{aligned} &M_{4,j} = \\ &E[\mathbf{S}_j \cdot \mathbf{S}_j^*]^2 + 2 \cdot E[\mathbf{N}_j \cdot \mathbf{N}_j^*]^2 + 4 \cdot E[\mathbf{S}_j \cdot \mathbf{S}_j^*] \cdot E[\mathbf{N}_j \cdot \mathbf{N}_j^*] = \\ &P_{S,j}^2 + 2 \cdot P_{N,j}^2 + 4 \cdot P_{S,j} \cdot P_{N,j} \end{aligned} \tag{9.7}$$

Recalling the well-known mathematical relation *var*[x]=*E*[x|^2] - *E*[x]^2, the normalized variance of each block can be obtained as follows:

$$\Omega_j = \frac{M_{4,j} - M_{2,j}^2}{M_{2,j}^2} = \frac{M_{4,j}}{M_{2,j}^2} - 1 \tag{9.8}$$

And after some algebra we :

$$\Omega_j = \frac{P_{N,j}^2 + 2 \cdot P_{S,j} P_{N,j}}{P_{S,j}^2 + P_{N,j}^2 + 2 \cdot P_{S,j} \cdot P_{N,j}} \tag{9.9}$$

Finally, the normalized variance is defined as the average of (9.9) over the *L* blocks, as follows:

$$\Omega = \sum_{j=1}^{L} \Omega_j, \tag{9.10}$$

Now, its estimation is used as the testing variable for discriminating about the presence and absence of the primary user. The new testing variable is hence estimated according to the following:

$$\hat{\Omega} = \sum_{j=1}^{L} \hat{\Omega}_j, \quad \text{with} \quad \hat{\Omega}_j = \frac{\hat{M}_{4,j} - \hat{M}_{2,j}^2}{\hat{M}_{2,j}^2} = \frac{\hat{M}_{4,j}}{\hat{M}_{2,j}^2} - 1, \tag{9.11}$$

where the estimates $\hat{M}_{2,j}$, and $\hat{M}_{4,j}$ of the second and fourth order moments are obtained, respectively, as:

$$\hat{M}_{2,j} = \frac{1}{K}\sum_{i=j\cdot K}^{j\cdot K+K-1} |r_i|^2$$
$$\hat{M}_{4,j} = \frac{1}{K}\sum_{i=j\cdot K}^{j\cdot K+K-1} |r_i|^4 \qquad 0 \le j \le L-1 \tag{9.12}$$

and r_i is the i-th sample of the received signal.

The testing variable in (9.11) is asymptotically ($L \to \infty$) Gaussian as a direct consequence of the central limit theorem. Hence, the test threshold can be asymptotically tuned from a straightforward evaluation of the Gaussian integral for a fixed probability of false alarm, under the null-hypothesis:

$$\eta = E[\hat{\Omega}] + \frac{1}{\sqrt{2\,\mathrm{var}[\hat{\Omega}]}} erfc^{-1}(2P_{FA}) \tag{9.13}$$

Then, the test is finally expressed as follows:

$$\hat{\Omega} \underset{H_0}{\overset{H_1}{\lessgtr}} \eta$$

(9.14)

It means that if the testing variable is greater than the threshold value (η) the algorithm decides for the hypothesis H_0 (i.e. absence of the primary signal) otherwise the choice is for H_1 (i.e. presence of the primary signal). The probability of detection P_D is determined in the H_1 hypothesis as:

$$P_D = \frac{1}{2} erfc\left(\frac{\eta - E\left[\hat{\Omega}\right]}{\sqrt{2var\left[\hat{\Omega}\right]}}\right) \tag{9.15}$$

9.3 Performance Analysis

In this section, we theoretically evaluate the performance of the proposed method, evaluating the bias and the variance of the testing variable in (9.11). It has to be noted that the testing variable is obtained as the sum of *L* statistically independent variables. Therefore, both its bias and its variance can be easily obtained as the sum of the biases and variances of these *L* independent variables, as:

$$E[\hat{\Omega}] = \sum_{j=1}^{L} E[\hat{\Omega}_j] \tag{9.16}$$

$$\text{var}[\hat{\Omega}] = \sum_{j=1}^{L} \text{var}[\hat{\Omega}_j] \tag{9.17}$$

Consequently, in the following analysis we focus our attention on the bias and the variance of $\hat{\Omega}_j$. Let us define, for the sake of the compactness $\varepsilon_{2,j} = \hat{M}_{2,j} - E[\hat{M}_{2,j}]$, $\varepsilon_{4,j} = \hat{M}_{4,j} - E[\hat{M}_{4,j}]$ as the two moment-estimation's errors, which are assumed to be zero-mean random variables. Then, under the assumption of small errors for the high-order moment estimators ($\hat{M}_{2,j}$, $\hat{M}_{4,j}$), the estimation errors can be accordingly evaluated by a two-dimensional (2-D) reduced Taylor expansion up to the second order:

$$E[\hat{\Omega}_j] = \frac{1}{2}\frac{\partial^2 \hat{\Omega}_j}{\partial \hat{M}_{2,j}^2}\bigg|_{\varepsilon_{2,j}=\varepsilon_{4,j}=0} \cdot E[\varepsilon_{2,j}^2] + \frac{1}{2}\frac{\partial^2 \hat{\Omega}_j}{\partial \hat{M}_{4,j}^2}\bigg|_{\varepsilon_{2,j}=\varepsilon_{4,j}=0} \cdot E[\varepsilon_{4,j}^2] + \frac{1}{2}\frac{\partial \hat{\Omega}_j}{\partial \hat{M}_{2,j}\partial \hat{M}_{4,j}}\bigg|_{\varepsilon_{2,j}=\varepsilon_{4,j}=0} \cdot E[\varepsilon_{2,j}\varepsilon_{4,j}] \tag{9.18}$$

$$\text{var}[\hat{\Omega}_j] = \left(\frac{\partial \hat{\Omega}_j}{\partial \hat{M}_{2,j}}\right)^2\bigg|_{\varepsilon_{2,j}=\varepsilon_{4,j}=0} \cdot E[\varepsilon_{2,j}^2] + \left(\frac{\partial \hat{\Omega}_j}{\partial \hat{M}_{4,j}}\right)^2\bigg|_{\varepsilon_{1,j}=\varepsilon_{2,j}=0} \cdot E[\varepsilon_{4,j}^2] + \frac{\partial \hat{\Omega}_j}{\partial \hat{M}_{2,j}}\bigg|_{\varepsilon_{2,j}=\varepsilon_{4,j}=0} \cdot \frac{\partial \hat{\Omega}_j}{\partial \hat{M}_{4,j},}\bigg|_{\varepsilon_{2,j}=\varepsilon_{4,j}=0} \cdot E[\varepsilon_{2,j}\varepsilon_{4,j}] \tag{9.19}$$

The algebraic expressions (9.18) and (9.19) are trivially derived from a mere computation of the partial derivatives of the expressions in (9.11). The variances $E[\varepsilon_{2,j}^2]$, $E[\varepsilon_{4,j}^2]$ and the covariance $E[\varepsilon_{2,j}\varepsilon_{4,j}]$ of the high-order estimators are obtained as follows. The variance of $E[\varepsilon_{2,j}^2]$ can be derived as:

$$E[\varepsilon_{2,j}^2] = \text{var}(\hat{M}_{2,j}) = E[\hat{M}_{2,j}\hat{M}_{2,j}] - E^2[\hat{M}_{2,j}] = E\left[\frac{1}{K}\sum_{i=j\cdot K}^{j\cdot K+K-1}|r_i|^2 \cdot \frac{1}{K}\sum_{m=j\cdot K}^{j\cdot K+K-1}|r_m|^2\right] - M_{2,j}^2$$
$$= \frac{1}{K^2}\cdot E\left[K\cdot\sum_{i=j\cdot K}^{j\cdot K+K-1}|r_i|^4 + \sum_{\substack{m=j\cdot K \\ i\neq m}}^{j\cdot K+K-1}|r_i|^2|r_m|^2\right] - M_{2,j}^2 = \frac{1}{K}M_{4,j} - \frac{1}{K}M_{2,j}^2 \quad (9.20)$$

And following the same approach the expression of $E[\varepsilon_{4,j}^2]$ is given by:

$$E[\varepsilon_{4,j}^2] = \text{var}(\hat{M}_{4,j}) = \frac{1}{K}M_{8,j} - \frac{1}{K}M_{4,j}^2 \quad (9.21)$$

Finally, the expression of the covariance can be obtained as follows:

$$E[\varepsilon_{2,j}\varepsilon_{4,j}] =$$
$$= \text{cov}(\hat{M}_{2,j},\hat{M}_{4,j}) = E[\hat{M}_{2,j}\hat{M}_{4,j}] - E[\hat{M}_{2,j}]\cdot[\hat{M}_{4,j}] = E\left[\frac{1}{K}\sum_{i=j\cdot K}^{j\cdot K+K-1}|r_i|^2\frac{1}{K}\sum_{m=j\cdot K}^{j\cdot K+K-1}|r_m|^4\right] - M_2M_4 \quad (9.22)$$
$$= \frac{1}{K^2}E\left[K\cdot\sum_{i=j\cdot K}^{j\cdot K+K-1}|r_i|^6 + \sum_{\substack{m=j\cdot K \\ i\neq m}}^{j\cdot K+K-1}|r_i|^2|r_m|^4\right] - M_{2,j}M_{4,j} = \frac{1}{K}M_{6,j} - \frac{1}{K}M_{2,j}M_{4,j}$$

In order to evaluate the covariance in (9.22) and the variance in (9.21), the sixth- (M_6) and eighth-(M_8) order moments need to be calculated. Recalling the analysis depicted in Section III, the sixth- and eighth-order moments can be derived as follows:

$$M_{6,j} = E\left[|\mathbf{R}_j|^6\right] = P_{S,j}^3 + 6P_{N,j}^3 + 9P_{S,j}^2P_{N,j} + 18P_{S,j}P_{N,j}^2 \quad (9.23)$$

$$M_{8,j} = E\left[|\mathbf{R}_j|^8\right] = P_{S,j}^4 + 24P_{N,j}^4 + 16P_{S,j}^3P_{N,j} + 72P_{S,j}^2P_{N,j}^2 + 96P_{S,j}P_{N,j}^3 \quad (9.24)$$

Then, by substituting each of the expressions (9.18)-(9.24) into (9.16) and (9.17), the desired expressions of the estimation errors are obtained as follows:

$$E[\hat{\Omega}_j] = \frac{2P_{S,j}^4 + 11P_S^2P_{N,j}^2 + 8P_{S,j}P_{N,j}^3 + 2P_{N,j}^4}{K\cdot\left(P_{S,j}+P_{N,j}\right)^4} \quad (9.25)$$

$$\text{var}[\hat{\Omega}_j] = \frac{8P_{S,j}^5P_{N,j} + 72P_{S,j}^4P_{N,j}^2 + 208P_{S,j}^3P_{N,j}^3 + 240P_{S,j}^2P_{N,j}^4 + 120P_{S,j}P_{N,j}^5 + 20P_{N,j}^6}{K\cdot\left(P_{S,j}+P_{N,j}\right)^6} \quad (9.26)$$

Finally, we can easily obtain the expressions of the bias and of the variance of the testing variable using (9.24) and (9.25) in (9.15) e (16). It has to be noted that both the estimations in (9.25) and (9.26) vary with $1/K$, meaning that the estimator is consistent (i.e. as K becomes larger and larger, the estimate tends to the true value).

9.4 Results

Several simulations have been performed to validate the proposed NV sensing procedure versus the conventional ED approach. Several Monte-Carlo simulation trials (10^5 independent runs) have been implemented to numerically evaluate the performance of the two methods. A QPSK modulation with rectangular pulse shaping has been used, with a target $P_{FA} = 10^{-2}$. In all the following results, we have evaluated the P_D both in an analytic way, i.e. using equation (9.15), and by means of simulations. The time record length is N_s = 50000 complex samples, and different values of the noise uncertainty have been considered. Moreover, in all the addressed cases a block length K = 1000 and different number of blocks L have been considered. Then, we have evaluated the performance of both the ED and the NV approach in terms of P_D versus SNR of practical interest. Fig. 9-1 reports the theoretical and simulated results for the P_D of the two methods with N_s =50000, L = 50, K =1000 and $\rho = 1$ dB (noise uncertainty).

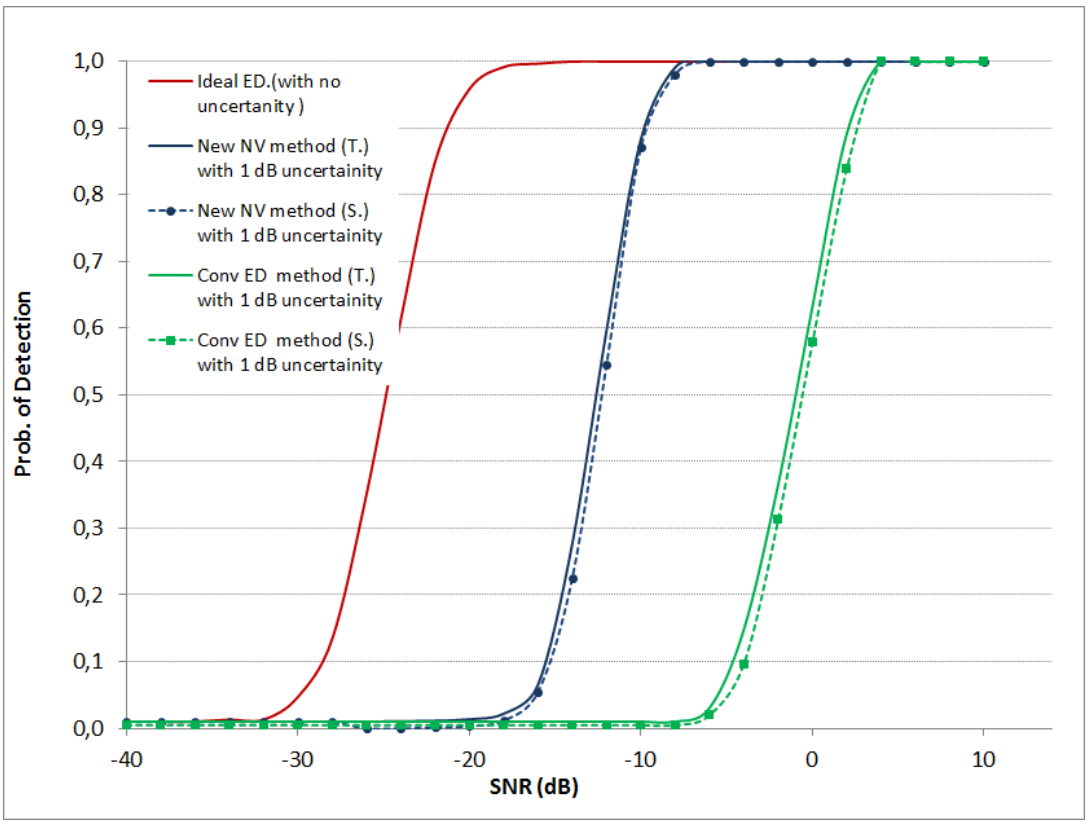

Figure 9-1 Theoretical (T.) and simulated (S.) results for the P_D vs. SNR of both the new NV and conv. ED methods, with 1 dB of noise uncertainty and N_s = 50000, K = 1000, L = 50.

The curve referring to the ideal ED (i.e. the detector with exact knowledge of the noise variance) is also reported as representative of the upper bound of the system performance. ED is used as a proof of concept of the new method here propsed.The simulation results (dotted lines) well match the theoretical ones (solid lines), thus validating the correctness of the mathematical analysis and assumptions of the previous Sections. It can be easily seen from the graphs that the NV method strongly outperforms the conventional ED approach. Then, the detection probabilities of the two methods for ρ = 0.5 dB are shown in Fig. 9-2: the proposed NV method outperforms the conventional one also in this case. It has to be noted that our method is not affected by the noise uncertainty problem since exact knowledge of the noise variance is not needed for setting the test threshold. On the other hand, in the ED approach the threshold depends on the noise variance, and if it is not exactly known the performance of the ED strongly reduces (see again fig.9-1, 9-2)

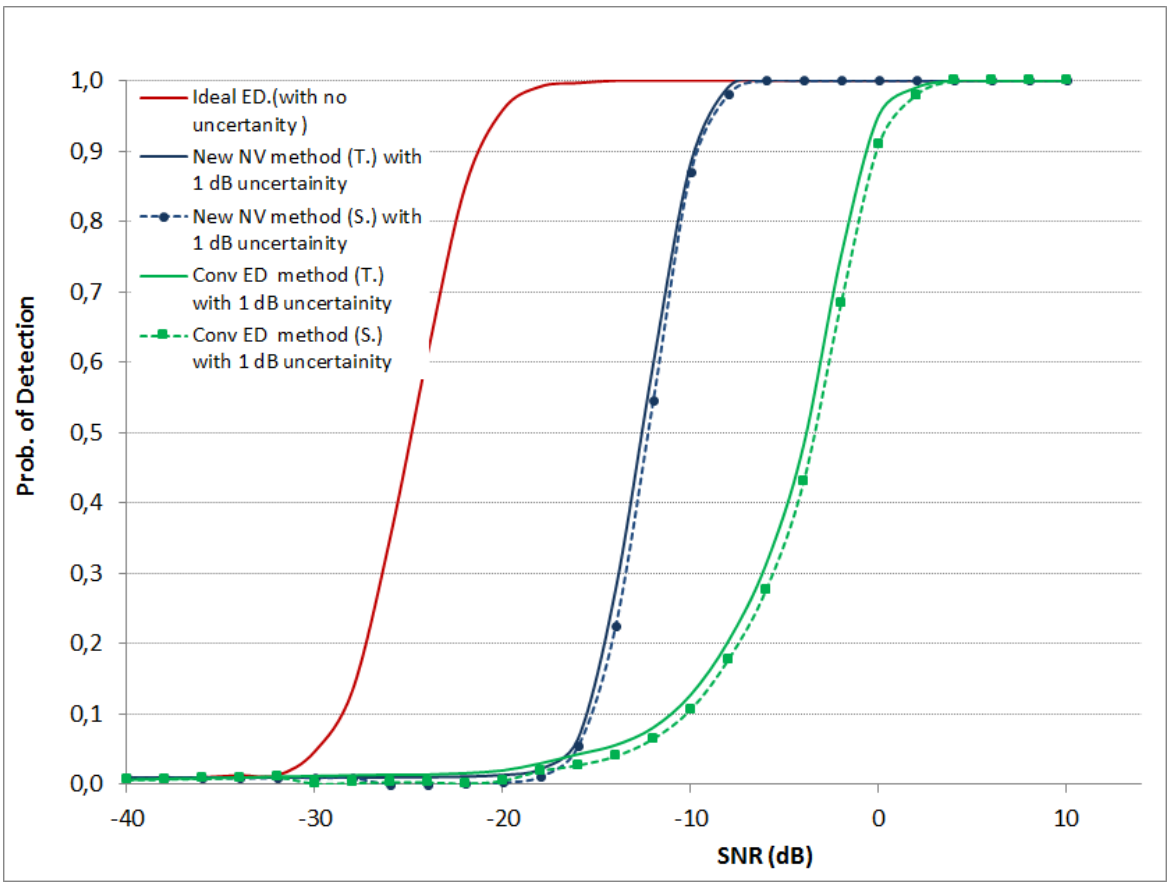

Figure 9-2. Theoretical (T.) and simulated (S.) results for the P_D vs. SNR of both the new NV and conv. ED methods, with 0.5 dB of noise uncertainty, and N_s = 50000, K = 1000, L = 50.

Then, we have evaluated the mean detection time (MDT) required by the two techniques for detecting a primary signal. Similar to the definition of MAT in code acquisition systems, the MDT is defined as the time (i.e. the number of samples) needed on average before a correct detection is declared. The MDT can be expressed as follows:

$$MDT = (M + P_{FA} \cdot T_P) \cdot \frac{2 - P_D}{2 \cdot P_D} \qquad (9.27)$$

where M is the number of sensing samples (i.e. $M = K{\cdot}L$ for the NV method and $M = N_s$ for the ED approach) and T_p is the time needed for recovery from a wrong decision when declaring empty a band where a primary user is actually transmitting. Since the term $(M + P_{FA} \cdot T_P)$ is the same for both method, we can define the MDT-gain as the ratio between

the MDT of the conventional and of the proposed methods, respectively. The MDT-gain is shown in Fig. 9-3 versus SNR values representative of typical operating cases.

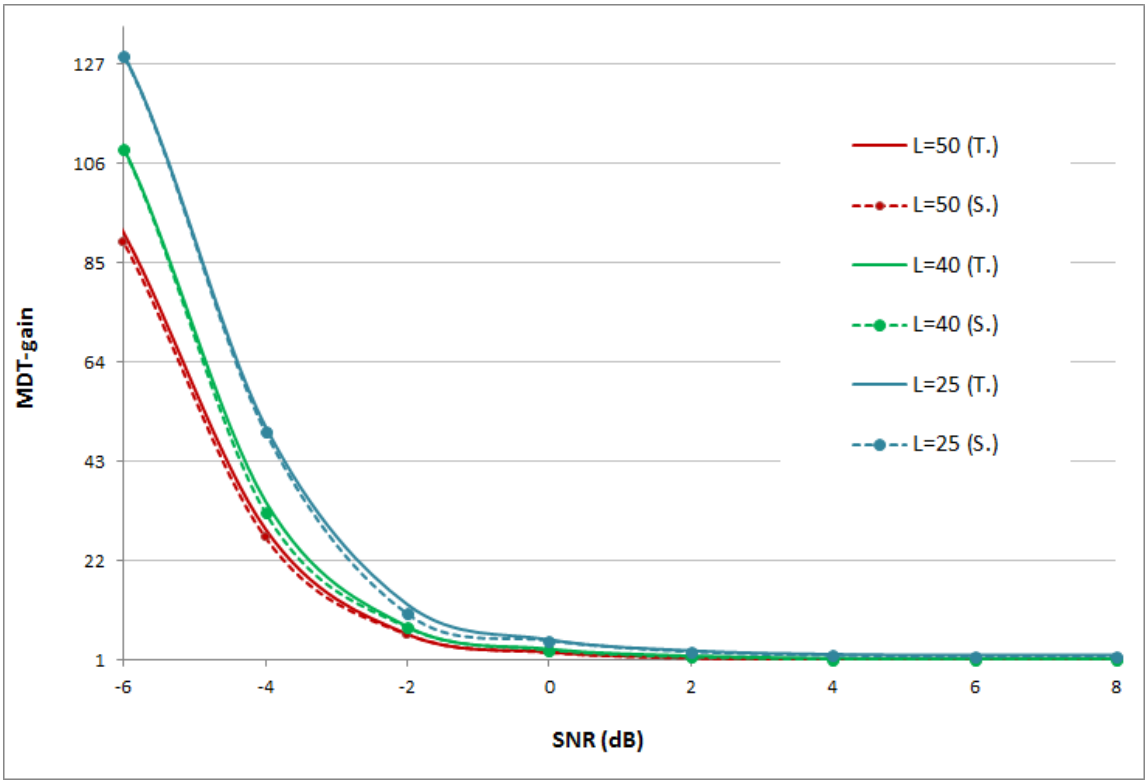

Figure 9-3 Theoretical (T.) and simulated (S.) results for the MDT-gain vs. SNR for several values of L and 1 dB of noise uncertainty.

We focus only on SNR values belonging to the interval [-6, 8] dB, since this situation corresponds to detection probabilities higher than 0.5. The MDT-gain is higher than 1 in all the addressed case: i.e. the NV approach strongly outperforms the conventional ED, allowing a faster detection of primary users. Higher MDT-gains are obtained with lower values of L, as expected. Moreover, for L = 50 (red solid line) we have $K{\cdot}L$=50000 and both the ED and the NV method exploit the same number of samples. Then, as L decreases, the number of samples used by our strategy becomes lower and the MAT-gain increases. Unfortunately, as L decreases, the P_D starts worsening (Fig. 9-4), since the test is now made on a lower number of sensing samples. The detection probabilities of the ED (with N_s=50000) and of the NV method (with L = 25, 40, 50 and K =2000, 1250, 1000) are

depicted in Fig. 9-4. As we can see, even with lower values of L the proposed method strongly outperforms the conventional ED approach, thus proving the effectiveness of the NV test for PUs' detection in cognitive radio networks. It has to be noted that the number of blocks used in the NV testing procedure can be dynamically changed according to the specific operating scenario. In particular, lower values of L can be used for reducing the sensing time, while higher values of L should be used for accurate PU's detection. In fact, using high values of L increases the number of sensing samples over which the decision is made, thus improving the detection probability. Unfortunately, the time needed for achieving the correct decision also increases, and fast PUs' detection is no longer possible.

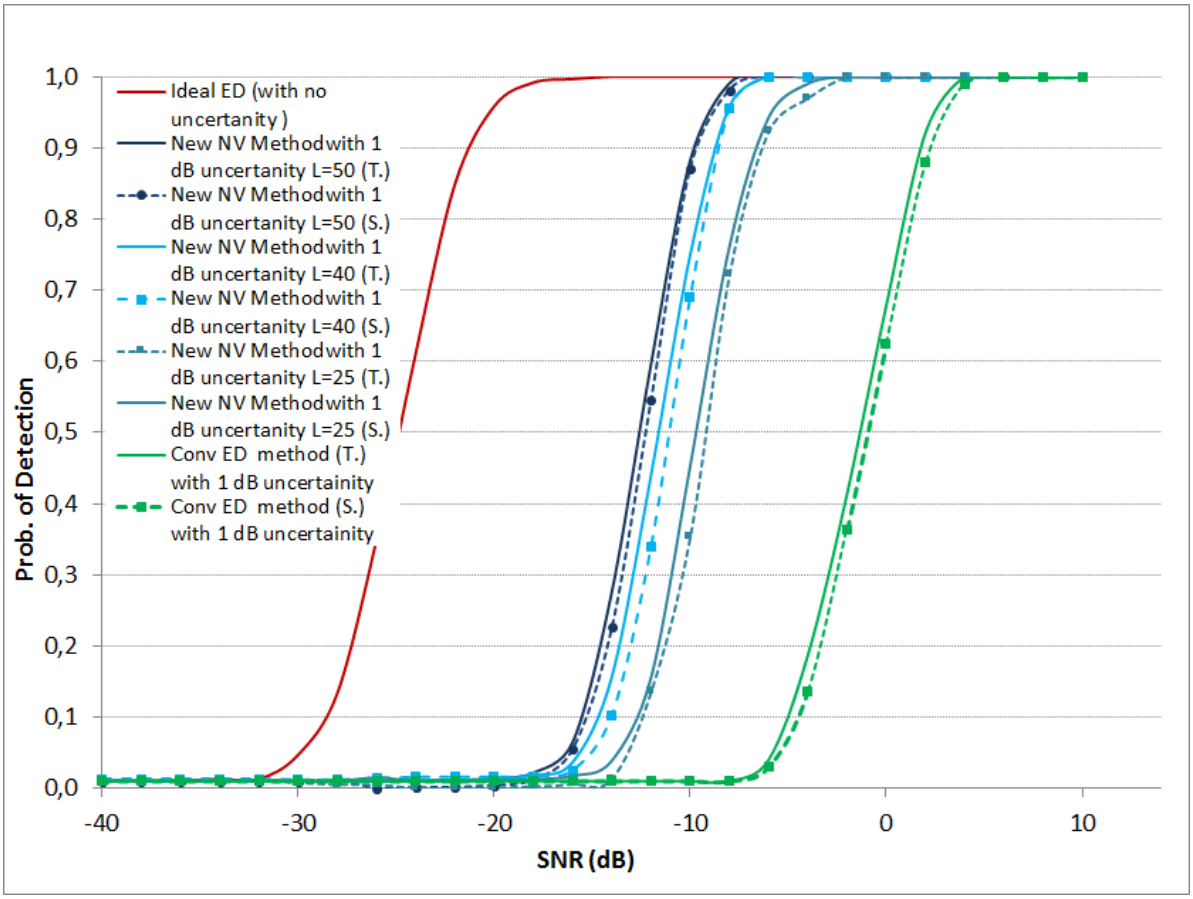

Figure 9-4. Theoretical (T.) and simulated (S.) results for the P_D vs. SNR of both the new NV (with L = 25, 40, 50 and K =2000, 1250, 1000) and the conv. ED (Ns = 50000) methods, with 1 dB of noise uncertainty.

9.5 Conclusions

This chapter has presented a novel spectrum sensing technique based on HOS of the received signal. A new metric has been first defined, namely the *normalized variance* (NV), and then used as the testing variable for primary user detection. The performance of the proposed technique is evaluated by theoretical analysis and computer simulations, in comparison with the conventional energy detector and in presence of noise uncertainty. The results have shown that the proposed method is characterized by higher detection probabilities and faster sensing time than the conventional approach.

Chapter 10 PERFORMANCE IMPROVEMENTS OF COOPERATIVE SPECTRUM SENSING WITH CORRELATED COGNITIVE USERS

10.1 Introduction

Cooperative sensing has been recently proposed has a possible solution for the sensing problems arising in presence of noise uncertainty and fading, where coherent combining at the receiver side is requested [115]. In cooperative spectrum sensing the final decision about the spectrum occupancy is obtained by combining the decision of each single SU [14]. Energy detection is used at the SUs in order to reduce the system complexity. The cooperation between SUs can occur in different ways, and many different methods have been proposed in the scientific literature [116]-[117]. However, conventional methods assume that the observations from the cooperative sensors are independent, in order to simplify the analysis. But, this assumption is not practical when the proximity of the sensors results in correlated observations. In particular, the authors in [118] analyze the impact of correlated SUs observations in terms of overall detection probability. In addition, they combine the correlated observation by fixing the fusion rule to one of the three decision rules: OR, AND, and Majority (MAJ) Voting.

In this chapter, a new test for the performance improvements of cooperative spectrum sensing in the presence of correlated users is proposed. In fact, in the presence of strong fading or shadowing effects, some correlated observations may be under the threshold of the conventional ED, even if the PU is effectively transmitting. This behavior results in a dramatic reduction of the detection probability of the system, thus increasing the interference with PUs. The method proposed in this chapter, which is based on the twin test that has been introduced in chapter 4, aims at recovering these unlucky cases. The performance of the new approach is matched to the method proposed in [118], under the same setting and channel conditions.

The remainder of this Chapter is organized as follows. Section 2 depicts the system model of cooperative spectrum sensing as well as the ED approach in the presence of correlated users. The new test for cooperative spectrum sensing in the presence of correlated users is depicted in Section 3, while comparisons and simulation results are discussed in Section 4. Finally, the conclusions are briefly depicted in Section 5.

10.2 Spectrum Sensing for Correlated Users

In conventional cooperative spectrum sensing each SU performs spectrum sensing locally and independently, and then sends its decision to a fusion center (or secondary base station) that makes the final decision about the occupancy of the frequency band. The fusion center can adopt the following fusion rules (see Fig. 10-1):

- *OR fusion rule*: the fusion center declares that the frequency band is not empty if at least one SU declares the presence of a PU.

- *AND fusion rule*: the fusion center declares that the frequency band is vacant if all the SUs state the absence of a PU.

- *MAJ or Majority voting fusion rule*: the fusion center identifies the frequency band as a spectrum hole, if more than half of the SUs decide for the absence of a PU.

The OR and MAJ voting rules are always superior to the AND rule: in fact, in the AND rule all the observations must be under the threshold to declare the presence of a spectrum hole, that is a too strict requirement to be satisfied for a large number M of SUs.

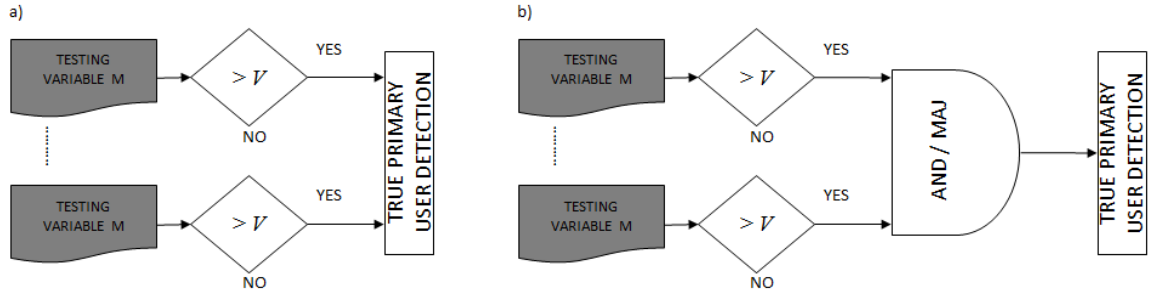

Figure 10-1. Cooperative sensing in the presence of correlated observations, with the: ***a)*** OR fusion rule; ***b)*** AND / MAJ voting fusion rules.

10.3 Proposed method

In large SNs, where there are many SUs, the spectrum observations may be strongly correlated, due to the proximity among SUs. In such case, the performance of the conventional independence based model drastically reduces. Moreover, the results in [20] showed that the performance of cooperative sensing in the presence of correlated users degrades with the increasing in correlation between the correlated observations for all the fusion rules. In this Section, we design a new test for the performance improvements of cooperative spectrum sensing in the presence of correlated observations. The method is based on the *twin test* for code acquisition, which has been described in chapter 4. In fact code synchronization is a task that is conceptually similar to spectrum sensing: in both case the problem is modeled as a binary hypothesis testing, where a testing variable is compared to a proper pre-selected threshold. Here, a modified version of the twin test, namely the *Modified Twin Test* (MTT), is proposed for application to cooperative spectrum sensing. In particular, since strong fading and shadowing effects may result in a degradation of the spectrum sensing performance, first a further threshold is introduced; then the correlated observations are processed by both OR and MAJ voting rules in order to improve the detection performance, while enabling faster rejection of occupied bands. The rationale of the MTT is as follows. An additional threshold V_L (lower than the conventional one) introduced, to be jointly overcame by the majority of the correlated observations (see Fig. 10-2). If the testing variables are under the upper threshold V_U (different from the

conventional threshold V) but more than half exceed the lower threshold V_L, it is still possible to declare reliable detection of a PU signal. The CFAR criterion is adopted for setting the threshold value. As happens in the original twin test, there is more than one possible pair of thresholds (V_L, V_U) that meet the CFAR criterion, and the best one is chosen as the pair maximizing the P_D.

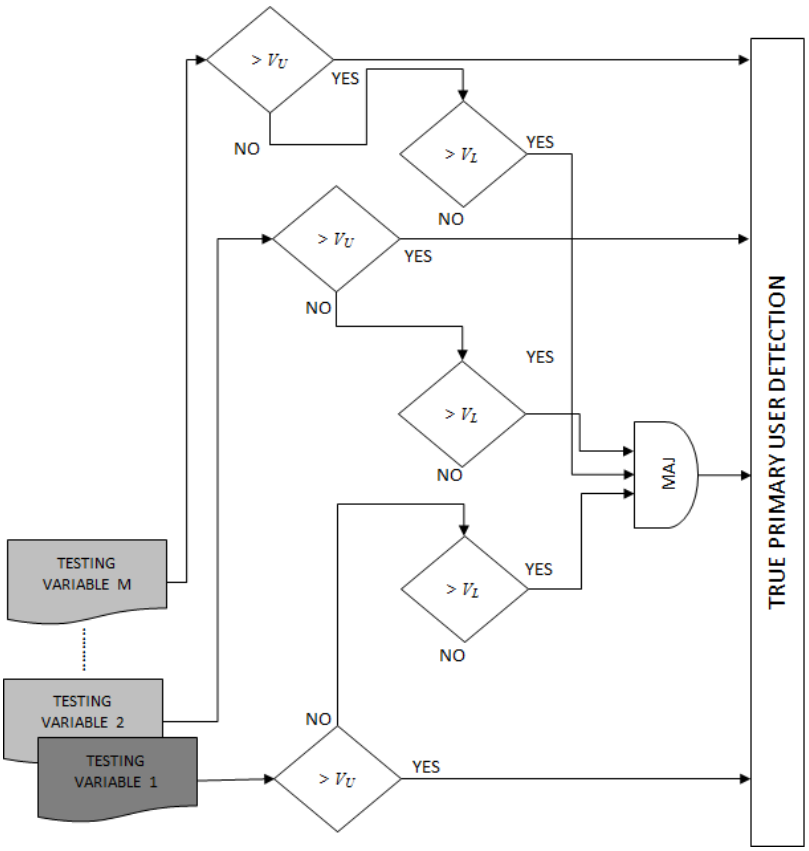

Figure 10-2 Cooperative sensing in the presence of correlated observations, with the: ***a)*** OR fusion rule; ***b)*** AND / MAJ voting fusion rules.

In the ED method, the testing variables are examined according to one out of the three rules AND, OR, MAJ. The modified twin test combines two rules at once (see Fig 10-2), and declares true PU detection if one of the corresponding testing variables exceeds the upper threshold V_U (OR strategy), or if half or more of the testing variables are between the lower and the upper thresholds (MAJ strategy). Moreover, since the testing variables are

strictly correlated, if they are jointly below the lower threshold it is unlikely to have PU detection in one of them, and can be both discarded.

10.4 Numerical Results

In this section, simulation results are presented and discussed to evaluate the performance of cooperative sensing in the presence of correlated users. In particular, we match the results of the method in [120], in order to state the effectiveness of the proposed MTT. The correlation between the M observations is represented by the correlation coefficient ρ, which is assumed to be equal under the two hypotheses H_0 and H_1. Following the same approach as in [120] we assume that the network consists of M cognitive users, and all the SUs participates in the final decision. The number of sensing symbols N is set to 1000, the target P_{FA} is considered equal to 10^{-3}, and all the cooperating users have equal unitary noise variance. Fig. 10-3 shows the detection probability of the two methods for the OR, AND, MAJ voting rules as well, versus the signal-to-noise ratio (SNR) for M = 3. Fig. 10-3a represents the case of ρ = 0.1, while Fig. 10-3b depicts the cases of ρ =0. 5, respectively.

In all the considered cases, the MTT always outperforms the conventional methods for all the fusion rules, showing higher detection probabilities in correspondence of the same SNR. It has to be underlined that, for high SNR values, i.e. when the channel is good enough so that the single CR user declares a correct decision on its own, the effects of correlated observations become weaker and weaker, and all the methods present the same performance. Fig. 10-4 reports here the cases of M = 5 for a correlation coefficient equal to 0.1 (see Fig. 10-4a) and 0.5 (see Fig. 10-4b).

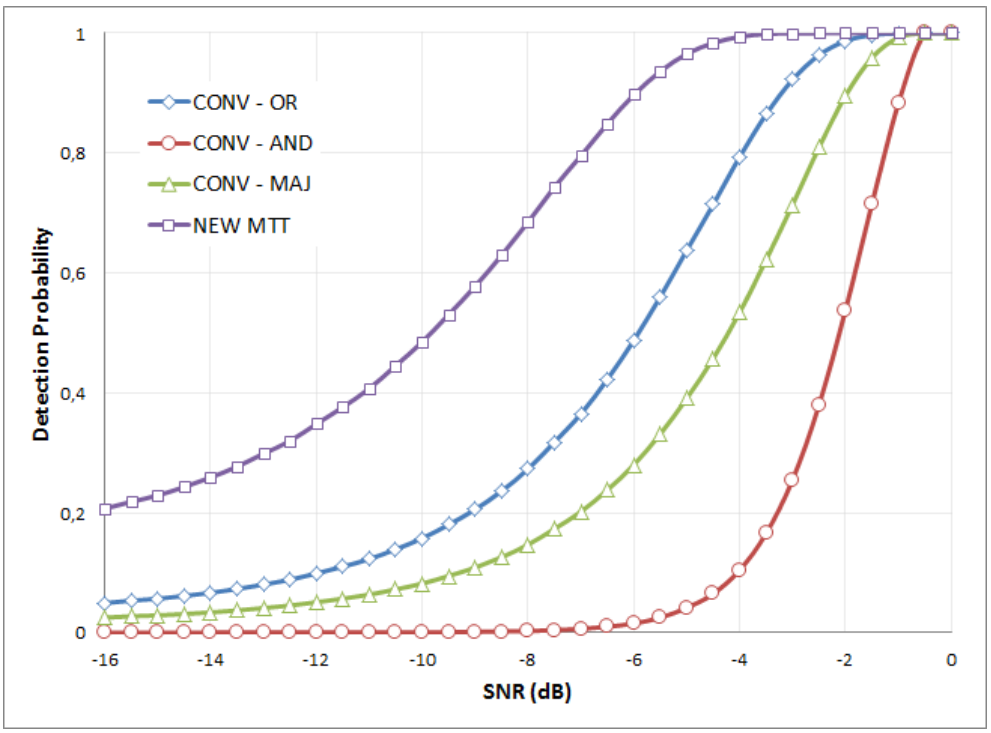

(a)

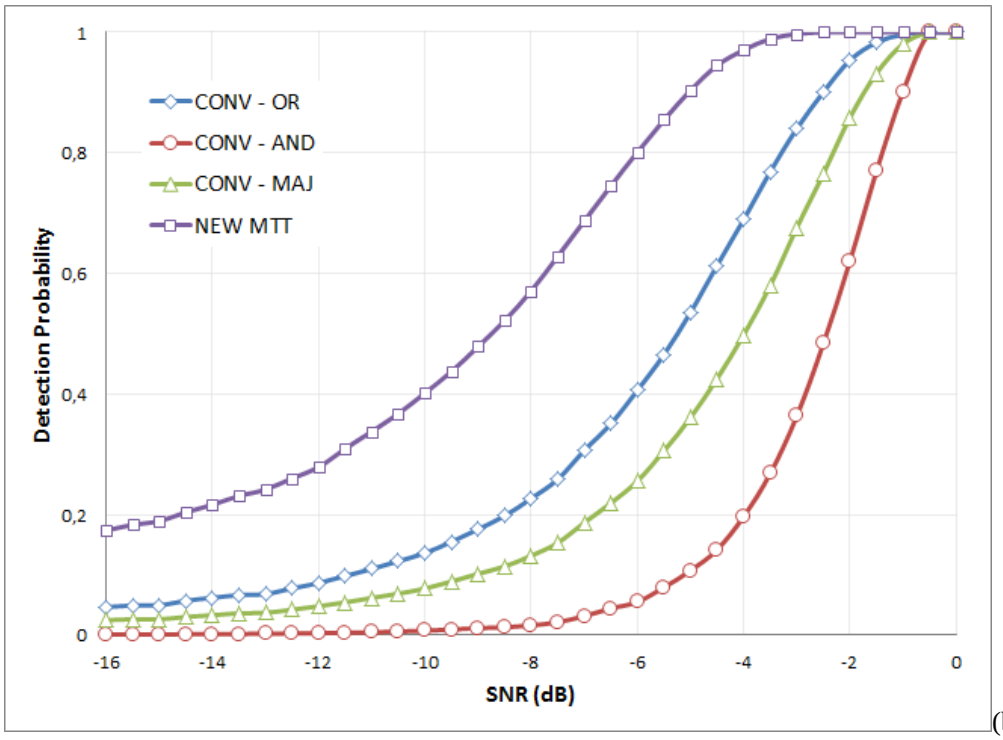

(b)

Figure 10-3 Detection Probability of all the considered methods for 3 correlated observations (a) $\rho = 0.1$; (b) $\rho = 0.5$.

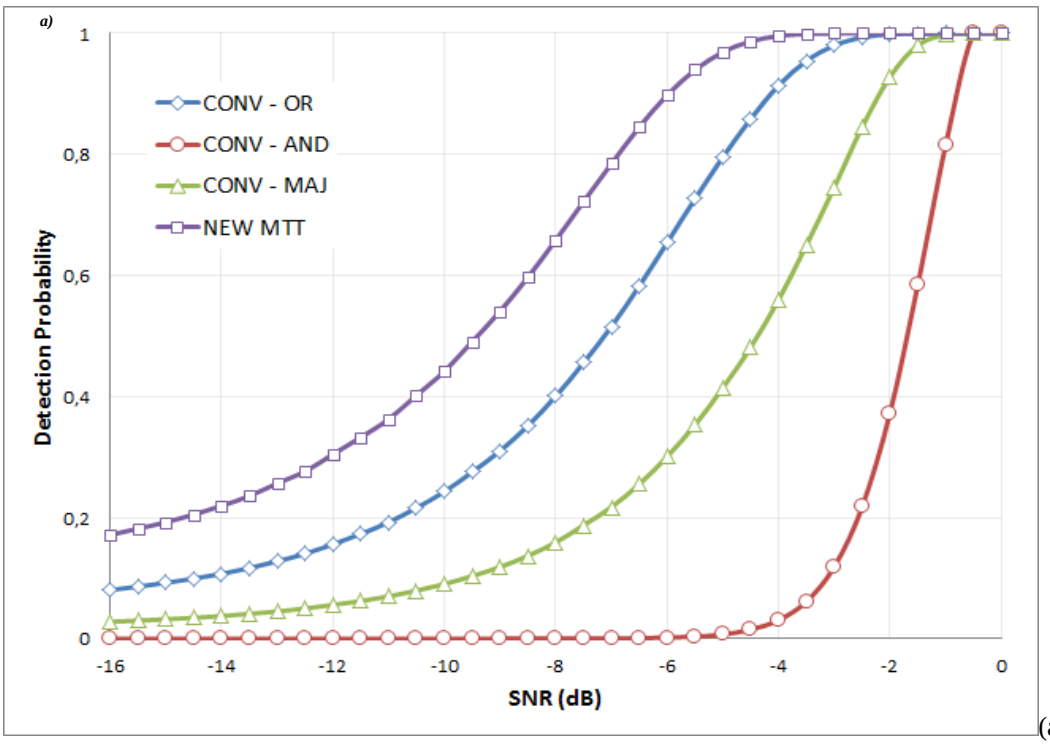

(a)

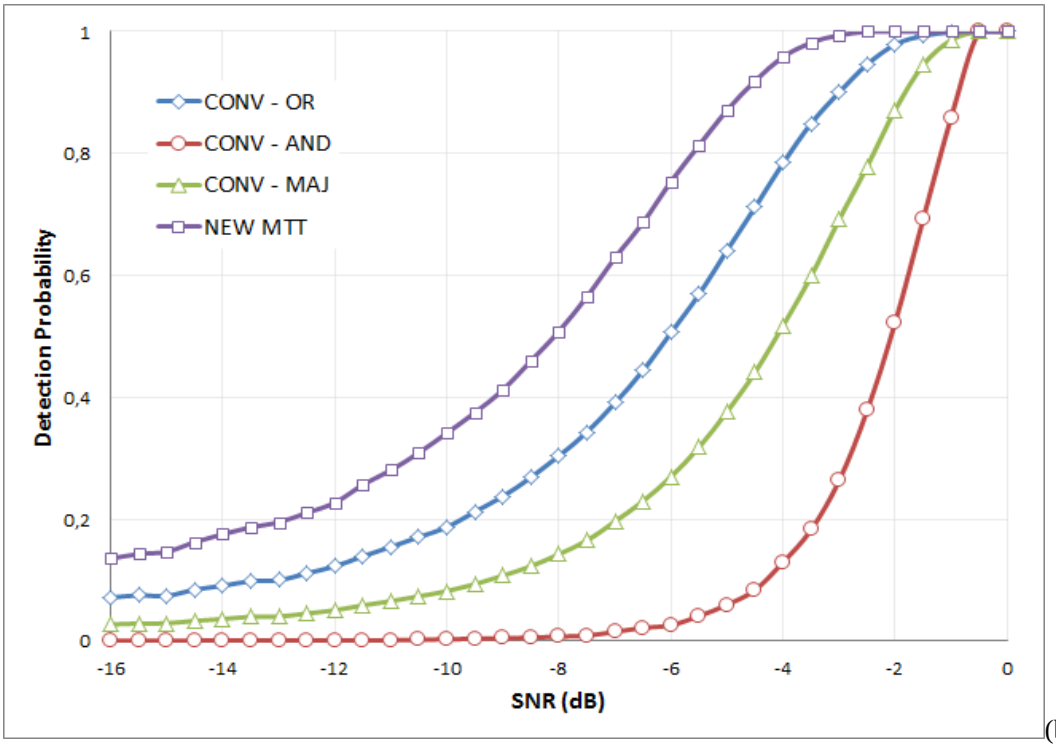

(b)

Figure 10-4. Detection Probability of all the considered methods for 5 correlated observation and: (a) $\rho = 0.1$; (b) $\rho = 0.5$.

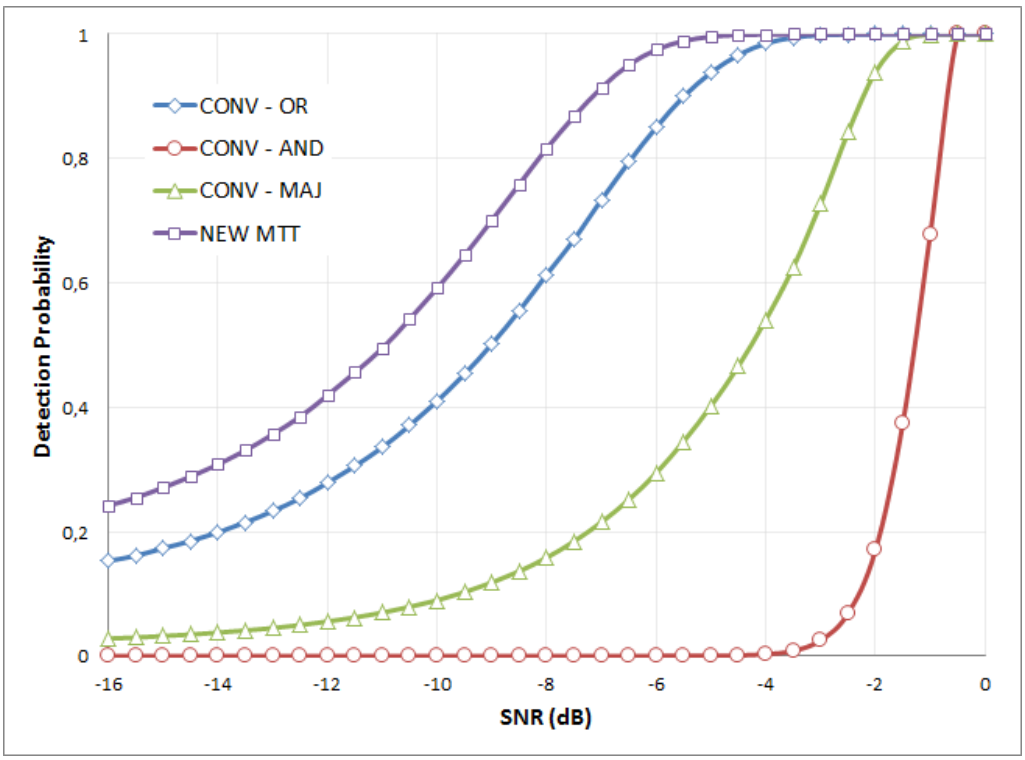

(a)

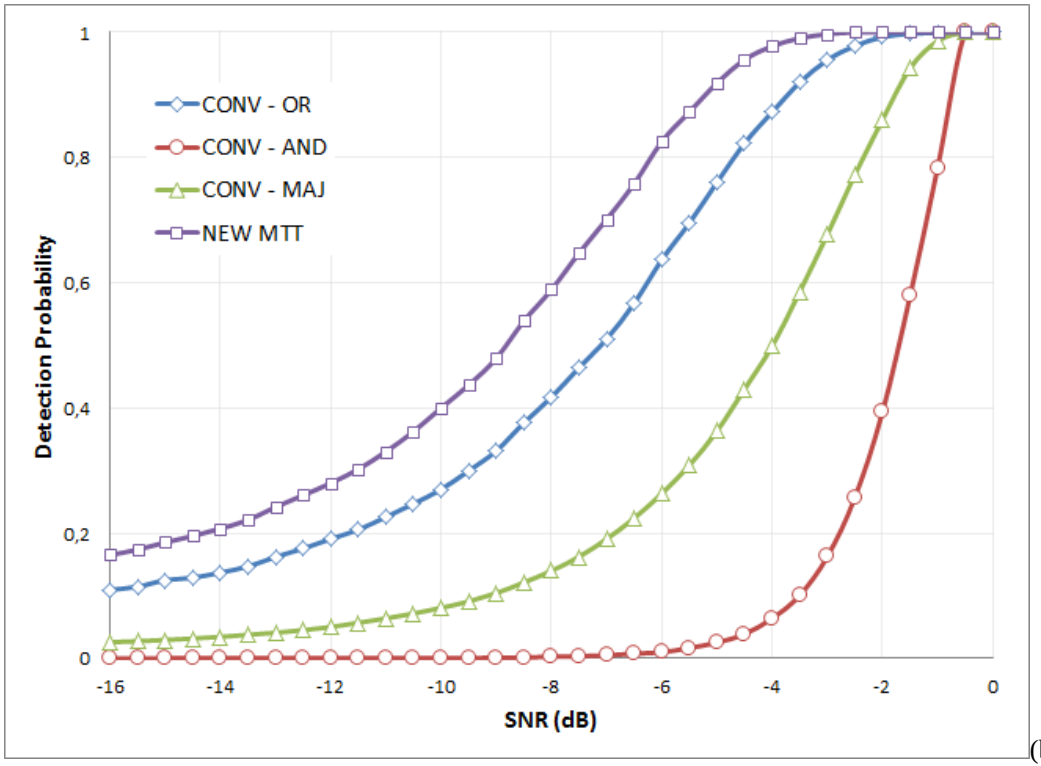

(b)

Figure 10-5. Detection Probability of all the considered methods for 5 correlated observation and: (a) $\rho = 0.1$; (b) $\rho = 0.5$.

It is interesting to note that the P_D increases with the increasing of the number of sensors (M), as the observations become more and more correlated (i.e. with higher correlation coefficients). This is due to the fact that in presence of correlated users, increasing the number of sensors means exploiting multi-user diversity, hence increasing the system performance.

Finally, we have analyzed how the performance improvement obtained with the MTT procedure reflects in a detection gain, varying the correlation coefficient. In particular, we have defined as detection gain (D_G) the ratio between the P_D of the MTT and the P_D of the conventional approach. Fig. 10-6 shows the D_G in the cases of M = 5, and 10 correlated users (see Fig. 10-6a, and Fig. 10-6b respectively). Again, it is easy to see that the MTT method is always superior, reaching detections of about 20%, if compared with the better conventional OR fusion strategy.

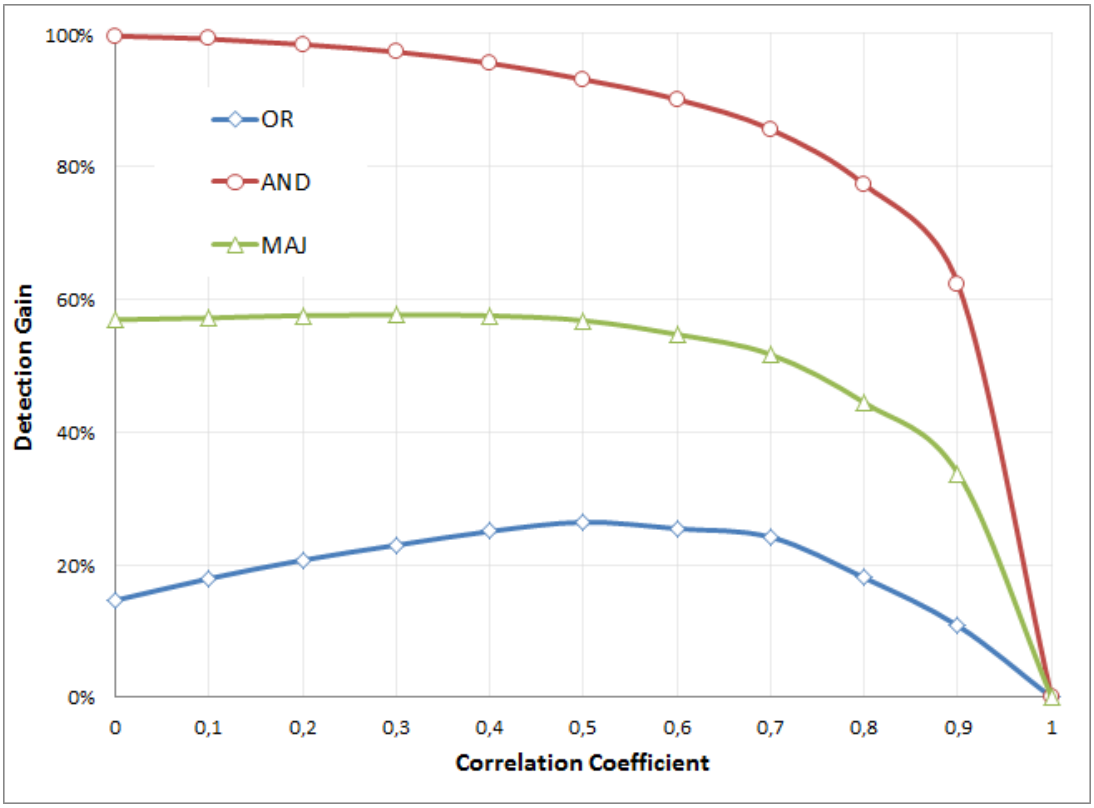

(a)

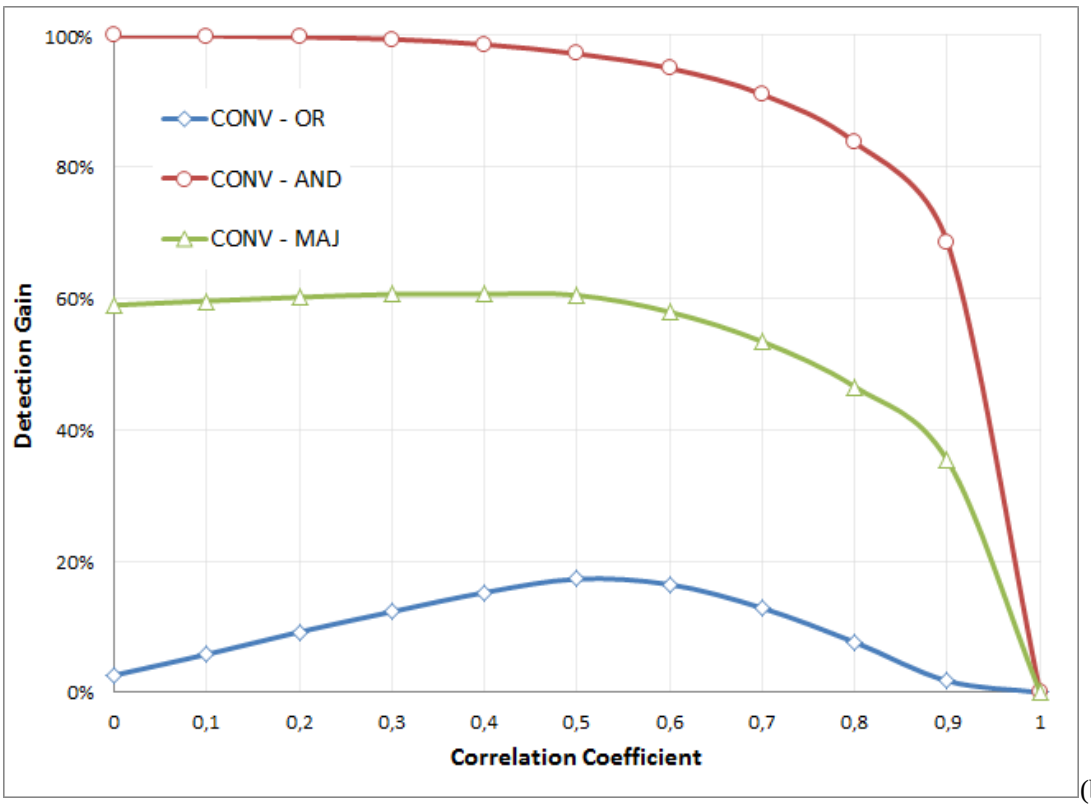

(b)

Figure 10-6 Detection Gain of all the considered methods versus the correlation coefficient for: a) M = 5 and; b) M = 10 correlated users.

10.5 Conclusions

This chapter has addressed the problem of cooperative spectrum sensing in the presence of correlated cognitive users. In particular, we have propose an innovative test, the modified twin test (MTT), has been proposed for recovering all those unlucky cases where strong fading and shadowing drastically reduce the system detection performance. Our method combines the OR and the Majority voting rules, in order to improve the detection performance, while enabling faster rejection of occupied bands. The obtained results, obtained from wide simulation trials, demonstrate the effectiveness of our MTT method for application in cognitive radio networks in the presence of correlated users.

Chapter 11

Effective Monitoring of Freeloading User in the Presence of Active User in Cognitive Radio Networks

11.1 Introduction

In a CR network, the possibility of trading the radio spectrum offers new business opportunities for both PUs and SUs [8]. PUs can lease unused resources to SUs in exchange for appropriate remuneration, while maintaining the ownership of the spectrum. On the other hand, SUs can use the frequency bands which could not otherwise access. In a CRN, two types of spectrum market can be identified: the primary market and secondary market. In a primary market, the spectrum leasing is performed directly among primary users (i.e., the spectrum holders) and secondary users in a long-term manner (e.g., weeks or months). In a secondary market, the spectrum can be traded among secondary users in a finer time scale (e.g. several minutes). In this scenario secondary service provider (SSP) can lease spectrum resources from spectrum brokers to provide service to secondary users.

Unfortunately, in this operating scenario there is also room for fraudulent users. In fact, a deceitful cognitive SU could use its technical advances for hiding himself under the noise floor, and not being charged for using the radio spectrum. The aim of such "freeloading" users (FLUs) is to use the spectrum secretly. Their transmit power must be as low as possible in order to be confused with the channel noise. Notwithstanding FLUs do not directly damage the communications of active users (either PUs or SUs), they represent a relevant economic loss for CRN providers. In fact, even if the freeloader does not deteriorate the authorized signal, it is illegally accessing the spectrum. This behavior reflects in a profit loss for the service providers, which, in turn, will enhance the fees for accessing the spectrum to the authorized users. In fact, the service providers aim at maximizing their profit

and hence, the price and supply of bandwidths in the secondary market will change, due to the presence of the freeloaders. To the best of our knowledge, this is an operating scenario that is completely different from what has been studied in the literature about cognitive radio users. In fact, FLUs cannot be considered as conventional SUs according to the OSA and CSA models. In the first case (OSA), the SU transmits high power signals, while in the new model the FLU transmit very low power signals. On the other hand, in the second situation (CSA) the SU is a cooperative user, while here, the FLU is fraudulent. In addition, this is not even the case of a fraudulent SU that pretends to be a PU, as in the case of the Primary User Emulation (PUE) attack [120]-[121], since in a PUE the SU exploits again very high power signals. Then, the detection of a SU hiding in between PUs is discussed in [122], but the authors exploit a completely different an approach. In particular, they introduce a cyclostationary detection method, assuming that the deceptive CR transmits only when there are no active PUs and using different signal parameters from those of the PUs. Conversely, in this dissertation we propose an innovative signal processing technique for the detection of an unknown low-power constant modulus signal (i.e. the FLU signal) in noise of unknown variance and in the presence of an active high power signal (i.e. either PU or SU). The proposed procedure exploits higher order statistics, up to the sixth moment, of the received signal to obtain an estimation of the fraudulent, of the noise and of the active user variances: we have these three afore-mentioned unknowns in three independent equations (i.e. the second, the fourth and the sixth order moment of the received signal). The estimated power of the freeloading signal is then the decision variable exploited, for discovery the hiding FLUs.

The remainder of this chapter is organized as follows. The operating scenario with a FLU transmitting in the presence of an active user is illustrated in the first half of Section 2, while the system model is depicted in the second half of the Section. The new signal processing algorithm for FLU detection is described in Section 3, and the noise and signals' variances are then theoretically derived. In Section 4, a theoretical analysis about the performance of the proposed method is carried out. Simulation and theoretical results are shown in Section 5, before our conclusions briefly depicted in Section 6.

11.2 FLU Transmission in the presence of an Active User

11.2.1 Operating scenario

A CRN is composed by a primary network, composed by a set of primary receivers and transmitters (PU-rx and PU-tx, respectively) and a secondary network that comprises secondary receivers and transmitters (SU-rx and SU-tx, respectively). According to the OSA model, primary and secondary users share the same portions of the radio spectrum in an opportunistic way. This means that the secondary network is active when the primary network is not operating and vice-versa. In the scenario of our interest, there is another network, the *freeloading network*, composed by freeloading receivers (FLU-rx) and transmitters (FLU-tx), illegally exploiting the spectrum resources. In particular, we assume that the FLU can operate in the presence of an active user, either PU or SU. This new scenario is depicted in Fig. 11-1, where the freeloading network secretly and illegally exploits the radio spectrum, in the presence of the active network. In the following, we refer to both PUs and SUs as Authorized Users (AUs), in order to distinguish them from the non-authorized user (i.e. the FLU). We assume that the power of the FLU signal is low enough to be confused with the channel noise, and that the FLU is located far away from the AU-tx, thus making it is impossible for the AUs themselves to detect the hidden FLU signal. Therefore, we include the presence of an additional mobile network element, namely the monitoring sensor (MS) that senses the spectrum with the aim of detecting the FLUs.

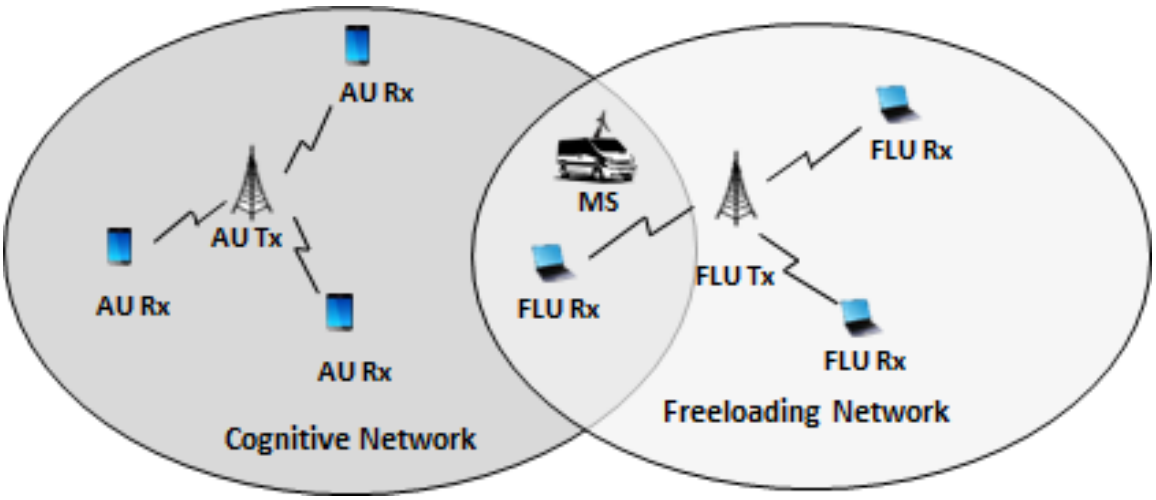

Figure 11-1. The operating scenario consisting of an active authorized user (AU), a freeloader (FLU), and a monitoring sensor (MS).

11.2.2 System Model

Spectrum sensing is the process of detecting the presence of the primary signals and identifying spectrum holes. In the consider model there is another signal (the FLU signal) which is transmitted at very low power.

More in details, let s_1(t) be the signal transmitted by an AU which is assumed to be affected by additive complex white Gaussian noise $n(t)$, with zero-mean and variance $2\sigma_n^2$. Let $s_2(t)$ be the signal transmitted by the FLU, then the signal received by the MN is $r(t) = s_1(t) + s_2(t) + n(t)$ under the H_1 hypothesis and $r(t) = s_1(t) + n(t)$ otherwise. In the following analysis, we assume that $s_1(t)$ and s_2(t) are independent CM signals, since pprimary transmissions usually take place by means of CM waveforms. For sake of compactness, all the signals are expressed in terms of their representative vectors. The signal $r(t)$ represented by the vector $\mathbf{r=s_1+s_2+n}$ is sampled at the MS side with a sampling period T_s. Now, the sequences (of N samples) of the received signal, of the AU, of the FLU, and of the noise are defined as, respectively:

$$\begin{aligned}
&\mathbf{r} = [r_0, r_1, r_2, \ldots r_{N-1}]^T, && \text{Received signal}\\
&\mathbf{s}_1 = [s_{1,0}, s_{1,1}, s_{1,2}, \ldots s_{1,N-1}]^T, && \text{AU signal}\\
&\mathbf{s}_2 = [s_{2,0}, s_{2,1}, s_{2,2}, \ldots s_{2,N-1}]^T, && \text{FLU signal}\\
&\mathbf{n} = [n_0, n_1, n_2, \ldots n_{N-1}]^T, && \text{Noise}
\end{aligned} \tag{11.1}$$

Finally, the detection problem of the FLU signal $\mathbf{s_2}$, in the presence of the AU signal $\mathbf{s_1}$ corrupted by the noise $\mathbf{n}$, can be formulated as follows:

$$\begin{aligned}
&H_0 : \mathbf{r} = \mathbf{s_1} + \mathbf{n}\\
&H_1 : \mathbf{r} = \mathbf{s_1} + \mathbf{s_2} + \mathbf{n}
\end{aligned} \tag{11.2}$$

11.3 Testing for the Presence of the Freeloader

In this section, we illustrate the proposed strategy for detecting the FLU illegally transmitting in a licensed spectrum band. The rationale behind the proposed approach is as follows. The second, the fourth and the sixth order moments of the received signal are evaluated. Then, the power of the FLU, of the AU, and of the noise are derived as functions of the higher order moments.

Let M_2 be the second-order moment of the received signal and expressed as follows:

$$\begin{aligned}
M_2 &= E[|\mathbf{s}_1 + \mathbf{s}_2 + \mathbf{n}|^2] = E[|\mathbf{s}_1|^2 + |\mathbf{s}_2|^2 + |\mathbf{n}|^2 + 2\,\mathrm{Re}(\mathbf{s}_1\mathbf{s}_2^*) + 2\,\mathrm{Re}(\mathbf{s}_1\mathbf{n}^*) + 2\,\mathrm{Re}(\mathbf{s}_2\mathbf{n}^*)]\\
&= E\left[|\mathbf{s}_1|^2\right] + E\left[|\mathbf{s}_2|^2\right] + E\left[|\mathbf{n}|^2\right] + 2E\left[\mathrm{Re}(\mathbf{s}_1\mathbf{s}_2^*)\right] + 2E\left[\mathrm{Re}(\mathbf{s}_1\mathbf{n}^*)\right] + 2E\left[\mathrm{Re}(\mathbf{s}_2\mathbf{n}^*)\right],
\end{aligned} \tag{11.3}$$

where $E[\cdot]$ denotes the expectation operator, $|\cdot|$ is the absolute value, and $\mathrm{Re}(\cdot)$ denotes the real part of complex number. Assuming that the noise, the authorized and the hidden signal and are zero-mean, mutually independent random processes, we have:

$$\begin{aligned} E\left[\mathbf{s}_1\mathbf{s}_2^*\right] &= 0 \\ E\left[\mathbf{s}_1\mathbf{n}^*\right] &= 0 \\ E\left[\mathbf{s}_2\mathbf{n}^*\right] &= 0. \end{aligned} \tag{11.4}$$

Then, (11.3) can be re-written as follows:

$$M_2 = E[|\mathbf{r}|^2] = E[|\mathbf{s}_1 + \mathbf{s}_2 + \mathbf{n}|^2] = E[|\mathbf{s}_1|^2] + E[|\mathbf{s}_2|^2] + E[|\mathbf{n}|^2] = P_1 + P_2 + P_n. \tag{11.5}$$

where $P_n=2\cdot\sigma_n^2$ is the noise variance and P_1 and P_2 are the powers of the AU and FLU signals, respectively. Now, let M_4 be the forth order moment of **r**, expressed by:

$$\begin{aligned} M_4 = E[|\mathbf{r}|^4] &= E[|\mathbf{s}_1 + \mathbf{s}_2 + \mathbf{n}|^4] = \\ &+E[|\mathbf{s}_1|^4 + |\mathbf{s}_2|^4 + |\mathbf{n}|^4 + 4\,\mathrm{Re}^2\left(\mathbf{s}_1\mathbf{s}_2^*\right) + 4\,\mathrm{Re}^2\left(\mathbf{s}_1\mathbf{n}^*\right) + 4\,\mathrm{Re}^2\left(\mathbf{s}_2\mathbf{n}^*\right) + 2|\mathbf{s}_1|^2|\mathbf{s}_2|^2 + 2|\mathbf{s}_1|^2|\mathbf{n}|^2 + 2|\mathbf{s}_2|^2|\mathbf{n}|^2 \\ &+ 4|\mathbf{s}_1|^2\,\mathrm{Re}\left(\mathbf{s}_1\mathbf{s}_2^*\right) + 4|\mathbf{s}_1|^2\,\mathrm{Re}\left(\mathbf{s}_1\mathbf{n}^*\right) + 4|\mathbf{s}_1|^2\,\mathrm{Re}\left(\mathbf{s}_2\mathbf{n}^*\right) + 4|\mathbf{s}_2|^2\,\mathrm{Re}\left(\mathbf{s}_1\mathbf{s}_2^*\right) + 4|\mathbf{s}_2|^2\,\mathrm{Re}\left(\mathbf{s}_1\mathbf{n}^*\right) + \\ &+ 4|\mathbf{s}_2|^2\,\mathrm{Re}\left(\mathbf{s}_2\mathbf{n}^*\right) + 4|\mathbf{n}|^2\,\mathrm{Re}\left(\mathbf{s}_1\mathbf{s}_2^*\right) + 4|\mathbf{n}|^2\,\mathrm{Re}\left(\mathbf{s}_1\mathbf{n}^*\right) + 4|\mathbf{n}|^2\,\mathrm{Re}\left(\mathbf{s}_2\mathbf{n}^*\right) + 8\,\mathrm{Re}\left(\mathbf{s}_1\mathbf{s}_2^*\right)\mathrm{Re}\left(\mathbf{s}_1\mathbf{n}\right) \\ &+ 8\,\mathrm{Re}\left(\mathbf{s}_1\mathbf{s}_2^*\right)\mathrm{Re}\left(\mathbf{s}_2\mathbf{n}^*\right) + 8\,\mathrm{Re}\left(\mathbf{s}_1\mathbf{n}^*\right)\mathrm{Re}\left(\mathbf{s}_2\mathbf{n}^*\right)]. \end{aligned} \tag{11.6}$$

Assuming that the real and the imaginary components of the noise and of the signals processes are orthogonal, we obtain the following simplifications:

$$\begin{aligned} E\left[2\,\mathrm{Re}^2\left(\mathbf{s}_1\mathbf{s}_2^*\right)\right] &= 2|\mathbf{s}_1|^2\cdot|\mathbf{s}_2|^2 \\ E\left[2\,\mathrm{Re}^2\left(\mathbf{s}_1\mathbf{n}^*\right)\right] &= 2|\mathbf{s}_1|^2\cdot|\mathbf{n}|^2 \\ E\left[2\,\mathrm{Re}^2\left(\mathbf{s}_2\mathbf{n}^*\right)\right] &= 2|\mathbf{s}_2|^2\cdot|\mathbf{n}|^2 \end{aligned} \tag{11.7}$$

Finally, substituting (11.4) and (11.7) in (11.6) the fourth order moment can be finally expressed as:

$$\begin{aligned} M_4 = E[|\mathbf{r}|^4] &= E[|\mathbf{s}_1 + \mathbf{s}_2 + \mathbf{n}|^2] = E[|\mathbf{s}_1|^4 + |\mathbf{s}_2|^4 + |\mathbf{n}|^4 + 4|\mathbf{s}_1|^2|\mathbf{s}_2|^2 + 4|\mathbf{s}_1|^2|\mathbf{n}|^2 + 4|\mathbf{s}_2|^2|\mathbf{n}|^2] \\ &= E[|\mathbf{s}_1|^4] + E[|\mathbf{s}_2|^4] + E[|\mathbf{n}|^4] + 4E[|\mathbf{s}_1|^2]E[|\mathbf{n}|^2] + 4E[|\mathbf{s}_2|^2]E[|\mathbf{n}|^2] + 4E[|\mathbf{s}_1|^2]E[|\mathbf{s}_2|^2] \\ &= P_1^2 + P_2^2 + 2P_n^2 + 4P_1P_2 + 4P_1P_n + 4P_2P_n \end{aligned} \tag{11.8}$$

Now, let M_6 be the sixth order moment of **r**:

$$\begin{aligned}
M_6 &= E[|\mathbf{r}|^6] = E[|\mathbf{s}_1+\mathbf{s}_2+\mathbf{n}|^6] \\
&= E[|\mathbf{s}_1|^6+|\mathbf{s}_2|^6+|\mathbf{n}|^6+3|\mathbf{s}_1|^4|\mathbf{s}_2|^2+3|\mathbf{s}_1|^2|\mathbf{s}_2|^4+3|\mathbf{s}_1|^4|\mathbf{n}|^2+6|\mathbf{s}_1|^2|\mathbf{s}_2|^2|\mathbf{n}|^2+3|\mathbf{s}_2|^4|\mathbf{n}|^2+3|\mathbf{s}_1|^2|\mathbf{n}|^4 \\
&+3|\mathbf{s}_2|^2|\mathbf{n}|^4+6|\mathbf{s}_1|^4\,\mathrm{Re}(\mathbf{s}_1\mathbf{s}_2^*)+12|\mathbf{s}_1|^2|\mathbf{s}_2|^2\,\mathrm{Re}(\mathbf{s}_1\mathbf{s}_2^*)+6|\mathbf{s}_2|^4\,\mathrm{Re}(\mathbf{s}_1\mathbf{s}_2^*)+12|\mathbf{s}_1|^2|\mathbf{n}|^2\,\mathrm{Re}(\mathbf{s}_1\mathbf{s}_2^*)+12|\mathbf{s}_2|^2|\mathbf{n}|^2\,\mathrm{Re}(\mathbf{s}_1\mathbf{s}_2^*) \\
&+6|\mathbf{n}|^4\,\mathrm{Re}(\mathbf{s}_1\mathbf{s}_2^*)+12|\mathbf{s}_1|^2\,\mathrm{Re}^2(\mathbf{s}_1\mathbf{s}_2^*)+12|\mathbf{s}_2|^2\,\mathrm{Re}^2(\mathbf{s}_1\mathbf{s}_2^*)+12|\mathbf{n}|^2\,\mathrm{Re}^2(\mathbf{s}_1\mathbf{s}_2^*)+8\,\mathrm{Re}^3(\mathbf{s}_1\mathbf{s}_2^*)+6|\mathbf{s}_1|^4\,\mathrm{Re}(\mathbf{s}_1\mathbf{n}^*) \\
&+12|\mathbf{s}_1|^2|\mathbf{s}_2|^2\,\mathrm{Re}(\mathbf{s}_1\mathbf{n}^*)+6|\mathbf{s}_2|^4\,\mathrm{Re}(\mathbf{s}_1\mathbf{n}^*)+12|\mathbf{s}_1|^2|\mathbf{n}|^2\,\mathrm{Re}(\mathbf{s}_1\mathbf{n}^*)+12|\mathbf{s}_2|^2|\mathbf{n}|^2\,\mathrm{Re}(\mathbf{s}_1\mathbf{n}^*)+6|\mathbf{n}|^4\,\mathrm{Re}(\mathbf{s}_1\mathbf{n}^*) \\
&+24|\mathbf{s}_1|^2\,\mathrm{Re}(\mathbf{s}_1\mathbf{n}^*)\mathrm{Re}(\mathbf{s}_1\mathbf{s}_2^*)+24|\mathbf{s}_2|^2\,\mathrm{Re}(\mathbf{s}_1\mathbf{n}^*)\mathrm{Re}(\mathbf{s}_1\mathbf{s}_2^*)+24|\mathbf{n}|^2\,\mathrm{Re}(\mathbf{s}_1\mathbf{n}^*)\mathrm{Re}(\mathbf{s}_1\mathbf{s}_2^*)+12\,\mathrm{Re}^2(\mathbf{s}_1\mathbf{n}^*)\mathrm{Re}(\mathbf{s}_1\mathbf{s}_2^*)+ \\
&+12\,\mathrm{Re}(\mathbf{s}_1\mathbf{n}^*)\mathrm{Re}^2(\mathbf{s}_1\mathbf{s}_2^*)+12|\mathbf{s}_1|^2\,\mathrm{Re}^2(\mathbf{s}_1\mathbf{n}^*)+12|\mathbf{s}_2|^2\,\mathrm{Re}^2(\mathbf{s}_1\mathbf{n}^*)+12|\mathbf{n}|^2\,\mathrm{Re}^2(\mathbf{s}_1\mathbf{n}^*)+8\,\mathrm{Re}^3(\mathbf{s}_1\mathbf{n}^*)+6|\mathbf{s}_1|^4\,\mathrm{Re}(\mathbf{s}_2\mathbf{n}) \\
&+12|\mathbf{s}_1|^2|\mathbf{s}_2|^2\,\mathrm{Re}\,\mathbf{s}_2\mathbf{n}^*)+6|\mathbf{s}_2|^4\,\mathrm{Re}(\mathbf{s}_2\mathbf{n}^*)+12|\mathbf{s}_1|^2|\mathbf{n}|^2\,\mathrm{Re}(\mathbf{s}_2\mathbf{n}^*)+12|\mathbf{s}_2|^2|\mathbf{n}|^2\,\mathrm{Re}(\mathbf{s}_2\mathbf{n}^*)+6|\mathbf{n}|^4\,\mathrm{Re}(\mathbf{s}_2\mathbf{n}^*) \\
&+24|\mathbf{s}_1|^2\,\mathrm{Re}(\mathbf{s}_2\mathbf{n})\mathrm{Re}(\mathbf{s}_1\mathbf{s}_2^*)+24|\mathbf{s}_2|^2\,\mathrm{Re}(\mathbf{s}_2\mathbf{n}^*)\mathrm{Re}(\mathbf{s}_1\mathbf{s}_2^*)+24|\mathbf{n}|^2\,\mathrm{Re}(\mathbf{s}_2\mathbf{n})\mathrm{Re}(\mathbf{s}_1\mathbf{s}_2^*)+12\,\mathrm{Re}^2(\mathbf{s}_2\mathbf{n}^*)\mathrm{Re}(\mathbf{s}_1\mathbf{s}_2^*) \\
&+12\,\mathrm{Re}(\mathbf{s}_2\mathbf{n})\,\mathrm{Re}^2(\mathbf{s}_1\mathbf{s}_2^*)12\,\mathrm{Re}^2(\mathbf{s}_1\mathbf{n}^*)\mathrm{Re}(\mathbf{s}_2\mathbf{n}^*)+12\,\mathrm{Re}(\mathbf{s}_1\mathbf{n}^*)\mathrm{Re}(\mathbf{s}_2\mathbf{n}^*)^2+4|\mathbf{s}_1|^2\,\mathrm{Re}(\mathbf{s}_1\mathbf{n}^*)\mathrm{Re}(\mathbf{s}_2\mathbf{n}^*) \\
&+24|\mathbf{s}_2|^2\,\mathrm{Re}(\mathbf{s}_1\mathbf{n}^*)\mathrm{Re}(\mathbf{s}_2\mathbf{n}^*)+24|\mathbf{n}|^2\,\mathrm{Re}(\mathbf{s}_1\mathbf{n}^*)\mathrm{Re}(\mathbf{s}_2\mathbf{n}^*)+48\,\mathrm{Re}(\mathbf{s}_1\mathbf{n}^*)\mathrm{Re}(\mathbf{s}_2\mathbf{n}^*)\mathrm{Re}(\mathbf{s}_1\mathbf{s}_2^*)+12|\mathbf{s}_1|^2\,\mathrm{Re}^2(\mathbf{s}_2\mathbf{n}^*) \\
&+12|\mathbf{s}_2|^2\,\mathrm{Re}^2(\mathbf{s}_2\mathbf{n}^*)+12|\mathbf{n}|^2\,\mathrm{Re}^2(\mathbf{s}_2\mathbf{n}^*)+8\,\mathrm{Re}^3(\mathbf{s}_1\mathbf{n}^*)] = \\
&= P_1^3+P_2^3+6P_n^3+9P_1^2P_2+9P_2^2P_1+9P_1^2P_n+9P_2^2P_n+18P_1P_n^2+18P_2P_n^2+36P_1P_2P_n.
\end{aligned} \tag{11.9}$$

Finally, the expressions of P_1, P_2 and P_n can be derived by solving the following system:

$$\begin{cases}
M_2 = P_1+P_2+P_n \\
M_4 = P_1^2+P_2^2+2P_n^2+4P_1P_2+4P_1P_n+4PP_n \\
M_6 = P_1^3+P_2^3+6P_n^3+9P_1^2P_2+9P_1P_2^2+9P_1P_n+9P_2P_n+18P_1P_n^2+18P_2P_n^2+36P_1P_2P_n
\end{cases} \tag{11.10}$$

The process of finding the solutions of (11.10) is a really cumbersome procedure, since it involves high power terms, but it can be simplified with the following useful substitutions:

$$\begin{aligned}
A &= P_1+P_2 \\
B &= P_1\cdot P_2
\end{aligned} \tag{11.11}$$

Now, (11.10) can be rewritten as follows:

$$\begin{cases}
A+P_n = M_2 \\
A^2+2B+2P_n^2+4AP_n = M_4 \\
A^3+6BA+9P_n\left(A^2+2B\right)+18P_n^2A+6P_n^3 = M_6
\end{cases} \tag{11.12}$$

that is a system of three unknowns (i.e., P_n, A and B) with three independent equations. Now, merging the two upper equations into the third one in (11.12), we can write the following equation, involving the unknown A and the three moments $\{M_2, M_4, M_6\}$:

$$2A^3 + 36A^2 \cdot M_2 - 12A \cdot M_2^2 + 6A \cdot M_4 = 9M_2 \cdot M_4 - M_6 - 12M_2^3 \tag{11.13}$$

that is a cubic equation in A. Hence, there are three possible solutions for (11.13), i.e. $\{A_1, A_2, A_3\}$, and hence three possible sets of solutions for (11.10), i.e. $\{A_1, B_1, P_{n1}\}$, $\{A_2, B_2, P_{n2}\}$, $\{A_3, B_3, P_{n3}\}$, but only one set is acceptable as detailed in the following.

The first set of solutions of (11.13) is as follows:

$$\begin{aligned} A_1 &= 2\sqrt{2M_2^2 - M_4}\cos\left(\frac{\gamma}{3}\right) \\ B_1 &= \frac{2M_2^2 - M_4}{2}\left(1 + 2\cos\left(\frac{2}{3}\gamma\right)\right) \\ P_{n1} &= M_2 - 2\sqrt{2M_2^2 - M_4}\cos\left(\frac{\gamma}{3}\right) \end{aligned} \tag{11.14}$$

where

$$\gamma = \arctan\left(\frac{\sqrt{16\left(2M_2^2 - M_4\right)^3 - \left(12M_2^3 - 9M_2M_4 + M_6\right)^2}}{-12M_2^3 + 9M_2M_4 - M_6}\right) + \pi \tag{11.15}$$

for $2M_2^2 \neq M_4$. In fact, the case $2M_2^2 = M_4$ corresponds to the limit solution $P_1 = P_2 = 0$ and $P_n > 0$, that models a noisy scenario with no transmitted signals. Then, the desired values of P_1, P_2 are then obtained in a straightforward way:

$$\begin{aligned} P_1 &= \sqrt{2M_2^2 - M_4}\cos\left(\frac{\gamma}{3}\right) + \sqrt{\frac{1}{2}\left(M_4 - 2M_2^2\right)\cos\left(2\frac{\gamma}{3}\right)} \\ P_2 &= \sqrt{2M_2^2 - M_4}\cos\left(\frac{\gamma}{3}\right) - \sqrt{\frac{1}{2}\left(M_4 - 2M_2^2\right)\cos\left(2\frac{\gamma}{3}\right)} \end{aligned} \tag{11.16}$$

The second set of solutions is as follows:

$$\begin{aligned} A_2 &= -2\sqrt{2M_2^2 - M_4}\left(\cos\left(\frac{\gamma}{3}\right) - \sqrt{3}\sin\left(\frac{\gamma}{3}\right)\right) \\ B_2 &= \frac{2M_2^2 - M_4}{2}\left(1 - \cos\left(2\frac{\gamma}{3}\right) - \sqrt{3}\sin\left(2\frac{\gamma}{3}\right)\right) \\ P_{n2} &= M_2 + 2\sqrt{2M_2^2 - M_4}\left(\cos\left(\frac{\gamma}{3}\right) - \sqrt{3}\sin\left(\frac{\gamma}{3}\right)\right) \end{aligned} \tag{11.17}$$

The desired values of P_1, P_2 are given by:

$$P_1 = \frac{1}{2}\left(\sqrt{2M_2^2 - M_4}\left(-\cos\left(\frac{\gamma}{3}\right)+\sqrt{3}\sin\left(\frac{\gamma}{3}\right)\right)+\sqrt{\left(M_4-2M_2^2\right)\left(\cos\left(2\frac{\gamma}{3}\right)+\sqrt{3}\sin\left(2\frac{\gamma}{3}\right)\right)}\right)$$
$$P_2 = \frac{1}{2}\left(\sqrt{2M_2^2 - M_4}\left(-\cos\left(\frac{\gamma}{3}\right)+\sqrt{3}\sin\left(\frac{\gamma}{3}\right)\right)-\sqrt{\left(M_4-2M_2^2\right)\left(\cos\left(2\frac{\gamma}{3}\right)+\sqrt{3}\sin\left(2\frac{\gamma}{3}\right)\right)}\right) \quad (11.18)$$

The third set of solutions is:

$$A_3 = -2\sqrt{2M_2^2 - M_4}\left(\cos\left(\frac{\gamma}{3}\right)+\sqrt{3}\sin\left(\frac{\gamma}{3}\right)\right)$$
$$B_3 = \frac{2M_2^2 - M_4}{2}\left(1-\cos\left(2\frac{\gamma}{3}\right)+\sqrt{3}\sin\left(2\frac{\gamma}{3}\right)\right) \quad (11.19)$$
$$P_{n3} = M_2 + 2\sqrt{2M_2^2 - M_4}\left(\cos\left(\frac{\gamma}{3}\right)-\sqrt{3}\sin\left(\frac{\gamma}{3}\right)\right)$$

The corresponding desired values of P_1, P_2 are:

$$P_1 = \frac{1}{2}\left(-\sqrt{2M_2^2 - M_4}\left(\cos\left(\frac{\gamma}{3}\right)+\sqrt{3}\sin\left(\frac{\gamma}{3}\right)\right)+\sqrt{\left(M_4-2M_2^2\right)\left(\cos\left(2\frac{\gamma}{3}\right)-\sqrt{3}\sin\left(2\frac{\gamma}{3}\right)\right)}\right)$$
$$P_2 = \frac{1}{2}\left(-\sqrt{2M_2^2 - M_4}\left(\cos\left(\frac{\gamma}{3}\right)+\sqrt{3}\sin\left(\frac{\gamma}{3}\right)\right)-\sqrt{\left(M_4-2M_2^2\right)\left(\cos\left(2\frac{\gamma}{3}\right)-\sqrt{3}\sin\left(2\frac{\gamma}{3}\right)\right)}\right) \quad (11.20)$$

In order to determine which solution is acceptable, we need to solve $A = P_1+P_2$ and $B = P_1 \cdot P_2$ in a straightforward way, in all the three possible cases (i.e. $A=A_1$, A_2, A_3 and $B=B_1$, B_2, B_3). In other words, we need to study the sign of $\Delta = (A^2 - 4 \cdot B)$ with the constraints: $P_1>0$ and $P_2>0$. Moreover, the expressions $A = P_1+P_2$ and $B = P_1 \cdot P_2$ represent the equation of a straight line and a hyperbola respectively, whose intersections, give the desired values of P_1 and P_2. In Fig. 11-2 the two curves are drawn on a Cartesian plane. Solution I is depicted in Fig. 11-2(a), while Solution II and Solution III are reported Fig. 11-2(b) and Fig. 11-2(c), respectively. In Solution I, we have $\Delta>0$, $A_1>0$ and $B_1>0$: the intersections between the two curves are in the first quadrant of the Cartesian plane, and hence, it is possible to find two distinct and positive values for P_1 and P_2, see Fig. 11-2(a), On the other hand, in Solution II, we have $\Delta>0$, $A_2>0$ but $B_2<0$: This solution is unacceptable since the term B_2 is negative only if either $P_1<0$ or $P_2<0$, but P_1 and P_2 represent the powers of the authorized and hidden signal, respectively, and cannot be negative. This case is depicted Fig. 11-2(b): the

intersections between the straight line and the hyperbola happen in the second quadrant of the Cartesian plane, where $P_1>0$ and $P_2<0$, and in the fourth quadrant, where conversely $P_1<0$ and $P_2>0$. Finally, in Solution III $\Delta<0$, $A_3<0$, and $B_3>0$ and there is no intersection between the two curves, Fig. 11-2(c).

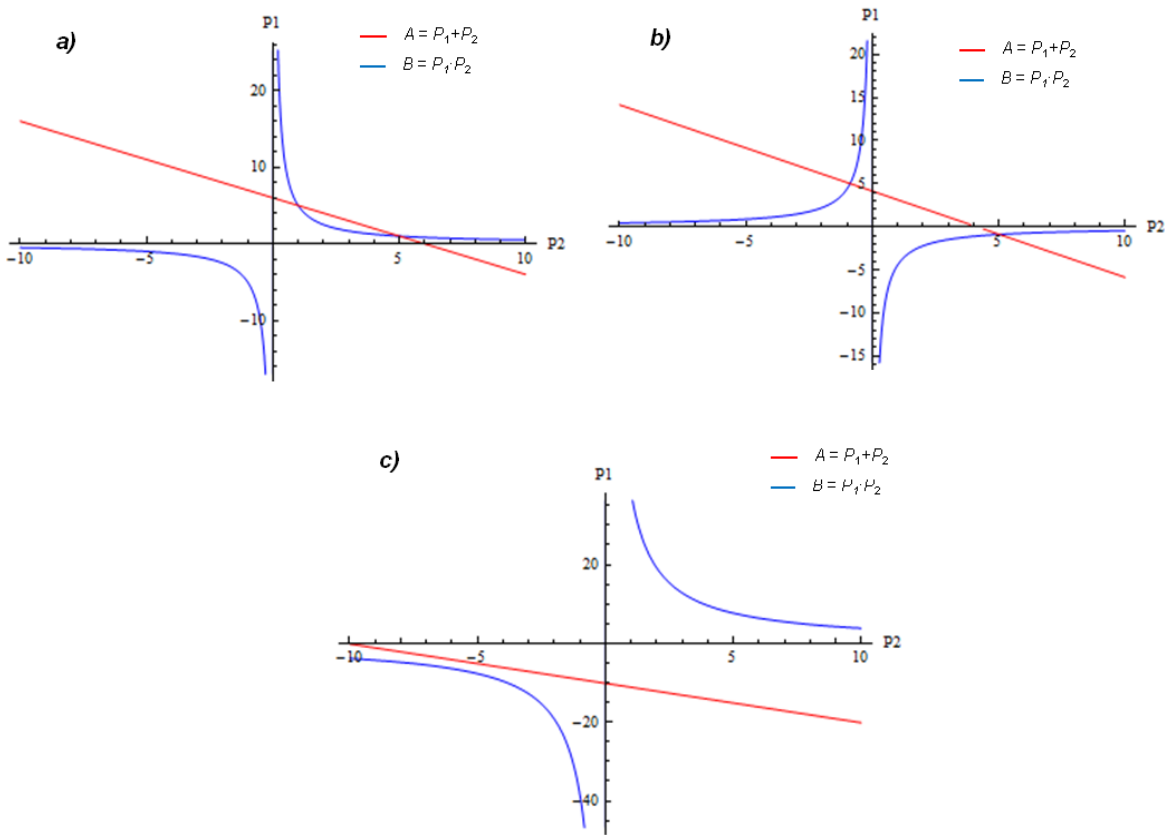

Figure 11-2 Graphical representation of $A= P_1+P_2$ and $B = P_1 \cdot P_2$ according to: ***a)*** Solution I, ***b)*** Solution II, ***c)*** Solution III.

It has to be noted that only Solution I is acceptable, while both Solution II and Solution III yield to impossible (i.e. absurd) results.

The power of the hidden signal P_2 is hence expressed by the second formula in (11.11). Now, its estimation $\hat{P}_2$ is used as the decision variable for the hypothesis testing about the presence or absence of the freeloader.

The decision variable is estimated according to the following:

$$\hat{P}_2 = \frac{1}{2}\left(\sqrt{2\hat{M}_2^2 - \hat{M}_4}\cos\left(\frac{\hat{\gamma}}{3}\right) - \sqrt{\left(\hat{M}_4 - 2\hat{M}_2^2\right)\cos\left(2\frac{\hat{\gamma}}{3}\right)} \right) \tag{11.21}$$

with the estimations $\hat{M}_2$, $\hat{M}_4$, $\hat{M}_6$ of the second, fourth, and sixth order moments respectively obtained as:

$$\hat{M}_2 = \frac{1}{N}\sum_{i=1}^{N}|r_i|^2, \tag{11.22}$$

$$\hat{M}_4 = \frac{1}{N}\sum_{i=1}^{N}|r_i|^4 \tag{11.23}$$

$$\hat{M}_6 = \frac{1}{N}\sum_{i=1}^{N}|r_i|^6. \tag{11.24}$$

where r_i is the i-th sample of the received signal and:

$$\hat{\gamma} = \arctan\left(\frac{\sqrt{16\left[\left(\frac{1}{N}\sum_{i=1}^{N}|r_i|^2\right)^2 - \frac{1}{N}\sum_{i=1}^{N}|r_i|^4\right]^3 + \left[12\left(\frac{1}{N}\sum_{i=1}^{N}|r_i|^2\right)^3 - 9\left(\frac{1}{N}\sum_{i=1}^{N}|r_i|^2\right)\left(\frac{1}{N}\sum_{i=1}^{N}|r_i|^4\right) + \frac{1}{N}\sum_{i=1}^{N}|r_i|^6\right]^2}}{12\left(\frac{1}{N}\sum_{i=1}^{N}|r_i|^2\right)^3 - 9\left(\frac{1}{N}\sum_{i=1}^{N}|r_i|^2\right)\left(\frac{1}{N}\sum_{i=1}^{N}|r_i|^4\right) + \frac{1}{N}\sum_{i=1}^{N}|r_i|^6} \right) + \pi \tag{11.25}$$

Now, considering a threshold η, the test is finally expressed as follows:

$$\begin{aligned} H_0 &: \ \hat{P}_2 < \eta \quad \text{absence of the freeloader} \\ H_1 &: \ \hat{P}_2 \geq \eta \quad \text{presence of the freeloader} \end{aligned} \tag{11.26}$$

11.4 Performance analysis

In this section, the performances of the new method for the detection of FLUs in CRNs are evaluated. In order to statistically quantify the estimation errors we are considering the mean value and the variance of the testing variable in (11-13), i.e. the estimation of the freeloader power $\hat{P}_2$. Let us define, for the sake of compactness $\varepsilon_2 = \hat{M}_2 - E[\hat{M}_2]$,

$\varepsilon_4 = \hat{M}_4 - E[\hat{M}_4]$, $\varepsilon_6 = \hat{M}_6 - E[\hat{M}_6]$, as the three moment-estimation's errors, which are assumed to be zero-mean random variables. Then, under the assumption of small errors for the high-order moment estimators ($\hat{M}_2, \hat{M}_4, \hat{M}_6$), the bias and variance of the estimation error can be accordingly evaluated by a three-dimensional (3-D) reduced Taylor expansion up to the second order as follows, respectively:

$$\begin{aligned} E[\hat{P}_2] = & \\ & \frac{1}{2}\frac{\partial^2 \hat{P}_2}{\partial \hat{M}_2^2}\bigg|_{\varepsilon_2=\varepsilon_4=\varepsilon_6=0} \cdot \mathrm{var}[\hat{M}_2] + \frac{1}{2}\frac{\partial^2 \hat{P}_2}{\partial \hat{M}_4^2}\bigg|_{\varepsilon_2=\varepsilon_4=\varepsilon_6=0} \cdot \mathrm{var}[\hat{M}_4] + \\ & \frac{1}{2}\frac{\partial^2 \hat{P}_2}{\partial \hat{M}_6^2}\bigg|_{\varepsilon_2=\varepsilon_4=\varepsilon_6=0} \cdot \mathrm{var}[\hat{M}_6] + \frac{1}{2}\frac{\partial \hat{P}_2}{\partial \hat{M}_2 \partial \hat{M}_4}\bigg|_{\varepsilon_2=\varepsilon_4=\varepsilon_6=0} \cdot \mathrm{cov}[\hat{M}_2 \hat{M}_4] + \\ & \frac{1}{2}\frac{\partial \hat{P}_2}{\partial \hat{M}_2 \partial \hat{M}_6}\bigg|_{\varepsilon_2=\varepsilon_4=\varepsilon_6=0} \cdot \mathrm{cov}[\hat{M}_2 \hat{M}_6] + \frac{1}{2}\frac{\partial \hat{P}_2}{\partial \hat{M}_4 \partial \hat{M}_6}\bigg|_{\varepsilon_2=\varepsilon_4=\varepsilon_6=0} \cdot \mathrm{cov}[\hat{M}_4 \hat{M}_6] \end{aligned} \tag{11.27}$$

$$\begin{aligned} \mathrm{var}[\hat{P}_2] = & \\ & \left(\frac{\partial \hat{P}_2}{\partial \hat{M}_2}\right)^2\bigg|_{\varepsilon_2=\varepsilon_4=\varepsilon_6=0} \cdot \mathrm{var}[\hat{M}_2] + \left(\frac{\partial \hat{P}_2}{\partial \hat{M}_4}\right)^2\bigg|_{\varepsilon_2=\varepsilon_4=\varepsilon_6=0} \cdot \mathrm{var}[\hat{M}_4] + \left(\frac{\partial \hat{P}_2}{\partial \hat{M}_3}\right)^2\bigg|_{\varepsilon_2=\varepsilon_4=\varepsilon_6=0} \cdot \mathrm{var}[\hat{M}_6] \\ & + \frac{\partial \hat{P}_2}{\partial \hat{M}_2}\bigg|_{\varepsilon_2=\varepsilon_4=\varepsilon_6=0} \cdot \frac{\partial \hat{P}_2}{\partial \hat{M}_4}\bigg|_{\varepsilon_2=\varepsilon_4=\varepsilon_6=0} \cdot \mathrm{cov}[\hat{M}_2 \hat{M}_4] + \frac{\partial \hat{P}_2}{\partial \hat{M}_2}\bigg|_{\varepsilon_2=\varepsilon_4=\varepsilon_6=0} \cdot \frac{\partial \hat{P}_2}{\partial \hat{M}_6}\bigg|_{\varepsilon_2=\varepsilon_4=\varepsilon_6=0} \cdot \mathrm{cov}[\hat{M}_2 \hat{M}_6] \\ & + \frac{\partial \hat{P}_2}{\partial \hat{M}_4}\bigg|_{\varepsilon_2=\varepsilon_4=\varepsilon_6=0} \cdot \frac{\partial \hat{P}_2}{\partial \hat{M}_6}\bigg|_{\varepsilon_2=\varepsilon_4=\varepsilon_6=0} \cdot \mathrm{cov}[\hat{M}_4 \hat{M}_6] \end{aligned} \tag{11.28}$$

where var[·] and cov[·] stand for variance and covariance, respectively. The above algebraic expressions are trivially derived from a mere computation of the partial derivatives of the three moments expressed by (11-5), (11-8), (11-9). Let us now evaluate the expressions for the mean values $E[\hat{M}_2]$, $E[\hat{M}_4]$, $E[\hat{M}_6]$, the variances $\mathrm{var}[\hat{M}_2]$, $\mathrm{var}[\hat{M}_4]$, $\mathrm{var}[\hat{M}_6]$, and the covariances $\mathrm{cov}[\hat{M}_2]$, $\mathrm{cov}[\hat{M}_4]$, $\mathrm{cov}[\hat{M}_6]$ of the estimators. In particular, since $E[\varepsilon_i] = 0$ with $i = 2, 4, 6$, for the mean values we have:

$$
\begin{aligned}
&E[\hat{M}_2] = M_2 = P_1 + P_2 + P_n \\
&E[\hat{M}_4] = M_4 = P_1^2 + P_2^2 + 2P_n^2 + 4P_1P_2 + 4P_1P_n + 4PP_n \\
&E[\hat{M}_6] = M_6 = P_1^3 + P_2^3 + 6P_n^3 + 9P_1^2P_2 + 9P_1P_2^2 + 9P_1P_n + 9P_2P_n + 18P_1P_n^2 + 18P_2P_n^2 + 36P_1P_2P_n
\end{aligned}
\tag{11.29}
$$

Then, the variances of the estimators can be evaluated by means of the following:

$$
\begin{aligned}
\mathrm{var}\left[\hat{M}_i\right] &= E[\varepsilon_i^2] = E[\hat{M}_i\hat{M}_i] - E^2[\hat{M}_i] = E\left[\frac{1}{N}\sum_{n=1}^{N}|r_n|^{2\cdot i}\,\frac{1}{N}\sum_{m=1}^{N}|r_m|^{2\cdot i}\right] - M_i^2 \\
&= \frac{1}{N^2}E\left[\sum_{n=1}^{N}\sum_{m=1}^{N}|r_n|^{2\cdot i}\,|r_m|^{2\cdot i}\right] - M_i^2 = \frac{1}{N^2}E\left[N\sum_{n=1}^{N}|r_n|^{2\cdot i} + \sum_{\substack{m=1\\ n\neq m}}^{N}|r_n|^{2\cdot i}\,|r_m|^{2\cdot i}\right] - M_i^2 \\
&= \frac{1}{N}E[|\mathbf{r}|^{2\cdot i}] + \frac{N^2-N}{N^2}E^2[|\mathbf{r}|^{2\cdot i}] - M_i^2 = \frac{1}{N}E[|\mathbf{r}|^{2\cdot i}] + \frac{N^2-N}{N^2}M_i^2 - M_i^2 \\
&= \frac{1}{N}M_{2\cdot i} - \frac{1}{N}M_i^2
\end{aligned}
\tag{11.30}
$$

with $i = 2,\ 4,\ 6$

In particular, exploiting (11-30), the variances are now given by:

$$
\mathrm{var}\left[\hat{M}_2\right] = \frac{1}{N}\left(2P_1P_2 + 2P_1P_n + 2P_2P_n + P_n^2\right)
$$

$$
\begin{aligned}
\mathrm{var}\left[\hat{M}_4\right] = \frac{1}{N}\big(&20P_n^4 + 80P_1P_n^3 + 80P_2P_n^3 - 20P_1^2P_n^2 + 52P_2^2P_n^2 + 8P_1^3P_n + 8P_2^3P_n + 72P_1^2P_n + \\
&+ 240P_1P_2P_n^2 + 104P_1P_2^2P_n + 104P_1^2P_2P_n + 8P_1P_2^3 + 18P_1^2P_2^2 + 8P_1^3P_2\big)
\end{aligned}
\tag{11.31}
$$

$$
\begin{aligned}
\mathrm{var}\left[\hat{M}_6\right] = \frac{1}{N}\big(&684P_n^6 + 4104P_1P_n^5 + 4104P_2P_n^5 + 4968P_1^2P_n^4 + 4968P_2^2P_n^4 + 20520P_1P_2P_n^4 \\
&+ 2064P_1^3P_n^3 + 2064P_2^3P_n^3 + 19872P_1P_2^2P_n^3 + 19872P_1^2P_2P_n^3 + 333P_1^4P_n^2 + 333P_2^4P_n^2 \\
&+ 6192P_1P_2^3P_n^2 + 14094P_1^2P_2^2P_n^2 + 6192P_1^3P_2P_n^2 + 18P_1^5P_n + 18P_2^5P_n + 666P_1P_2^4P_n \\
&+ 2772P_1^2P_2^3P_n 2772P_1^3P_2^2P_n + 666P_1^4P_2P_n + 18P_1P_2^5 + 126P_1^2P_2^4 + 236P_1^3P_2^3 + 126P_1^4P_2^2 + 18P_1^5P_2\big)
\end{aligned}
$$

In the same way, the covariances of the estimators can be evaluated by means of:

$$\begin{aligned}
\operatorname{cov}\left[\hat{M}_i\hat{M}_j\right] &= E[\varepsilon_i\varepsilon_j] = E[\hat{M}_i\hat{M}_j] - E^2[\hat{M}_i]E^2[\hat{M}_j] \\
&= E\left[\frac{1}{N}\sum_{n=1}^{N}|r_n|^i \frac{1}{N}\sum_{m=1}^{N}|r_m|^j\right] - M_i^2M_j^2 = \frac{1}{N^2}E\left[\sum_{n=1}^{N}\sum_{m=1}^{N}|r_n|^i|r_m|^j\right] - M_i^2M_j^2 \\
&= \frac{1}{N^2}E\left[N\sum_{n=1}^{N}|r_n|^{i+j} + \sum_{\substack{m=1\\ n\neq m}}^{N}|r_n|^j|r_m|^i\right] - M_i^2M_j^2 \\
&= \frac{1}{N}E[|\mathbf{r}|^{i+j}] + \frac{N^2-N}{N^2}E^2[|\mathbf{r}|^i] - M_i^2M_j^2 \\
&= \frac{1}{N}E[|\mathbf{r}|^{i+j}] + \frac{N^2-N}{N^2}M_i^2M_j^2 - M_i^2M_j^2 = \frac{1}{N}M_{i+j} - \frac{1}{N}M_i^2M_j^2 \\
&\qquad \text{with } i = 2,\ 4,\ 6\ ;\ j = 2,\ 4,\ 6 \text{ and } i \neq j
\end{aligned} \tag{11.32}$$

and exploiting (11.32), we can obtain the expressions of all the covariances as follows:

$$\operatorname{cov}\left[\hat{M}_2\hat{M}_4\right] = \frac{1}{N}\left(4P_n^3 + 12P_1P_n^2 + 12P_2P_n^2 + 4P_1^2P_n + 4P_2^2P_n + 24P_1P_2P_n + 4P_1P_2^2 + 4P_1^2P_2\right)$$

$$\begin{aligned}
\operatorname{cov}\left[\hat{M}_4\hat{M}_6\right] = \frac{1}{N}\big(&108P_n^5 + 540P_1P_n^4 + 540P_2P_n^4 + 504P_1^2P_n^3 + 504P_2^2P_n^3 + 2160P_1P_2P_n^3 + 144P_1^3P_n^2 \\
&+ 144P_2^3P_n^2 + 1512P_1P_2^2P_n^2 + 1512P_1^2P_2P_n^2 + 12P_1^4P_n + 12P_2^4P_n + + 288P_1P_2^3P_n \\
&+ 666P_1^2P_2^2P_n + 288P_1^3P_2P_n + 12P_1P_2^4 + 54P_1^2P_2^3 + 54P_1^3P_2^2 + 12P_1^4P_2\big)
\end{aligned} \tag{11.33}$$

$$\begin{aligned}
\operatorname{cov}\left[\hat{M}_6\hat{M}_2\right] = \frac{1}{N}\big(&18P_n^4 + 72P_1P_n^3 + 72P_2P_n^3 - 27P_1^2P_n^2 + 45P_2^2P_n^2 + 216P_1P_2P_n^2 \\
&+ 6P_1^3P_n + 6P_2^3P_n + 72P_1^2P_n + 90P_1P_2^2P_n + 90P_1^2P_2P_n + 6P_1P_2^3 + 18P_1^2P_2^2 + 6P_1^3P_2\big)
\end{aligned}$$

In order to evaluate the variances in (11.31) and the covariances in (11.33), the eighth, M_8, tenth, M_{10} and twelfth, $M_{12,}$ order moments need to be calculated. Recalling the system model described in Section II and following the same approach as in the previous section, the above mentioned high-order moments can be easily derived as follows:

$$M_8 = E[|\mathbf{r}|^8] = E[|\mathbf{s}_1 + \mathbf{s}_2 + \mathbf{n}|^8] = \\ = P_1^4 + P_2^4 + 24P_n^4 + 36P_1^2P_2^2 + 16P_1^3P_2 + 16P_1P_2^3 + 16P_1^3P_n + 72P_1^2P_n + 96P_1P_n^3 + 16P_2^3P_n \\ + 72P_2^2P_n^2 + 96P_2P_n^3 + 288P_1P_2P_n^2 + 144P_1^2P_2P_n + 144P_1P_2^2P_n \quad (11.34)$$

$$M_{10} = E[|\mathbf{r}|^{10}] = E[|\mathbf{s}_1 + \mathbf{s}_2 + \mathbf{n}|^{10}] = \\ = P_1^5 + P_2^5 + 120P_n^5 + 25P_1^4P_2 + 100P_1^3P_2^2 + 100P_1^2P_2^3 + 25P_1P_2^4 + 25P_1^4P_n + 200P_1^3P_n^2 \\ + 600P_1^2P_n^3 + 600P_1P_n^4 + 25P_2^4P_n + 200P_2^3P_n^2 + 600P_2^2P_n^3 + 600P_2P_n^4 + 400P_1^3P_2P_n \\ + 900P_1^2P_2^2P_n + 400P_1P_2^3P_n + 1800P_1^2P_2P_n^2 + 1800P_1P_2^2P_n^2 + 2400P_1P_2P_n^3 \quad (11.35)$$

$$M_{12} = E[|\mathbf{r}|^{12}] = E[|\mathbf{s}_1 + \mathbf{s}_2 + \mathbf{n}|^{12}] \\ = P_1^6 + P_2^6 + 720P_n^6 + 36P_1^5P_2 + 225P_1^4P_2^2 + 400P_1^3P_2^3 + 225P_1^2P_2^4 + 36P_1P_2^5 + 36P_1^5P_n \\ + 450P_1^4P_n^2 + 2400P_1^3P_n^3 + 5400P_1^2P_n^4 + 4320P_1P_n^5 + 36P_2^5P_n + 450P_2^4P_n^2 + 2400P_2^3P_n^3 \\ + 5400P_2^2P_n^4 + 4320P_2P_n^5 + 900P_1^4P_2P_n + 7200P_1^3P_2P_n^2 + 3600P_1^3P_2^2P_n + 21600P_1^2P_2P_n^3 \\ + 16200P_1^2P_2^2P_n^2 + 900P_1P_2^4P_n + 7200P_1P_2^3P_n^2 + 3600P_1^2P_2^3P_n + 21600P_1P_2^2P_n^3 + 21600P_1P_2P_n^4 \quad (11.36)$$

Finally, the desired expressions of the bias $E[\hat{P}_2]$ and the variance $\mathrm{var}[\hat{P}_2]$ can be obtained, as functions of the actual values P_1, P_2, and P_n. The obtained results, are reported in the Appendix II of this chapter. Then, the testing variable in (11-21) is asymptotically Gaussian as a direct consequence of the central limit theorem. In fact, both the first and the second terms are the difference of two asymptotically Gaussian variables with non-zero mean. Nonetheless the testing variable represents the estimation $\hat{P}_2$ of the hidden user power, it is obtained as the difference of two estimated terms, and hence, can assume also negative values. In fact, the testing variable $\hat{P}_2$ is a Gaussian variable with a mean equal to P_2 in the H_1 hypothesis and a Gaussian variable with zero mean in the H_0 hypothesis. The test threshold can be now evaluated from a straightforward evaluation of the Gaussian integral, under the null-hypothesis:

$$\eta = E[\hat{P}_2] + \frac{1}{\sqrt{2\,\mathrm{var}[\hat{P}_2]}} erfc^{-1}(2P_{FA}) \quad (11.37)$$

for $P_2 = 0$

Again, the probability of detection P_D is determined in the H_1 hypothesis as:

$$P_D = \frac{1}{2} erfc\left(\frac{v - E\left[\hat{P}_2\right]}{\sqrt{2var\left[\hat{P}_2\right]}} \right)$$

for $P_2 \neq 0$

(11.38)

11.5 Results

In this Section, wide simulation trials are conducted to prove the sensitivity of the theoretical approach and to verify the efficiency of the proposed test. In all the following results, we have evaluated the P_D both in an analytic way, i.e. using (11.38), and by means of simulations. The time record length is equal to 10^7 complex samples, and several Monte-Carlo simulation trials (10^5 independent runs) have been implemented to numerically evaluate the performance of our method. In the reported analysis, a $P_{FA}=10^{-2}$ and additive white Gaussian noise (AWGN) have been used. Then, the P_D of the new detector is evaluated under the Constant False Alarm (CFAR) procedure versus several values of P_1 and P_2 of practical interest (i.e. $P_1 > P_n > P_2$). In fact, the proposed method must be able to detect the FLU, with power P_2 that hides its radio signal under the noise floor (P_n) in the presence of an active (either primary or secondary) user, with power P_1.

The P_D of the proposed method versus the power of the signal transmitted by the freeloader user P_2 is showed in Fig. 11-2 for different values of P_1, and for a unitary noise variance (i.e. P_n = 0 dB). The simulation results (dotted lines) well match the theoretical ones (solid lines), thus validating the correctness of the mathematical analysis and assumptions of the previous Sections. As P_1 increases (from 5 dB to 30 dB) the performance of the proposed procedure starts worsening, as expected. In fact, if the power of the signal transmitted by the AU is too high, it covers all the weaker signals. Thus making it impossible for the monitoring sensor to detect the freeloader that is transmitting with very low power.

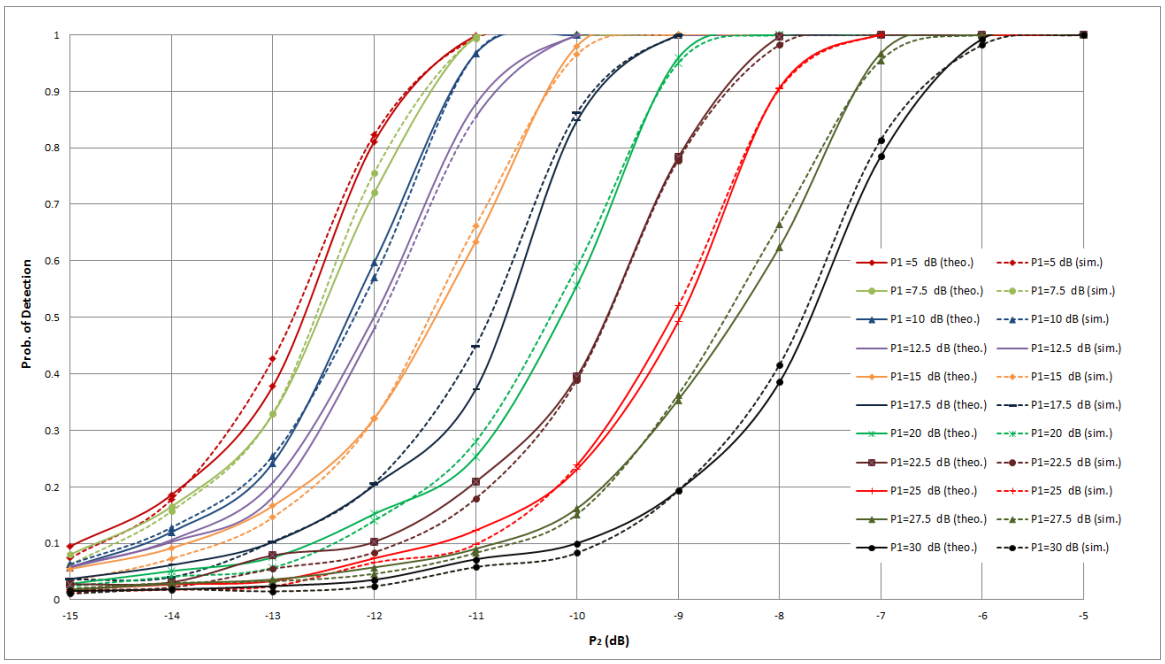

Figure 11-3 Probability of detection of the proposed method vs. the power of the freeloader P_2, for several values of the active user power P_1, and a noise power P_n = 0 dB. Simulation (dotted lines); theory (solid lines).

Fig. 11-3 shows the P_D of the proposed method versus the power of the authorized user P_1, for several values of P_2 (spanning from -15 dB to -5 dB) and for P_n = 0 dB. Again, the simulated results corroborate the theoretical curves also in Fig. 11-3. As it can be seen, larger detection probabilities are achieved in correspondence of higher values of P_2. That is because, as the power of the freeloader signal decreases, it becomes harder to distinguish it from the channel noise. However, exploiting the innovative method, large detection probabilities (up to 100%) can be achieved even with low powers (i.e. P_2 = -10 dB). This is very important for security and economic reasons. In fact, under a security viewpoint, by exploiting our test the monitoring sensor can be truly sense if hidden transmissions take place without authorization. Then, even if FLUs do not directly damage the communications of the active operator, they represent a relevant economic loss for CRN providers.

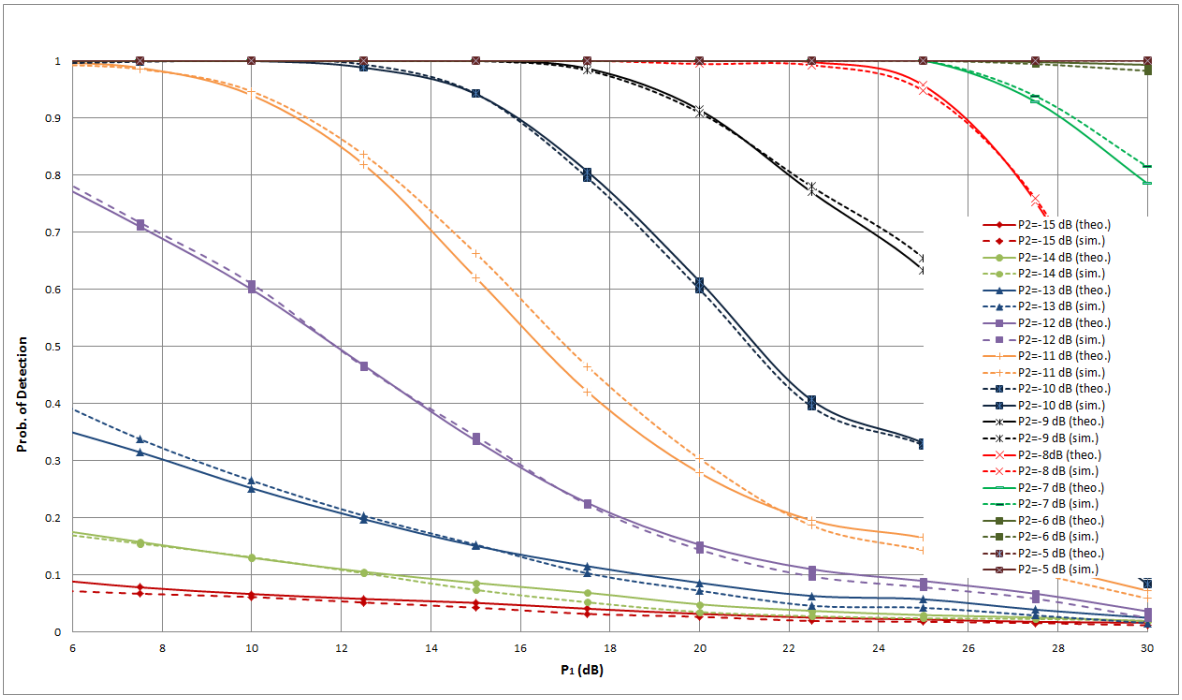

Figure 11-4 Probability of detection of the proposed method vs. the power of the authorized user P_1, for several values of the freeloader power P_2, and a noise power P_n = 0 dB. Simulation (dotted lines); theory (solid lines).

Finally, in order to completely define the performance of our method, we have investigated how the detection and false alarm probabilities are related each other. The theoretical ROC curves, i.e. P_D vs. P_{FA}, are then depicted in Figs. 4 and 5, again for P_n = 0 dB. In particular, Fig. 11-4 shows the ROC of the system for a fixed value of P_2 = -10 dB, varying the values of P_1, while in Fig. 11-5 the ROC curves for a fixed value of P_1 = 15 dB are presented, varying the values of P_2. As we can see from the graphs, larger detection probabilities are achieved with lower values of P_1, thus demonstrating the effectiveness of our test for application to the detection of hidden users in cognitive radios.

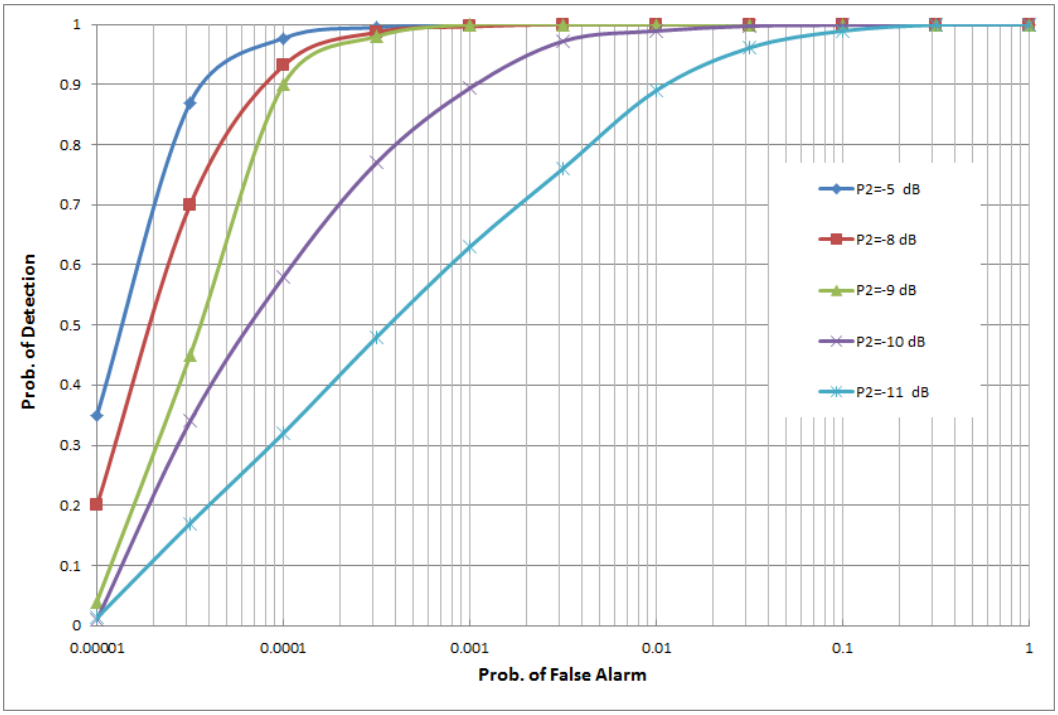

Figure 11-5. Theoretical probability of detection vs. the probability of false alarm for a freeloader power P_2 =-10 dB, and several values of the active user power P_1, and a noise power P_n = 0 dB.

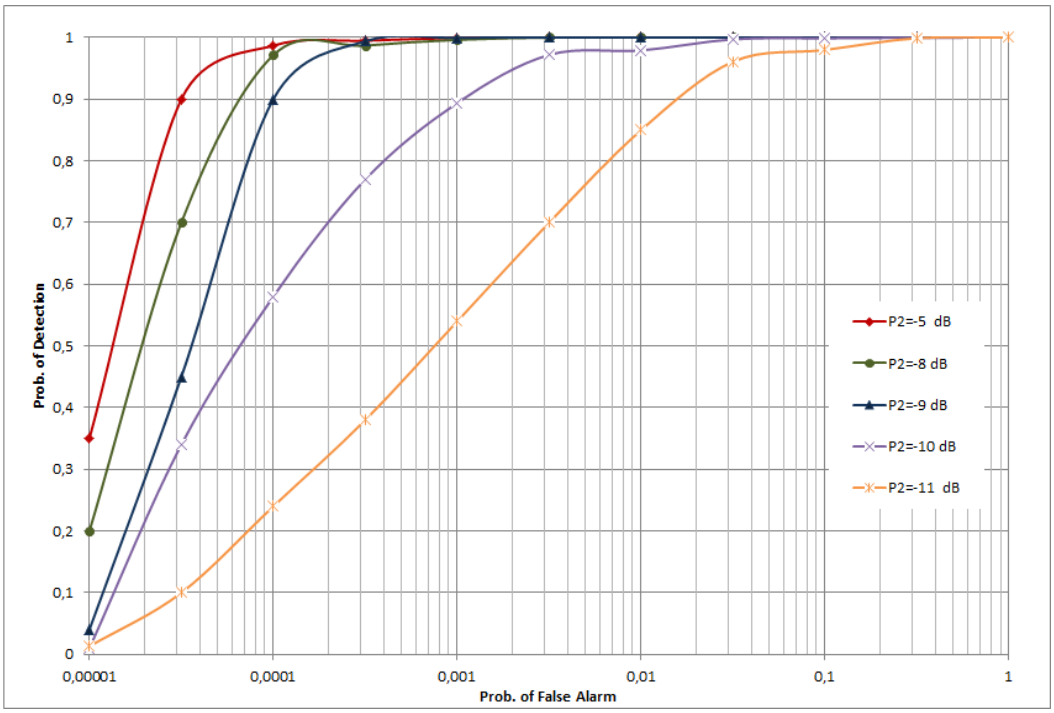

Figure 11-6. Theoretical probability of detection vs. the probability of false alarm for a freeloader power P_1 =15 dB, and several values of the active user power P_2, and a noise power P_n = 0 dB.

11.6 Conclusions

This chapter has presented a novel method for the detection of hidden freeloader users in cognitive radio networks. This is an innovative scenarios that has been investigated for the very first time during the research activity of my doctorate. In addition, the fast and reliable identification of FLUs is a very important task for the security of the cognitive radio market. The innovative signal processing technique discussed allows the detection of a freeloader that hides its radio signal under the noise floor in the presence of an active (either primary or secondary) user. A theoretical and simulated performance analysis has been carried out. In particular, the detection probability of the freeloader has been expressed as a parametric function of the powers of the authorized user and the background noise under typical operating scenarios. Moreover, the ROC curves of the proposed method have been evaluated for several values of false alarm probability. The theoretical results, sustained by wide simulation trials, have evidenced the efficiency of our method for detecting hidden users in cognitive radio communications.

11.7 Appendix I

In this section we report the expression of the bias $E[\hat{P}_2]$ and the variance $\mathrm{var}[\hat{P}_2]$ of the testing variable in (11-21).

$E[\hat{P}_2] =$

$$
\begin{aligned}
&P_2 + \Bigg(324\left(\sqrt{2}\cos\left(\frac{\gamma}{3}\right)+\sqrt{1-2\cos^2\left(\frac{\gamma}{3}\right)}\right)\left(\sin(\gamma)-\sin\left(\frac{\gamma}{3}\right)\right)(P_2+P_n)P_1^{12}+\\
&\quad 54\left(\sqrt{2}\cos\left(\frac{\gamma}{3}\right)+\sqrt{1-2\cos^2\left(\frac{\gamma}{3}\right)}\right)\left(\sin(\gamma)-\sin\left(\frac{\gamma}{3}\right)\right)\left(48P_2^2+154P_nP_2+(96-19P_n)P_n\right)P_1^{11}+\\
&\quad 24\left(\sqrt{2}\cos\left(\frac{\gamma}{3}\right)+\sqrt{1-2\cos^2\left(\frac{\gamma}{3}\right)}\right)\left(\sin(\gamma)-\sin\left(\frac{\gamma}{3}\right)\right)\\
&\quad \left(239P_2^3+1674P_nP_2^2+198P_n(7P_n+6)P_2+66(18-5P_n)P_n^2\right)P_1^{10}+\\
&\quad 18\Bigg(274\left(\sqrt{2}\cos\left(\frac{\gamma}{3}\right)+\sqrt{1-2\cos^2\left(\frac{\gamma}{3}\right)}\right)\left(\sin(\gamma)-\sin\left(\frac{\gamma}{3}\right)\right)P_2^4+2854\left(\sqrt{2}\cos\left(\frac{\gamma}{3}\right)+\sqrt{1-2\cos^2\left(\frac{\gamma}{3}\right)}\right)\\
&\qquad \left(\sin(\gamma)-\sin\left(\frac{\gamma}{3}\right)\right)P_nP_2^3+12\left(\sqrt{2}\cos\left(\frac{\gamma}{3}\right)+\sqrt{1-2\cos^2\left(\frac{\gamma}{3}\right)}\right)\left(\sin(\gamma)-\sin\left(\frac{\gamma}{3}\right)\right)P_n\\
&\qquad (731P_n+72)P_2^2+3\Bigg(1760\left(\sqrt{2}\cos\left(\frac{\gamma}{3}\right)+\sqrt{1-2\cos^2\left(\frac{\gamma}{3}\right)}\right)\left(\sin(\gamma)-\sin\left(\frac{\gamma}{3}\right)\right)P_n^3+\\
&\qquad\quad 1584\left(\sqrt{2}\cos\left(\frac{\gamma}{3}\right)+\sqrt{1-2\cos^2\left(\frac{\gamma}{3}\right)}\right)\left(\sin(\gamma)-\sin\left(\frac{\gamma}{3}\right)\right)P_n^2+\Bigg(2\sqrt{1-2\cos^2\left(\frac{\gamma}{3}\right)}\cos\left(\frac{\gamma}{3}\right)+\\
&\qquad\quad 2\sqrt{-\cos\left(\frac{2\gamma}{3}\right)}\cos(\gamma)+\sqrt{2}\left(\cos\left(\frac{4\gamma}{3}\right)+3\right)\Bigg)\sqrt{P_1^3P_2^2\left(3P_1^2-2P_2P_1+3P_2^2\right)}\Bigg)P_2+\\
&\quad 3P_n\Bigg(44\left(\sqrt{2}\cos\left(\frac{\gamma}{3}\right)+\sqrt{1-2\cos^2\left(\frac{\gamma}{3}\right)}\right)\left(\sin(\gamma)-\sin\left(\frac{\gamma}{3}\right)\right)P_n^3+\\
&\qquad 792\left(\sqrt{2}\cos\left(\frac{\gamma}{3}\right)+\sqrt{1-2\cos^2\left(\frac{\gamma}{3}\right)}\right)\left(\sin(\gamma)-\sin\left(\frac{\gamma}{3}\right)\right)P_n^2+\Bigg(2\sqrt{1-2\cos^2\left(\frac{\gamma}{3}\right)}\cos\left(\frac{\gamma}{3}\right)+\\
&\qquad 2\sqrt{1-2\cos^2\left(\frac{\gamma}{3}\right)}\cos(\gamma)+\sqrt{2}\left(\cos\left(\frac{4\gamma}{3}\right)+3\right)\Bigg)\sqrt{P_1^3P_2^2\left(3P_1^2-2P_2P_1+3P_2^2\right)}\Bigg)\\
&P_1^9+3\Bigg(1336\left(\sqrt{2}\cos\left(\frac{\gamma}{3}\right)+\sqrt{1-2\cos^2\left(\frac{\gamma}{3}\right)}\right)\left(\sin\left(\frac{\gamma}{3}\right)-\sin(\gamma)\right)P_2^5+\\
&\quad 16332\left(\sqrt{2}\cos\left(\frac{\gamma}{3}\right)+\sqrt{1-2\cos^2\left(\frac{\gamma}{3}\right)}\right)\left(\sin(\gamma)-\sin\left(\frac{\gamma}{3}\right)\right)P_nP_2^4+\\
&\quad 6\left(\sqrt{2}\cos\left(\frac{\gamma}{3}\right)+\sqrt{1-2\cos^2\left(\frac{\gamma}{3}\right)}\right)\left(\sin(\gamma)-\sin\left(\frac{\gamma}{3}\right)\right)P_n(7823P_n+1344)P_2^3+\\
&\quad 48\Bigg(1846\left(\sqrt{2}\cos\left(\frac{\gamma}{3}\right)+\sqrt{1-2\cos^2\left(\frac{\gamma}{3}\right)}\right)\left(\sin(\gamma)-\sin\left(\frac{\gamma}{3}\right)\right)P_n^3+3\Bigg(2\sqrt{1-2\cos^2\left(\frac{\gamma}{3}\right)}\cos\left(\frac{\gamma}{3}\right)+
\end{aligned}
$$

$$2\sqrt{1-2\cos^2\left(\frac{\gamma}{3}\right)}\cos(\gamma)+\sqrt{2}\left(\cos\left(\frac{4\gamma}{3}\right)+3\right)\Bigg)\sqrt{P_1^2P_2^2\left(3P_1^2-2P_2P_1+3P_2^2\right)}\Bigg)P_2^2+$$

$$6P_n\Bigg(10800\left(\sqrt{2}\cos\left(\frac{\gamma}{3}\right)+\sqrt{1-2\cos^2\left(\frac{\gamma}{3}\right)}\right)\left(\sin(\gamma)-\sin\left(\frac{\gamma}{3}\right)\right)P_n^3+$$

$$77\left(2\sqrt{1-2\cos^2\left(\frac{\gamma}{3}\right)}\cos\left(\frac{\gamma}{3}\right)+2\sqrt{1-2\cos^2\left(\frac{\gamma}{3}\right)}\cos(\gamma)+\sqrt{2}\left(\cos\left(\frac{4\gamma}{3}\right)+3\right)\right)$$

$$\sqrt{P_1^2P_2^2\left(3P_1^2-2P_2P_1+3P_2^2\right)}\Bigg)P_2+$$

$$3P_n\Bigg(4320\left(\sqrt{2}\cos\left(\frac{\gamma}{3}\right)+\sqrt{1-2\cos^2\left(\frac{\gamma}{3}\right)}\right)\left(\sin(\gamma)-\sin\left(\frac{\gamma}{3}\right)\right)P_n^4-$$

$$19\left(2\sqrt{1-2\cos^2\left(\frac{\gamma}{3}\right)}\cos\left(\frac{\gamma}{3}\right)+2\sqrt{1-2\cos^2\left(\frac{\gamma}{3}\right)}\cos(\gamma)+\sqrt{2}\left(\cos\left(\frac{4\gamma}{3}\right)+3\right)\right)$$

$$\sqrt{P_1^2P_2^2\left(3P_1^2-2P_2P_1+3P_2^2\right)}\,P_n+96\Bigg(2\sqrt{1-2\cos^2\left(\frac{\gamma}{3}\right)}\cos\left(\frac{\gamma}{3}\right)+$$

$$2\sqrt{1-2\cos^2\left(\frac{\gamma}{3}\right)}\cos(\gamma)+\sqrt{2}\left(\cos\left(\frac{4\gamma}{3}\right)+3\right)\Bigg)\sqrt{P_1^2P_2^2\left(3P_1^2-2P_2P_1+3P_2^2\right)}\Bigg)\Bigg)$$

$$P_1^8+4\Bigg(1770\left(\sqrt{2}\cos\left(\frac{\gamma}{3}\right)+\sqrt{1-2\cos^2\left(\frac{\gamma}{3}\right)}\right)\left(\sin\left(\frac{\gamma}{3}\right)-\sin(\gamma)\right)P_2^6+$$

$$7146\left(\sqrt{2}\cos\left(\frac{\gamma}{3}\right)+\sqrt{1-2\cos^2\left(\frac{\gamma}{3}\right)}\right)\left(\sin(\gamma)-\sin\left(\frac{\gamma}{3}\right)\right)P_nP_2^5+$$

$$27\left(\sqrt{2}\cos\left(\frac{\gamma}{3}\right)+\sqrt{1-2\cos^2\left(\frac{\gamma}{3}\right)}\right)\left(\sin(\gamma)-\sin\left(\frac{\gamma}{3}\right)\right)P_n\left(2379P_n+56\right)P_2^4+$$

$$\Bigg(23472\left(\sqrt{2}\cos\left(\frac{\gamma}{3}\right)+\sqrt{1-2\cos^2\left(\frac{\gamma}{3}\right)}\right)\left(\sin(\gamma)-\sin\left(\frac{\gamma}{3}\right)\right)P_n^3+$$

$$54648\left(\sqrt{2}\cos\left(\frac{\gamma}{3}\right)+\sqrt{1-2\cos^2\left(\frac{\gamma}{3}\right)}\right)\left(\sin(\gamma)-\sin\left(\frac{\gamma}{3}\right)\right)P_n^2+$$

$$\left(1270\sqrt{1-2\cos^2\left(\frac{\gamma}{3}\right)}\cos\left(\frac{\gamma}{3}\right)+1270\sqrt{1-2\cos^2\left(\frac{\gamma}{3}\right)}\cos(\gamma)+\sqrt{2}\left(635\cos\left(\frac{4\gamma}{3}\right)+1473\right)\right)$$

$$\sqrt{P_1^2P_2^2\left(3P_1^2-2P_2P_1+3P_2^2\right)}\Bigg)P_2^3+$$

$$9P_n\Bigg(1386\left(\sqrt{2}\cos\left(\frac{\gamma}{3}\right)+\sqrt{1-2\cos^2\left(\frac{\gamma}{3}\right)}\right)\left(\sin(\gamma)-\sin\left(\frac{\gamma}{3}\right)\right)P_n^3+$$

$$2376\left(\sqrt{2}\cos\left(\frac{\gamma}{3}\right)+\sqrt{1-2\cos^2\left(\frac{\gamma}{3}\right)}\right)\left(\sin(\gamma)-\sin\left(\frac{\gamma}{3}\right)\right)P_n^2+$$

$$2\left(230\sqrt{1-2\cos^2\left(\frac{\gamma}{3}\right)}\cos\left(\frac{\gamma}{3}\right)+230\sqrt{1-2\cos^2\left(\frac{\gamma}{3}\right)}\cos(\gamma)+\sqrt{2}\left(115\cos\left(\frac{4\gamma}{3}\right)+321\right)\right)$$

$$\sqrt{P_1^2 P_2^2 \left(3 P_1^2 - 2 P_2 P_1 + 3 P_2^2\right)}\Bigg) P_2^2 +$$

$$18 P_n \Bigg(666 \left(\sqrt{2}\ \cos\left(\frac{\gamma}{3}\right) + \sqrt{1 - 2\cos^2\left(\frac{\gamma}{3}\right)}\right)\left(\sin(\gamma) - \sin\left(\frac{\gamma}{3}\right)\right) P_n^4 +$$

$$77 \left(2\sqrt{1 - 2\cos^2\left(\frac{\gamma}{3}\right)}\ \cos\left(\frac{\gamma}{3}\right) + 2\sqrt{1 - 2\cos^2\left(\frac{\gamma}{3}\right)}\ \cos(\gamma) + \sqrt{2}\left(\cos\left(\frac{4\gamma}{3}\right) + 3\right)\right)$$

$$\sqrt{P_1^2 P_2^2 \left(3 P_1^2 - 2 P_2 P_1 + 3 P_2^2\right)}\ P_n + 66 \Bigg(2\sqrt{1 - 2\cos^2\left(\frac{\gamma}{3}\right)}\ \cos\left(\frac{\gamma}{3}\right) +$$

$$2\sqrt{1 - 2\cos^2\left(\frac{\gamma}{3}\right)}\ \cos(\gamma) + \sqrt{2}\left(\cos\left(\frac{4\gamma}{3}\right) + 3\right)\Bigg)\sqrt{P_1^2 P_2^2 \left(3 P_1^2 - 2 P_2 P_1 + 3 P_2^2\right)}\Bigg) P_2 +$$

$$3 P_n^2 \Bigg(666 \left(\sqrt{2}\ \cos\left(\frac{\gamma}{3}\right) + \sqrt{1 - 2\cos^2\left(\frac{\gamma}{3}\right)}\right)\left(\sin(\gamma) - \sin\left(\frac{\gamma}{3}\right)\right) P_n^4 -$$

$$110 \left(2\sqrt{1 - 2\cos^2\left(\frac{\gamma}{3}\right)}\ \cos\left(\frac{\gamma}{3}\right) + 2\sqrt{1 - 2\cos^2\left(\frac{\gamma}{3}\right)}\ \cos(\gamma) + \sqrt{2}\left(\cos\left(\frac{4\gamma}{3}\right) + 3\right)\right)$$

$$\sqrt{P_1^2 P_2^2 \left(3 P_1^2 - 2 P_2 P_1 + 3 P_2^2\right)}\ P_n + 396 \Bigg(2\sqrt{1 - 2\cos^2\left(\frac{\gamma}{3}\right)}\ \cos\left(\frac{\gamma}{3}\right) +$$

$$2\sqrt{1 - 2\cos^2\left(\frac{\gamma}{3}\right)}\ \cos(\gamma) + \sqrt{2}\left(\cos\left(\frac{4\gamma}{3}\right) + 3\right)\Bigg)\sqrt{P_1^3 P_2^2 \left(3 P_1^2 - 2 P_2 P_1 + 3 P_2^2\right)}\Bigg)\Bigg)$$

$$P_1^7 + 12 \Bigg(590 \left(\sqrt{2}\ \cos\left(\frac{\gamma}{3}\right) + \sqrt{1 - 2\cos^2\left(\frac{\gamma}{3}\right)}\right)\left(\sin\left(\frac{\gamma}{3}\right) - \sin(\gamma)\right) P_2^7 +$$

$$1524 \left(\sqrt{2}\ \cos\left(\frac{\gamma}{3}\right) + \sqrt{1 - 2\cos^2\left(\frac{\gamma}{3}\right)}\right)\left(\sin(\gamma) - \sin\left(\frac{\gamma}{3}\right)\right) P_n P_2^6 +$$

$$6 \left(\sqrt{2}\ \cos\left(\frac{\gamma}{3}\right) + \sqrt{1 - 2\cos^2\left(\frac{\gamma}{3}\right)}\right)\left(\sin(\gamma) - \sin\left(\frac{\gamma}{3}\right)\right) P_n \left(2651 P_n + 84\right) P_2^5 +$$

$$6 \Bigg(8758 \left(\sqrt{2}\ \cos\left(\frac{\gamma}{3}\right) + \sqrt{1 - 2\cos^2\left(\frac{\gamma}{3}\right)}\right)\left(\sin(\gamma) - \sin\left(\frac{\gamma}{3}\right)\right) P_n^3 +$$

$$792 \left(\sqrt{2}\ \cos\left(\frac{\gamma}{3}\right) + \sqrt{1 - 2\cos^2\left(\frac{\gamma}{3}\right)}\right)\left(\sin\left(\frac{\gamma}{3}\right) - \sin(\gamma)\right) P_n^2 +$$

$$\left(234\sqrt{1 - 2\cos^2\left(\frac{\gamma}{3}\right)}\ \cos\left(\frac{\gamma}{3}\right) + 234\sqrt{1 - 2\cos^2\left(\frac{\gamma}{3}\right)}\ \cos(\gamma) + \sqrt{2}\left(117\cos\left(\frac{4\gamma}{3}\right) + 217\right)\right)$$

$$\sqrt{P_1^2 P_2^2 \left(3 P_1^2 - 2 P_2 P_1 + 3 P_2^2\right)}\Bigg) P_2^4 +$$

$$3 P_n \Bigg(10026 \left(\sqrt{2}\ \cos\left(\frac{\gamma}{3}\right) + \sqrt{1 - 2\cos^2\left(\frac{\gamma}{3}\right)}\right)\left(\sin(\gamma) - \sin\left(\frac{\gamma}{3}\right)\right) P_n^3 +$$

$$1188 \left(\sqrt{2}\ \cos\left(\frac{\gamma}{3}\right) + \sqrt{1 - 2\cos^2\left(\frac{\gamma}{3}\right)}\right)\left(\sin(\gamma) - \sin\left(\frac{\gamma}{3}\right)\right) P_n^2 +$$

$$\left(1774\sqrt{1-2\cos^2\left(\frac{\gamma}{3}\right)}\cos\left(\frac{\gamma}{3}\right)+1774\sqrt{1-2\cos^2\left(\frac{\gamma}{3}\right)}\cos(\gamma)+\sqrt{2}\left(887\cos\left(\frac{4\gamma}{3}\right)+1973\right)\right)$$

$$\sqrt{P_1^2P_2^2\left(3P_1^2-2P_2P_1+3P_2^2\right)}\Bigg)P_2^3+$$

$$9P_n\Bigg(636\left(\sqrt{2}\cos\left(\frac{\gamma}{3}\right)+\sqrt{1-2\cos^2\left(\frac{\gamma}{3}\right)}\right)\left(\sin(\gamma)-\sin\left(\frac{\gamma}{3}\right)\right)P_n^4+$$

$$\left(362\sqrt{1-2\cos^2\left(\frac{\gamma}{3}\right)}\cos\left(\frac{\gamma}{3}\right)+362\sqrt{1-2\cos^2\left(\frac{\gamma}{3}\right)}\cos(\gamma)+\sqrt{2}\left(181\cos\left(\frac{4\gamma}{3}\right)+567\right)\right)$$

$$\sqrt{P_1^2P_2^2\left(3P_1^2-2P_2P_1+3P_2^2\right)}\,P_n+8\Bigg(50\sqrt{1-2\cos^2\left(\frac{\gamma}{3}\right)}\cos\left(\frac{\gamma}{3}\right)+50\sqrt{1-2\cos^2\left(\frac{\gamma}{3}\right)}$$

$$\cos(\gamma)+\sqrt{2}\left(25\cos\left(\frac{4\gamma}{3}\right)+57\right)\Bigg)\sqrt{P_1^2P_2^2\left(3P_1^2-2P_2P_1+3P_2^2\right)}\Bigg)P_2^2+$$

$$132\Bigg(2\sqrt{1-2\cos^2\left(\frac{\gamma}{3}\right)}\cos\left(\frac{\gamma}{3}\right)+2\sqrt{1-2\cos^2\left(\frac{\gamma}{3}\right)}\cos(\gamma)+\sqrt{2}\left(\cos\left(\frac{4\gamma}{3}\right)+3\right)\Bigg)$$

$$\sqrt{P_1^2P_2^2\left(3P_1^2-2P_2P_1+3P_2^2\right)}\,P_n^2(10P_n+9)P_2+$$

$$33\Bigg(2\sqrt{1-2\cos^2\left(\frac{\gamma}{3}\right)}\cos\left(\frac{\gamma}{3}\right)+2\sqrt{1-2\cos^2\left(\frac{\gamma}{3}\right)}\cos(\gamma)+\sqrt{2}\left(\cos\left(\frac{4\gamma}{3}\right)+3\right)\Bigg)$$

$$\sqrt{P_1^2P_2^2\left(3P_1^2-2P_2P_1+3P_2^2\right)}\,P_n^3(P_n+18)\Bigg)P_1^6+$$

$$\Bigg(1002\left(\sqrt{2}\cos\left(\frac{\gamma}{3}\right)+\sqrt{1-2\cos^2\left(\frac{\gamma}{3}\right)}\right)\left(\sin\left(\frac{\gamma}{3}\right)-\sin(\gamma)\right)P_2^8+$$

$$7146\left(\sqrt{2}\cos\left(\frac{\gamma}{3}\right)+\sqrt{1-2\cos^2\left(\frac{\gamma}{3}\right)}\right)\left(\sin(\gamma)-\sin\left(\frac{\gamma}{3}\right)\right)P_nP_2^7+$$

$$18\left(\sqrt{2}\cos\left(\frac{\gamma}{3}\right)+\sqrt{1-2\cos^2\left(\frac{\gamma}{3}\right)}\right)\left(\sin(\gamma)-\sin\left(\frac{\gamma}{3}\right)\right)P_n(2399P_n+336)P_2^6+$$

$$\Bigg(11304\left(\sqrt{2}\cos\left(\frac{\gamma}{3}\right)+\sqrt{1-2\cos^2\left(\frac{\gamma}{3}\right)}\right)\left(\sin(\gamma)-\sin\left(\frac{\gamma}{3}\right)\right)P_n^3+$$

$$54648\left(\sqrt{2}\cos\left(\frac{\gamma}{3}\right)+\sqrt{1-2\cos^2\left(\frac{\gamma}{3}\right)}\right)\left(\sin(\gamma)-\sin\left(\frac{\gamma}{3}\right)\right)P_n^2+$$

$$\left(2486\sqrt{1-2\cos^2\left(\frac{\gamma}{3}\right)}\cos\left(\frac{\gamma}{3}\right)+2486\sqrt{-\cos\left(\frac{2\gamma}{3}\right)}\cos(\gamma)+\sqrt{2}\left(1243\cos\left(\frac{4\gamma}{3}\right)+4665\right)\right)$$

$$\sqrt{P_1^2P_2^2\left(3P_1^2-2P_2P_1+3P_2^2\right)}\Bigg)P_2^5+$$

$$
\begin{aligned}
&27 P_n \Bigg(2378 \left(\sqrt{2}\, \cos\left(\frac{\gamma}{3}\right) + \sqrt{1 - 2\cos^2\left(\frac{\gamma}{3}\right)} \right) \left(\sin(\gamma) - \sin\left(\frac{\gamma}{3}\right) \right) P_n^3 + \\
&\quad 396 \left(\sqrt{2}\, \cos\left(\frac{\gamma}{3}\right) + \sqrt{1 - 2\cos^2\left(\frac{\gamma}{3}\right)} \right) \left(\sin(\gamma) - \sin\left(\frac{\gamma}{3}\right) \right) P_n^2 + \\
&\quad \Bigg(718 \sqrt{-\cos\left(\frac{2\gamma}{3}\right)}\, \cos\left(\frac{\gamma}{3}\right) + 718 \sqrt{-\cos\left(\frac{2\gamma}{3}\right)}\, \cos(\gamma) + \sqrt{2} \left(359 \cos\left(\frac{4\gamma}{3}\right) + 981 \right) \Bigg) \\
&\quad \sqrt{P_1^2 P_2^2 \left(3P_1^2 - 2P_2 P_1 + 3P_2^2 \right)} \Bigg) P_2^4 + \\
&18 P_n \Bigg(1914 \left(\sqrt{2}\, \cos\left(\frac{\gamma}{3}\right) + \sqrt{1 - 2\cos^2\left(\frac{\gamma}{3}\right)} \right) \left(\sin(\gamma) - \sin\left(\frac{\gamma}{3}\right) \right) P_n^4 + \\
&\quad \left(2162 \sqrt{1 - 2\cos^2\left(\frac{\gamma}{3}\right)}\, \cos\left(\frac{\gamma}{3}\right) + 2162 \sqrt{1 - 2\cos^2\left(\frac{\gamma}{3}\right)}\, \cos(\gamma) + \sqrt{2} \left(1081 \cos\left(\frac{4\gamma}{3}\right) + 2499 \right) \right) \\
&\quad \sqrt{P_1^2 P_2^2 \left(3P_1^2 - 2P_2 P_1 + 3P_2^2 \right)}\, P_n + 12 \Bigg(22 \sqrt{1 - 2\cos^2\left(\frac{\gamma}{3}\right)}\, \cos\left(\frac{\gamma}{3}\right) + \\
&\quad 22 \sqrt{1 - 2\cos^2\left(\frac{\gamma}{3}\right)}\, \cos(\gamma) + \sqrt{2} \left(11 \cos\left(\frac{4\gamma}{3}\right) + 45 \right) \Bigg) \sqrt{P_1^2 P_2^2 \left(3P_1^2 - 2P_2 P_1 + 3P_2^2 \right)} \Bigg) \\
&P_2^3 + 6 P_n^2 \Bigg(666 \left(\sqrt{2}\, \cos\left(\frac{\gamma}{3}\right) + \sqrt{1 - 2\cos^2\left(\frac{\gamma}{3}\right)} \right) \left(\sin(\gamma) - \sin\left(\frac{\gamma}{3}\right) \right) P_n^4 + \\
&\quad 8 \left(502 \sqrt{1 - 2\cos^2\left(\frac{\gamma}{3}\right)}\, \cos\left(\frac{\gamma}{3}\right) + 502 \sqrt{1 - 2\cos^2\left(\frac{\gamma}{3}\right)}\, \cos(\gamma) + \sqrt{2} \left(251 \cos\left(\frac{4\gamma}{3}\right) + 663 \right) \right) \\
&\quad \sqrt{P_1^2 P_2^2 \left(3P_1^2 - 2P_2 P_1 + 3P_2^2 \right)}\, P_n + 792 \Bigg(2 \sqrt{1 - 2\cos^2\left(\frac{\gamma}{3}\right)}\, \cos\left(\frac{\gamma}{3}\right) + \\
&\quad 2 \sqrt{1 - 2\cos^2\left(\frac{\gamma}{3}\right)}\, \cos(\gamma) + \sqrt{2} \left(\cos\left(\frac{4\gamma}{3}\right) + 3 \right) \Bigg) \sqrt{P_1^2 P_2^2 \left(3P_1^2 - 2P_2 P_1 + 3P_2^2 \right)} \Bigg) P_2^2 + \\
&8100 \left(2 \sqrt{1 - 2\cos^2\left(\frac{\gamma}{3}\right)}\, \cos\left(\frac{\gamma}{3}\right) + 2 \sqrt{1 - 2\cos^2\left(\frac{\gamma}{3}\right)}\, \cos(\gamma) + \sqrt{2} \left(\cos\left(\frac{4\gamma}{3}\right) + 3 \right) \right) \\
&\sqrt{P_1^2 P_2^2 \left(3P_1^2 - 2P_2 P_1 + 3P_2^2 \right)}\, P_n^4 P_2 + \\
&1620 \left(2 \sqrt{1 - 2\cos^2\left(\frac{\gamma}{3}\right)}\, \cos\left(\frac{\gamma}{3}\right) + 2 \sqrt{1 - 2\cos^2\left(\frac{\gamma}{3}\right)}\, \cos(\gamma) + \sqrt{2} \left(\cos\left(\frac{4\gamma}{3}\right) + 3 \right) \right) \\
&\quad \sqrt{P_1^2 P_2^2 \left(3P_1^2 - 2P_2 P_1 + 3P_2^2 \right)}\, P_n^5 \Bigg) P_1^5 + \\
&6 \Bigg(822 \left(\sqrt{2}\, \cos\left(\frac{\gamma}{3}\right) + \sqrt{1 - 2\cos^2\left(\frac{\gamma}{3}\right)} \right) \left(\sin(\gamma) - \sin\left(\frac{\gamma}{3}\right) \right) P_2^9 +
\end{aligned}
$$

$$
\begin{aligned}
&8166\left(\sqrt{2}\,\cos\left(\frac{\gamma}{3}\right)+\sqrt{1-2\cos^2\left(\frac{\gamma}{3}\right)}\right)\left(\sin(\gamma)-\sin\left(\frac{\gamma}{3}\right)\right)P_n P_2^8+\\
&18\left(\sqrt{2}\,\cos\left(\frac{\gamma}{3}\right)+\sqrt{1-2\cos^2\left(\frac{\gamma}{3}\right)}\right)\left(\sin(\gamma)-\sin\left(\frac{\gamma}{3}\right)\right)P_n\left(2291\,P_n+144\right)P_2^7+\\
&12\left(7966\left(\sqrt{2}\,\cos\left(\frac{\gamma}{3}\right)+\sqrt{1-2\cos^2\left(\frac{\gamma}{3}\right)}\right)\left(\sin(\gamma)-\sin\left(\frac{\gamma}{3}\right)\right)P_n^3+\right.\\
&\quad\left(234\sqrt{1-2\cos^2\left(\frac{\gamma}{3}\right)}\,\cos\left(\frac{\gamma}{3}\right)+234\sqrt{1-2\cos^2\left(\frac{\gamma}{3}\right)}\,\cos(\gamma)+\sqrt{2}\left(117\cos\left(\frac{4\gamma}{3}\right)+217\right)\right)\\
&\quad\left.\sqrt{P_1^2P_2^2\left(3P_1^2-2P_2P_1+3P_2^2\right)}\right)P_2^6+\\
&18P_n\left(1982\left(\sqrt{2}\,\cos\left(\frac{\gamma}{3}\right)+\sqrt{1-2\cos^2\left(\frac{\gamma}{3}\right)}\right)\left(\sin(\gamma)-\sin\left(\frac{\gamma}{3}\right)\right)P_n^3+\right.\\
&\quad 792\left(\sqrt{2}\,\cos\left(\frac{\gamma}{3}\right)+\sqrt{1-2\cos^2\left(\frac{\gamma}{3}\right)}\right)\left(\sin(\gamma)-\sin\left(\frac{\gamma}{3}\right)\right)P_n^2+\\
&\quad\left(718\sqrt{1-2\cos^2\left(\frac{\gamma}{3}\right)}\,\cos\left(\frac{\gamma}{3}\right)+718\sqrt{1-2\cos^2\left(\frac{\gamma}{3}\right)}\,\cos(\gamma)+\sqrt{2}\left(359\cos\left(\frac{4\gamma}{3}\right)+981\right)\right)\\
&\quad\left.\sqrt{P_1^2P_2^2\left(3P_1^2-2P_2P_1+3P_2^2\right)}\right)P_2^5+\\
&3P_n\left(3312\left(\sqrt{2}\,\cos\left(\frac{\gamma}{3}\right)+\sqrt{1-2\cos^2\left(\frac{\gamma}{3}\right)}\right)\left(\sin(\gamma)-\sin\left(\frac{\gamma}{3}\right)\right)P_n^4+\right.\\
&\quad\left(6590\sqrt{1-2\cos^2\left(\frac{\gamma}{3}\right)}\,\cos\left(\frac{\gamma}{3}\right)+6590\sqrt{1-2\cos^2\left(\frac{\gamma}{3}\right)}\,\cos(\gamma)+\right.\\
&\qquad\left.\sqrt{2}\left(3295\cos\left(\frac{4\gamma}{3}\right)+11229\right)\right)\sqrt{P_1^2P_2^2\left(3P_1^2-2P_2P_1+3P_2^2\right)}\,P_n+\\
&\quad 48\left(50\sqrt{1-2\cos^2\left(\frac{\gamma}{3}\right)}\,\cos\left(\frac{\gamma}{3}\right)+50\sqrt{-\cos\left(\frac{2\gamma}{3}\right)}\,\cos(\gamma)+\sqrt{2}\left(25\cos\left(\frac{4\gamma}{3}\right)+57\right)\right)\\
&\quad\left.\sqrt{P_1^2P_2^2\left(3P_1^2-2P_2P_1+3P_2^2\right)}\right)P_2^4+\\
&2P_n^2\left(666\left(\sqrt{2}\,\cos\left(\frac{\gamma}{3}\right)+\sqrt{1-2\cos^2\left(\frac{\gamma}{3}\right)}\right)\left(\sin(\gamma)-\sin\left(\frac{\gamma}{3}\right)\right)P_n^4+\right.\\
&\quad 2\left(6238\sqrt{1-2\cos^2\left(\frac{\gamma}{3}\right)}\,\cos\left(\frac{\gamma}{3}\right)+6238\sqrt{1-2\cos^2\left(\frac{\gamma}{3}\right)}\,\cos(\gamma)+\right.\\
&\qquad\left.\sqrt{2}\left(3119\cos\left(\frac{4\gamma}{3}\right)+9117\right)\right)\sqrt{P_1^2P_2^2\left(3P_1^2-2P_2P_1+3P_2^2\right)}\,P_n+
\end{aligned}
$$

$$1584\left(2\sqrt{1-2\cos^2\left(\frac{\gamma}{3}\right)}\cos\left(\frac{\gamma}{3}\right)+2\sqrt{1-2\cos^2\left(\frac{\gamma}{3}\right)}\cos(\gamma)+\sqrt{2}\left(\cos\left(\frac{4\gamma}{3}\right)+3\right)\right)$$

$$\sqrt{P_1^2P_2^2\left(3P_1^2-2P_2P_1+3P_2^2\right)}\Bigg)P_2^3+18\sqrt{P_1^2P_2^2\left(3P_1^2-2P_2P_1+3P_2^2\right)}\,P_n^3$$

$$\left(132\left(2\sqrt{1-2\cos^2\left(\frac{\gamma}{3}\right)}\cos\left(\frac{\gamma}{3}\right)+2\sqrt{1-2\cos^2\left(\frac{\gamma}{3}\right)}\cos(\gamma)+\sqrt{2}\left(\cos\left(\frac{4\gamma}{3}\right)+3\right)\right)+\right.$$

$$\left.\left(434\sqrt{1-2\cos^2\left(\frac{\gamma}{3}\right)}\cos\left(\frac{\gamma}{3}\right)+434\sqrt{1-2\cos^2\left(\frac{\gamma}{3}\right)}\cos(\gamma)+\sqrt{2}\left(217\cos\left(\frac{4\gamma}{3}\right)+611\right)\right)P_n\right)$$

$$P_2^2+1332\left(2\sqrt{1-2\cos^2\left(\frac{\gamma}{3}\right)}\cos\left(\frac{\gamma}{3}\right)+2\sqrt{1-2\cos^2\left(\frac{\gamma}{3}\right)}\cos(\gamma)+\sqrt{2}\left(\cos\left(\frac{4\gamma}{3}\right)+3\right)\right)$$

$$\sqrt{P_1^2P_2^2\left(3P_1^2-2P_2P_1+3P_2^2\right)}\,P_n^5P_2+$$

$$222\left(2\sqrt{1-2\cos^2\left(\frac{\gamma}{3}\right)}\cos\left(\frac{\gamma}{3}\right)+2\sqrt{1-2\cos^2\left(\frac{\gamma}{3}\right)}\cos(\gamma)+\sqrt{2}\left(\cos\left(\frac{4\gamma}{3}\right)+3\right)\right)$$

$$\sqrt{P_1^2P_2^2\left(3P_1^2-2P_2P_1+3P_2^2\right)}\,P_n^6\Bigg)P_1^4+$$

$$2P_2^2\left(2868\left(\sqrt{2}\cos\left(\frac{\gamma}{3}\right)+\sqrt{1-2\cos^2\left(\frac{\gamma}{3}\right)}\right)\left(\sin(\gamma)-\sin\left(\frac{\gamma}{3}\right)\right)P_2^8+\right.$$

$$25686\left(\sqrt{2}\cos\left(\frac{\gamma}{3}\right)+\sqrt{1-2\cos^2\left(\frac{\gamma}{3}\right)}\right)\left(\sin(\gamma)-\sin\left(\frac{\gamma}{3}\right)\right)P_nP_2^7+$$

$$9\left(\sqrt{2}\cos\left(\frac{\gamma}{3}\right)+\sqrt{1-2\cos^2\left(\frac{\gamma}{3}\right)}\right)\left(\sin(\gamma)-\sin\left(\frac{\gamma}{3}\right)\right)P_n\left(7583P_n+1584\right)P_2^6+$$

$$2\left(56736\left(\sqrt{2}\cos\left(\frac{\gamma}{3}\right)+\sqrt{1-2\cos^2\left(\frac{\gamma}{3}\right)}\right)\left(\sin(\gamma)-\sin\left(\frac{\gamma}{3}\right)\right)P_n^3+\right.$$

$$21384\left(\sqrt{2}\cos\left(\frac{\gamma}{3}\right)+\sqrt{1-2\cos^2\left(\frac{\gamma}{3}\right)}\right)\left(\sin(\gamma)-\sin\left(\frac{\gamma}{3}\right)\right)P_n^2+$$

$$\left(1270\sqrt{1-2\cos^2\left(\frac{\gamma}{3}\right)}\cos\left(\frac{\gamma}{3}\right)+1270\sqrt{1-2\cos^2\left(\frac{\gamma}{3}\right)}\cos(\gamma)+\sqrt{2}\left(635\cos\left(\frac{4\gamma}{3}\right)+1473\right)\right)$$

$$\left.\sqrt{P_1^2P_2^2\left(3P_1^2-2P_2P_1+3P_2^2\right)}\right)P_2^5+$$

$$18P_n\left(11214\left(\sqrt{2}\cos\left(\frac{\gamma}{3}\right)+\sqrt{1-2\cos^2\left(\frac{\gamma}{3}\right)}\right)\left(\sin(\gamma)-\sin\left(\frac{\gamma}{3}\right)\right)P_n^3+\right.$$

$$\left(1774\sqrt{1-2\cos^2\left(\frac{\gamma}{3}\right)}\cos\left(\frac{\gamma}{3}\right)+1774\sqrt{1-2\cos^2\left(\frac{\gamma}{3}\right)}\cos(\gamma)+\sqrt{2}\left(887\cos\left(\frac{4\gamma}{3}\right)+1973\right)\right)$$

$$\left.\sqrt{P_1^2P_2^2\left(3P_1^2-2P_2P_1+3P_2^2\right)}\right)P_2^4+$$

$$
\begin{aligned}
&36 P_n \left(1914 \left(\sqrt{2}\ \cos\left(\frac{\gamma}{3}\right)+\sqrt{1-2\cos^2\left(\frac{\gamma}{3}\right)}\right)\left(\sin(\gamma)-\sin\left(\frac{\gamma}{3}\right)\right) P_n^4+\right.\\
&\left(2294\sqrt{1-2\cos^2\left(\frac{\gamma}{3}\right)}\ \cos\left(\frac{\gamma}{3}\right)+2294\sqrt{1-2\cos^2\left(\frac{\gamma}{3}\right)}\ \cos(\gamma)+\sqrt{2}\left(1147\cos\left(\frac{4\gamma}{3}\right)+2841\right)\right)\\
&\sqrt{P_1^2 P_2^2\left(3P_1^2-2P_2P_1+3P_2^2\right)}\ P_n+66\left(2\sqrt{1-2\cos^2\left(\frac{\gamma}{3}\right)}\ \cos\left(\frac{\gamma}{3}\right)+\right.\\
&\left.\left.2\sqrt{1-2\cos^2\left(\frac{\gamma}{3}\right)}\ \cos(\gamma)+\sqrt{2}\left(\cos\left(\frac{4\gamma}{3}\right)+3\right)\right)\sqrt{P_1^3 P_2^2\left(3P_1^2-2P_2P_1+3P_2^2\right)}\right) P_2^3+\\
&6P_n^2\left(666\left(\sqrt{2}\ \cos\left(\frac{\gamma}{3}\right)+\sqrt{1-2\cos^2\left(\frac{\gamma}{3}\right)}\right)\left(\sin(\gamma)-\sin\left(\frac{\gamma}{3}\right)\right) P_n^4+\right.\\
&2\left(6634\sqrt{-\cos\left(\frac{2\gamma}{3}\right)}\ \cos\left(\frac{\gamma}{3}\right)+6634\sqrt{1-2\cos^2\left(\frac{\gamma}{3}\right)}\ \cos(\gamma)+\sqrt{2}\left(3317\cos\left(\frac{4\gamma}{3}\right)+9711\right)\right)\\
&\sqrt{P_1^2 P_2^2\left(3P_1^2-2P_2P_1+3P_2^2\right)}\ P_n+1188\left(2\sqrt{-\cos\left(\frac{2\gamma}{3}\right)}\ \cos\left(\frac{\gamma}{3}\right)+\right.\\
&\left.\left.2\sqrt{1-2\cos^2\left(\frac{\gamma}{3}\right)}\ \cos(\gamma)+\sqrt{2}\left(\cos\left(\frac{4\gamma}{3}\right)+3\right)\right)\sqrt{P_1^3 P_2^2\left(3P_1^2-2P_2P_1+3P_2^2\right)}\right) P_2^3+\\
&720\left(90\sqrt{-\cos\left(\frac{2\gamma}{3}\right)}\ \cos\left(\frac{\gamma}{3}\right)+90\sqrt{1-2\cos^2\left(\frac{\gamma}{3}\right)}\ \cos(\gamma)+\sqrt{2}\left(45\cos\left(\frac{4\gamma}{3}\right)+137\right)\right)\\
&\sqrt{P_1^2 P_2^2\left(3P_1^3-2P_2P_1+3P_2^2\right)}\ P_n^4 P_2+\\
&7236\left(2\sqrt{1-2\cos^2\left(\frac{\gamma}{3}\right)}\ \cos\left(\frac{\gamma}{3}\right)+2\sqrt{1-2\cos^2\left(\frac{\gamma}{3}\right)}\ \cos(\gamma)+\sqrt{2}\left(\cos\left(\frac{4\gamma}{3}\right)+3\right)\right)\\
&\left.\sqrt{P_1^2 P_2^2\left(3P_1^2-2P_2P_1+3P_2^2\right)}\ P_n^5\right) P_1^3+\\
&12P_2^2\left(216\left(\sqrt{2}\ \cos\left(\frac{\gamma}{3}\right)+\sqrt{1-2\cos^2\left(\frac{\gamma}{3}\right)}\right)\left(\sin(\gamma)-\sin\left(\frac{\gamma}{3}\right)\right) P_2^9+\right.\\
&3348\left(\sqrt{2}\ \cos\left(\frac{\gamma}{3}\right)+\sqrt{1-2\cos^2\left(\frac{\gamma}{3}\right)}\right)\left(\sin(\gamma)-\sin\left(\frac{\gamma}{3}\right)\right) P_n P_2^8+\\
&18\left(\sqrt{2}\ \cos\left(\frac{\gamma}{3}\right)+\sqrt{1-2\cos^2\left(\frac{\gamma}{3}\right)}\right)\left(\sin(\gamma)-\sin\left(\frac{\gamma}{3}\right)\right) P_n\left(779P_n+24\right) P_2^7+\\
&12\left(1648\left(\sqrt{2}\ \cos\left(\frac{\gamma}{3}\right)+\sqrt{1-2\cos^2\left(\frac{\gamma}{3}\right)}\right)\left(\sin(\gamma)-\sin\left(\frac{\gamma}{3}\right)\right) P_n^3+\right.
\end{aligned}
$$

$$198\left(\sqrt{2}\,\cos\left(\frac{\gamma}{3}\right)+\sqrt{1-2\cos^2\left(\frac{\gamma}{3}\right)}\right)\left(\sin(\gamma)-\sin\left(\frac{\gamma}{3}\right)\right)P_n^2+3\left(2\sqrt{1-2\cos^2\left(\frac{\gamma}{3}\right)}\,\cos\left(\frac{\gamma}{3}\right)+2\sqrt{1-2\cos^2\left(\frac{\gamma}{3}\right)}\,\cos(\gamma)+\sqrt{2}\left(\cos\left(\frac{4\gamma}{3}\right)+3\right)\right)\sqrt{P_1^2P_2^2\left(3P_1^2-2P_2P_1+3P_2^2\right)}\Bigg)P_2^6+$$

$$3P_n\Bigg(2574\left(\sqrt{2}\,\cos\left(\frac{\gamma}{3}\right)+\sqrt{1-2\cos^2\left(\frac{\gamma}{3}\right)}\right)\left(\sin(\gamma)-\sin\left(\frac{\gamma}{3}\right)\right)P_n^3+$$

$$1188\left(\sqrt{2}\,\cos\left(\frac{\gamma}{3}\right)+\sqrt{-\cos\left(\frac{2\gamma}{3}\right)}\right)\left(\sin(\gamma)-\sin\left(\frac{\gamma}{3}\right)\right)P_n^2+$$

$$2\left(230\sqrt{1-2\cos^2\left(\frac{\gamma}{3}\right)}\,\cos\left(\frac{\gamma}{3}\right)+230\sqrt{-\cos\left(\frac{2\gamma}{3}\right)}\,\cos(\gamma)+\sqrt{2}\left(115\cos\left(\frac{4\gamma}{3}\right)+321\right)\right)$$

$$\sqrt{P_1^2P_2^2\left(3P_1^2-2P_2P_1+3P_2^2\right)}\Bigg)P_2^5+$$

$$9P_n\Bigg(636\left(\sqrt{2}\,\cos\left(\frac{\gamma}{3}\right)+\sqrt{1-2\cos^2\left(\frac{\gamma}{3}\right)}\right)\left(\sin(\gamma)-\sin\left(\frac{\gamma}{3}\right)\right)P_n^4+$$

$$\left(746\sqrt{1-2\cos^2\left(\frac{\gamma}{3}\right)}\,\cos\left(\frac{\gamma}{3}\right)+746\sqrt{1-2\cos^2\left(\frac{\gamma}{3}\right)}\,\cos(\gamma)+\sqrt{2}\left(373\cos\left(\frac{4\gamma}{3}\right)+999\right)\right)$$

$$\sqrt{P_1^2P_2^2\left(3P_1^2-2P_2P_1+3P_2^2\right)}\,P_n+8\Bigg(2\sqrt{1-2\cos^2\left(\frac{\gamma}{3}\right)}\,\cos\left(\frac{\gamma}{3}\right)+2\sqrt{1-2\cos^2\left(\frac{\gamma}{3}\right)}\,\cos(\gamma)+\sqrt{2}\left(\cos\left(\frac{4\gamma}{3}\right)+3\right)\Bigg)\sqrt{P_1^2P_2^2\left(3P_1^2-2P_2P_1+3P_2^2\right)}\Bigg)P_2^4+$$

$$2P_n^2\Bigg(666\left(\sqrt{2}\,\cos\left(\frac{\gamma}{3}\right)+\sqrt{1-2\cos^2\left(\frac{\gamma}{3}\right)}\right)\left(\sin(\gamma)-\sin\left(\frac{\gamma}{3}\right)\right)P_n^4+$$

$$2\Bigg(2602\sqrt{1-2\cos^2\left(\frac{\gamma}{3}\right)}\,\cos\left(\frac{\gamma}{3}\right)+2602\sqrt{1-2\cos^2\left(\frac{\gamma}{3}\right)}\,\cos(\gamma)+\sqrt{2}\left(1301\cos\left(\frac{4\gamma}{3}\right)+3543\right)\Bigg)\sqrt{P_1^2P_2^2\left(3P_1^2-2P_2P_1+3P_2^2\right)}\,P_n+$$

$$198\left(2\sqrt{1-2\cos^2\left(\frac{\gamma}{3}\right)}\,\cos\left(\frac{\gamma}{3}\right)+2\sqrt{1-2\cos^2\left(\frac{\gamma}{3}\right)}\,\cos(\gamma)+\sqrt{2}\left(\cos\left(\frac{4\gamma}{3}\right)+3\right)\right)$$

$$\sqrt{P_1^2P_2^2\left(3P_1^2-2P_2P_1+3P_2^2\right)}\Bigg)P_2^3+9\sqrt{P_1^2P_2^2\left(3P_1^2-2P_2P_1+3P_2^2\right)}\,P_n^3$$

$$\Bigg(66\left(2\sqrt{1-2\cos^2\left(\frac{\gamma}{3}\right)}\,\cos\left(\frac{\gamma}{3}\right)+2\sqrt{1-2\cos^2\left(\frac{\gamma}{3}\right)}\,\cos(\gamma)+\sqrt{2}\left(\cos\left(\frac{4\gamma}{3}\right)+3\right)\right)+$$

$$\left(566\sqrt{1-2\cos^2\left(\frac{\gamma}{3}\right)}\,\cos\left(\frac{\gamma}{3}\right)+566\sqrt{1-2\cos^2\left(\frac{\gamma}{3}\right)}\,\cos(\gamma)+\sqrt{2}\left(283\cos\left(\frac{4\gamma}{3}\right)+809\right)\right)P_n\Bigg)$$

$$P_2^2 + 1206\left(2\sqrt{1-2\cos^2\left(\frac{\gamma}{3}\right)}\cos\left(\frac{\gamma}{3}\right) + 2\sqrt{1-2\cos^2\left(\frac{\gamma}{3}\right)}\cos(\gamma) + \sqrt{2}\left(\cos\left(\frac{4\gamma}{3}\right)+3\right)\right)$$

$$\sqrt{P_1^2 P_2^2\left(3P_1^2 - 2P_2P_1 + 3P_2^2\right)}\,P_n^5 P_2 +$$

$$222\left(2\sqrt{1-2\cos^2\left(\frac{\gamma}{3}\right)}\cos\left(\frac{\gamma}{3}\right) + 2\sqrt{1-2\cos^2\left(\frac{\gamma}{3}\right)}\cos(\gamma) + \sqrt{2}\left(\cos\left(\frac{4\gamma}{3}\right)+3\right)\right)$$

$$\sqrt{P_1^2 P_2^2\left(3P_1^2 - 2P_2P_1 + 3P_2^2\right)}\,P_n^6\Bigg)P_1^2 +$$

$$18P_2^4\left(6\left(\sqrt{2}\cos\left(\frac{\gamma}{3}\right) + \sqrt{1-2\cos^2\left(\frac{\gamma}{3}\right)}\right)\left(\sin(\gamma) - \sin\left(\frac{\gamma}{3}\right)\right)P_2^3 +\right.$$

$$\left(2\sqrt{1-2\cos^2\left(\frac{\gamma}{3}\right)}\cos\left(\frac{\gamma}{3}\right) + 2\sqrt{1-2\cos^2\left(\frac{\gamma}{3}\right)}\cos(\gamma) + \sqrt{2}\left(\cos\left(\frac{4\gamma}{3}\right)+3\right)\right)$$

$$\left.\sqrt{P_1^2 P_2^2\left(3P_1^2 - 2P_2P_1 + 3P_2^2\right)}\right)$$

$$\left(3P_2^5 + 77P_nP_2^4 + 572P_n^2P_2^3 + 1672P_n^3P_2^2 + 1800P_n^4P_2 + 444P_n^5\right)$$

$$P_1 + 3$$

$$P_2^4$$

$$\left(6\left(\sqrt{2}\cos\left(\frac{\gamma}{3}\right) + \sqrt{1-2\cos^2\left(\frac{\gamma}{3}\right)}\right)\left(\sin(\gamma) - \sin\left(\frac{\gamma}{3}\right)\right)P_2^3 +\right.$$

$$\left(2\sqrt{1-2\cos^2\left(\frac{\gamma}{3}\right)}\cos\left(\frac{\gamma}{3}\right) + 2\sqrt{1-2\cos^2\left(\frac{\gamma}{3}\right)}\cos(\gamma) + \sqrt{2}\left(\cos\left(\frac{4\gamma}{3}\right)+3\right)\right)$$

$$\left.\sqrt{P_1^2 P_2^2\left(3P_1^2 - 2P_2P_1 + 3P_2^2\right)}\right)P_n$$

$$\left(18P_2^5 + 231P_nP_2^4 + 1144P_n^2P_2^3 + 2508P_n^3P_2^2 + 2160P_n^4P_2 + 444P_n^5\right)\Big/\Big(1152$$

$$N\left(1-2\cos^2\left(\frac{\gamma}{3}\right)\right)^{3/2}$$

$$\left(P_1^2 + P_2^2\right)^{3/2}$$

$$\left.\left(P_1^2P_2^2\left(3P_1^2 - 2P_2P_1 + 3P_2^2\right)\right)^{3/2}\right)$$

11.8 Variance

$\text{var}[\hat{P}_2] =$

$$\left(\left(P_1^4 + 16P_2P_1^3 + 16P_nP_1^3 + 36P_2^2P_1^2 + 144P_2P_nP_1^2 + 72P_nP_1^2 + 16P_2^3P_1 + 96P_n^3P_1 + 288P_2P_n^2P_1 + 144P_2^2P_n\right.\right.$$
$$\left.\left.P_1 + P_2^4 + 24P_n^4 + 96P_2P_n^3 + 72P_2^2P_n^2 - \left(P_1^2 + 4P_2P_1 + 4P_nP_1 + P_2^2 + 2P_n^2 + 4P_2P_n\right)^2 + 16P_2^3P_n\right)$$
$$\left(-2\cos\left(\frac{\gamma}{3}\right) + \sqrt{2 - 4\cos^2\left(\frac{\gamma}{3}\right)} + \left(2\left(\sqrt{2}\,\cos\left(\frac{\gamma}{3}\right) + \sqrt{1 - 2\cos^2\left(\frac{\gamma}{3}\right)}\right)\sin\left(\frac{\gamma}{3}\right)\right.\right.$$
$$\left(-P_1^3 - 9P_2P_1^2 - 9P_nP_1^2 - 9P_2^2P_1 - 18P_n^2P_1 - 36P_2P_nP_1 - P_2^3 - 6P_n^3 - 18P_2P_n^2 -\right.$$
$$\left.\left.\left.9P_2^2P_n + 3(P_1 + P_2 + P_n)\left(P_1^2 + 4P_2P_1 + 4P_nP_1 + P_2^2 + 2P_n^2 + 4P_2P_n\right)\right)\right)\Big/$$
$$\left(\sqrt{1 - 2\cos^2\left(\frac{\gamma}{3}\right)}\,\sqrt{\left(16\left(-P_1^2 - 4P_2P_1 - 4P_nP_1 - P_2^2 - 2P_n^2 + 2(P_1 + P_2 + P_n)^2 - 4P_2P_n\right)^3 -\right.\right.$$
$$\left.\left.9P_2^2P_n + 3(P_1 + P_2 + P_n)\left(P_1^2 + 4P_2P_1 + 4P_nP_1 + P_2^2 + 2P_n^2 + 4P_2P_n\right)\right)\right)\Big/$$
$$\left(\sqrt{1 - 2\cos^2\left(\frac{\gamma}{3}\right)}\,\sqrt{\left(16\left(-P_1^2 - 4P_2P_1 - 4P_nP_1 - P_2^2 - 2P_n^2 + 2(P_1 + P_2 + P_n)^2 - 4P_2P_n\right)^3 -\right.\right.$$
$$\left(P_1^3 + 9P_2P_1^2 + 9P_nP_1^2 + 9P_2^2P_1 + 18P_n^2P_1 + 36P_2P_nP_1 +\right.$$
$$P_2^3 + 6P_n^3 + 12(P_1 + P_2 + P_n)^3 + 18P_2P_n^2 + 9P_2^2P_n -$$
$$\left.\left.\left.9(P_1 + P_2 + P_n)\left(P_1^2 + 4P_2P_1 + 4P_nP_1 + P_2^2 + 2P_n^2 + 4P_2P_n\right)\right)^2\right)\right)\Big/$$
$$\left(8N\left(-P_1^2 - 4P_2P_1 - 4P_nP_1 - P_2^2 - 2P_n^2 + 2(P_1 + P_2 + P_n)^2 - 4P_2P_n\right)\right) +$$
$$\left(\left(P_1^5 + 25P_2P_1^4 + 25P_nP_1^4 + 100P_2^2P_1^3 + 200P_n^2P_1^3 +\right.\right.$$
$$400P_2P_nP_1^3 + 100P_2^3P_1^2 + 600P_n^3P_1^2 +$$
$$1800P_2P_n^2P_1^2 + 900P_2^2P_nP_1^2 + 25P_2^4P_1 +$$
$$600P_2^4P_1 + 2400P_2P_n^3P_1 + 1800P_2^2P_n^2P_1 +$$
$$400P_2^3P_nP_1 + P_2^5 + 120P_n^5 + 600P_2P_n^4 +$$
$$600P_2^2P_n^3 + 200P_2^3P_n^2 + 25P_2^4P_n -$$
$$\left(P_1^2 + 4P_2P_1 + 4P_nP_1 + P_2^2 + 2P_n^2 + 4P_2P_n\right)$$
$$\left.\left.\left(P_1^3 + 9P_2P_1^2 + 9P_nP_1^2 + 9P_2^2P_1 + 18P_n^2P_1 + 36P_2P_nP_1 + P_2^3 + 6P_n^3 + 18P_2P_n^2 + 9P_2^2P_n\right)\right)\right.$$

$$\left(P_1^3+9P_2P_1^2+9P_nP_1^2+9P_2^2P_1+18P_n^2P_1+36P_2P_nP_1+P_2^3+6P_n^3+12(P_1+P_2+P_n)^3+18P_2P_n^2+9P_2^2P_n-9(P_1+P_2+P_n)\left(P_1^2+4P_2P_1+4P_nP_1+P_2^2+2P_n^2+4P_2P_n\right)\right)^2\Bigg)\Bigg)^2\Bigg)\Bigg/$$

$$\left(16N\left(-P_1^2-4P_2P_1-4P_nP_1-P_2^2-2P_n^2+2(P_1+P_2+P_n)^2-4P_2P_n\right)\right)+$$

$$\Bigg(\Big(P_1^4+16P_2P_1^3+16P_nP_1^3+36P_2^2P_1^2+144P_2P_nP_1^2+72P_nP_1^2+16P_2^3P_1+96P_2^3P_1+288P_2P_n^2P_1+144P_2^2P_nP_1+P_2^4+24P_n^4+96P_2P_n^3+72P_2^2P_n^2+16P_2^3P_n-(P_1+P_2+P_n)\left(P_1^2+4P_2P_1+4P_nP_1+P_2^2+2P_n^2+4P_2P_n\right)\Big)$$

$$\left(4\cos\left(\frac{\gamma}{3}\right)(P_1+P_2+P_n)-2\sqrt{2-4\cos^2\left(\frac{\gamma}{3}\right)}\,(P_1+P_2+P_n)-\left(2\left(\sqrt{2}\,\cos\left(\frac{\gamma}{3}\right)+\sqrt{-\cos\left(\frac{2\gamma}{3}\right)}\right)\sin\left(\frac{\gamma}{3}\right)\left(3\left(P_1^2+4P_2P_1+4P_nP_1+P_2^2+2P_n^2+4P_2P_n\right)^2-2(P_1+P_2+P_n)\left(P_1^3+9P_2P_1^2+9P_nP_1^2+9P_2^2P_1+18P_n^2P_1+36P_2P_nP_1+P_2^3+6P_n^3+18P_2P_n^2+9P_2^2P_n\right)\right)\Bigg/\left(\sqrt{-\cos\left(\frac{2\gamma}{3}\right)}\sqrt{\left(16\left(-P_1^2-4P_2P_1-4P_nP_1-P_2^2-2P_n^2+2(P_1+P_2+P_n)^2-4P_2P_n\right)^3-\left(P_1^3+9P_2P_1^2+9P_nP_1^2+9P_2^2P_1+18P_n^2P_1+36P_2P_nP_1+P_2^3+6P_n^3+12(P_1+P_2+P_n)^3+18P_2P_n^2+9P_2^2P_n-9(P_1+P_2+P_n)\left(P_1^2+4P_2P_1+4P_nP_1+P_2^2+2P_n^2+4P_2P_n\right)\right)^2\right)}\right)\Bigg)\Bigg)$$

$$\left(-2\cos\left(\frac{\gamma}{3}\right)+\sqrt{2-4\cos^2\left(\frac{\gamma}{3}\right)}+\left(2\left(\sqrt{2}\,\cos\left(\frac{\gamma}{3}\right)+\sqrt{1-2\cos^2\left(\frac{\gamma}{3}\right)}\right)\sin\left(\frac{\gamma}{3}\right)\left(-P_1^3-9P_2P_1^2-9P_nP_1^2-9P_2^2P_1-18P_n^2P_1-36P_2P_nP_1-P_2^3-6P_n^3-18P_2P_n^2-\right.\right.\right.$$

$$\left(\sqrt{2}\,\sqrt{1-2\cos^2\left(\frac{\gamma}{3}\right)}\,\tan\left(\frac{2\gamma}{3}\right)-2\sin\left(\frac{\gamma}{3}\right)\right)$$

$$\left(-2\cos\left(\frac{\gamma}{3}\right)+\sqrt{2-4\cos^2\left(\frac{\gamma}{3}\right)}+\left(2\left(\sqrt{2}\,\cos\left(\frac{\gamma}{3}\right)+\sqrt{1-2\cos^2\left(\frac{\gamma}{3}\right)}\right)\sin\left(\frac{\gamma}{3}\right)\left(-P_1^3-9P_2P_1^2-9P_nP_1^2-9P_2^2P_1-18P_n^2P_1-36P_2P_nP_1-P_2^3-6P_n^3-18P_2P_n^2-9P_2^2P_n+3(P_1+P_2+P_n)\left(P_1^2+4P_2P_1+4P_nP_1+P_2^2+2P_n^2+4P_2P_n\right)\right)\Bigg/\left(\sqrt{1-2\cos^2\left(\frac{\gamma}{3}\right)}\sqrt{\left(16\left(-P_1^2-4P_2P_1-4P_nP_1-P_2^2-2P_n^2+2(P_1+P_2+P_n)^2-4P_2P_n\right)^3-\left(P_1^3+9P_2P_1^2+9P_nP_1^2+9P_2^2P_1+18P_n^2P_1+36P_2P_nP_1+P_2^3+6P_n^3+12(P_1+P_2+P_n)^3+18P_2P_n^2+9P_2^2P_n-9(P_1+P_2+P_n)\left(P_1^2+4P_2P_1+4P_nP_1+P_2^2+2P_n^2+4P_2P_n\right)\right)^2\right)}\right)\Bigg)\Bigg)\Bigg)\Bigg/$$

$$\left(24N\sqrt{\left(16\left(-P_1^2-4P_2P_1-4P_nP_1-P_2^2-2P_n^2+2(P_1+P_2+P_n)^2-4P_2P_n\right)^3-\left(P_1^3+9P_2P_1^2+9P_nP_1^2+9P_2^2P_1+18P_n^2P_1+36P_2P_nP_1+P_2^3+6P_n^3+12(P_1+P_2+P_n)^3+18P_2P_n^2+9P_2^2P_n-9(P_1+P_2+P_n)\left(P_1^2+4P_2P_1+4P_nP_1+P_2^2+2P_n^2+4P_2P_n\right)\right)^2\right)}\right)+$$

$$\Bigg(\left(P_1^2+4P_2P_1+4P_nP_1+P_2^2+2P_n^2-(P_1+P_2+P_n)^2+4P_2P_n\right)$$

$$\left(4\cos\left(\frac{\gamma}{3}\right)(P_1+P_2+P_n)-2\sqrt{2-4\cos^2\left(\frac{\gamma}{3}\right)}\,(P_1+P_2+P_n)-\left(2\left(\sqrt{2}\,\cos\left(\frac{\gamma}{3}\right)+\sqrt{-\cos\left(\frac{2\gamma}{3}\right)}\right)\sin\left(\frac{\gamma}{3}\right)\right.\right.$$
$$\left(3\left(P_1^2+4P_2P_1+4P_nP_1+P_2^2+2P_n^2+4P_2P_n\right)^2-2(P_1+P_2+P_n)\left(P_1^3+9P_2P_1^2+\right.\right.$$
$$\left.\left.\left.9P_nP_1^2+9P_2^2P_1+18P_n^2P_1+36P_2P_nP_1+P_2^3+6P_n^3+18P_2P_n^2+9P_2^2P_n\right)\right)\right)\Big/$$
$$\left(\sqrt{-\cos\left(\frac{2\gamma}{3}\right)}\,\sqrt{\left(16\left(-P_1^2-4P_2P_1-4P_nP_1-P_2^2-2P_n^2+2(P_1+P_2+P_n)^2-4P_2P_n\right)^3-\right.\right.$$
$$\left(P_1^3+9P_2P_1^2+9P_nP_1^2+9P_2^2P_1+18P_n^2P_1+36P_2P_nP_1+\right.$$
$$P_2^3+6P_n^3+12(P_1+P_2+P_n)^3+18P_2P_n^2+9P_2^2P_n-$$
$$\left.\left.\left.9(P_1+P_2+P_n)\left(P_1^2+4P_2P_1+4P_nP_1+P_2^2+2P_n^2+4P_2P_n\right)\right)^2\right)\right)^2\Big)\Big/$$
$$\left(4N\left(-P_1^2-4P_2P_1-4P_nP_1-P_2^2-2P_n^2+2(P_1+P_2+P_n)^2-4P_2P_n\right)\right)+$$

$$\left(4N\left(-P_1^2-4P_2P_1-4P_nP_1-P_2^2-2P_n^2+2(P_1+P_2+P_n)^2-4P_2P_n\right)\right)+$$
$$\left(\left(-P_1^2-4P_2P_1-4P_nP_1-P_2^2-2P_n^2+2(P_1+P_2+P_n)^2-4P_2P_n\right)\right.$$
$$\left(P_1^5+25P_2P_1^4+25P_nP_1^4+100P_2^2P_1^3+\right.$$
$$200P_n^2P_1^3+400P_2P_nP_1^3+100P_2^3P_1^2+600P_n^3P_1^2+$$
$$1800P_2P_n^2P_1^2+900P_2^2P_nP_1^2+25P_2^4P_1+600P_n^4P_1+$$
$$2400P_2P_n^3P_1+1800P_2^2P_n^2P_1+400P_2^3P_nP_1+$$
$$P_2^5+120P_n^5+600P_2P_n^4+600P_2^2P_n^3+200P_2^3P_n^2-$$
$$\left(P_1^3+9P_2P_1^2+9P_nP_1^2+9P_2^2P_1+18P_n^2P_1+36P_2P_nP_1+P_2^3+6P_n^3+18P_2P_n^2+9P_2^2P_n\right)^2+$$
$$\left.25P_2^4P_n\right)$$
$$\left.\left(\sqrt{2}\,\sqrt{1-2\cos^2\left(\frac{\gamma}{3}\right)}\,\tan\left(\frac{2\gamma}{3}\right)-2\sin\left(\frac{\gamma}{3}\right)\right)^2\right)\Big/$$
$$\left(36N\left(16\left(-P_1^2-4P_2P_1-4P_nP_1-P_2^2-2P_n^2+2(P_1+P_2+P_n)^2-4P_2P_n\right)^3-\right.\right.$$
$$\left(P_1^3+9P_2P_1^2+9P_nP_1^2+9P_2^2P_1+18P_n^2P_1+36P_2P_nP_1+P_2^3+6P_n^3+12(P_1+P_2+P_n)^3+\right.$$
$$\left.\left.18P_2P_n^2+9P_2^2P_n-9(P_1+P_2+P_n)\left(P_1^2+4P_2P_1+4P_nP_1+P_2^2+2P_n^2+4P_2P_n\right)\right)^2\right)\right)+$$
$$\left(\left(P_1^4+16P_2P_1^3+16P_nP_1^3+36P_2^2P_1^2+144P_2P_nP_1^2+72P_nP_1^2+16P_2^3P_1+96P_n^3P_1+\right.\right.$$
$$288P_2P_n^2P_1+144P_2^2P_nP_1+P_2^4+24P_n^4+$$
$$96P_2P_n^3+72P_2^2P_n^2+16P_2^3P_n-(P_1+P_2+P_n)$$
$$\left.\left(P_1^3+9P_2P_1^2+9P_nP_1^2+9P_2^2P_1+18P_n^2P_1+36P_2P_nP_1+P_2^3+6P_n^3+18P_2P_n^2+9P_2^2P_n\right)\right)$$
$$\left(4\cos\left(\frac{\gamma}{3}\right)(P_1+P_2+P_n)-2\sqrt{2-4\cos^2\left(\frac{\gamma}{3}\right)}\,(P_1+P_2+P_n)-\right.$$

$$\left(2\left(\sqrt{2}\,\cos\left(\frac{\gamma}{3}\right)+\sqrt{-\cos\left(\frac{2\gamma}{3}\right)}\right)\sin\left(\frac{\gamma}{3}\right)\right.$$
$$\left(3\left(P_1^3+4P_2P_1+4P_nP_1+P_2^2+2P_n^2+4P_2P_n\right)^2-2\left(P_1+P_2+P_n\right)\left(P_1^3+9P_2P_1^2+\right.\right.$$
$$\left.\left.9P_nP_1^2+9P_2^2P_1+18P_n^2P_1+36P_2P_nP_1+P_2^3+6P_n^3+18P_2P_n^2+9P_2^2P_n\right)\right)\Big/$$
$$\left(\sqrt{-\cos\left(\frac{2\gamma}{3}\right)}\,\sqrt{\left(16\left(-P_1^2-4P_2P_1-4P_nP_1-P_2^2-2P_n^2+2\left(P_1+P_2+P_n\right)^2-4P_2P_n\right)^3-\right.\right.$$
$$\left(P_1^3+9P_2P_1^2+9P_nP_1^2+9P_2^2P_1+18P_n^2P_1+36P_2P_nP_1+P_2^3+6P_n^3+\right.$$
$$12\left(P_1+P_2+P_n\right)^3+18P_2P_n^2+9P_2^2P_n-9\left(P_1+P_2+P_n\right)\left(P_1^2+4P_2P_1+4P_nP_1+\right.$$
$$\left.\left.\left.\left.P_2^2+2P_n^2+4P_2P_n\right)\right)^2\right)\right)\left(\sqrt{2}\,\sqrt{1-2\cos^2\left(\frac{\gamma}{3}\right)}\,\tan\left(\frac{2\gamma}{3}\right)-2\sin\left(\frac{\gamma}{3}\right)\right)\Big/$$
$$\left(12N\sqrt{\left(16\left(-P_1^2-4P_2P_1-4P_nP_1-P_2^2-2P_n^2+2\left(P_1+P_2+P_n\right)^2-4P_2P_n\right)^3-\right.\right.$$
$$\left(P_1^3+9P_2P_1^2+9P_nP_1^2+9P_2^2P_1+18P_n^2P_1+36P_2P_nP_1+P_2^3+6P_n^3+12\left(P_1+P_2+P_n\right)^3+\right.$$
$$\left.\left.\left.18P_2P_n^2+9P_2^2P_n-9\left(P_1+P_2+P_n\right)\left(P_1^2+4P_2P_1+4P_nP_1+P_2^2+2P_n^2+4P_2P_n\right)\right)^2\right)\right)$$

Chapter 12 APPLICATIONS OF THE FLU METHOD FOR SPECTRUM SENSING

12.1 Introduction

In this chapter a modified version of the method for detection of the FLUproposed in the previous chapter is presented and applied for conventional spectrum sensing. First we refer to the OSA model and apply the method for detecting the presence of a hidden unknown low-power CM signals in noise of unknown variance. The hidden user (HU) can be either an authorized (licensed or unlicensed) or an unauthorized (freeloader) one. Then, referring to the CSA model, we exploit an estimation of the noise variance for improving the performance of the interference temperature methods. The basic rational behind the new approach is as follows. The FLUs detection method exploits the second, fourth and sixth order of the received signal to obtain an estimation of the freeloader, authorized and noise signal power. Now, assuming that the FLU and the AU are active alternatively, the same procedure can be applied for conventional spectrum sensing. More in details, the second and forth order moments are used for estimating the signal (either authorized or illegal) and noise power. In fact, we are now solving a system of two unknowns (the noise and signal power) in two independent equations (the two abovementioned moments). Then the signal power is used for transmission detection while the noise power is exploited for estimating the interference temperature. The remainder of this chapter is organized as follows. The proposed method is described in section 2. In particular, the transmission detection method is presented in the first half of the section, while the IT method is depicted in the second half. Results are shown in Section 3, before conclusions briefly depicted in section 4.

12.2 Proposed method

Following the same analysis of the previous chapter, let M_2 be the second-order moment of the received signal expressed as follows:

$$M_2 = E[|\mathbf{r}|^2] = E[|\mathbf{s}+\mathbf{n}|^2] = E[|\mathbf{s}|^2] + E[|\mathbf{n}|^2] = P_S + P_n. \quad (12.1)$$

where P_s and P_n are the hidden user and noise powers, respectively. Now, let M_4 denote the fourth order moment of the received signal expressed by

$$\begin{aligned} M_4 &= E[|\mathbf{r}|^4] = E[|\mathbf{s}+\mathbf{n}|^2] = E[|\mathbf{s}|^4 + |\mathbf{n}|^4 + 4|\mathbf{s}|^2 |\mathbf{n}|^2] = \\ &= E[|\mathbf{s}|^4] + E[|\mathbf{n}|^4] + 4E[|\mathbf{s}|^2]E[|\mathbf{n}|^2] = P_s^2 + 2P_n^2 + 4P_s P_n \end{aligned} \quad (12.2)$$

Finally, P_s and P_n can be derived by solving (12.1) and (12.2) in a straightforward way:

$$\begin{aligned} P_s &= \sqrt{2M^2 - Q} \\ P_n &= M - \sqrt{2M^2 - Q} \end{aligned} \quad (12.3)$$

12.2.1 Hidden user detection

The estimation of the signal power can be used for detecting a low power signal hidden under the noise power. To avoid dealing with complex numbers, the decision variable for the hypothesis testing is the estimation of the (squared) hidden signal power:

$$x = 2\hat{M}^2 - \hat{Q} = \left(\frac{1}{N} \sum_{n=1}^{N} |r_n|^2 \right)^2 - \frac{1}{N} \sum_{n=1}^{N} |r_n|^4 \quad (12.4)$$

The testing variable in (12.4) is asymptotically Gaussian as a direct consequence of the central limit theorem. In fact, the first term is the square of an asymptotically Gaussian variable with non-zero mean. The second term, consisting of a sum of random variables, is asymptotically Gaussian from a direct application of the central limit theorem. Nonetheless the testing variable in (12.5) represents the estimation $\hat{P}_s^2$ of the hidden user power P_s^2, it is obtained as the difference of two estimated moments, and hence, can assume also negative values. In fact, the testing variable x is a Gaussian variable with a mean equal to P_s^2 in the H_1 hypothesis and a Gaussian variable with zero mean in the H_0 hypothesis. Finally, the testing variable is compared with a threshold value, in order to determine the presence of hidden users.

12.2.1 Improving the Interference Temperature Estimation

In this section, the innovative method for evaluating the IT is proposed. The method is based on the same procedure described in the previous sections, but now we exploit the estimation of the noise power for providing an improved estimation of the interference temperature. More in details, and according to (12.3) the noise powers can be estimated as follows

$$\hat{P}_n = \hat{M}_2 - \sqrt{2\hat{M}_2{}^2 - \hat{M}_4} = \\ = \left(\frac{1}{N}\sum_{n=1}^{N}|r_n|^2\right)^2 - \sqrt{\left(\frac{1}{N}\sum_{n=1}^{N}|r_n|^2\right)^2 - \frac{1}{N}\sum_{n=1}^{N}|r_n|^4} \tag{12.5}$$

Then, P_n can be used for evaluating the interference temperature as follows:

$$\hat{T}_I = \frac{\hat{P}_n}{K \cdot B} \tag{12.6}$$

Eq. (12.6) provides a finer estimation of the IT than the one expressed by the conventional ED approach in (6.7), and here reported for the sake of readability:

$$T_I = \frac{P_R}{K \cdot B} \tag{12.7}$$

In fact the ideal model, the IT is estimated from the power of the SUs, but this means that the CRs can identify the licensed signals. However, plain energy detection cannot be used for distinguishing the noise from the transmitted signal, and some a priori knowledge about the primary signal is needed. Then, in the generalized model the received power P_R is used for the interference's estimation, but P_R includes both noise and useful signal powers. As the noise increases the IT value, the licensed signal does not. Hence, with the generalized model, the IT may be incorrectly estimated, thus providing bad working conditions for the SU.

12.3 Numerical results

12.3.1 Hidden users detection method

Several simulations have been performed to validate the proposed spectrum sensing procedure versus the conventional energy detection approach. Several Monte-Carlo simulation trials (10^5 independent runs) have been implemented to numerically evaluate the performance of the two methods. A QPSK modulation with rectangular pulse shaping has been used, with a target $P_{FA} = 10^{-2}$. The performance of the proposed HU detection method is evaluated in terms of P_D versus SNR of practical interest and compared with the ED approach. ρ=1 dB of noise uncertainty is considered as the worst-case scenario for the channel noise variance estimation. Results are shown in Fig. 12-1 where it can be seen that the new method strongly outperforms the conventional ED approach. Moreover, the curve referring to the ideal ED (i.e. the detector with exact knowledge of the noise variance) is also reported as representative of the upper bound of the system performance.

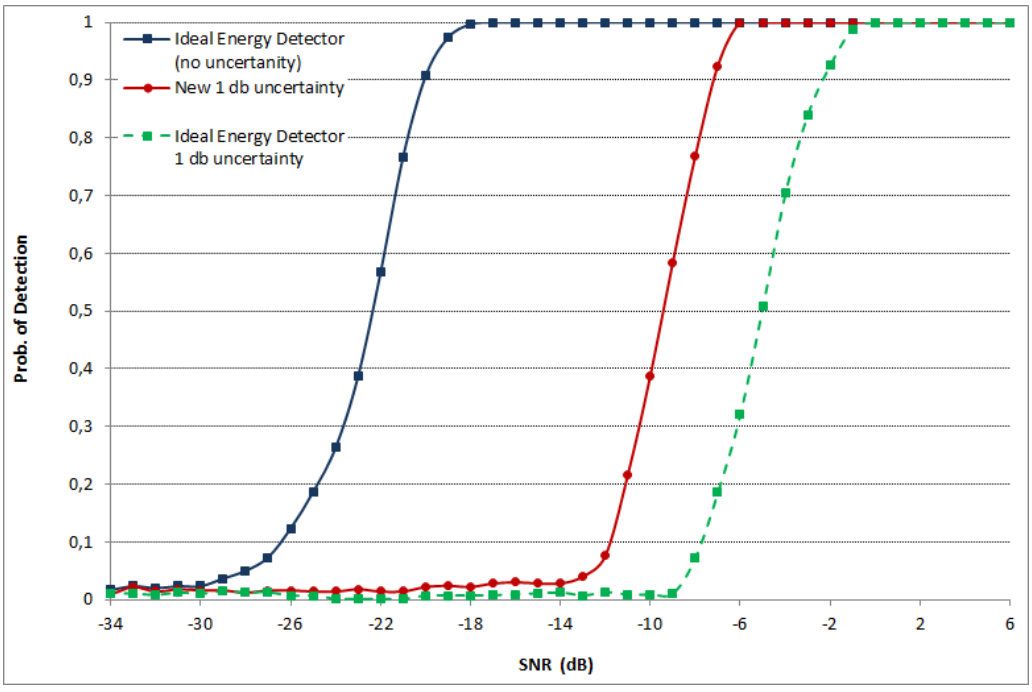

Figure 12-1. P_D of the conventional energy detector and of the new method with 1dB of noise uncertainty

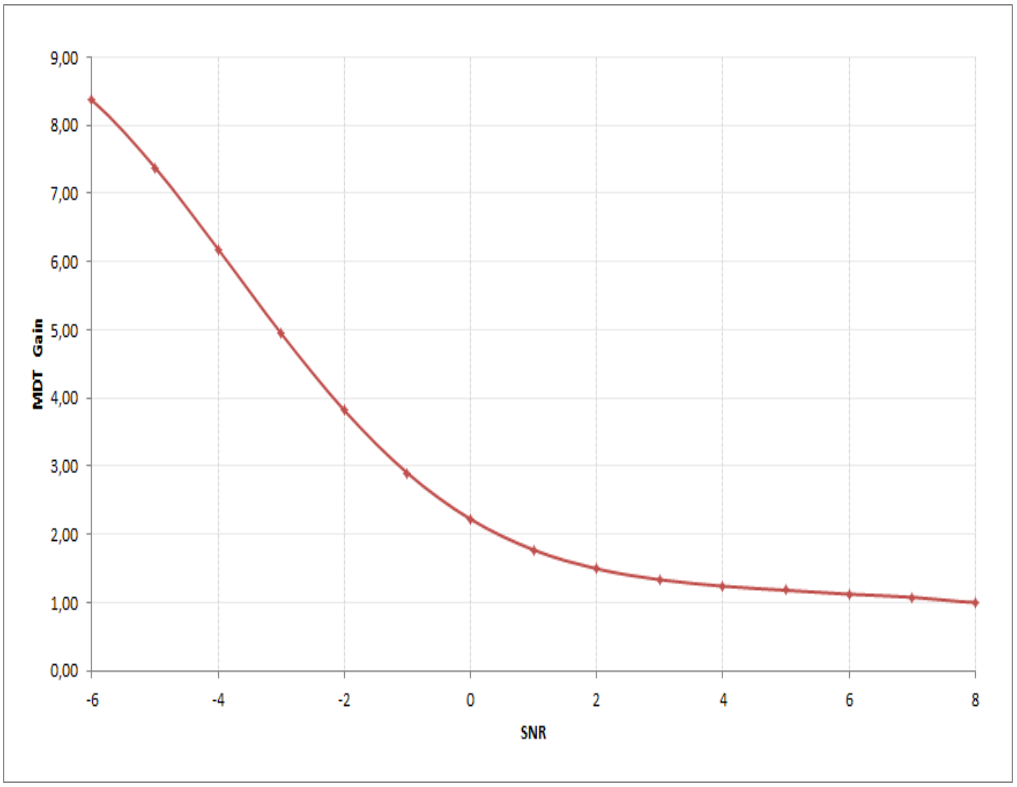

Figure 12-2. MDT gain vs. SNR values representative of typical operating cases, for Case I and with 1 dB of noise uncertainty.

In addition in order to determine how much the increase in P_D reflects in the reduction of the mean detection time, we evaluated the MDT gain of the new strategy as the ratio between the proposed and conventional method. We focus only on SNR values belonging to the interval [-6, 8] dB, since this situation corresponds to detection probabilities higher than 0.5. It can be easily seen from Fig. 12-2 that the MDT gain is always higher than 1: i.e. the new method strongly outperforms the conventional approach, allowing a faster detection of hidden users than the conventional ED.

12.3.2 Interference Temperature

Several simulations have been performed to validate the proposed method versus the conventional ED approach, in estimating the interference temperature under the generalized case. In particular, we assume that the power of the primary user signal is higher the noise

power, and consequently we focus our attention in the region SNR > 0 dB. The time record length is equal to 10^6 complex samples and a bandwidth B = 8 MHz (i.e. typical of digital television systems [123]) is used for both the proposed and ED methods. The performance of the two methods are evaluated in terms of the maximum accepted IT (i.e. T_{SU}) versus the allowable SU power. In particular, Fig. 12-3 shows the performance of the two approaches in the generalized case, for an SNR = 3 dB. As it can be easily seen from the graph, the new method drastically outperforms the conventional ED, in terms of allowable SU power. In fact, the advantage of the proposed method is twofold: the SU can transmit with a higher power than the one obtained through the ED method, or conversely, more SUs can transmit altogether at the same power level defined by the classic ED. In fact the conventional method the interference exceeds the IT limit in correspondence of a SU power of 0.15. Any transmission with a higher value of P_{SU} interferes with the primary user. Conversely, in the proposed method the interference exceeds the IT limit for a P_{SU} = 0.85 thus allowing the SU to safely coexist with primary users in a wider range of operating cases (or allowing the transmission of a maximum of 5 SUs all transmitting at the maximum allowable power P_{SU}=0.15). The innovative strategy can obtain a finer estimation of the noise power that reflects in a performance improvement of the overall system.

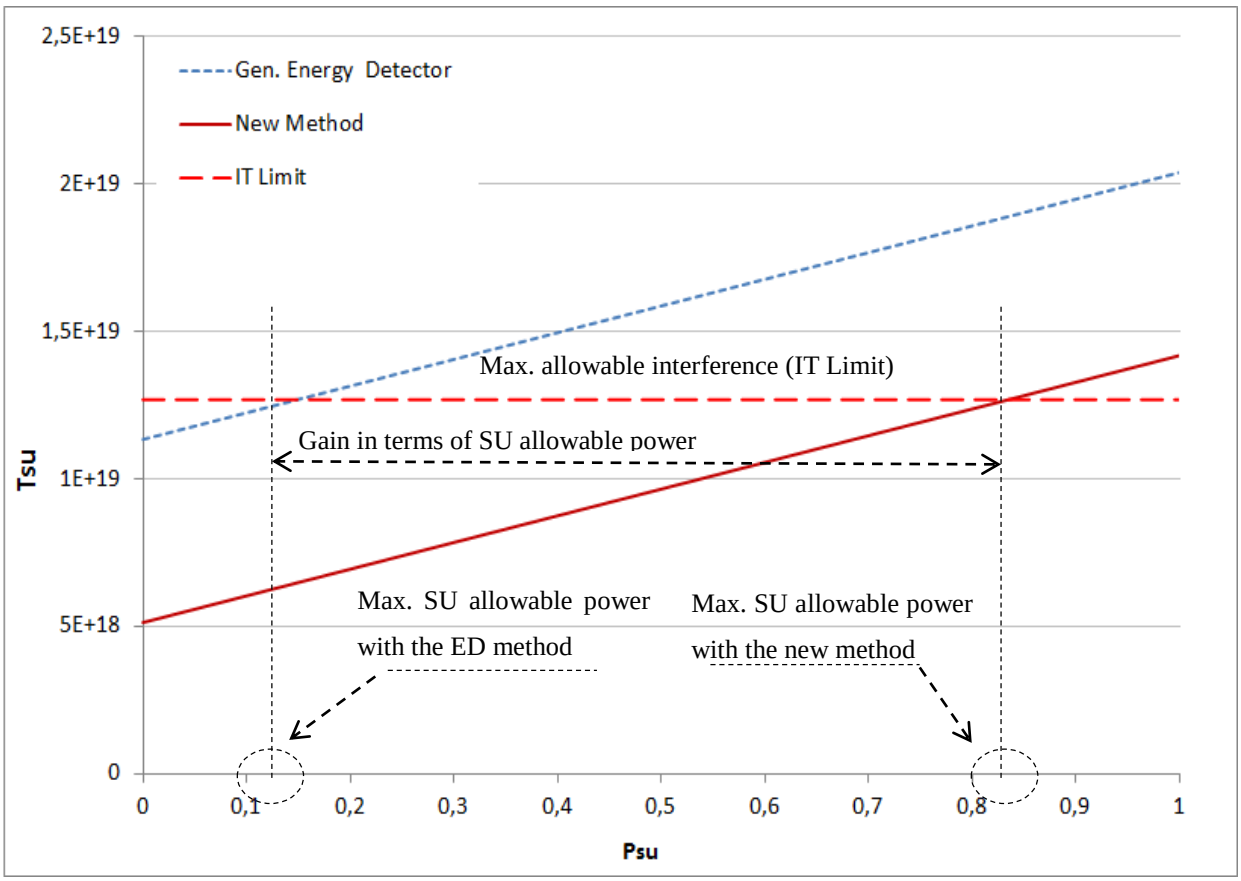

Figure 12-3. Interference caused by the SU to the primary receiver (T_{su}) versus the SU transmitted power (P_{su}).

12.4 Conclusions

This chapter has presented two application of the FLUs detection method for spectrum sensing in CRN. In particular, an innovative technique for the detection of unknown low-power CM signals in noise of unknown variance for cognitive radio networks. The proposed method estimates the signal and noise powers, exploiting higher order moments of the received signal. Then the power of the hidden user signal is used as the testing variable of HU detection, while the noise power has be used for IT estimation. The results of several simulation trials have evidenced the effectiveness of the two proposed methods for application in CRNs.

Chapter 13 **CONCLUSIONS**

This dissertation has focused on the signal processing techniques for cognitive radio networks. The main goal of the research activity has been proposing innovative, efficient methods for improving the spectrum utilization and mitigating the ever increasing spectrum scarcity problem. This document is the result of a three year research activity which has been mainly concentrated into two fields: primary networks and secondary networks.

The research field dedicated to the primary networks has been mainly concentrated on 4G/5G systems for their inherit flexibility in managing the frequency resources. In such systems achieving and maintaining time and frequency synchronization between the transmitter and the receiver is one the most critical issues. For such reasons, the research activities in the field of primary networks has been concentrated on time synchronization in 4G and 5G networks. In conventional methods based on matched filter correlators, the time uncertainty of the incoming signal is divided into a finite number of cells, each corresponding to a sample of the time delay between the received signal and its local replica. Here, the case of taking the cell size as a fraction of the actual sample period has been analyzed. This choice improves the acquisition performance in terms of detection probability and mean detection time. However, unlike the case of one cell per sample, the detection variables between contiguous cells, are not independent and possibly strongly correlated. In such cases, it is extremely difficult to find a closed form expression for the systems error probabilities. In this thesis a new class of function, the extended-MGQ (EMGQ) functions, has been defined for expressing the false alarm and detection probabilities of the system in a closed form. The novelty introduced in this thesis is twofold. First a new method, the twin test, has been introduced for the performance improvement of initial code acquisition, taking into account correlated cells. Then, the EMGQ functions are derived and used to express the system error probabilities in a closed form. The analytical results show that the new procedure can offer better performance than the conventional scheme based on the cell-by-cell detection, with only a negligible increasing of the system

computational complexity. Moreover, the twin test can be effectively used for reducing the mean acquisition time in code synchronization wireless communications.

The research activity has been also focused on improving the performance of initial synchronization in the LTE systems. LTE uses OFDM modulation and OFDMA technique for the downlink transmissions in order to provide high data rate and mobility. The initial synchronization process is especially important for LTE systems, which rely heavily on the orthogonality of the uplink and downlink transmission and reception. In this doctorate thesis an innovative signal processing method for the initial synchronization of LTE wireless networks has been proposed. The proposed procedure exploits the primary synchronization signal, and can be applied to any LTE transmission standard. The rationale behind the innovative approach is to maximize the main peak of the cross-correlation between the received signal and its locally generated replica, at the same time minimizing the side-lobes. The numerical results, obtained from wide simulation trials under operating settings, have evidenced the effectiveness of the devised method.

The second part of the research activity has been dedicated to the secondary networks. In particular, one of the more important operations of a SN is the spectrum sensing where the SU identifies and the access the spectrum holes. The research activity in this field has been manly focused on proposing effective, blind spectrum sensing methods. All the proposed algorithms have been applied for detecting primary communications in the 4G and 5G systems.

A method for detection of OFDM signal based on the autocorrelation of the received signal has been proposed. The method is based on a modified version of the Rayleigh-ness test which has been recently introduced for code acquisition purposes DS-CDMA systems. The decision whether a primary user is active, or not, can be made on the presence of a non-zero mean value of a Gaussian distributed random variable. This is also equivalent to state whether the observed series is a portion of one realization of a Rayleigh (or Rice) distributed random process, and hence the Rayleigh-ness can be applied for spectrum sensing purposes. The Rayleigh-ness test in its original form makes use of matched filter correlation.

Notwithstanding matched filter are the optimal detector, they require a priori knowledge about the signal of interest. Therefore, the proposed method is based on a modified the conventional Rayleigh-ness test, which exploits the autocorrelation of the received signal. The numerical results, obtained from wide simulation trials have evidenced the effectiveness of the devised method in different operating scenarios. The innovative strategy has been applied using typical operating parameters for OFDM signal of wireless local area networks and multimedia communications, thus proving the applicability of the new method for spectrum sensing in CRNs.

Another aspect that has been considered is the fast detection of primary users. In fact, since secondary user are guest of the radio spectrum, they must yield to the primary user whenever it start to access the band in operation. Then the secondary communication should continue on another spectrum holes without interruptions. Therefore, a cognitive radio device should be able to sense wide portions of the radio spectrum in order to identify multiple spectrum holes. A possible solution for multiband sensing is using banks of band-pass filters. Conventional filter banks methods use analog hardware, because the RF imperfections can be better handled in the analog domain. However, this choice reduces the system's flexibility and re-configurability. In this dissertation a software radio implementation of FFT filter banks, has been proposed. A performance analysis of the proposed method has been carried out in comparison with a two stage sensing approach that exploits analog band-pass filters. Numerical results show that the FFT filter banks, allows achieving both higher detection probabilities and lower mean detection time.

One of the most relevant drawbacks of many spectrum sensing methods is that the noise variance has to be perfectly known in order to correctly set the threshold. Then, if this information is unavailable or not accurate, the system performance dramatically reduces. In order to overcame these limitations, in this dissertation an innovative normalized variance method has been proposed. The NV exploits the second and fourth order moments of the received signal and evaluates the ratio between the variance and the second order moment. The performance of the proposed technique has been evaluated by theoretical analysis and computer simulations, in comparison with the conventional energy detector and in presence

of noise uncertainty. The results have shown that the proposed method is characterized by higher detection probabilities and faster sensing time than the conventional approach.

In addition, the research has been focused also on cooperative sensing strategies. In cooperative spectrum sensing the final decision about the spectrum occupancy is obtained by combining the decision of many SU. Conventional methods assume that the observations from the cooperative sensors are independent, in order to simplify the analysis. But, this assumption is not practical when the proximity of the sensors results in correlated observations. In this doctorate thesis an innovative testing procedure for cooperative spectrum sensing in the presence of correlated users is proposed. The devised method, based on a modified version of the twin test, allows to recover all those unlucky cases where strong fading and shadowing drastically reduce the system detection performance. The method combines OR and Majority voting rules, in order to improve the detection performance, while enabling faster rejection of occupied bands. The numerical results, obtained from wide simulation trials, demonstrate the effectiveness of the proposed method for application in cognitive radio networks in the presence of correlated users.

In addition, a new scenario and a security treat in cognitive radio networks has been identified and a possible countermeasure proposed. In fact in CRN the possibility of trading the spectrum offers news business opportunity to primary and secondary providers. The primary providers can rent their unused resources to the secondary providers, which gain access to radio spectrum. Unfortunately, in this operating scenario there is also room for fraudulent users that could hide themselves under the noise floor, to avoid being charged for using the radio spectrum. The aim of such freeloader users is to use the spectrum secretly. Notwithstanding they do not directly damage the communications of active users they represent a relevant economic loss for CRN providers, and therefore must be promptly detected and blocked. This is a new operating scenario, which to the best of our knowledge, is completely different from what has been studied in the literature about cognitive radio users. In this thesis an innovative signal processing technique is discussed that allows the detection of a freeloader user that hides its radio signal under the noise floor in the presence of an active user. More in details, the second, fourth and sixth order moments of the received signal are evaluated. Then, an estimation of the fraudulent, active and noise signal power is

derived from the above mention moments, and the fraudulent power used as a testing variable to determine the presence of such deceitful users. A theoretical and simulated performance analysis has been carried out and the theoretical results, sustained by wide simulation trials, have evidenced the efficiency of the devised method for detecting hidden users in cognitive radio communications.

Finally two applications of the FLUs detection procedure for conventional spectrum sensing have been proposed. More in details the second and fourth order moments of the received signal are derived and used for estimating the signal and noise power. The signal power has been used for determine the presence of a low power transmission in the frequency band of interest. On the other hand, the noise power has been exploited for estimating the interference temperature and determine if the SUs can safely accessing the band, without causing harmful interference to the primary users.

Future development and applications of the methods described in this doctorate thesis aims at sustaining the diffusions of the cognitive radio networks and offering a more rational usage of the radio spectrum. Nowadays, the spectrum shortage is a critical bottle neck of the system that obstacles the diffusion of high-data rate multi-media services. Cognitive radio technology can offer an effective solutions to this problem. However, they poses several issues with efficient spectrum management, real time implementation, CR security and applications, as well as regulatory and standardization aspects. While spectrum sensing is a well investigated aspect, CR security and applications is still an open issue. In particular, the scenario of the freeloader users, introduced for the very first time in this thesis, could open new interesting research prospective in the field of the economy of cognitive radio networks. In fact, markets and business opportunity will play a fundamental role in the development o the cognitive technology and hence should be taken into proper account.

REFERENCE

[1] A. Molish, “Wireless Communications” in “Applications and Requirements of Wireless Services”, *Wiley-IEEE Press*, pp 3-25, 2011. M.

[2] P. Jacobs, CEO at Qualcomm. Qualcomm opening keynote, CES 2013

[3] FCC. Spectrum Policy Task Force, “Report of the Spectrum Efficiency Working Group,” Nov. 2002. Online: http://www.fcc.gov/sptf/reports.html.

[4] M. A. McHenry and McCloskey, “Multi-band, multi-location spectrum occupancy measurements,” in *Proc. Int. Symposium. Advanced. Radio Technology*, Boulder, CO, Mar. 2006.

[5] Survey on Spectrum Utilization in Europe: Measurements, Analyses and Observations

[6] Y.C. Liang, K.-C. Chen, G. Ye Li, P. Mähönen, "Cognitive radio networking and communications: An overview", *IEEE Trans. On Vehic. Tech*., vol. 60, no. 7, pp. 3386-3406 Sept. 2011.

[7] Q. Zhao, B. M. Sadler, "A survey of dynamic spectrum access", *IEEE Sign. Proc. Magazine*, vol. 24, no. 3. Pp. 79-8, May 2007

[8] M. Zander, “Technical and economic trends in wireless applications”, *in Proc. ESSCIRC*, pp. 37-44, 2010.

[9] J. Mitola, G. Q. Maguire, "Cognitive radio: Making software radios more personal," *IEEE Pers. Commun*., vol. 6, no. 4, pp. 13-18, Aug. 1999.

[10] T. Yucek, H. Arslan, "A survey of spectrum sensing algorithms for cognitive radio applications", *IEEE Commun. Survs&Tuts*., vol. 11, no.1, pp. 116-130, 2009.

[11] E. Axell, G. Leus, E.G. Larsson and H.V. Poor, "Spectrum Sensing for Cognitive Radio", *IEEE Sig. Proc. Magazines*, vol. 29, no. 3, pp. 101-116, 2012

[12] G. Giunta, L. Vandendorpe, “A “Rayleigh-ness” Test for DS/SS Code Acquisition”, *IEEE Trans. on Commun*., vol. 51, no. 9, pp.1492-1501, Sept. 2003

[13] Y.-C.Liang, K.-C. Chen,G. Ye Li, P. Mähönen, "Cognitive radio networking and communications: An overview", *IEEE Trans. On Vehic. Tech*., vol. 60, no. 7, pp. 3386-3406 Sept. 2011.

[14] D. Datla, A. M. Wyglinski, G. J. Minden, "A spectrum surveying framework for dynamic spectrum access networks", *IEEE Trans. Vehic.Technol*., vol.58, no. 8, pp. 4158-4168, Oct. 2009.

[15] Xu L., Tonjes R., Paila T., Hansmann W., Frank M., and Albrecht M., “DRiVE-ing to the Internet: Dynamic radio for IP services in vehicular environments,” *Proc.25th Annual IEEE on. Local Computer Networks*, Nov. 2000, pp. 281–289.

[16] C. Carlos, C. Kiran , and B. Dagnachew , S. Sai**.** IEEE 802.22: An Introduction to the First Wireless Standard based on Cognitive Radios, *IEEE J. Communications*, Vol. 1, no.1, Apr. 2006.

[17] I. F. Akaylidz., W. Lee, M. C. Vuran, S. Mohant, “NeXt generation/dynamic spectrum access/cognitive radio wireless networks: a survey”. In *Computer Networks* pp. 2127–2159, 2006

[18] J.A. Stine, Spectrum management: the killer application of ad hoc and mesh networking, in*: Proc. IEEE DySPAN 2005, November* 2005, pp. 184–193.

[19] IEEE Std. 9001Definitions and Concepts for Dynamic Spectrum Access: terminology relating to Emerging wireless networks system functionality and spectrum management

[20] D. Hatfield and P. Weiser, "Property rights in spectrum: Taking the next step". Proc. 1st IEEE Symp. New
Frontiers Dynamic Spectrum Access Networks, Nov. 2005, pp. 43-5

[21] Leri O., Samardzija D., N.B. Mandayam. "Dynamic Property Rights Spectrum Access: Flexible Ownership Based Spectrum Management", in 2nd *IEEE International Symposium on New Frontiers in Dynamic Spectrum Access Networks*, 2007. (DySPAN 2007), June 2007.

[22] W. Lehr, J. Crowcroft, "Managing shared access to a spectrum commons," *in Proc. 1st IEEE Int. Symp. DySPAN*, pp. 420–444, 2005.

[23] C. Peng, H. Zheng, B.Y. Zhao, "Utilization and fairness in spectrum assignment for opportunistic spectrum access" in. *ACM Mobile Networks Appl*. pp. 555–76, Aug. 2006

[24] R. Menon, R.M. Buehrer, J.H. Reed, "Outage probability based comparison of underlay and overlay spectrum sharing techniques". *Proc. IEEE DySPAN 2005*, pp. 101–109Nov. 2005

[25] R. Tandra, S. Mubaraq Mishra, A. Sahai, "What is a spectrum hole and what does it take to recognize one?" *Proc.IEEE:* vol.97 no. 5, pp 824-848, May 2009.

[26] M. Sharma, A. Sahoo, and K. D. Nayak, "Channel modeling based on interference temperature in underlay cognitive wireless networks," in *Proc. IEEE Int. Symp. Wireless Commun. Syst. (ISWCS)*, Reykjavik, Iceland, Oct. 2008, pp. 224–228.

[27] T. C. Clancy, "On the use of interference temperature for dynamic spectrum access," *Ann. Telecomm., Springer*, vol. 64, no. 7, pp. 573–585, Aug. 2009.

[28] J. S. Pang, G. Scutari, D. P. Palomar, "Design of Cognitive Radio System under Temperature-Interference Constrains: a Variation Inequality Approach", *IEEE Trans. on Sig. Proc*. vol. 58, no. 6, pp. 3251-3271, 2010.

[29] Xing Y., Mathur C.N., Haleem M., Chandramouli R., and Subbalakshmi K.. "Dynamic spectrum access with QoS and interference temperature constraints". *On IEEE Transactions on Mobile Computing*, vol. 6, no. 4, pp. 423–433, 2007.

[30] ITU-R WP8A Working document towards a PDNReport "Software Defined Radio in the Land Mobile Service" *document 8A/228-E*, Sept. 2005.

[31] SDR Forum. "What are Cognitive Radio and dynamic Spectrum Access". *www.sdr-forum.org.* available online at *www.sdr-forum.org*.

[32] S. Brandes, I. Cosovic, M. Schnell, "Sidelobe suppression in OFDM systems by insertion of cancellation carriers" in *IEEE vehicular technology conference*, vol. 1; pp. 152–6.Sept. 2005

[33] J.A.C. Bingham, "Multicarrier modulation for data transmission: an idea whose time has come," *IEEE Commun. Mag.*, vol. 28. 110.5, May 1990, pp. 5-14

[34] Pandharipande A., "Principles of OFDM," IEEE Potentials, vol. 21, no. 2, pp.16 – 19, Apr.–May 2002.

[35] L. Hanzo, Y. Akhtman, L. Wang, M. Jiang, "*OFDM Standards*", in MIMO-OFDM for LTE, WiFi and WiMAX:Coherent versus Noncoherent and Cooperative Turbo Transceivers, *Wiley-IEEE Press*, pp. 37-60

[36] H. Wang and B. Chen, BA comparison of the subcarrier allocation schemes for uplink OFDMA systems", in Proc. CISS'2004, Princeton, NJ, Mar. 2004.

[37] I.van de Beek. M. Sandell. and P. O. Brjesson. "ML estimation of timing and frequency offset in OFDM systems," *IEEE Trans. Signal Processing*. vol. 45, July 1997, pp. 1800-1805.

[38] J.H. Wena, G.-R. Lee, J.-W. Liuc, T.-L. Kung, "Frame synchronization, channel estimation scheme and signal compensation using regression method in OFDM systems", Computer Communications Vol. 31 pp 2124–2130, 2008

[39] H. Wang; L. Zhu;2, Y. Shi 1, T. Xing, Y. Wang, "A Novel Synchronization Algorithm for OFDM Systems with Weighted CAZAC Sequence", Journal of Computational Information Systems, Vol. 8, no. 6 pp. 2275-2283, 2012

[40] J. L. Zhang, M. Z. Wang and W. L. Zhu, "A Novel OFDM Frame Synchronization Scheme", *in Proceedings of the IEEE International Conference on Communications, Circuits and Systems and West Sino Expositions*, 2002, pp. 119-123.

[41] F. Tufvesson, O. Edfors and M. Faulkner, "Time and Frequency Synchronization for OFDM Using PN-sequence Preambles", *in Proceedingsof the IEEE Vehicular Technology Conference*, 1999, vol. 4, pp. 2203-2207.

[42] J. L. Zhang, M. Z. Wang and W. L. Zhu, "A Novel OFDM Frame Synchronization Scheme", *in Proceedings of the IEEE International Conference on Communications, Circuits and Systems and West Sino Expositions*, 2002, pp. 119-123.

[43] J. E. Kleider and S. Gifford, "Synchronization for Broadband OFDM Mobile Ad Hoc Networking: Simulation and Implementation", *in Proc. of the IEEE International Conference on Acoustics, Speech,and Signal Processing*, 2002, vol. 4, pp. 3756-3759.

[44] H. Minn, M. Zeng and V. K. Bhargava, "On Timing Offset Estimation for OFDM Systems", *IEEE Communication Letters*, vol. 4, no. 7, pp.242 - 244, July 2000.

[45] B. Park, H. Cheon, C. Kang and D. Hong, "A Novel Timing Estimation Method for OFDM Systems", *IEEE Communication Letters*, vol. 7, no. 5, pp. 239 - 241, May 2003.

[46] H. Puska, H. Saarnisaari "Matched filter time and frequency synchronization method for OFDM systems using PN-sequence preambles", Proc. 18th *IEEE International Symposium on Personal, Indoor and Mobile Radio Communications (PIMRC'07)*

[47] J. C. Lin, "Non-coherent sequential PN code acquisition using sliding correlation for chip-asynchronous direct-sequence spread-spectrum communications," *IEEE Trans. Commun.*, vol. 50, no. 4, pp. 664–676, Apr. 2002.

[48] G. Giunta and F. Benedetto, "Spread-spectrum code acquisition in the presence of cell correlation," *IEEE Trans. Commun.*, vol. 55, no. 2, pp. 257–261, Feb. 2007.

[49] W. Sheen, J. Tzeng, and C. Tzou, "Effects on cell correlation in a matched filter PN code acquisition for direct sequence spread-spectrum systems," *IEEE Trans. Veh. Technol.*, vol. 48, no. 3, pp. 724–732, May 1999

[50] F. Benedetto and G. Giunta, "A self-synchronizing method for asynchronous code acquisition in band-limited spread spectrum communications," *IEEE Trans. Commun.*, vol. 57, no. 8, pp. 2410–2419, Aug. 2009.

[51] G. Giunta, "Generalized Q-functions for application to noncoherent serial detection of spread-spectrum communication signals," *IEEE Trans. Signal Process.*, vol. 48, no. 5, pp. 1506–1513, May 2000.

[52] E. W. Weisstein, Regularized hyper-geometric function, From Math-World-A Wolfram Web Resource, http://mathworld.wolfram.com/RegularizedHypergeometricFunction.html

[53] G. Giunta, A. Neri, and M. Carli, "Constrained optimization of noncoherent serial acquisition of spread-spectrum code by exploiting the generalized Q-functions," *IEEE Trans. Veh. Technol.*, vol. 52, no. 5, pp. 1378–1385, Sep. 2003.

[54] L. Khalid, A. Anpalagan, "Emerging cognitive radio technology: Principles, challenges and opportunities", *Computers and Electrical Eng*., vol. 36, no. 3, pp. 358-366, 2009.

[55] S. Haykin, "Cognitive radio: Brain-empowered wireless communications", *IEEE J. Sel. Areas Commun*., vol. 23, no. 2, pp. 201–220, 2005.

[56] T. Charles Clancy, "Formalizing the Interference Temperature Model" *Wiley J. on Wireless Com. and mobile Comp*. vol. 7 no.9, pp. 1077-1086, 2007.

[57] D. Cabric, S.M. Mishra, R.W. Brodersen, "Implementation issues in spectrum sensing for cognitive radio"s, in Proc. *38th Asilomar Conference on Signals, Systems and Computers* 2004, November 2004, pp. 772–776.

[58] D. Cabric, R.W Brodersen, "Physical layer design issues unique to cognitive radio systems", Proc. *IEEE Personal Indoor and Mobile Radio Communications (PIMRC2005)*,September 2005.

[59] R. Murty, Software-defined reconfigurability radios: smart, agile, cognitive, and interoperable, Technology @Intel Magazine, July 2003.

[60] Y. Tsai, G. Zhang, D. Grieco, F. Ozluturk, "Cell search in 3GPP Long Term Evolution Systems", *IEEE Vehicular Technol. Magazine*, vol. 2, no. 2, pp. 23-29, June 2007.

[61] Manolakis, K.; Gutierrez Estevez, D.M.; Jungnickel, V.; Wen Xu; Drewes, C., "A Closed Concept for Synchronization and Cell Search in 3GPP LTE Systems", *IEEE Wireless Commun. and Networking Conf.* (WCNC 2009), pp. 1 – 6, 2009

[62] B. Lindoff;T. Ryden;D. Astely, "A robust cell search algorithm for 3GPP LTE", *European Wireless Conf. (EW 2009)*, pp. 303 – 307, 17-20 May 2009

[63] Sälzer, T. and Baker, M. (2011) Introduction and Background, in LTE - The UMTS Long Term Evolution: From Theory to Practice, Second Edition (eds S. Sesia, I. Toufik and M. Baker), John Wiley & Sons, Ltd, Chichester, UK

[64] 3rd Generation Partnership Project TS 36.211 V8.7.0, "Physical Channels and Modulation", May 2009.

[65] Moray Rumney, "LTE and the Evolution to 4G Wireless: Design and Measurement Challenges", Agilent Technologies, Jun. 2009.

[66] H. Setiawn, M. Hurosaki, H. Ochi, "LTE Phisycal Layer Identity Detection Frequency Vs Time Domain", *IEEE Int. Conf. on Communications (ICC 2011)*, pp. 1-5, 2011.

[67] 3rd Generation Partnership Project TS 36.211 V8.7.0, "*Physical Channels and Modulation*", May 2009.

[68] 3rd Generation Partnership Project, R1-051329, "*Cell Search and Initial Acquisition for OFDM Downlink*", Motorola, Nov. 2005.

[69] W. R. Braun, "PN Acquisition and Tracking Performance in DS/CDMA Systems with Symbol-Length Spreading Sequences", *IEEE Trans. on Commun.*, vol. 45, pp. 1595-1601, Dec. 1997.

[70] 3rd Generation Partnership Project, R1-061065, E-UTRA Cell Search, Ericsson.

[71] 3rd Generation Partnership Project, R1-051329, Cell Search and Initial Acquisition for OFDM Downlink, Motorola

[72] 3rd Generation Partnership Project, R1-062129, "Non-hierarchical Cell Search with Symmetric and periodic SCH Signals", Huawei.

[73] 3rd Generation Partnership Project, R1-062164, "Channel Structure and Hybrid Detection for Evolved UTRA Cell Search", InterDigital.

[74] T. Sälzer, M. Baker, "*Introduction and Background, in LTE - The UMTS Long Term Evolution: From Theory to Practice*", Second Edition (ed. S. Sesia, I. Toufik and M. Baker), John Wiley & Sons, Ltd, Chichester, UK, July 2011

[75] F. Benedetto, G. Giunta, ""A Fast Time-Delay Estimator of PN Signal", *IEEE Trans. on Commun.*, vol. 62, no. 3, pp. 1350-1355, 2013

[76] F. Benedetto, G. Giunta, E. S. Lohan, M. Renfors, "A Fast Unambiguous Acquisition Algorithm for BOC-Modulated Signals", *IEEE Trans. on Vehic. Techn.*, in press, 2013.

[77] Y.-P.E. Wang, T. Ottosson, "Cell search in W-CDMA", *IEEE J. on Selected Areas in Commun.*, vol. 18, no. 8, pp. 1470-1482, Aug. 2000.

[78] S. Chaudhari, V. Koivunen, V. Poor, "Autocorrelation-Based decentralized sequential detection of OFDM Signals in Cognitive Radio", *IEEE Trans. on Sign. Proc*., vol. 57, no. 7, pp. 2690-2700, 2009.

[79] A. V. Dandawate, G. B. Giannakis, "Statistical test for presence of cyclostationarity", IEEE Trans. on Sign. Proc., vol. 42, no. 9, pp. 2355-2369, 1994.

[80] F. F. Digham, M. S. Alouini, M. K. Simon, "On the energy detection of unknown signals over fading channels", *IEEE Trans. On Commun.*, vol. 55, no. 1, pp. 21-24, 2007.

[81] M. S. Oude Alink, A. B. J. Kokkeler, E. A. M. Klumperink, G. J. M. Smit, and Bram Nauta, "Lowering the SNR Wall for Energy Detection Using Cross-Correlation" *IEEE Tran. on Vehic. Techn*., vol. 60, no. 8, pp. 3748-3756, 2011.

[82] R. Tandra and A. Sahai, "SNR walls for signal detection", *IEEE J. on Selected Topics on Sign. Proc*., vol. 2, no.1, pp. 4-17, 2008.

[83] M. S. Oude Alink, A. B. J. Kokkeler, E. A. M. Klumperink, G. J. M. Smit, and Bram Nauta, "Lowering the SNR Wall for Energy Detection Using Cross-Correlation" *IEEE Tran. on Vehic. Techn*., vol. 60, no. 8, pp. 3748-3756, 2011

[84] Zeng, Y.-C. Liang, "Eigenvalue-based spectrum sensing algorithms for cognitive radio", *IEEE Trans. on Commun*.,vol. 57, no. 6, pp. 1784-1793, 2009.

[85] H. Sadeghi, P. Azmi, H. Arezumand, "Cyclostationarity based soft cooperative spectrum sensing for cognitive radio networks", *IET Commun.*, vol. 6, no.1, pp. 29 - 38, 2012.

[86] F. Benedetto, G. Giunta, S. Bucci, "A Unified Approach for Time Delay Estimation in Spread Spectrum Communications", *IEEE Trans. on Commun.*,vol. 59, no. 12, pp. 3421-3429, Dec. 2011.

[87] B. Wild, K. Ramchandran, "Detecting primary receivers for cognitive radio applications", *IEEE Dyn. Spect. Access Net. (DySpan 2005)*, pp.124-130 Nov. 2005

[88] J. S. Chitode J. G. Proakis,, "Data Transmission" in *Digital Communications*, pp. 4.22-4.29 D, McGraw-Hill International Editions, New York, 2001.

[89] V. I. Kostylev, "Energy detection of a signal with random amplitude", *IEEE Int. Conf. on Commun. (ICC 2002)*, vol. 3, pp. 1606- 1610, 2002.

[90] H. H. Choi, T. I. Hyon, K. H. Jang, Y. Kim, I. S. Lee, "*Cognitive radio communication apparatus and method which adaptably controls sensing reference level*", E. Patent 2077624 A3. Aug. 2012

[91] H.-Y. Hsieh, H.-K. Chang, M.-L. Ku, "Higher-order statistics based sequential spectrum sensing for cognitive radio", *IEEE 11th int. Conf. On ITS Telecomu. (ITST2011)*, pp. 696-701, Aug. 2011.

[92] B. Wild, K. Ramchandran, "Detecting primary receivers for cognitive radio applications", *IEEE Dyn. Spect. Access Net. (DySpan 2005)*, pp.124-130 Nov. 2005

[93] J. D. Vlok, J.C. Olivier, "Non-cooperative detection of weak spread-spectrum signals in additive white Gaussian noise", *IET Commun*., vol. 6, no. 4, pp. 2513-2524, Nov. 2012

[94] A. Ghasemi and E. S. Sousa, “Collaborative spectrum sensing for opportunistic access in fading environments,” *IEEE 1st Int. Symp.on Dynam. Spect. Access Net. (DySPAN)*, Baltimore, MD, Nov. 2005, pp. 131–136.

[95] G. Ganesan and G. Y. Li, “Cooperative spectrum sensing in cognitive radio—Part II: Multiuser networks,” *IEEE Trans. Wireless Commun*., vol. 6, no. 6, pp. 2214–2222, 2007.

[96] G. Ganesan and G. Y. Li, “Cooperative spectrum sensing in cognitive radio—Part I: Two user networks,*IEEE Trans. Wireless Commun*., vol. 6, no. 6, pp. 2204–2213, 2007.

[97] Z. Qaun, S. Cui, H.V. Poor, and A. Sayed “Collaborative wideband sensing for cognitive radio”, *IEEE Sign. Proc. Magazine*, vol.25, no. 6, pp. 60-73, 2008.

[98] J. Zhao, H. Zheng, and G.H. Yang, “Distributed coordination if Dynamic spectrum allocation networks”, *IEEE 5th Int. Symp.on Dynam. Spect. Access Net. (DySpan’05)*, pp.259-268, 2005

[99] W. Ahang and L.B. Kaheld, “Robust cooperative spectrum sensing for cognitive radios” U.S. Patent 765641, 2010

[100] J. Kronander, Y.SELÉN and H. Tullberg, “*Method and apparatus relating to spectrum sensing*” WO patent 2009148393A, 2011.

[101]] M. Al-Shalash, D.Li, A. C.K. Soong, D.Wang, C. Yang and G Zhao, “*System and Method for Cooperative Spectrum Sensing*

[102] R. Murty, R. Chandra, T. Moscibroda, P. (V.) Bahl. "SenseLess: A Database-Driven White Spaces Network", *IEEE Trans. on Mobile Computing*, vol. 11 no.2, pp 189-203, Feb 2012.

[103] C. Sun; H. Harada "On the effect of local sensing database to cognitive radio systems", *IEEE Int. Symp. on Wireless Personal Multimedia Commun. (WPMC2011),* pp 1-5. Oct. 2011.

[104] L. Li, J. Yee, "*System and method of implementing a cognitive radio device using spectrum sensing and location information*", E.Patent 2533559 A1, 8 June 2012.

[105] H. A. Hannel, J, Jari, P. J Hermannim, "*Method, apparatus and computer program for self-adjusting spectrum sensing for cognitive radio*", U.S. Patent 7885229 Feb. 2011.

[106] S. Wang, R. Inkol, S. Rajan, F. Patenaude, “On the performance gain of the FFT Filter-Bank-based summation and majority CFAR Detectors”, *IEEE Trans Instrum. and Measur.*, vol. 58, no. 5, pp 1778-1788, May 2009.

[107] S. Wang, S. Inkol, S. Rajan, F. Patenaude, “Detection of narrow band signals through the FFT and Polyphase FFT filter banks: Non-Coherent versus Coherent Integration”, *IEEE Trans on Instrum. and Measur*., vol. 59, no. 5, pp. 1424-1438, May 2010.

[108] S. Dikmese, S. Srinivasan, M. Renfors, “FFT and Filter Bank Based Spectrum Sensing And Spectrum Utilization for Cognitive Radios”, *Proc. 5th IEEE ISCCSP*, pp. 1-5, May 2012.

[109] S. Dikmese, A. Gokceoglu, M. Renfors, “Optimized FFT and Filter Bank based spectrum sensing for Bluethooth signals”, *Proc. WCNC*, pp. 792-797, Apr. 2012.

[110] S. Dikmese, M. Renfors, H. Dincer, "FFT and Filter Bank based spectrum sensing for WLAN signals", *Proc. ECCTD*, pp. 781-784, Aug. 2011.

[111] L. Luo, N. M. Neihart, S. Roy, D. J. Allstot, "A Two-Stage sensing technique for dynamic spectrum access", *IEEE Trans on Wireless Commun.*, vol. 8, no. 6, pp. 4181 – 4185, June 2009.

[112] P. Duhamel, "Algorithms meeting the lower bounds on the multiplicative complexity of length-2N DFTs and their connection with practical algorithms", *IEEE Trans. Acoust. Speech. Sign. Proc*., vol. 38, no. 9, pp. 1504-1511, 1990.

[113] D.Romero, R. Lopez-Valcarce, "Multiantenna detection of constant-envelope signals in noise of unknown variance", *in Proc. of the IEEE 12th Int. Workshop on Signal Proc. Adv. in Wireless Commun. (SPAWC)*, pp. 446 – 450, 2011.

[114] F. Benedetto, G. Giunta, L. Vandendorpe, "A Blind Equalization Algorithm Based on Minimization of Normalized Variance for DS/CDMA Communications", *IEEE Trans. on Vehic. Techn*., vol. 57, no. 6, pp. 3453-3461, 2008

[115] I. F. Akyildiz, L. Won-Yeol, C. M.Vuran, S.Mohanty, "A survey on spectrum management in cognitive radio networks",*IEEE Commun. Mag.*, vol.46, no.4, pp.40,48, 2008.

[116] K. N. Steadman, A. D. Rose, T. T. N. Nguyen, "Dynamic Spectrum Sharing Detectors", *in proc. of IEEE Int. Symp. on New Frontiers in Dynamic Spectrum Access Networks (DySPAN 2007)*, pp. 276-282, 2007.

[117] Federal Communications Commission, "*Facilitating Opportunities for Flexible, Efficient and Reliable Spectrum Use Employing Cognitive Radio Technologies*", notice of proposed rulemaking and order, FCC 03- 322, 2003.

[118] L. Khalid, A.Anpalagan, "Performance of cooperative spectrum sensing with correlated cognitive users' decisions",in proc. of the IEEE 22nd Int.Symp. onPersonal Indoor and Mobile Radio Commun. pp.635-639, 2011.

[119] M. Zander, "Technical and economic trends in wireless applications", *in Proc. ESSCIRC*, pp. 37-44, 2010.

[120] A. G. Fragkiadakis, E. Z. Tragos, I. G. Askoxylakis, "A Survey on Security Threats and Detection Techniques in Cognitive Radio Networks", *IEEE Commun. Survs &Tuts.*, vol. 15, no. 1, pp. 428-445, 2013.

[121] Z. Jin, S. Anand, K. P. Subbalakshmi, "Impact of Primary User Emulation Attacks on Dynamic Spectrum Access Networks", *IEEE Trans. on Commun.*, vol. 60, no. 9, pp. 2635-2643, 2012.

[122] Y. H. Zeng, Y.-C. Liang, "Spectrum-sensing algorithms for cognitive radio based on statistical covariance", *IEEE Trans. on Vehic. Techn.*, vol. 58, no. 4, pp. 1804–1815, 2009.

[123] G. Jacovitti and G. Scarano, "Discrete time techniques for time delay estimation," *IEEE Trans. Signal Processing*, vol. 41, pp. 525–533, 1993